Polarized growth and septation in the filamentous ascomycete *Ashbya gossypii* analyzed by live cell imaging

Inauguraldissertation

zur

Erlangung der Würde eines Doktors der Philosophie

vorgelegt der Philosophisch-Naturwissenschaftlichen Fakultät

der Universität Basel

von

Andreas Kaufmann

aus Ebikon, Luzern

Basel, 2008

Genehmigt von der Philosophisch-Naturwissenschaftlichen Fakultät

auf Antrag von

Prof. Dr. Peter Philippsen und Dr. Robert Arkowitz

Basel, den 24. April 2007

Prof. Dr. Hans-Peter Hauri

Dekan

Table of contents

Table of contents

Summary

Summary

Pathogenic filamentous fungi are responsible for huge crop losses worldwide and play an important role in human diseases. The morphological requirements for the development of a fungal mycelium, i.e. a network of fungal hyphae, include germ tube formation, permanent hyphal tip extension, lateral branching, tip splitting, and septation. These events, also termed landmarks of filamentous growth, represent different processes summarized as polarized growth. In this study we wanted to investigate the role of genes that are involved in polarized growth in the filamentous ascomycete *Ashbya gossypii*.

This thesis is structured in three parts that can be regarded as individual studies but all share the common purpose to increase our understanding of polarized growth in filamentous fungi. In Part I we characterize the role of the formin *Ag*Bni1 that is involved in germ tube formation, permanent hyphal tip extension, and tip splitting. The data presented suggests a novel pathway to transform one axis into two new axes of polar growth. Part II includes the functional analysis of genes involved in septation with focus on one gene essential for septation, encoding the novel PCH protein*Ag*Hof1. This allows us to draw a refined model of septation in *A. gossypii* in particular and filamentous fungi in general. Part III describes the construction of novel tools for the functional analysis of genes and proteins in *A. gossypii* and related fungi. These tools consist of three series of modules for PCR-based gene targeting, combining all markers presently available for *A. gossypii* with many different fluorescent protein and epitope tags. The three series can be used for C- or N-terminal tagging of proteins in combination with the exchange of the promoter. The first series has been extensively used for strain construction in Part II of this thesis.

Part I (Published in *Mol Biol Cell*, 2006, **17**:130-45)

We identified the formin *Ag*Bni1 as an essential factor for germ tube formation, permanent hyphal tip extension, and tip splitting. *Ag*Bni1 is apparently lacking functional overlaps with the two additional *A. gossypii* formins that are nonessential. Consistent with the essential role in hyphal development, *Ag*Bni1 locates to tips, but not to septa. Deletion of a C-terminal domain of *Ag*Bni1, which should render *Ag*Bni1 constitutively active, completely changes the branching pattern of young hyphae. New axes of polarity are no longer established subapically (lateral branching) but by symmetric divisions of hyphal tips (tip splitting). In wild-type hyphae, tip splitting is induced much later and only at much higher growth rates. We could show that *Ag*Bni1 interacts with the Rho-type GTPase *Ag*Cdc42. Consistently, young hyphae expressing mutated *AgCDC42* split at their tips, similar to the mutants expressing truncated *AgBNI1*. These data suggest a pathway for transforming one axis into two new axes of polar growth, in which an increased activation of *Ag*Bni1 by a pulse of activated *Ag*Cdc42 stimulates additional actin cable formation and tip-directed vesicle transport, thus enlarging and ultimately splitting the polarity site.

Part II (Manuscript in revision)

The knowledge about the molecular details of septation in filamentous fungi is still very limited, although it is comparable to cytokinesis and septation in *Saccharomyces cerevisiae*. 3D life cell imaging allowed the analysis of the events that take place during septation in *A. gossypii* and gave new insight into the role of cytokinetic key players, i.e. actin, PCH protein, myosin II, septins, formins, landmark proteins, and IQGAP. Septins constantly localize to the cortex of apical compartments and mark future septa at the very hyphal tip when localizing as a collar of cortical bars (CCB). The PCH protein *Ag*Hof1 colocalizes with septins as CCBs at future septa. These bars condense to a single ring colocalizing with the actin ring. The ring contracts as the septum is formed. CCBs and rings can persist up to five hours but ring contraction speed is comparable to *S. cerevisiae*. Concomitant with ring contraction cytokinesis occurs and the septum is formed but finally the hyphal compartments do not separate. Based on these studies, septation in *A. gossypii* can be divided into five stages: Site selection, bar-to-ring transition, contractile ring assembly and persistence, cytokinesis and septation, and septum maturation. It is to emphasize that all these events take place simultaneously in a continuous cytoplasm at different septa of one hypha. A possible reason for cell separation not to occur is that homologs of two genes required for cell separation in *S. cerevisiae* are not present in *A. gossypii.*

Part III (Manuscript in preparation)

Tagging of genes with PCR-amplified cassettes is an efficient and widely used method to label proteins *in vivo*. Generation of N- and C-terminally tagged proteins or the exchange of the promoter of a gene has thus become a straightforward method to analyze protein function. For the yeast *S. cerevisiae* many plasmid collections covering a wide selection of tags and markers are available. Unfortunately, most of these cassettes cannot be used in *A. gossypii*. So far, only a limited number of modules for C-terminal and none for N-terminal tagging were available for *A. gossypii*. Therefore I constructed three different series of totally 103 novel cassettes, containing a broad variety of C-terminal tags as well as promoter substitutions in combination with N-terminal tags. Many of these new modules have been successfully used in Part II of this thesis. This new toolbox should help to speed up the analysis of gene function in *A. gossypii*

and in other organisms in which *S. cerevisiae* promoter sequences are functional and that are amenable for PCR-based gene targeting.

Note:

Movies from the supplemental material of Part I of this thesis are freely available online at http://www.molbiolcell.org/cgi/content/full/E05-06-0479/DC1. The movies referred to in Part II are stored on a CD located at the end of this manuscript. The movies are available in uncompressed QuickTime, uncompressed AVI, and compressed MPEG4 format. The sequence of all pAGT plasmids constructed in Part III of this thesis are available as commented GenBank files on the same CD.

Purpose of this thesis

Purpose of this thesis

Filamentous growth is a very efficient strategy of pathogenic fungi to spread on or within their hosts. Insight into the function and regulation of conserved polarity factors should help to elucidate the principles of filamentous growth. Understanding the basis of the development of filamentous fungi will eventually lead to the discovery of new highly specific drug targets, thus reducing health threats and agricultural damage caused by filamentous fungi while limiting unwanted side effects and environmental problems.

The three parts of my thesis address different topics but share the common purpose to increase our understanding of polarized growth in filamentous fungi in general and in the model organism *Ashbya gossypii* in particular.

The goal of Part I of my thesis was the detailed analysis of the formin *Ag*Bni1. Formins are conserved nucleators of actin filaments, which are essential for filamentous growth. The genome of *A. gossypii* encodes three formins whereas the genome of the closely related yeast *Saccharomyces cerevisiae* encodes only two, which share redundant functions. Thus we addressed the questions if this could be one reason for the completely different life styles of the two organisms and whether formins play so far uncharacterized roles in morphogenesis and filamentous growth of *A. gossypii*.

The work presented in Part II aimed at the first dynamic analysis of septation and cytokinesis in filamentous fungi. This included the precise characterization of the events that lead to septum formation as well as the identification of new factors involved in these events. *Ag*Hof1 is the first PCH protein described in filamentous fungi. Additionally, it was intended to set an end to an ongoing debate whether septa in *A. gossypii* contain pores that would allow nuclear migration from one hyphal compartment to another. Finally, we found a plausible answer to the question why cytokinesis and septation is not followed by cell separation in *A. gossypii*.

The purpose of Part III of my thesis was to expand the repertoire of molecular tools for *A. gossypii*. The availability of a so-called versatile toolbox for PCR-based gene targeting should help to speed up functional analysis of genes and proteins in *A. gossypii* and potentially in other related fungi. The plasmid collection was designed to be modular, which facilitates the introduction of new tags and markers and reduces the need for gene-specific primers to a minimum making it very cost-effective. I integrated into the different series of this toolbox well established variants of fluorescent proteins and epitope tags as well as new fluorescent protein variants.

Background

Figures 2, 4, and 5 in this general introduction to my thesis are adapted versions of figures I contributed to the review "Homologues of yeast polarity genes control the development of multinucleated hyphae in *Ashbya gossypii*" by Peter Philippsen, Andreas Kaufmann, and Hans-Peter Schmitz. It was published in *Current Opinion in Microbiology* (2005), **8**(4): 370-7 and copyrights are property of Elsevier.

Background

The filamentous fungus *Ashbya gossypii*

Fungi represent by far the largest group of plant pathogens. Spores of phytopathogenic fungi may be disseminated by water, wind, or insects, and infection of plants is often facilitated by tissue damage caused by insects (Agrios, 1997). The ability of piercing-sucking insects to transmit plant disease is closely linked to feeding mode and target tissue. The true bugs (*Heteroptera*) are generally considered to be of minimal importance as vectors of plant pathogens. Nevertheless, they have been associated with a variety of plant diseases caused by fungi (Agrios, 1980). The majority of these fungi are ascomycetes. In some cases the association simply involves creation of an infection court through wound lesions, as in bacterial transmission, but more frequently, *Heteroptera* are directly implicated in vectoring, or represent the primary facilitator of spore transmission (Mitchell, 2004). Infection of cotton (*Gossypium hirsutum*; Figure 1, A) by the filamentous ascomycete *Ashbya gossypii* in association with hemipteran feeding was referred to as stigmatomycosis (Ashby and Nowell, 1926). On pistachio, this term is still commonly used (Michailides and Moragan, 1990), but other terms are used for cotton (internal boll disease), beans (yeast spot), tomato (fruit rot), citrus (fruit lesions), and coffee (bean rot). *A. gossypii* causes internal boll disease of cotton throughout the tropics, and is strongly associated with cotton stainers in the genus *Dysdercus* (Mitchell, 2004; Figure 1, B). In the first half of the twentieth century, the fungus caused severe economic losses and made in virtually impossible to grow cotton in several regions of the subtropics (Batra, 1973). Frazer (1944) considered transmission to be mechanical, with spores and mycelium carried as an external contaminant on the mouthparts and within the stylet pouches; however, the insect is obligatory for the spread of the fungus. Therefore the spread of the disease can be readily controlled with insecticides (Dammer and Ravelo, 1990).

Soon after its first description *A. gossypii* was recognized for its ability to produce large quantities of riboflavin (vitamin B_2; Figure 1, C), which is responsible for its yellow color (Demain, 1972; Stahmann *et al.*, 2001; Wickerham *et al.*, 1946). Riboflavin is a successful commercial product and is used not only as a vitamin and food additive but also as food coloring (E101). Analysis of riboflavin production dominated research in *A. gossypii* for more than half a century prior to the introduction of molecular genetic tools and the sequencing of its genome (Altmann-Johl and Philippsen, 1996; Dietrich *et al.*, 2004; Steiner *et al.*, 1995; Wright and Philippsen, 1991).

The annotation of the genome sequence of *A. gossypii* surprisingly revealed a gene set very similar to that of *Saccharomyces cerevisiae* and allowed the reconstruction of the evolutionary history of both organisms. *A. gossypii* and *S. cerevisiae* originate from a common ancestor which carried about 5000 genes (Figure 2, A). The genome of *A. gossypii* with 9 million base pairs and 4700 protein coding genes has evolved from this common ancestor during 100 million years by up to 100 viable genome rearrangements (translocations and inversions), a few million base pair changes, and a limited number of gene deletions, duplications, and additions. The genome of *S. cerevisiae* underwent a more eventful evolution, which includes a whole-genome duplication, 200 or more viable genome

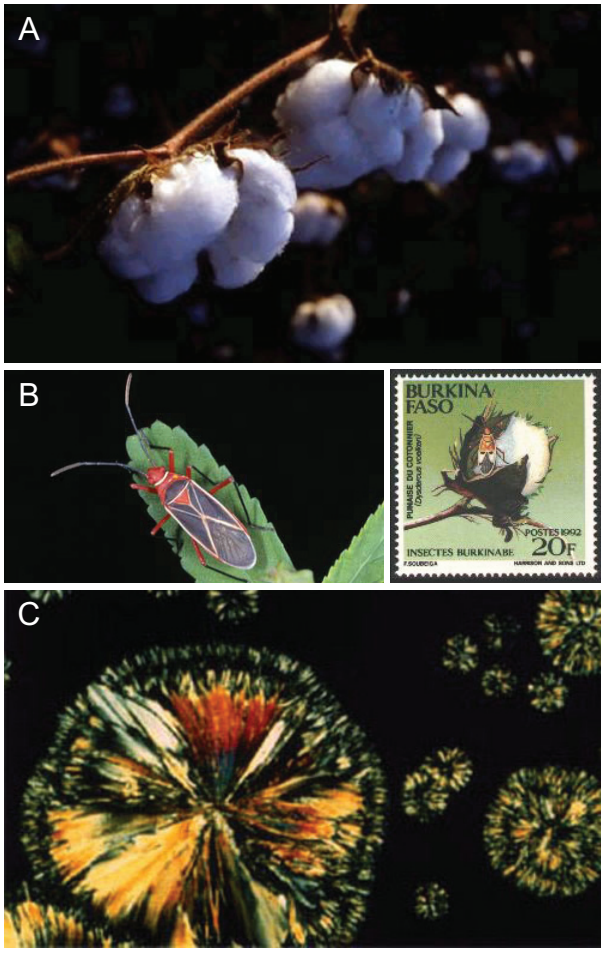

Figure 1: Origin of *A. gossypii*.
(A) Cotton bolls (FAO). (B) Cotton stainers of the genus *Dysdercus* (SquashBug; Buss). (C) Riboflavin crystals (TransGEN, 2007).

rearrangements, a few million base pair changes, 4000 to 4500 gene deletions after the genome duplication, and a limited number of gene additions. The complete synteny map of both genomes reveales that 95 % of *A. gossypii* genes are orthologs of *S. cerevisiae* genes and 90 % map within blocks of synteny (syntenic homologs) (Dietrich *et al.*, 2004; reviewed by Philippsen *et al.*, 2005).

Polarized growth in *A. gossypii*

The life cycle of *A. gossypii* starts with a phase of isotropic growth (Figure 3, A). The center part of the needle-shaped spore swells and forms a round germ bubble, where actin patches localize randomly to the cortex. Then actin patches start to concentrate at one region at the cortex thus marking the site of germ tube emergence. The polarized actin cytoskeleton directs growth to this region causing the first germ tube to extend, perpendicular to the axis of the needle, and to form a unipolar germling (Figure 3, B). Actin localizes as cortical patches polarized to the tip of the germ tube and less frequently to the hyphal cortex. Actin cables emanate from the tip and run along the hyphal cortex. The germ tube maintains polarization and, under favorable growth conditions, extends incessantly in one direction. Opposite of the first germ tube a second germ tube emerges from the germ bubble to give rise to a bipolar germling. New sites of polarity are established during hyphal growth leading to the formation of lateral branches distant from the growing tip (Figure 3, C). This is different from budding yeast cells, which only initiate one new polarity axis after completion of the cell cycle. Hyphal tip growth speed increases during maturation and apical tip splitting occurs in mature mycelium (Figure 3, D). Older parts of mature mycelia eventually form sporangia containing the asexually produced spores, attached to each other through a filament, that are set free by lysis (Figure 3, E and F; Ashby and Nowell, 1926; Ayad-Durieux *et al.*, 2000; Knechtle *et al.*, 2003; Schmitz *et al.*, 2006; Wendland and Philippsen, 2000).

Figure 4 highlights the differences in growth forms between *A. gossypii* and *S. cerevisiae*. In contrast to the developmental pattern of the filamentous fungus *A. gossypii*, uninucleate *S. cerevisiae* cells proliferate by growing buds (daughter cells). These different patterns of growth lead to very different colony sizes after three days of budding and filamentous growth, respectively (Figure 2, C). As outlined in Figure 4, A, polar growth in *S. cerevisiae* is tightly linked to the cell cycle and to morphogenesis of the yeast cells (reviewed by Pruyne and Bretscher, 2000). Polarity is established at the end of each G1 phase, with selection of a new growth site followed by polar growth of the emerging bud during S phase. During cell cycle progression, bud development switches from polar to isotropic growth. During mitosis (M), one of the two daughter nuclei migrates through the bud neck into the daughter cell, which induces polar growth at the bud neck to complete cytokinesis and cell separation (CK/CS). The mother cell enters its next cycle whereas the new-born daughter cell grows isotropically to increase its size before entering another cell cycle round.

Analysis of sustained polar growth in *A. gossypii* revealed that it involves the same polarity factors that function during the polar growth phases of yeast (Ayad-Durieux *et al.*, 2000; Bauer *et al.*, 2004; Knechtle *et al.*, 2003; Knechtle *et al.*, 2006; Schmitz *et al.*, 2006; Wendland and Philippsen, 2000; Wendland and Philippsen, 2001). Compared to budding yeast the multitude of morphological phenotypes associated

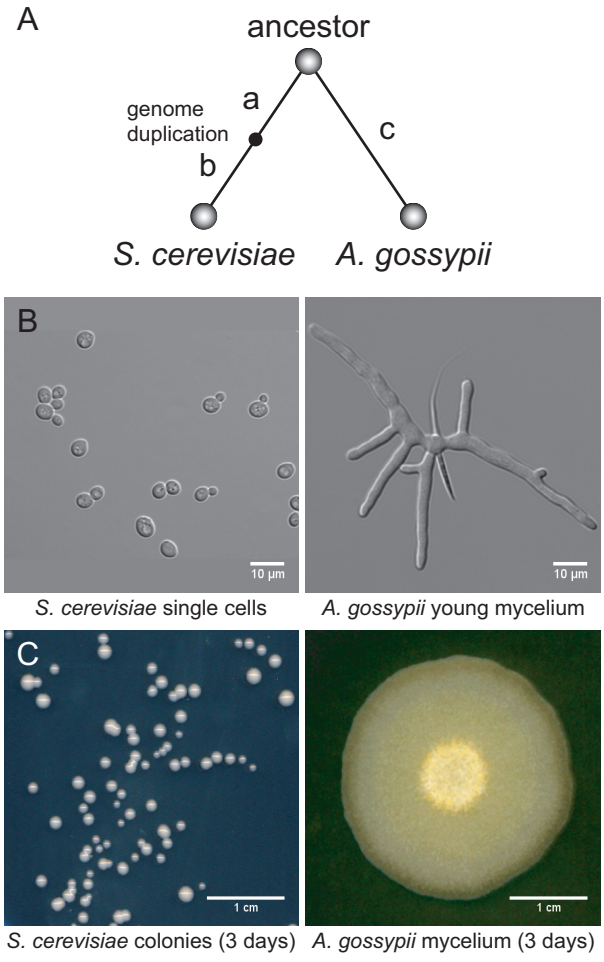

Figure 2: Evolution of different lifestyles from one fungal ancestor.

(A) *A. gossypii* and *S. cerevisiae* diverged from a common ancestor over one hundred million years ago. (B) DIC images of single budding *S. cerevisiae* cells and young lateral-branching *A. gossypii* mycelium. (C) Different diameters of yeast and fungal colonies after three days of growth.

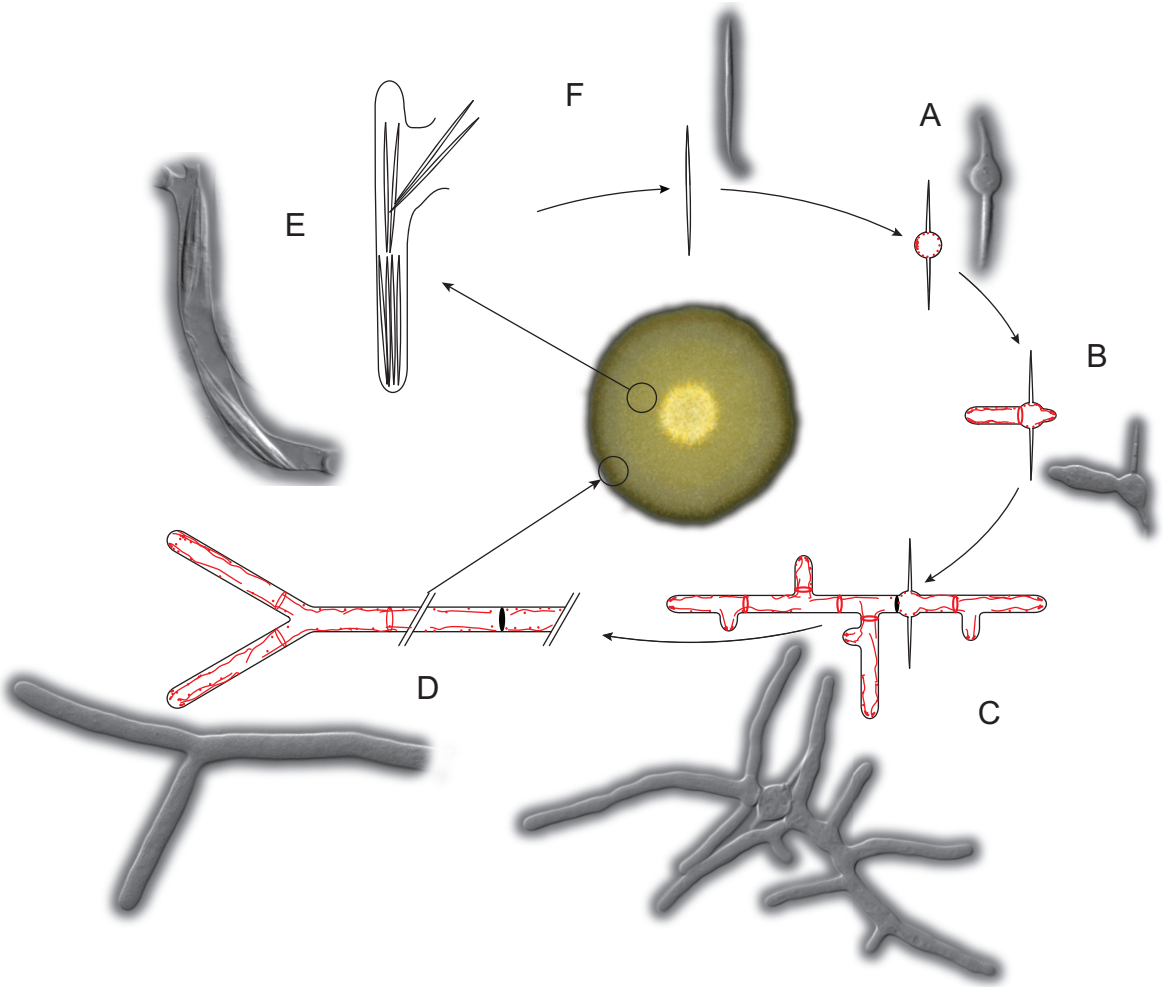

Figure 3: Life cycle of *A. gossypii.*

In the centre, an *A. gossypii* colony is shown that was inoculated in the middle of an agar plate and incubated for three days at 30 °C. The yellow color is caused by riboflavin production. The inner part of the colony is sporulating. Schematic drawings and DIC images of characteristic developmental stages show: (A) isotropic growth phase during germination, (B) germ tube formation, (C) lateral branching of young mycelium, (D) tip splitting of mature mycelium, (E) sporulation, and (F) rupture of sporangia to release the spores. The actin cytoskeleton consists of actin patches (red dots), actin cables (red lines), and actin rings (red circles). Septa are indicated as black bars.

with *A. gossypii* mutants of these genes was surprising and led, in some cases, to the assignment of new roles to these polarity factors. Some examples have been reviewed by Philippsen *et al.* (2005), are summarized in Figure 5, and are briefly discussed here. One example is the Rho-type GTPase Rho3. Mutants in budding yeast form enlarged cold-sensitive cells with bud site selection defects (Adamo *et al.*, 1999). Hyphae of *A. gossypii* lacking *Ag*Rho3 still grow along a stable polarity axis but alternate between polar and isotropic growth phases (Wendland and Philippsen, 2001). Thus *Ag*Rho3 is important for maintenance but not initial establishment of cell polarity. Similarly, *Agbem2Δ* mutants lose sustained polarity and switch to isotropic growth. Although these mutants can reestablish polarity, like *Agrho3Δ* mutants, polarity reestablishment occurs at multiple sites (Wendland and Philippsen, 2000). In contrast, loss of *Sc*Bem2, the GAP (GTPase activating protein) of the small GTPase *Sc*Rho1, causes mutant cells to become multinucleated and to enlarge (Cid *et al.*, 1998; Wang and Bretscher, 1995). The lack of the GAP probably leads to prolonged activation of the GTPase, which apparently causes different responses in both systems. A multitude of phenotypes can be observed in hyphae lacking *Ag*Rsr1/Bud1, the homolog of the small GTPase *Sc*Rsr1. While *S. cerevisiae rsr1* mutants grow like wild type except for the random budding pattern (Bender and Pringle, 1989), *A. gossypii Agrsr1/bud1Δ* hyphae grow much slower caused by pausing of hyphal tip extension. The polarity axis in this mutant is unstable causing the hyphae to change growth direction frequently. Additionally, unsuccessful branching attempts at random sites vaguely resemble at the random bud site selection in *Scrsr1Δ* mutants

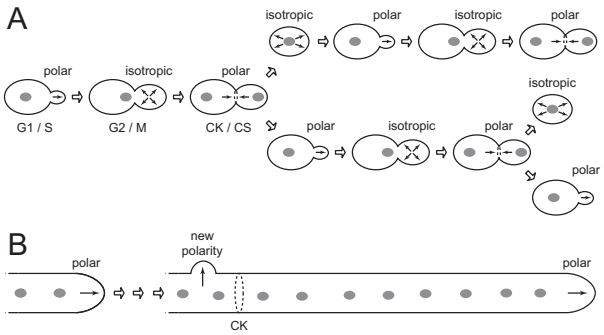

Figure 4: Different modes of polar growth.
(A) In *S. cerevisiae* transitions between polar and isotropic growth are tightly coupled to cell cycle phases. After cytokinesis and cell separation (CK/CS) the bigger mother cell immediately selects a new site for bud growth, whereas the smaller daughter cell first increases its size, thereby prolonging the G1 phase before selecting the site for but growth. (B) Constant polar growth, establishment of new sites of polar growth, and cytokinesis are uncoupled from the nuclear cycles in hyphae of *A. gossypii* and occur simultaneously only spatially separated from each other. Solid arrows mark directions of surface extensions and grey circles represent nuclei.

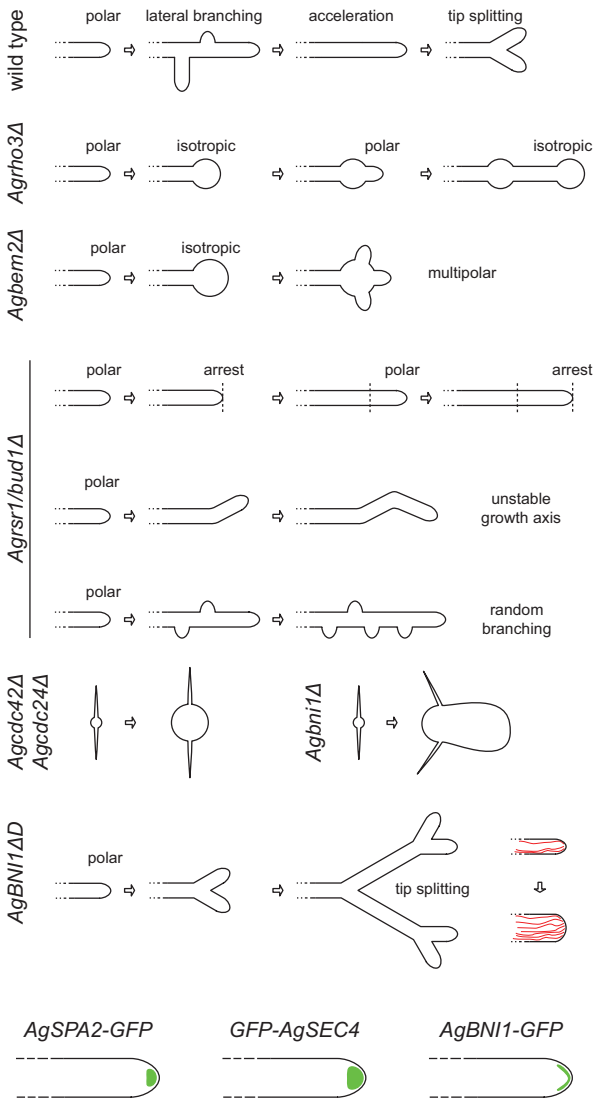

Figure 5: Growth phenotypes of *A. gossypii* mutants that lack polarity factors.
Changes in hyphal growth that are associated with gene deletions and the localization of GFP-tagged proteins (green areas) are shown. Red lines represent actin cables.

(Bauer *et al.*, 2004). The observation that the polarisome component *Ag*Spa2 (Knechtle *et al.*, 2003) frequently dis- and reappears at hyphal tips of *Agrsr1/bud1Δ* mutants led to the assignment of a novel function for the Rsr1 GTPase in stabilizing the polarisome (Bauer *et al.*, 2004). In mutants lacking either the Rho-type GTPase *Ag*Cdc42 or its GEF (Guanine nucleotide exchange factor) *Ag*Cdc24 polarity establishment was completely abolished causing germinating spores to form large round cells with many nuclei (Wendland and Philippsen, 2001). This phenotype was not surprising as this GTPase module has a conserved central role in polarity establishment of many eukaryotes (reviewed by Etienne-Manneville, 2004). Formins are a growing protein family and have a conserved role in nucleation and assembly of unbranched actin filaments and are usually activated by Rho-type GTPases (reviewed by Kovar, 2006). In *A. gossypii* three formins are present whereas only two have been found in *S. cerevisiae*. The importance of formin-mediated actin cable assembly in filamentous growth is demonstrated by the deletion of a single formin in *A. gossypii*, *AgBNI1*. Whereas deletion of either one of the two formins present in *S. cerevisiae* does not have a drastic phenotype (Imamura *et al.*, 1997), deletion of *AgBNI1* is lethal and germinating mutant spores expand to giant potato-shaped cells completely lacking actin cables (Part I of this thesis: Schmitz *et al.*, 2006). Furthermore deletion of the C-terminal autoinhibitory domain leads to an increase in hyphal diameter and actin cables. This probably causes an increase in tip-directed transport of secretory vesicles leading to premature hyphal tip splitting. The bottom part of Figure 5 shows examples of the localization patterns of polarity factors in *A. gossypii*. The polarisome component *Ag*Spa2 (Knechtle, 2002) and the formin *Ag*Bni1 (Schmitz *et al.*, 2006) constantly localize to the hyphal tip. The Ras-like GTPase *Ag*Sec4, which probably attaches to late Golgi vesicles as shown in budding yeast (Mulholland *et al.*, 1997), accumulates just behind the growing tip (Schmitz *et al.*, 2006). Additionally, the PAK kinase *Ag*Cla4, a putative downstream effector of *Ag*Cdc42, localizes to the growing tip as well (Ayad-Durieux *et al.*, 2000). Recent results show that many other proteins with a conserved role in cell polarization constantly localize to the hyphal tip, e.g., the Rho-type GTPase *Ag*Cdc42 and its GEF *Ag*Cdc42, the polarisome components *Ag*Bud6 and *Ag*Pea2, the exocyst component *Ag*Exo70,

the small GTPase *Ag*Rho1b, as well as the SH3 domain-containing proteins *Ag*Boi1 and *Ag*Bem1 (Knechtle *et al.*, 2006; Michael Köhli, Philipp Knechtle, and Kamila Boudier, personal communication). Interestingly, the localization patterns of these proteins slightly differ allowing the definition of individual zones of the hyphal apical cortex. Additionally, the localization of many of these markers changes from cortical to an intracellular spheroid as hyphal tip growth speed increases (Michael Köhli, PhD thesis 2007).

Septation in *A. gossypii*

Cytokinesis (division of the cytoplasm) is a process that is conserved between animal and fungal cells. Basically all these cells use an actin-based contractile ring to constrict the plasma membrane and to separate the cytoplasm of the two daughter cells during cytokinesis (reviewed by Balasubramanian *et al.*, 2004). As outlined in Figure 4, A, polarized growth alternates with phases of isotropic growth during cell cycle progression in yeast. First in G1/S phase the future site of cytokinesis and septation is chosen during bud site selection. Later during the cell cycle, after one of the two nuclei migrated into the bud, the contractile ring at the bud neck contracts and the primary septum is formed. Secondary septa and new cell walls will form on either side of the primary septum that is finally degraded. These processes lead to complete cell separation and to the formation of two cells. Cytokinesis and septation are tightly coupled to the cell cycle to happen only once per cycle and after the end of mitosis (reviewed by Pruyne and Bretscher, 2000).

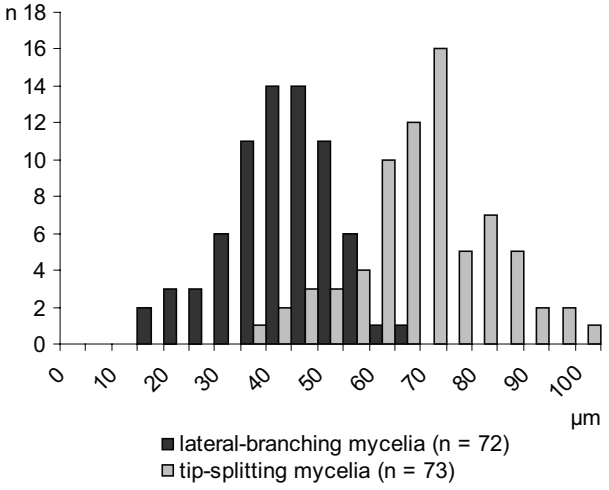

Figure 6: Distance distribution between septa in *A. gossypii*.
The distance between 72 and 73 septa has been measured in young lateral-branching mycelia (dark grey) and mature tip-splitting mycelia (light grey), respectively.

In contrast to yeast, *A. gossypii* produces septa distant from the growing tip. Nevertheless, septation in filamentous fungi is homologous to cytokinesis and septation in yeasts (reviewed by Walther and Wendland, 2003; Wendland and Walther, 2005). Homologs of all major components required for cytokinesis are encoded in the genome of *A. gossypii* (Table 1). Cytokinesis and septation are obviously uncoupled from individual nuclear cycles in *A. gossypii* as compartments between septa contain many nuclei (Ashby and Nowell, 1926). Figure 3 illustrates the normal septation pattern of *A. gossypii* wild type. Actin rings (red circles) are present at sites where septa (black bars) will form (Knechtle *et al.*, 2003). The first septum forms between the base of the germ tube and the germ bubble. In young mycelia, i.e. lateral-branching mycelia, septa can be found either at the base of lateral branches or in the main hypha in proximity to lateral branches (reviewed by Wendland and Walther, 2005). In mature mycelia, i.e. tip-splitting mycelia with hyphae growing faster than 80 µm/h (Schmitz *et al.*, 2006), septa are found along the hyphae and at the bases of the two hyphae resulting from a tip-splitting event. The distance between septa is not constant and apparently depends on the developmental stage of the mycelium and/or the growth speed of the hyphae. Figure 6 shows the distances between septa measured in slow-growing lateral-branching and fast-growing tip-splitting mycelia (this study). The knowledge about the molecular details of septation in *A. gossypii* in particular and filamentous fungi in general is still very limited. For example, the homologs of the bud protein *Sc*Bud3 and the IQGAP *Sc*Iqg1 are important for actin ring localization and formation, respectively, in yeast and *A. gossypii*, however the IQGAP is essential in yeast but not in *A. gossypii* (Wendland, 2003a; Wendland and Philippsen, 2002). Additionally, members of the septin family of filamentous fungi have been found not only to be involved in septation but in general hyphal morphogenesis (Helfer, 2006; Helfer and Gladfelter, 2006 and reviewed by Gladfelter, 2006).

Molecular tools for *A. gossypii*

Many of the molecular tools for *A. gossypii* were introduced by the Philippsen group in the 1990s. It became evident that *A. gossypii* is more similar, in terms of its molecular genetics, to yeast than to filamentous fungi. Plasmids containing autonomously replicating sequence (ARS) elements of *S. cerevisiae* are able to freely replicate in *A. gossypii* (Wright and Philippsen, 1991). Moreover, *A. gossypii* integrates DNA exclusively via homologous recombination (Steiner *et al.*, 1995). The absence of ectopic integration of DNA, which occurs frequently in other filamentous

Table 1: Major components involved in cytokinesis in different fungi.

	S. cerevisiae	*S. pombe*	*A. gossypii*[1]
Contractile ring positioning			
Bud proteins	Axl1, Axl2, Bud3, Bud4, Bud8, Bud9, Rsr1/ Bud1,Bud2, Bud5	na/nr	AGR251C, AER417W, Bud3, AGL306C, ACL193C, ACL193C, AFR464W, ABR021W, AFR630C
Cdc42 GTPase module	Cdc42, Cdc24,	Cdc42	Cdc42, Cdc24
Septin	Cdc3, Cdc10, Cdc11, Cdc12, Shs1/Sep7, Spr3, Spr28	Spn1-7	Cdc3, Cdc10, Cdc11a, Cdc11b, Cdc12, Sep7, AAR146W, AGR175C
Anillin and anillin-related	na	Mid1, Mid2	na
Contractile ring assembly			
Myosin II heavy chain	Myo1	Myo2, Myp2	ACR068W
Myosin essential light chain	Mlc1	Cdc4	AFL030C
Myosin regulatory light chain	Mlc2	Rlc1	AEL280W
Actin	Act1	Act1	ABR222W
Profilin	Pfy1	Cdc3	ACL168C
Formin	Bni1, Bnr1	Cdc12	Bni1, Bnr1, Bnr2
ADF/Cofilin	Cof1	Cof1	ADR235W
IQGAP	Iqg1/Cyk1	Rng2	Cyk1
PCH proteins	Hof1/Cyk2	Cdc15	ABR082W
RhoA	Rho1	Rho1	Rho1, ABR183W
Rho GEF	Rom1, Rom2	Gef1, Scd1	AFR585W
Membrane insertion			
Syntaxin	Sso1, Sso2	Psy1	AFL139W
Exocyst complex	Sec3, Sec5, Sec6, Sec8, Sec10, Sec15, Exo70, Exo80	Sec6, Sec8, Sec10, Exo70	ADR012C, AGL158C, ACL047W, ADL317C, AGL130C, AFR251C, AFR100W, ADL321W
Myosin V	Myo2, Myo4	Myo52	ADR354W
Coordination with nuclear division			
MEN/SIN pathway	Tem1, Lte1, Bub2, Bfa1, Cdc15, Dbf2, Dbf20, Mob1, Cdc14, Net1	Cdc7, Cdc11, Cdc14, Cdc16, Sid1, Sid2, Spg1, Sid4, Mob1, Byr4, Clp1/ Flp1	AER132W, ACR292W, ADR132W, ACL090C, AER223C, ADR033W, ADR033W, ADL236W, AEL025W, AAL181C
Regulatory molecules			
Polo kinase	Cdc5	Plo1	ACL006W
Aurora B kinase complex	Ipl1, Sli15, Bir1	Ark1, Cut17, Pic1	AFL101C, AGL269W, AER399C
Cdk1/Cyclin B	Cdc28, Clb1, Clb2, Clb3, Clb4	Cdc2, Cdc13	Cdc28, Clb1/2, Clb3/4

[1] systematic ORF names are given for uncharacterized proteins

na: apparently absent in genome

nr: related molecules known, but no known function in cytokinesis

adapted from Balasubramanian *et al.* (2004)

fungi, enabled the development of very powerful tools for functional genomics including one-step PCR-based gene targeting (Wach *et al.*, 1994; Wendland *et al.*, 2000) and recombinant plasmid technology (Steiner and Philippsen, 1994; Steiner *et al.*, 1995). Hyphae of *A. gossypii* are multinucleated, so primary transformants, so-called heterokaryons, will harbor two types of nuclei that contain either the mutant allele or the wild-type allele within a hyphal segment. Such a heterokaryotic mycelium will generate uninucleate spores that carry either wild-type or mutant nuclei. Selection for mutant spores allows propagation of mycelia carrying only mutant nuclei, so-called homokaroyns, and therefore the analysis of mutant phenotypes. Compared with other filamentous fungi, gene analysis in *A. gossypii* is therefore particularly convenient. A heterologous selectable marker for dominant selection (Wendland *et al.*, 2000), strains auxotrophic for leucine biosynthesis (Altmann-

Johl and Philippsen, 1996), and GFP modules for C-terminal tagging of proteins (Knechtle *et al.*, 2003) have been developed. Additionally, several fluorescent dyes can be used in *A. gossypii* to stain the actin cytoskeleton, cell wall, vacuoles, ER, and mitochondria.

Fluorescent proteins

Fluorescent proteins (FPs) are not new to science, nor were they always a hot topic; rather, it is biotechnology that has made FPs what they are today. The Green Fluorescent Protein (GFP) was discovered by (Shimomura *et al.*, 1962) as a protein isolated during the purification of aequorin, the famous chemiluminescent protein from the jellyfish *Aequorea victoria*. Marine biochemists labored in relative obscurity for 30 years before the GFP gene was first cloned by Prasher *et al.* (1992). With the cDNA sequence at hand the use of GFP as a reporter molecule was straightforward. Gene expression was monitored with GFP first in *Escherichia coli* then in the nematode *Caenorhabditis elegans* and the fruit fly *Drosophila melanogaster* (Chalfie *et al.*, 1994; Heim *et al.*, 1994; Inouye and Tsuji, 1994; Wang and Hazelrigg, 1994). The applications of GFP to detect gene expression *in vivo* were somewhat disappointing due to the inherent lack of sensitivity of GFP as a reporter gene, a direct result of its lack of amplification. GFP is not an enzyme that catalytically processes an indefinite number of substrate molecules. Instead, each GFP molecule produces at most one fluorophore. The most successful and numerous GFP applications have been fusions to host proteins to monitor their localization and fate. The open reading frame (ORF) encoding GFP is fused in frame with the ORF encoding the endogenous protein and the resulting chimera expressed in the cell or organism of interest. The ideal result is a fusion protein that maintains the normal functions and localizations of the host protein but is now fluorescent. GFP has been targeted successfully to practically every major organelle of the cell, including plasma membrane, nucleus, endoplasmic reticulum, Golgi apparatus, secretory vesicles, mitochondria, peroxisomes, vacuoles, and phagosomes. Thus the size and shape of GFP and the differing pHs and redox potentials of such organelles do not seem to impose any serious barrier (reviewed by Tsien, 1998). Even specific chromosomal loci can be tagged indirectly by inserting multiple copies of Lac operator sites and decorating them with a fusion of GFP with the Lac repressor protein (Straight *et al.*, 1997). In general, fusions can be attempted at either the amino or carboxyl terminus of the host protein, sometimes with intervening spacer peptides. However, the crystal structures of GFP (Ormo *et al.*, 1996; Yang *et al.*, 1996) show that the N- and C-termini of its core domain are not far apart, so it might be possible to splice GFP into a non-critical exterior loop or domain boundary of the host protein. For example, residues 2–233 of GFP have been inserted between the last transmembrane segment and the long cytoplasmic tail of a Shaker potassium channel (Siegel and Isacoff, 1997). Although the prime advantage of GFP is its ability to generate fluorescence *in vivo*, its fluorescence does survive formaldehyde fixatives (Chalfie *et al.*, 1994). Occasional problems in maintaining fluorescence during fixation may result from uncontrolled acidity of the fixative solution, which denatures the protein and destroys the fluorescence (Ward *et al.*, 1980).

Low expression of target proteins, slow folding kinetics of GFP, photobleaching of the fluorophore, and phototoxicity of the excitation wavelength limited the observation of wild-type GFP *in vivo*. These obstacles could be alleviated by *in vitro* mutagenesis of GFP and screening for better folding kinetics, higher extinction coefficient, and longer excitation wavelength. The first and still most widely used mutant that encountered these requirements carries a single point mutation at the position 65 converting the serine, involved in building the fluorophore, to a threonine. This increases the relative brightness of the S65T variant compared to wild-type GFP about a factor of 2. In addition, the time for the protein required to become fluorescent is drastically reduced from 90 to about 20 min (Heim *et al.*, 1995). The possibility of altering the excitation and emission spectra of GFP by mutagenesis and increasing knowledge about the functional and structural relationship of individual amino acid residues raised the hope to produce artificially engineered GFP variants that could be used for *in vivo* double labeling. A red-shifted variant together with a blue-shifted variant showed to be suitable (Ellenberg *et al.*, 1998; Heim *et al.*, 1995). This FP pair is now generally referred to as YFP (Yellow Fluorescent Protein) and CFP (Cyan Fluorescent Protein), respectively, and has successfully been used for many of colocalizations and interaction studies based on fluorescence resonance energy transfer (FRET). cDNA extraction from colored body parts of various *Anthozoa* corrals and comparison of sequence motifs believed to be essential for the β-barrel structure based on the crystal structure of GFP revealed eight different GFP homologs (Matz *et al.*, 1999). The emission wavelength of these proteins ranged from blue to red. Variants shifted to longer wavelengths are of special interest because longer wavelengths are less phototoxic and clear spectrum separation compared with the CFP/YFP variants would allow for *in vivo* triple labeling. In addition, the intrinsic background fluorescence of many tissues and organisms is considerably lower in the red spectrum. This made the red fluorescent protein from *Discosoma striata* (DsRed) an interesting candidate for further analysis. Unfortunately, DsRed is an obligate tetramer *in vitro* and maturation of the protein takes days (Baird *et al.*,

Table 2: Spectral properties of some fluorescent proteins.

Class	Protein	Ex (nm)	Em (nm)	Brightness[1]	Photostability[2]	$t_{0.5}$ for maturation	Oligomerization
Far-red	mPlum	590	649	4.1	53	1 h	Monomer
Red	mCherry	587	610	16	96	15 min	Monomer
	tdTomato	554	581	95	98	1 h	Tandem dimer
	mStrawberry	574	596	26	15	50 min	Monomer
	DsRed	558	583	na	na	days	Tetramer
	RedStar2	558	583	na	na	~40 min	Dimer
Orange	mOrange	548	562	49	9.0	2.5 h	Monomer
Yellow	mCitrine	516	529	59	49	na	Monomer
	Venus	515	528	53	15	na	Weak dimer[3]
	EYFP	514	527	51	60	na	Weak dimer[3]
Green	EGFP	488	507	34	174	na	Weak dimer[3]
	GFP(S65T)	489	510	na	na	~20 min	Weak dimer[3]
	wtGFP	395	504	na	na	~90 min	Weak dimer[3]
Cyan	ECFP	435	495	na	na	na	Weak dimer[3]
	mCFP	433	475	13	64	na	Monomer
	Cerulean	433	475	27	36	na	Weak dimer[3]

[1] Product of extinction coefficient and quantum yield at pH 7.4 (Shaner *et al.*, 2005).

[2] Time for bleaching from an initial emission rate of 1,000 photons/s down to 500 photons/s (Shaner *et al.*, 2005).

[3] Can be made monomeric by introducing A206K mutation

na not available

adapted from Heim *et al.*(1995), Knop *et al.* (2002), Shaner *et al.* (2005), and Stewart (2006)

2000) resulting in many unsuccessful attempts to create functional fusion proteins.

In recent years, random and site-directed mutagenesis of DsRed (Campbell *et al.*, 2002; Janke *et al.*, 2004; Knop *et al.*, 2002; Shaner *et al.*, 2004) as well as anthozoan-derived FPs (Griesbeck *et al.*, 2001; Nagai *et al.*, 2002; Nguyen and Daugherty, 2005; Rizzo *et al.*, 2004; Zacharias *et al.*, 2002) led to an explosion in the diversity of available fluorescent proteins promising a wide variety of new tools for biological imaging (Table 2). These new FPs have been selected for brightness, i.e. extinction coefficient and quantum yield, photostability, folding efficiency, and the absence of oligomerization. Their excitation and emission spectra reach from the UV to the far red part of the light spectrum. Using adequate filter sets simultaneous labeling with cyan, yellow, orange and red FPs (e.g., Cerulan, YFP, mOrange, mCherry) with minimal crosstalk is possible. Furthermore, the coding sequences of many FPs have been codon optimized for efficient expression in a given organism (Cormack *et al.*, 1997; Sheff and Thorn, 2004). However, the drawback of this variety is that there is no unified standard for assessing these tools. Which FPs are best for general use? Which are the brightest? What additional factors determine which are best for a given experiment? In many cases, a trial-and-error approach may still be necessary in determining the answers to these questions. Shaner *et al.* (2005) tried to characterize the best available FPs and provided a useful guide to narrow down the options.

Part I

The work presented in this part of my PhD thesis was published in *Molecular Biology of the Cell* (2006), **17**: 130 – 45, by the authors Hans-Peter Schmitz, Andreas Kaufmann, Michael Köhli, Pierre Philippe Laissue, and Peter Philippsen. The copyrights are porperty of the American Society for Cell Biology (ASCB) and a free version of the manuscript is accessible at http://www.molbiolcell.org/cgi/content/full/17/1/130. For clarity, the whole manuscript is presented here. My personal contribution is the functional analysis of the formin *AgBNI1*, one main part of this publication. This includes construction and characterization of *Agbni1Δ* and *Agbni1ΔD* mutants, the introduction of point mutations in *AgBNI1*, and the strain construction and analysis of the localization patterns of *Ag*Spa2-GFP in *Agbni1Δ* mutants, *Ag*Bni1-GFP, and *Ag*bni1ΔD-GFP.

Molecular Biology of the Cell
Vol. 17, 130–145, January 2006

From Function to Shape: A Novel Role of a Formin in Morphogenesis of the Fungus *Ashbya gossypii*[V]

Hans-Peter Schmitz, Andreas Kaufmann, Michael Köhli, Pierre Philippe Laissue, and Peter Philippsen

Biozentrum der Universität Basel, 4056 Basel, Switzerland

Submitted June 3, 2005; Accepted October 11, 2005
Monitoring Editor: Sandra Schmid

Morphogenesis of filamentous ascomycetes includes continuously elongating hyphae, frequently emerging lateral branches, and, under certain circumstances, symmetrically dividing hyphal tips. We identified the formin *Ag*Bni1p of the model fungus *Ashbya gossypii* as an essential factor in these processes. *Ag*Bni1p is an essential protein apparently lacking functional overlaps with the two additional *A. gossypii* formins that are nonessential. *Agbni1* null mutants fail to develop hyphae and instead expand to potato-shaped giant cells, which lack actin cables and thus tip-directed transport of secretory vesicles. Consistent with the essential role in hyphal development, *Ag*Bni1p locates to tips, but not to septa. The presence of a diaphanous autoregulatory domain (DAD) indicates that the activation of *Ag*Bni1p depends on Rho-type GTPases. Deletion of this domain, which should render *Ag*Bni1p constitutively active, completely changes the branching pattern of young hyphae. New axes of polarity are no longer established subapically (lateral branching) but by symmetric divisions of hyphal tips (tip splitting). In wild-type hyphae, tip splitting is induced much later and only at much higher elongation speed. When GTP-locked Rho-type GTPases were tested, only the young hyphae with mutated *Ag*Cdc42p split at their tips, similar to the DAD deletion mutant. Two-hybrid experiments confirmed that *Ag*Bni1p interacts with GTP-bound *Ag*Cdc42p. These data suggest a pathway for transforming one axis into two new axes of polar growth, in which an increased activation of *Ag*Bni1p by a pulse of activated *Ag*Cdc42p stimulates additional actin cable formation and tip-directed vesicle transport, thus enlarging and ultimately splitting the polarity site.

INTRODUCTION

Elongated cells, such as neurites, pollen tubes, and root hair cells, are generated when polar growth is maintained for extended time periods. An extreme case of polar growth has evolved in filamentous fungi, which are able to extend the tips of their tubelike cells, called hyphae, for unlimited time, provided nutrients are available (Gow, 1995; Momany, 2002; Harris *et al.,* 2005). Hyphae not only very efficiently elongate but regularly establish new axes of polarity along their cortex, thus forming lateral branches, which themselves again generate lateral branches. This results in a fast spreading network of hyphae and the typical appearance of a fungal mycelium. In most filamentous fungi the initial hyphal tip elongation speed can increase by an order of magnitude or even more. Some filamentous fungi display hyphal tip splitting, the unique ability to simultaneously generate at tips of fast growing hyphae two sister hyphae.

The ascomycete *Ashbya gossypii* shows all the hallmarks of fungal filamentous growth, including tip splitting, although its recently completed genome sequence reveals an evolutionary relation with the *Saccharomyces cerevisiae* genome (Dietrich *et al.,* 2004). *A. gossypii* is amenable to functional genome analysis using gene targeting methods or autonomously replicating plasmids (Wright and Philippsen, 1991; Steiner and Philippsen, 1994; Steiner *et al.,* 1995; Wendland *et al.,* 2000), which have promoted functional analyses of polarity genes in this fungus. Polar growth in *A. gossypii* starts from an isotropically growing germ bubble. The first steps in polarity establishment involve the *A. gossypii* proteins *Ag*Cdc24p and *Ag*Cdc42p (Wendland and Philippsen, 2001). Once the first germ tube has emerged hyphal growth of *A. gossypii* proceeds with frequent lateral branching and a steadily increasing elongation speed from initially 5 μm/h up to a maximum of 170 μm/h (Knechtle *et al.,* 2003). For this process of hyphal maturation *Ag*Bem2p, *Ag*Rho3p, *Ag*Cla4p, *Ag*Spa2p, and *Ag*Rsr1p are important (Ayad-Durieux *et al.,* 2000; Wendland and Philippsen, 2000, 2001; Knechtle *et al.,* 2003; Bauer *et al.,* 2004). Although *Ag*Bem2p, *Ag*Rho3p and *Ag*Rsr1p are responsible for maintenance of polarity, both *Ag*Cla4p and *Ag*Spa2p are necessary to reach maximal growth speed.

An important late step in the development to a fast spreading *A. gossypii* mycelium is the splitting of hyphal tips which, under optimal growth conditions, begins 12–14 h after emergence of the first hypha (Ayad-Durieux *et al.,* 2000). A study with a GFP-labeled *Ag*Spa2p showed that during tip splitting the existing polarity control center divides into two new centers of polarity, yielding two hyphae that elongate, after a short lag phase, with a speed similar to that before tip splitting (Knechtle *et al.,* 2003). So far, the molecular basis for the initiation of hyphal tip splitting is unknown. We assumed that the apparent duplication of polar growth capacity depends on an approximately twofold increase in secretory vesicle transport at or shortly after

This article was published online ahead of print in *MBC in Press* (http://www.molbiolcell.org/cgi/doi/10.1091/mbc.E05–06–0479) on October 19, 2005.

[V] The online version of this article contains supplemental material at *MBC Online* (http://www.molbiolcell.org).

Address correspondence to: Peter Philippsen (peter.philippsen@unibas.ch).

tip splitting and that, before this increase, additional tip-located actin cables had to form. Given the conserved role of formins in nucleating actin cables (Pruyne *et al.*, 2002; Sagot *et al.*, 2002b), we therefore hypothesized that a formin homolog could play an important role for the regulation of tip splitting.

Formins are common to all eukaryotic species and participate in many different processes, from cell polarization to embryonic development (see Wallar and Alberts (2003) and Evangelista *et al.* (2003) for reviews). Except for some cases in higher cells where a formin is involved in signaling (Habas *et al.*, 2001), most formins participate in the organization of the actin cytoskeleton. Recently, the ability of formins to nucleate actin at the barbed end of actin filaments was described for different organisms (Pruyne *et al.*, 2002; Sagot *et al.*, 2002b; Kobielak *et al.*, 2003; Kovar *et al.*, 2003; Li and Higgs, 2003). Actin nucleation is mediated by the conserved formin homology domain FH2. As found by analyzing the crystal structures of the mouse formin, mDIA, and the yeast formin, *Sc*Bni1p, the core of the FH2 domain seems to have actin binding capacity, whereas adjacent amino acids are necessary for oligomerization and gain of polymerization capability (Shimada *et al.*, 2004; Xu *et al.*, 2004). A subclass of formins, the so-called diaphanous related formins (DRFs), are defined by two properties: First, they are activated when a GTP-bound Rho-type protein interacts with their amino terminus (Kohno *et al.*, 1996; Evangelista *et al.*, 1997; Imamura *et al.*, 1997; Watanabe *et al.*, 1997; Habas *et al.*, 2001). Second, they posses a carboxy-terminal diaphanous autoregulatory domain (DAD), which binds to the amino-terminus in the inactive state of these formins (Watanabe *et al.*, 1999; Alberts 2001).

In fungi, six formins have been studied to date. In *S. cerevisiae*, the two formins Bni1p and Bnr1p are required for cell polarity and cytokinesis with some overlapping and some different functions (Zahner *et al.*, 1996; Evangelista *et al.*, 1997; Imamura *et al.*, 1997; Kamei *et al.*, 1998; Pruyne *et al.*, 2004). In *Schizosaccharomyces pombe*, three formins exist which are also involved in cell polarity and cytokinesis. The protein *Sp*Cdc12p is involved in cytokinesis (Chang *et al.*, 1997; Kovar *et al.*, 2003), *Sp*Fus1p in cell fusion (Petersen *et al.*, 1998b) and *Sp*For3p in cell polarity control via regulation of the actin and microtubule network (Feierbach and Chang, 2001; Nakano *et al.*, 2002). The only formin family member described so far in a filamentous fungus is the SepA protein of *Aspergillus nidulans*. SepA is an essential protein that locates to growing hyphal tips and to sites of cytokinesis (septation). Some SepA mutants still grow in a filamentous manner although they can no longer form septa (Harris *et al.*, 1997; Sharpless and Harris, 2002).

In this article we first document by videomicroscopy the distinct differences in polar growth of budding yeast and *A. gossypii* and compare the domain compositions of the three *A. gossypii* formins with the two *S. cerevisiae* formins. Then we show that mutants lacking the *Ag*Bnr1p or *Ag*Bnr2p formin develop like wild type and that mutants lacking both formins are unable to grow. We next provide evidence that the *Ag*Bni1p formin is essential for hyphal emergence and elongation, that it localizes at hyphal tips, and that it is essential for organization of actin cables and thus tip-directed transport of secretory vesicles. In addition, we demonstrate that constitutively active *Ag*Bni1p leads to premature tip splitting and that this is most likely triggered by *Ag*Cdc42p-GTP.

MATERIALS AND METHODS

A. gossypii Strains and Growth Conditions

All strains were constructed by PCR-based gene targeting according to the method described by Wendland *et al.* (2000). Either pGEN3 (Wendland *et al.*, 2000), pGUG (Knechtle *et al.*, 2003), or pUC19NATPS (D. Hoepfner, personal communication) were used as templates to generate gene-targeting cassettes encoding geneticin-resistance, GFP plus geneticin-resistance, and ClonNAT-resistance, respectively. Strains and names of the oligonucleotides and templates used are given in Table 1. The strains were verified by PCR using a PTC 100 thermocycler (MJ Research, Waltham, MA). All oligonucleotides are listed in Table 2. Strains were grown at 30°C in AFM (Ashbya Full Medium) with or without geneticin or ClonNAT or at room temperature on synthetic medium for live cell imaging (Knechtle *et al.*, 2003).

DNA Manipulations and Sequencing

All DNA manipulations were carried out according to Sambrook *et al.* (2001) with DH5αF′ as host (Hanahan, 1983). Sequencing was done using an ABI prism 377 DNA sequencer (PE Applied Biosystems, Foster City, CA) according to the manufacturer's instructions. Plasmids were isolated from yeast using the High Pure Plasmid Purification Kit (Roche Diagnostics, Mannheim, Germany) according to the instruction manual for plasmid preparation from *Escherichia coli* but with the following modifications: 5 ml of a yeast culture was collected by centrifugation and the supernatant was discarded. The cells were resuspended in solution 1 and 0.2 g of 0.5-mm glass beads were added. Cells were lysed by vortexing for 8 min at 4°C. From here on the instructions of the manufacturer were followed, only the elution volume was decreased to 20 μl. Ten microliters of the elute were transformed into *E. coli* for plasmid amplification.

Plasmids and Constructs

All plasmids are listed in Table 3. All constructs carrying genes for Rho-type GTPases were constructed using the same scheme. Each gene was amplified from *A. gossypii* genomic DNA using the corresponding primers from Table 2 for PCR. All primers were designed to amplify the open reading frame (ORF) from the start codon to the end, excluding the nucleotides coding for the CAAX motif at the carboxy terminus, thus avoiding lipid modification (primers AgRHOx-ATG, AgRHOx-TAG and AgCDC42-ATG, and AgCDC42-TAG). To facilitate cloning, *Eco*RI and *Bam*HI restriction sites were added to the oligonucleotides. The fragments were purified, cut, and ligated into pUC19 (Vieira and Messing, 1991). Activated alleles of all Rho-GTPases were constructed using the method by Boles and Miosga (1995) with primers named AgRHOx and AgCDC42 plus the corresponding nucleotide exchange. DNA of wild-type and mutant alleles was cloned into pGBT9 (Bartel *et al.*, 1993) using again *Eco*RI and *Bam*HI. The resulting plasmids were verified by sequencing. *AgBNI1* was amplified by PCR from genomic *A. gossypii* DNA using primers AgBNI1-ATG2Hy and AgBNI1-TAG2Hy, which add on both sides of the amplified *AgBNI1* 45 base pairs homologous to pGBT9 for in vivo cloning. This PCR product was cotransformed with *Eco*RI- and *Bam*HI-digested pGBT9 into the yeast strain DHD5. Transformants were restreaked on selective medium, and recombinant plasmids were isolated from the yeast cells and amplified in *E. coli*. This resulted in pGBT9AgBNI1. From this, a 2.5-kb *Eco*RI-*Bgl*II fragment was cut out and ligated into the *Eco*RI-*Bam*HI sites of pGAD424 (Bartel *et al.*, 1993). Again the plasmid was first verified by digestion and sequencing.

The plasmid carrying *AgBNI1* (pAMK1) was constructed by ligation of an *Hin*dIII/*Sma*I fragment generated by PCR using primers AgBNI1-P_HindIII and AgBNI1-T_SmaI from genomic *A. gossypii* DNA. *GFP* was fused to the gene by in vivo recombination in *S. cerevisiae* strain DHD5 with a PCR fragment derived from pGUG with primers AgBNI1-GS1 and AgBNI1-GS2. The fusion was verified by sequencing.

An amino-terminal fusion of *Ag*SEC4 to GFP was constructed by a sequential series of PCR amplification and cloning steps. First, the *AgSEC4* promoter was amplified by PCR out of the genome using primers Sec4P-Hind and Sec4P-Bam and cloned into YCPlac111 using *Hin*dIII and *Bam*HI. The resulting plasmid was cut with *Bam*HI and *Eco*RI to allow fusion of the *SEC4* promoter to GFP that was amplified by PCR from pGUG with primers GFP-Eco and GFP-Bam. In a final step the *AgSEC4* ORF and terminator were fused to the GFP-ORF using the enzymes *Eco*RI and *Spe*I and a fragment generated from genomic DNA using primers Sec4-Eco and Sec4-Spe.

The $S_{1642}G$ allele of *AgBNI1* was generated using the method described by Storici *et al.* (2001) using primers Agbni1–12C1, Agbni1–12C2, Agbni1–12IRO1, and Agbni1–12IRO2 and *S. cerevisiae* strain CEN/PK2 (http://www.rz.uni-frankfurt.de/FB/fb16/mikro/euroscarf/) transformed with pAMK1. The resulting plasmid pAMK1ts12 was isolated from yeast digested with *Asc*I and dephosphorylated. The linearized vector was cotransformed together with a PCR product generated with primers AgBNRCFP-N and AgBNI1-GS2 from pGUG for in vivo recombination to integrate the *URA3* terminator from *S. cerevisiae* behind the mutagenized *Agbni1* gene. The resulting vector was isolated and verified by sequencing of the altered regions. An *Xba*I fragment containing the altered region of *AgBNI1*, the *URA3* terminator and the G418 resistance cassette was cloned into pUC19. The resulting plas-

Table 1. *Ashbya gossypii* strains and details of construction

Strain	Genotype	Oligo-nucleotides	Template	Reference
ATCC10895	Wild type	—	—	Ashby and Nowell (1926)
Δ*l*Δ*t*	*Agleu2*Δ *Agthr4*Δ	—	—	Altmann-Johl and Philippsen (1996)
*Agbni1*Δ*2*	*Agbni1*Δ*::GEN3, Agleu2*Δ *Agthr4*Δ	AgBNI1-S1 AgBNI1-S2	pGEN3	This study
*AgBNI1*Δ*D*	*AgBNI1*Δ*5308–5757::GEN3*	AgBNI1dD-S1 AgBNI1dD-S2	pGEN3	This study
AgBNI1-GFP	*AgBNI1-GFP-GEN3, Agleu2*Δ *Agthr4*Δ	AgBNI1-GS1 AgBNI1-GS2	pGUG	This study
AgSPA2-GFP	*AgSPA2-GFP-GEN3, Agleu2*Δ *Agthr4*Δ	—	—	Knechtle *et al.* (2003)
*Agbni1*Δ *AgSPA2-GFP*	*Agbni1*Δ*::NAT1, AgSPA2-GFP-GEN3, Agleu2*Δ *Agthr4*Δ	AgBNI1-NS1 AgBNI1-NS2	pUC19NATPS	This study
Agbni1S$_{1642}$*G*	*Agbni1T4924G, C4925G-GEN3, Agleu2*Δ *Agthr4*Δ	See text for details		This study
*Agbni1*Δ$_{1530}$*G, K*$_{1620R}$	*Agbni1A4589G, A4859G-GEN3, Agleu2*Δ *Agthr4*Δ	See text for details		This study
*Agbnr1*Δ*-GEN3*	*Agbnr1*Δ*::GEN3, Agleu2*Δ *Agthr4*Δ	AgBNR1-S1 AgBNR1-S2	pGEN3	This study
*Agbnr1*Δ*-NAT1*	*Agbnr1*Δ*::NAT1, Agleu2*Δ *Agthr4*Δ	AgBNR1-NS1 AgBNR1-NS2	pUC19NATPS	This study
*Agbnr2*Δ	*Agbnr2*Δ*::GEN3, Agleu2*Δ *Agthr4*Δ	AgBNR2-S1 AgBNR2-S2	pGEN3	This study
*Agbnr1,2*Δ*GL*	*Agbnr1*Δ*::GEN3, Agbnr2*Δ*::LEU2, Agleu2*Δ *Agthr4*Δ	AgBNR2-S1 AgBNR2-S2	pScLEU2	This study
*Agbnr1,2*Δ*GN*	*Agbnr1*Δ*::GEN3, Agbnr2*Δ*::NAT1*	AgBNR1-NS1 AgBNR1-NS2	pUC19NATPS	This study
*Agcdc42**	*Agcdc42G183C-GEN3, Agleu2*Δ *Agthr4*Δ	See text for details		This study
*AgBNI1*Δ*D-GFP*	*AgBNI1*Δ*D-GFP-GEN3, Agleu2*Δ *Agthr4*Δ	AgBNI1dD-F1 AgBNI1dD-F2	pAGT141	This study

mid pHPS232 was cut again with *Xba*I and transformed into the *A. gossypii* Δ*l*Δ*t* strain. Construction of the $D_{1530}R,K_{1620}R$ allele of *AgBNI1* was identical to the $S_{1642}G$ allele except for a sequential round of mutagenesis first using primers Agbni1–11.1C1, Agbni1–11.1C2, Agbni1–11.1IRO1 and Agbni1–11.1IRO2 and Agbni1–11.2C1, Agbni1–11.2C2, Agbni1–11.2IRO1 and Agbni1–11.2IRO2 respectively.

For construction of the $Q_{61}H$ allele of *AgCDC42* the gene was first PCR-amplified from genomic *A. gossypii* DNA using primers cdc42genom_sense and cdc42genom_antisense. The resulting product was cut with *Eco*RV, and *Pst*I was ligated into pRS415 cut with *Sma*I and *Pst*I. In the resulting plasmid pCDC42 the codon CAG starting at position 181 was deleted by integration of the pCORE-cassette (Storici *et al.*, 2001) using primers AgCdc42_Q-H-sense and AgCdc42_Q-H-antisense. This resulted in plasmid pCDC42cas. By homologous recombination in yeast with annealed primers and counterselection, the pCORE-cassette was replaced by the mutagenized codon, resulting in pcdc42cons. The Gen3 resistance cassette was amplified from pGEN3 using primers INT_CDC42*_S1 and INT_CDC42*_S2. The resulting PCR product was integrated behind the *cdc42* gene in the vector pcdc42cons yielding pcdc42kanr. The 3.1-kb *Bam*HI/*Pst*I fragment from pcdc42kanr carrying the mutagenized *cdc42* and the resistance cassette was cloned into pUC19, resulting in pUC19cdc42cons. DNA of this vector was again cut with *Bam*HI/*Pst*I and transformed into *A. gossypii*. Transformants resistant against G418 were sporulated and spores were separated to get homokaryotic Geneticin (G418) resistant mycelium. From this mycelium the *CDC42* gene was amplified by PCR using primers AgCDC42-ATG and AgCDC42-TAG. The resulting PCR product was sequenced to verify the presence of the desired mutation.

Image Acquisition and Processing

The microscopy setup used was the same as described in Knechtle *et al.* (2003). Actin staining was done according to Knechtle *et al.* (2003). The illumination time and light intensity for standard phase contrast, DIC, or fluorescence acquisitions was chosen to reach minimally 25% of the maximal intensity. For multiple exposures of the same sample bleaching of the sample had to be taken into account. The *Z*-distance between two planes in stack acquisitions was set between 0.1 and 0.5 μm. Phase contrast, DIC, and single-plane fluorescence images were processed using the "scale image" and "unsharp mask" feature in MetaMorph (Universal Imaging, West Chester, PA). Stacks were deblurred with MetaMorph's "remove haze," flattened by maximum projection with "stack arithmetics" and scaled as mentioned above. Fluorescence and phase-contrast images were colored and overlaid using MetaMorph's "overlay images" tool. For time-lapse acquisition spores were cultured on a slide with a cavity (time-lapse slide) that was filled with solid medium (Ashbya Full Medium). Spores were incubated in a humid chamber without coverslip until they reached the required developmental stage. Then a coverslip was applied. For Supplementary Movies S1 to S7 cells or spores were cultured on Petri plates with AFM agar, cultivated in a humid chamber, and placed for image acquisitions under a light microscope. The acquisition frequency varied between 1 and 0.2 min^{-1}. The time-lapse picture series were exported from MetaMorph as 8-bit TIFF files converted to a QuickTime (Apple Computer, Redmond, WA) or AVI movie with Adobe Premiere 4.2 (Adobe Systems, San Jose, CA).

Two-hybrid Experiments

For two-hybrid experiments prey and bait plasmids were cotransformed into *S. cerevisiae* strain PJ69-4a (James *et al.*, 1996) and selected on minimal medium lacking leucine and tryptophan but containing a fourfold concentration (80 mg/l) of adenine. Transformants were grown in the same liquid medium to an OD_{600} of ~1. Of these, 5 μl were spotted on plates lacking in addition to leucine and tryptophan either histidine or adenine to monitor activity of the reporter genes.

RESULTS

Filamentous Growth of A. gossypii Compared with Unicellular Growth of S. cerevisiae

A. gossypii grows like a filamentous ascomycete (Momany, 2002) and the main differences to yeastlike growth are shown in Figure 1A. Sustained polar growth results in continuous tip extensions of hyphae and lateral branches. Thus, growth of the hyphal surface is restricted to the tips, and isotropic growth phases are absent. In a yeast cell, a short phase of polar growth of the emerging bud is followed by isotropic growth of the bud. Then a septum grows at the junction between the mother cell and the bud and both cells

Table 2. Oligonucleotides used in this study

Name	Sequence[a]	Purpose
AgBNI1-S1	CTCGACCGTAGAGTCGATAGCGAGTTCTGCTCTAGCAAAATCCCCGCTAGGGATAACAGGGTAAT	Deletion
AgBNI1-S2	GAGTTGTTCGATGGAGATCTTGACCACCTGAAGTACAGGTTCAAGAGGCATGCAAGCTTAGATCT	Deletion
AgBNI1-G1	CCCGACCACCGTCTTGGACC	Verification
AgBNI1-G2	GGGCATTTGCGCCGGGAGAG	Verification
AgBNI1-GS1	CGGTGAACACCCGGAGTCTCGCAAGTCAATGCTCGATGAGCACAAGGGTGCAGGCGCTGGAGCTG	GFP-tagging
AgBNI1-GS2	GCGGCGCGGCGGCGACATCGCGCTGGTCTATCAGTTTCTTGGTGCGGCAGGGACCTGGCACGGAGC	GFP-tagging
AgBNI1-I1	CAGATCGGGCCTGTGTTACC	Verification
AgBNR2-S1	GATAAAGAACATCGCTAGTTAATTTTGCTAATAAAGAAGAGACCTTTAAgctagggataacagggtaat	Deletion
AgBNR2-S2	GGCCGATAAGTGTGGAATCGGATAAGTGTTGAATAGGGTAACGGAAGAGGCATGCAAGCTTAGATCT	Deletion
AgBNR2-I1	CGCACTCCGCACCGTGGACC	Verification
BNR2G1neu	CTGTCGAGGAATTAACTTTAAG	Verification
BNR2G2neu	GCCAGCGCATTTTGCACCGG	Verification
AgBNR1-S2	GCCCGAGCGCCGAAGGCGAAGGGATGCGAAAAGTATATAGATGCAAGTTGaggcatgcaagcttagatct	Deletion
AgBNR1-S1	GCGGGAGCAGTAGATTTGTGCCTGGGCCCCTCCCCCGCGAGTGCGCAATGgctagggataacagggtaat	Deletion
AgBNR1-I1	CAGGCTGTGCGGCGCGCGCG	Verification
BNR1G1neu	GAGCAGCTGGTCGCTGGGCATCTCGTGG	Verification
BNR1G4neu	GCCTCGAATCACCAATCCCC	Verification
AgBNR1-NS1	GGCGGGAGCAGTAGATTTGTGCCTGGGCCCCTCCCCCGCGAGTGCGCAccagtgaattcgagctcgg	Deletion
AgBNR1-NS2	GCCCGAGCGCCGAAGGCGAAGGGATGCGAAAAGTATATAGATGCAAGTTG tacgccaagcttgcatgcct	Deletion
V2PDC1P	GAACAAACCCAAATCTGATTGCAAGGAGAGTGAAAGAGCCTT	Verification
V3PDC1T	GACCAGACAAGAAGTTGCCGACAGTCTGTTGAATTGGCCTG	Verification
AgBNI1dD-S1	TCTGGAGTACAAGCGCGCGCAGGAGTTTAACCGCAAGATCTAAGCTAGGGATAACAGGGTAAT	Deletion
AgBNI1dD-S2	GCTGGTCTATCAGTTTCTTGGTGCGGCGCTGGCGAACCTTAGGCATGCAAGCTTAGATCT	Deletion
Agbni1-12 C1	CTTGAACTACGTGGAACGCATCGTCAGCCAGAATTATCCAgagctcgttttcgacactgg	pCORE integration
Agbni1-12 C2	CCTGAAGTACAGGTTCAAGTTCCTGGAGAAAGCTGTTGAAtccttaccattaagttgatc	pCORE integration
Agbni1-12 IRO1	ATGACTTTCTTGAACTACGTGGAACGCATCGTCAGCCAGAATTATCCAGGGTTCAACAGC	Mutagenesis
Agbni1-12 IRO2	TTGACCACCTGAAGTACAGGTTCAAGTTCCTGGAGAAAGCTGTTGAACCCTGGATAATTC	Mutagenesis
Agbni1-11.1 C1	TAAGTCTCCGGAAAAGGATCCAAGCGAGCTTCAGCGATCAgagctcgttttcgacactgg	pCORE integration
Agbni1-11.1 C2	AGTAGCTTTGAAGATTAACAATGAGGTTCAAGAATAACTGtccttaccattaagttgatc	pCORE integration
Agbni1-11.1 IRO1	GAGGATGCTAAGTCTCCGGAAAAGGATCCAAGCGAGCTTCAGCGATCAGGCCAGTTATTC	Mutagenesis
Agbni1-11.1 IRO2	TGAGCTCCAGTAGCTTTGAAGATTAACAATGAGGTTCAAGAATAACTGGCCTGATCGCTG	Mutagenesis
Agbni1-11.2 C1	GGGGTTCAAGTTGAGTACATTGCAGAGGCTCACCTTCATTgagctcgttttcgacactgg	pCORE integration
Agbni1-11.2 C2	GTTCCACGTAGTTCAAGAAAGTCATGCTGTTTTTCTCGTCtccttaccattaagttgatc	pCORE integration
Agbni1-11.2 IRO1	GCACAGGGGTTCAAGTTGAGTACATTGCAGAGGCTCACCTTCATTAGAGACGAGAAAAAC	Mutagenesis
Agbni1-11.2 IRO2	CTGACGATGCGTTCCACGTAGTTCAAGAAAGTCATGCTGTTTTTCTCGTCTCTAATGAAG	Mutagenesis
AgBNRCFP-N	CCAGCATGTCAACCACTATATTGATCACCGATATATGGACTTCCACACCAACTAGacgcggccgccagctgaagc	In vivo recombination
AgBNI1-GS2	GCGGCGCGGCGGCGACATCGCGCTGGTCTATCAGTTTCTTGGTGCGGCagggacctggcacggagc	In vivo recombination
AgRHO1a-ATG	GAGATCGAATTCATGGCGTACCAGACAGGCGGCA	Cloning
AgRHO1aG204C	GCCGGTCGTAGTCCTCcTGGCCCGCTGTATCCC	Mutagenesis
AgRHO1a-TAG	CGACGGATCCCTTTCTTCTTCTTCTTGTCACCGT	Cloning
AgRHO1b-ATG	GATCGAATTCATGTCTCAGCAAATGCATAAC	Cloning
AgRHO1bG207C	GCCTGTCGTAATCCTCGTGCCCAGCCGTATCC	Mutagenesis
AgRHO1b-TAG	CGACGGATCCCCTTTTTCTTCTTCTTCTTGTCAGAC	Cloning
AgRHO2-ATG	GAGATCGAATTCATGACGGTCAACGTTGTGAGAC	Cloning
AgRHO2G195C	CAGACGCTCGTATTCTTCGTGACCAGCAGTATCC	Mutagenesis
AgRHO2-TAG	CGACGGATCCCGCCTTGACCCGGCTCCTTGTTCAC	Cloning
AgRHO3-ATG	GATCGAATTCATGCCTCTGTGTGGGTCGAG	Cloning
AgRHO3G219C	GCAACCGGTCAAACTCCTCGTGCCCAGCAGTGTCCCACAGG	Mutagenesis
AgRHO3-TAG	GACGGATCCCACTGCTGCTTTCGGCCTCGG	Cloning
AgRHO4-ATG	GAGATCGAATTCATGAGCGCAGGGCCGTTGCAAG	Cloning
AgRHO4G333C	CAGCCGGCTGTACTCCTCGTGCCCAGCAGTGTCCCACAGC	Mutagenesis
AgRHO4-TAG	GACGGATCCCGCGGTGCTTGCGCACCCGCTTG	Cloning
AgRHO5-ATG	GATCGAATTCATGTGTTTTTCGCAGAGCGGCAG	Cloning
AgRHO5G255Cneu	CCGCAACCGGTCGTACTCCTCGTGCCCCGCCGTGTCCCACAG	Mutagenesis
AgRHO5-TAG	CGACGGATCCCTCTAGATCTCTTCCTCCTCTTTTTC	Cloning
AgCDC42-ATG	GATCGAATTCATGCAGACATTGAAGTGCGTGGTC	Cloning
AgCDC42-TAG	CGACGGATCCCCTTCTTGCTCTTCTTGATG	Cloning
AgCDC42G183C	GCCGCAACCTGTCGTAGTCCTCGTGGCCGGCAGTGTCGAACAAGC	Mutagenesis
u-40	GTTTTCCCAGTCACGAC	Mutagenesis
Reverse	CAGGAAACAGCTATGACCATG	Mutagenesis
Sec4-ECO	cgcgaattcTCGGGGCTAAGAACGGTGTC	Cloning
Sec4P-BAM	ccggatccCATTATAGCTACTGTACTGC	Cloning
Sec4P-HIND	ggaagcttCTACTACGCCTGAGCGCCGC	Cloning
Sec4-SPE	caccaactagtTGGGCGGCCTGTGCTGCAAAG	Cloning
GFP-BAM	cgggatccAGTAAAGGAGAAGAACTTTTCAC	Cloning
GFP-ECO	cgcgaattcTTTGTATAGTTCATCCATGCC	Cloning
AgBNI1-ATG2Hy	GTAGTAACAAAGGTCAAAGACAGTTGACTGTATCGCCGGAATTCatgaagaagtccacgcactcgaac	In vivo recombination
AgBNI1-TAG2Hy	CATAAGAAATTCGCCCCGGAATTAGCTTGGCTGCAGGTCGACGGATCCttacttgtgctcatcgagcattg	In vivo recombination
AgBNI1-P_HindIII	gcgcgcaagcttCTGGGACGACGACAAGCCTAC	Cloning
AgBNI1-T_SmaI	gcgccccgggCCTGCACCGAAATCCGCCGA	Cloning
AgBNI1-GS1	CGGTGAACACCCGGAGTCTCGCAAGTCAATGCTCGATGAGCACAAGggtgcaggcgctggagctg	In vivo recombination
AgBNI1-GS2	GCGGCGCGGCGGCGACATCGCGCTGGTCTATCAGTTTCTTGGTGCGGCagggacctggcacggagc	In vivo recombination
AgBNI1-NS1	GGTATAGTGGCAGCGTCGGCGGCTGGGCACATATGCAAGGccagtgaattcgagctcgg	Deletion
AgBNI1-NS2	GCTGGTCTATCAGTTTCTTGGTGCGGCGCTGGCGAACCTTtacgccaagcttgcatgcct	Deletion
Gal4-ad	GTTTGGAATCACTACAGGG	sequencing
Gal4-bd	GATTGGCTTCAGTGGAG	sequencing
Gad-term	GAGATGGTGCACGATGCACAGTTG	sequencing
Gbt-term	CGTTTTAAAACCTAAGAGTCAC	sequencing
AgCdc42_c1	GGACGAGCCGTACACGTTGGGCTTGTTCGACACTGCCGGGgagctcgttttcgacactgg	pCORE integration
AgCdc42_c2	GTCGACGGGTACGACAACGGCCGCAACCTGTCGTAGTCCTCtccttaccattaagttgatc	pCORE integration
AgCdc42_Q-H-antisense	cacgtccgtcgacgggtacgacaacggccgcaacctgtcgtagtcctcgtgcccggcagtg	Mutagenesis
AgCdc42_Q-H-sense	gtgatgatcggggacgagccgtacacgttgggcttgttcgacactgccgggcacgaggac	Mutagenesis
INT_CDC42*_S1	ACCAAGTGCCAGCTCTAGCGCCAGGACCCGCGCGAGACCTGCTAGGGATAACAGGGTAAT	Mutagenesis
INT_CDC42*_S2	TTGCCGATTTTTGGGCAGGGCGCAAAGACAGATATAGCAGAGGCATGCAAGCTTAGATCT	Mutagenesis
AgCDC42-ATG	GATCGAATTCATGCAGACATTGAAGTGCGTGGTC	Verification
AgCDC42-TAG	CGACGGATCCCCTTCTTGCTCTTCTTGATG	Verification
AgBNI1dD-F1	GACTTTATTCTGGAGTACAAGCGCGCGCAGGAGTTTAACCGCAAGATCaaaacgacggccagtgaattcg	In vivo recombination
AgBNI1dD-F2	GACATCGCGCTGGTCTATCAGTTTCTTGGTGCGGCGCTGGCGAACCTTaccatgattacgccaagcttgc	In vivo recombination

[a] Underscore indicates nucleotides exchanged for mutagenesis.

Table 3. Plasmids

Name	Insert	Reference
pUC19	—	Vieira and Messing (1991)
pGBT9	—	Bartel *et al.* (1993)
pGAD424	—	Bartel *et al.* (1993)
YCPlac111	—	Gietz and Sugino (1988)
pRS415	—	Sikorski and Hieter (1989)
pUC19NATPS	—	D. Hoepfner, personal communication
pAGT141	pUC19 carrying the *Pst*I fragment from pGEN and the *Sac*I fragment from pGUG	A. Kaufmann, personal communication
pCORE	—	Storici *et al.* (2001)
pUC19AgRHO1a	*A. gossypii RHO1a* from nucleotide 1–615	This study
pUC19AgRHO1b	*A. gossypii RHO1b* from nucleotide 1–609	This study
pUC19AgRHO2	*A. gossypii RHO2* from nucleotide 1–546	This study
pUC19AgRHO3	*A. gossypii RHO3* from nucleotide 1–660	This study
pUC19AgRHO4	*A. gossypii RHO4* from nucleotide 1–765	This study
pUC19AgRHO5	*A. gossypii RHO5* from nucleotide 1–870	This study
pUC19AgCDC42	*A. gossypii CDC42* from nucleotide 1–561	This study
pGBTAgRHO1a	*A. gossypii RHO1a* from nucleotide 1–615	This study
pGBTAgRHO1b	*A. gossypii RHO1b* from nucleotide 1–609	This study
pGBTAgRHO2	*A. gossypii RHO2* from nucleotide 1–546	This study
pGBTAgRHO3	*A. gossypii RHO3* from nucleotide 1–660	This study
pGBTAgRHO4	*A. gossypii RHO4* from nucleotide 1–765	This study
pGBTAgRHO5	*A. gossypii RHO5* from nucleotide 1–870	This study
pGBTAgCDC42	*A. gossypii CDC42* from nucleotide 1–561	This study
pGBTAgRHO1a*	*A. gossypii RHO1a* G204C from nucleotide 1–615	This study
pGBTAgRHO1b*	*A. gossypii RHO1b* G207C from nucleotide 1–609	This study
pGBTAgRHO2*	*A. gossypii RHO2* G195C from nucleotide 1–546	This study
pGBTAgRHO3*	*A. gossypii RHO3* G219C from nucleotide 1–660	This study
pGBTAgRHO4*	*A. gossypii RHO4* G333C from nucleotide 1–765	This study
pGBTAgRHO5*	*A. gossypii RHO5* G255C from nucleotide 1–870	This study
pGBTAgCDC42*	*A. gossypii CDC42* from nucleotide 1–561	This study
pGBTAgBNI1-N	*A. gossypii BNI1* from nucleotide 1–3152	This study
pGADAgBNI1-N	*A. gossypii BNI1* from nucleotide 1–3152	This study
YCp111GFPSEC4	N-terminal Fusion of *GFP* to *A. gossypii SEC4*	This study
pAMK1	*A. gossypii BNI1* from nucleotide −682 to +523	This study
pCDC42	*AgCDC42* including promoter and terminator	This study
pCDC42cas	*Agcdc42* with codon CAG starting at position 181 replaced by pCORE	This study
pcdc42cons	pCDC42 with codon CAG starting at position 181 altered to CAC	This study
pcdc42kanr	pcdc42cons with integrated GEN3 cassette behind ORF	This study
pUC19cdc42cons	3.1 kb *Bam*HI/*Pst*I fragment from pcdc42kanr with pUC19 backbone	This study
pSEC4NAT	*Pst*I fragment from pUC19NATPS carrying ClonNAT cassette ligated into *Pst*I site of YCP111GFPSEC4. Orientation reverse	This study

separate. Septation in *A. gossypii* like in other filamentous ascomycetes occurs in the growing hyphae and at the base of branches but separation of hyphal segments does not occur. Lateral branching leads to the successive establishment of several novel axes of polarity at the cortex of growing hyphae, in *A. gossypii* usually in an about right angle from the growth axis of the mother hyphae. In budding yeast, only one novel axis of polarity (site of bud emergence) is established in each cell cycle. Finally, the process of dividing the polarity-axis at the tip of mature hyphae (tip splitting) is restricted to a subset of filamentous ascomycetes including *A. gossypii*. Budding yeasts do not simultaneously generate two buds (two axes of polarity).

To visualize the differences in growth dynamics of *S. cerevisiae* and *A. gossypii*, we simultaneously monitored, by time-lapse video microscopy, growth of both fungi on AFM agar (Movie S1). Four representative frames were selected to show the development of *S. cerevisiae* mini colonies and of an *A. gossypii* mycelium (Figure 1B). Arrows in the zero minute frame point to eight *S. cerevisiae* cells, which have just finished the first division, and to one germinated *A. gossypii* spore from which the first hypha has emerged. After 225 min, the *S. cerevisiae* cells have undergone only one or two additional divisions whereas the *A. gossypii* young mycelium has already developed nine growing hyphae. At 450 min, the *S. cerevisiae* cells have divided one or two more times, and the *A. gossypii* young mycelium is now spreading from 23 hyphal tips. After nearly 700 min, the fastest hyphae (marked with open arrow heads) have started to symmetrically divide at their tips, the common mode of branching when hyphal tip speeds have reached 80 μm/h or more. This switch in branching pattern allows optimal radial spreading of an *A. gossypii* mycelium. The apparently symmetric division of the polar growth machinery leads only to a transient decrease of tip elongation speeds by ~20% as determined for seven tip splitting events in Supplementary Movie S1 (unpublished data). Using similar conditions, Knechtle *et al.* (2003) presented the dynamics of successive tip splitting events every 90–120 min at the edge of a radially expanding mature *A. gossypii* mycelium.

How can these differences in morphogenesis be explained when both organisms carry a very similar set of proteins? One possible answer is that homologous polar growth components may exert not only common functions but also

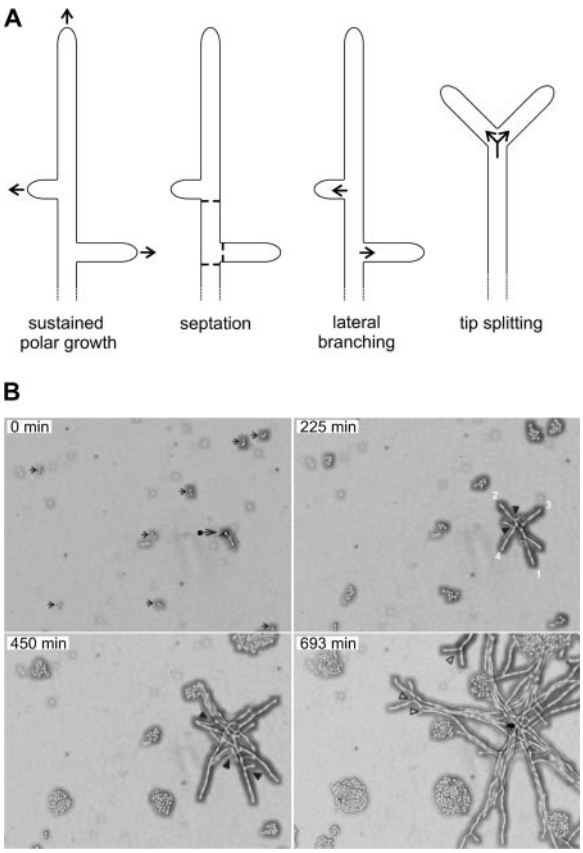

Figure 1. Differences in polar growth between *A. gossypii* and *S. cerevisiae*. (A) Schematic presentation of landmarks of hyphal growth of *A. gossypii*: Sustained polar growth (accelerating growth along a selected polarity-axis by continuous surface expansion at the tip), septation (growth of chitin-containing open rings at 30–50-μm distances at the cortex of hyphae and at the base of branches), lateral branching (successive selection of new axes of polarity at the cortex of elongating hyphae), and tip splitting (simultaneous generation of two new axes of polarity at fast growing tips). (B) Simultaneous monitoring of *A. gossypii* and *S. cerevisiae* growth. *A. gossypii* spores and *S. cerevisiae* cells were mixed and plated on AFM agar. After 4 h the agar surface was screened under the microscope. An area was selected for the start of the video (top left panel) showing eight *S. cerevisiae* cells after their first division (small arrows) and one germinated *A. gossypii* spore with the first emerged hypha (●). Growth in this area was monitored for 15 h at 25°C with pictures taken every 3 min (Supplementary Movie S1). After 225 min, the *S. cerevisiae* mini-colonies consist of four to eight cells, whereas the *A. gossypii* young mycelium has already developed nine extending hyphae. Two emerged, in addition to the first hypha, from the germinated spore and six originated from the initiation of lateral branches at the cortex of growing hyphae (two branches are marked by black arrow heads). At 450 min, the *S. cerevisiae* minicolonies have 12–32 cells and the *A. gossypii* young mycelium now consists of 23 hyphae due to 14 newly emerged lateral branches (black arrow heads). At 690 min the fastest hyphae, marked with open arrowheads, have started to symmetrically divide at their tips. Ten additional tip-splitting events were observed until the end of the movie at 897 min. The elongation speeds of the main hyphae during early mycelial development are ~10 μm/h (0 min), 15 μm/h (225 min), and 25 μm/h (450 min), as determined from the elongation of the four hyphae marked in frame 225 min, which were measured every four frames until 501 min. For technical reasons 21 frames were not recorded during the early period between the frames representing 132 and 135 min. To determine hyphal speeds at tip splitting hyphal elongations were measured during 18 frames before and after tip splitting. This mode of branching starts at elongation speeds of 80 μm/h. The highest speed observed at the end of Supplementary Movie S1 before a tip splitting was 140 μm/h. Four cases of consecutive tip splitting events were observed with an average distance of 190 μm and an average time interval of 140 min. Scale bar, 20 μm.

distinct functions in the cellular networks of both organisms. One example for shared and specific functions is *Ag*Spa2p, the first component identified in *A. gossypii* to permanently localize at hyphal tips, where it plays an essential role to reach maximal tip speeds (Knechtle *et al.*, 2003). These are properties specific for *A. gossypii*, because *Sc*Spa2p, the homolog in *S. cerevisiae*, does not localize permanently but only transiently to the bud tip and because a cellular process, controlling maximal bud tip speed, is unknown in morphogenesis of *S. cerevisiae* (Sheu *et al.*, 1998). Because *Sc*Spa2p is part of the polarisome, we speculated that *A. gossypii* homologues of other components of the polarisome complex, in particular the formin homology protein *Sc*Bni1p (Evangelista *et al.*, 2002; Sagot *et al.*, 2002a), could fulfill, in addition to common functions, also specific functions in sustained hyphal tip growth and tip splitting. Therefore, we searched for homologues in *A. gossypii* to *Sc*Bni1p and the related formin *Sc*Bnr1p and investigated to which degree the homologues would contribute to sustained hyphal tip growth and tip splitting.

The A. gossypii Formin Family Members

Using FASTA database searches (Pearson, 1990), we identified three formin homology members in the genome of *A. gossypii* (Dietrich *et al.*, 2004). By combining information from homology searches with synteny, these proteins can be categorized as follows: one syntenic homolog to the *S. cerevisiae BNI1* gene (*AFR669W*, in the following referred to as *AgBNI1*) and one syntenic and one nonsyntenic, telomere-located homolog to the *S. cerevisiae BNR1* gene (*AFR301C* and *AGL364C*, referred to as *AgBNR1* and *AgBNR2*, respectively). The formins *Sc*Bni1p and *Ag*Bni1p have almost the same size and domain composition (Figure 2A) using the domain definition from Evangelista *et al.* (2002). The two homologues to *Sc*Bnr1p differ much more in size and, interestingly, these size differences are located exclusively within the FH1 domains leading to differences in the number of short polyproline stretches (Figure 2B).

It was shown that the FH1 domain of formins can mediate interactions with profilin, an abundant actin-binding protein, thereby sequestering actin monomers (Pruyne *et al.*, 2002; Sagot *et al.*, 2002b; Moseley *et al.*, 2004). The FH2 domain provides the activity for nucleation of actin cables (Pruyne *et al.*, 2002; Sagot *et al.*, 2002a; Kovar *et al.*, 2003; Harris *et al.*, 2004; Moseley *et al.*, 2004). This domain is the most conserved and best characterized domain within formins and was used as a basis for the phylogenetic classification of over a hundred formins (Higgs and Peterson, 2005). The FH3 or Formin Homology 3 domain is only loosely conserved among formins and is defined by its role, in *S. cerevisiae*, to help locating *Sc*Bni1p to the bud tip (Ozaki-Kuroda *et al.*, 2001).

Other domains shown in Figure 2 are known to be involved in diverse protein interactions in *S. cerevisiae*. The Spa2-binding domain (SBD) and to a lesser degree the Bud6-binding domain (BBD) are important for localization of ScBni1p to the growing bud tip (Ozaki-Kuroda *et al.*, 2001; Sagot *et al.*, 2002a). The Rho-binding domain (RBD) interacts with small GTPases of the Rho-type and also undergoes an intramolecular association with a short carboxy-terminal domain called diaphanous autoregulatory domain (DAD). This association, indicated by the arrow in Figure 2A, prevents actin cable assembly unless an activated GTPase binds to this domain (Alberts, 2001). A short sequence similar to the known functional DAD residues of *Sc*Bni1p is also found in all members of the Bnr1 group (small black bars in Figure 2B) but its function remains unclear. Importantly, in contrast to *Sc*Bnr1p, am RBD could not be identified in the *A. gossypii*

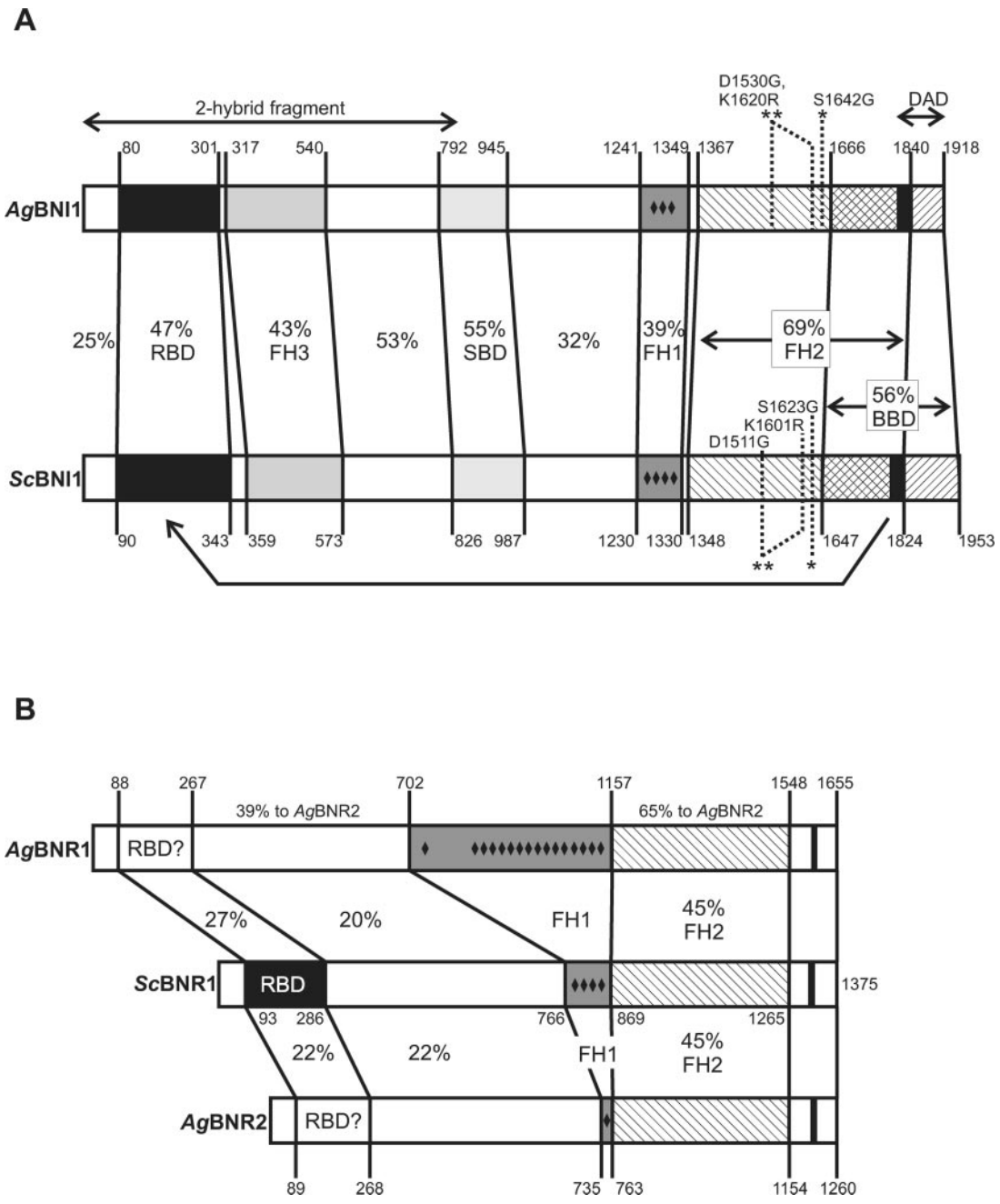

Figure 2. Domain comparisons between formin homologues of *S. cerevisiae* and *A. gossypii.* (A) Comparison of *Ag*Bni1p and *Sc*Bni1p. The domain structure of *Sc*Bni1p is based on the one published by Evangelista *et al.* (2002). Domain borders were first determined using the gap program of the GCG Wisconsin Package (Accelrys), which uses an Needleman-Wunsch algorithm (Needleman and Wunsch, 1970). Each domain was realigned and the identity values were taken from the output. All distances are drawn to a relative scale. RBD, Rho-binding domain; FH1–3, Formin Homology domain 1–3; SPD, Spa2-binding domain; BBD, Bud6-binding domain; DAD, diaphanous autoregulatory domain, which is drawn as black bar within BBD. The point mutations and the DAD deletion used in this work are indicated as well as the boundaries of the amino-terminal fragment used in two-hybrid studies. (B) Comparison of *Ag*Bnr1p and *Ag*Bnr2p with *Sc*Bnr1p. The domain structure of *Sc*Bnr1p is based on that of *Sc*Bni1p. Domain borders were determined and marked as described in A. No clear indication of an RBD was found in the two *A. gossypii* homologues. Small black diamonds indicate positions of short stretches of two or more prolines that are not separated by more than one other residue.

homologues searching for this domain (DRF_GBD) in PFAM version 17.0. This result is consistent with our finding that neither full-length nor amino-terminal parts of *Ag*Bnr1p and *Ag*Bnr2p bind to wild-type or activated forms of all *A. gossypii* Rho-GTPases in a two-hybrid test (unpublished data).

Because the two *S. cerevisiae* formins have partially overlapping functions allowing, for example, single deletions to grow, we expected, based on the domain comparisons, also to find overlapping functions in the three formins of *A. gossypii*.

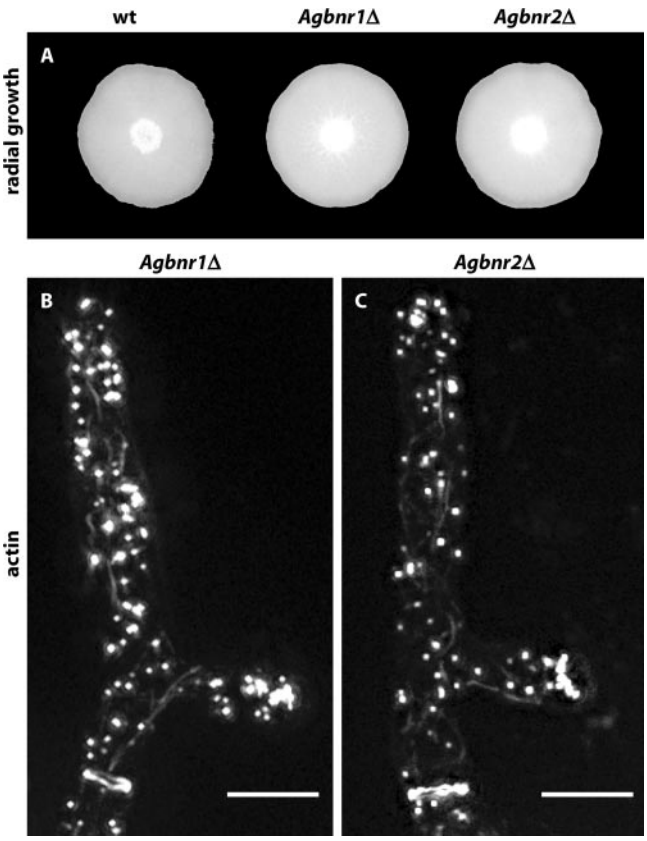

Figure 3. Wild type-like growth of *Agbnr1* and *Agbnr2* deletions. (A) Mycelial colonies from *A. gossypii* wild-type and single deletion strains. Small aliquots of mycelia were transferred to the middle of full medium plates and grown for 6 d at 30°C. Bar, 1.0 cm. (B and C) Visualization of actin patches, actin cables, and actin rings by staining young mycelium of the respective deletion strains with Alexa-phalloidin (Knechtle *et al.,* 2003). In both panels a growing tip is at the top and an actin ring is seen at the bottom below an emerged lateral branch. Bars, 5 μm.

Single Deletions of Agbnr1 and Agbnr2 Are Viable But Not the Double Deletion

To investigate the cellular function of the two homologues of *Sc*Bnr1p, we first deleted the entire ORFs of *AgBNR1* and *AgBNR2* by PCR-based gene targeting using a cassette coding for resistance against geneticin (G418). Young mycelium with 20–40 nuclei was transformed to geneticin-resistance. These primary transformants are heterokaryotic because their haploid nuclei carry either the wild-type or the deletion allele. Homokaryotic deletion transformants were obtained from spores that contain single nuclei and that were dissected on selective agar medium. Growing homokaryotic transformants were rechecked for the loss of the wild-type and presence of the deletion allele and were phenotypically characterized.

As can be seen in Figure 3A, the mycelial development of both single deletions is not perturbed. Consistent with this wild type-like growth, all actin structures can be observed by Alexa-phalloidin staining as shown in Figure 3, B and C. Staining with calcofluor white revealed an increased number of incomplete chitin rings in the *Agbnr2* deletion, and a fusion with GFP revealed that at least a fraction of the *Ag*Bnr2p-GFP proteins locates at septa, whereas no fluorescence was detected at the tips (unpublished data). Several attempts to locate an *Ag*Bnr1-GFP fusion remained unsuccessful.

The viability of both deletions indicates that the two *Ag*Bnrp homologues probably encode overlapping functions. The genomic arrangement of the *A. gossypii BNR* genes indeed suggests that *AgBNR2* most likely originates from a duplication of an ancient *AgBNR1* gene involving transposition of one copy to the telomere region of chromosome VI. We therefore constructed and tested double deletions of both homologues. Because of the lack of a functional mating system in *A. gossypii,* we had to delete the *AgBNR2* gene in a strain already deleted for the *AgBNR1* gene. This resulted in transformants that are homokaryotic for the *Agbnr1* deletion (ClonNAT resistance marker) and heterokaryotic for the *Agbnr2* deletion (geneticin resistance marker). PCR-verified heterokaryotic transformants were sporulated and spores were dissected on different selection media. Spores were viable on ClonNAT, selecting for the *Agbnr1* deletion, but nonviable on geneticin, selecting for the *Agbnr1/Agbnr2* double deletion ($n > 100$). To avoid the possibility that the *Agbnr1* deletion strain used to construct the double deletion carried an unknown mutation, which is colethal with the introduced *Agbnr2* deletion, we repeated the experiment with a newly constructed *Agbnr1* transformant as the recipient strain, now marked by geneticin resistance. Then we used leucine auxotrophy as selection for the *Agbnr2* deletion. Again, we were unable to isolate any mature mycelium carrying a homokaryotic *Agbnr1/Agbnr2* double deletion. To see if the nonviable spores showed residual growth, we looked for germination structures under the microscope. None of the spores formed a germ bubble ($n > 100$), indicating a common function of *Ag*Bnr1p and *Ag*Bnr2p essential very early in germination.

Deletion of AgBNI1 Is Lethal

To investigate the functions of *AgBNI1,* we first deleted the entire ORF. More than 100 spores obtained from the primary heterokaryotic mycelium were dissected and placed on selective medium. None of these spores gave rise to a mature mycelium. Thus, deletion of *AgBNI1* is lethal despite the presence of the two other formin genes, *AgBNR1* and *AgBNR2*, indicating an essential role of the formin *Ag*Bni1p. In *S. cerevisiae*, mutants with deletions of either one of the two formin genes, *ScBNI1* and *ScBNR1*, are viable and only deletion of both genes is lethal (Imamura *et al.,* 1997).

Microscopic observation of *Agbni1*Δ (Figure 4) revealed that spores started swelling like wild type, but were not able to initiate hyphal growth. Instead, irregular isotropic growth proceeded for at least 20 h, generating giant, potatolike cells containing over 100 nuclei. Because formins were reported to catalyze actin cable polymerization (Pruyne *et al.,* 2002; Sagot *et al.,* 2002b), we investigated the actin cytoskeleton of *Agbni1*Δ stained with Alexa-phalloidin. Long, polarized actin cables, reaching the tips, have been reported for *A. gossypii* wild type (Knechtle *et al.* (2003) and Figure 4D). The images in Figure 4, E and F, show that *Agbni1* deletion mutants do not contain polarized actin cables and that actin patches are distributed all over the cell cortex. This is in contrast to wild-type hyphae, where patches are concentrated at the tips The only concentration of actin patches is observed along structures which, according to the DIC images in Figure 4, B and C, most likely mark sites of septum formation as described before (Knechtle *et al.,* 2003). Thus, *AgBNI1* might not be essential for septum formation but is required for actin cable formation and hyphal morphology.

The loss of actin cable formation in the *Agbni1* deletion raises an important question. Why is this loss not compen-

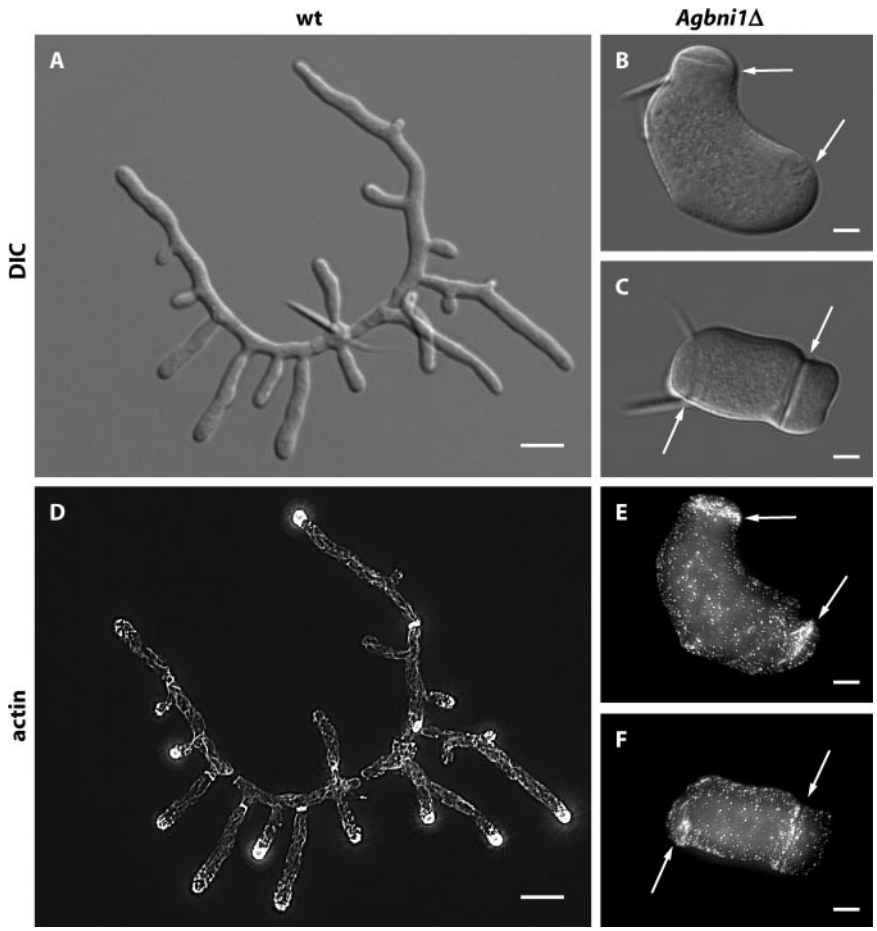

Figure 4. Lack of mycelial development after deletion of the single formin gene *AgBNI1.* Spores from wild type and from heterokaryotic *Agbni1*Δ transformants were grown over night at 30°C in AFM and AFM-Geneticin medium, respectively. DIC images are shown for wild-type (A) and *Agbni1*Δ (B and C), and fluorescence images for rhodamine-stained wild-type (D) and Alexa-phalloidin-stained *Agbni1*Δ (E and F). Arrows mark giant septumlike structures in *Agbni1*Δ that are visible by DIC and by actin staining. The needlelike structures attached to the middle of the young mycelium (A) and to one pole of the giant cells (B and C) originate from the spores, which have the shape of ~20-μm-long needles. Bars, (A and D) 10 μm and 5 μm for all other images.

sated, as in *S. cerevisiae*, by one of the two other formin homology members? The domain comparisons of Figure 2 do not reveal an answer because there is no significant difference between formin homologues of both organisms with respect to the domains responsible for actin cable formation. Therefore we hypothesized that *Ag*Bni1p is essential because its essential function may be connected to its location.

AgBni1p Locates to Hyphal Tips

To determine the location of *Ag*Bni1p, we constructed a GFP fusion at the genomic locus of *AgBNI1* and first tested whether the fusion protein is functional. Spores expressing *Ag*Bni1p-GFP developed to a young mycelium with actin cables, actin patches, and actin rings indistinguishable from wild type. Mature hyphae displayed regular tip splitting, only their maximal elongation speed was slightly slower than wild type (unpublished data). Microscopic images revealed a very weak GFP signal, always located at the tip of hyphae, which was detectable in both, young mycelium (Figure 5A) and mature hyphae (Figure 5B). Interestingly, no signal could be detected at sites of septation in over hundred apical regions inspected. This is in contrast to *S. cerevisiae* where Bni1p-GFP localizes, in addition to polarized bud tips, also as ringlike structures at sites of septation (Ozaki-Kuroda *et al.*, 2001), where it is most likely involved in cell separation, a process that does not occur in growing *A. gossypii* hyphae. Therefore the observed localization is consistent with an exclusive role for *Ag*Bni1p in tip growth.

Localization of the Polarisome Component AgSpa2p in the Agbni1Δ Mutant

One possible essential process *Ag*Bni1p that could be involved in at hyphal tips is the assembly or stabilization of a polarisome-like structure, which acts as a polarity control complex. For example, Bauer *et al.* (2004) could recently demonstrate that the GTPase *Ag*Bud1p is important to stably maintain the polarisome marker *Ag*Spa2p-GFP at hyphal tips and that transient loss of this tip marker in an *Agbud1* deletion causes an immediate arrest of polar growth. To test a possible essential role for *Ag*Bni1p in the assembly or stabilization of the "polarisome complex," we deleted *AgBNI1* in a strain expressing GFP-labeled *Ag*Spa2p. *Ag*Spa2p permanently localizes to the tips of elongating hyphae (Knechtle *et al.*, 2003). In the giant *Agbni1*Δ cells *Ag*Spa2p-GFP is always found at the cortex of the slowly expanding zone opposite from the spore needle (Figure 5C), indicating that *Ag*Bni1p does not play an essential role in polarizing *Ag*Spa2p. The observed polarization may be the reason why giant *Agbni1*Δ cells form potato-shaped structures instead of large round cells, like mutants of *Agcdc24* and *Agcdc42,* which are blocked in early steps of polarity establishment (Wendland and Philippsen, 2001).

Mutation of a Single Amino Acid in the FH2 Domain of AgBni1p Is Lethal

The experiments presented so far and the domain comparison of Bni1p from *A. gossypii* and *S. cerevisiae* discussed in Figure 2 suggest similar molecular properties of both pro-

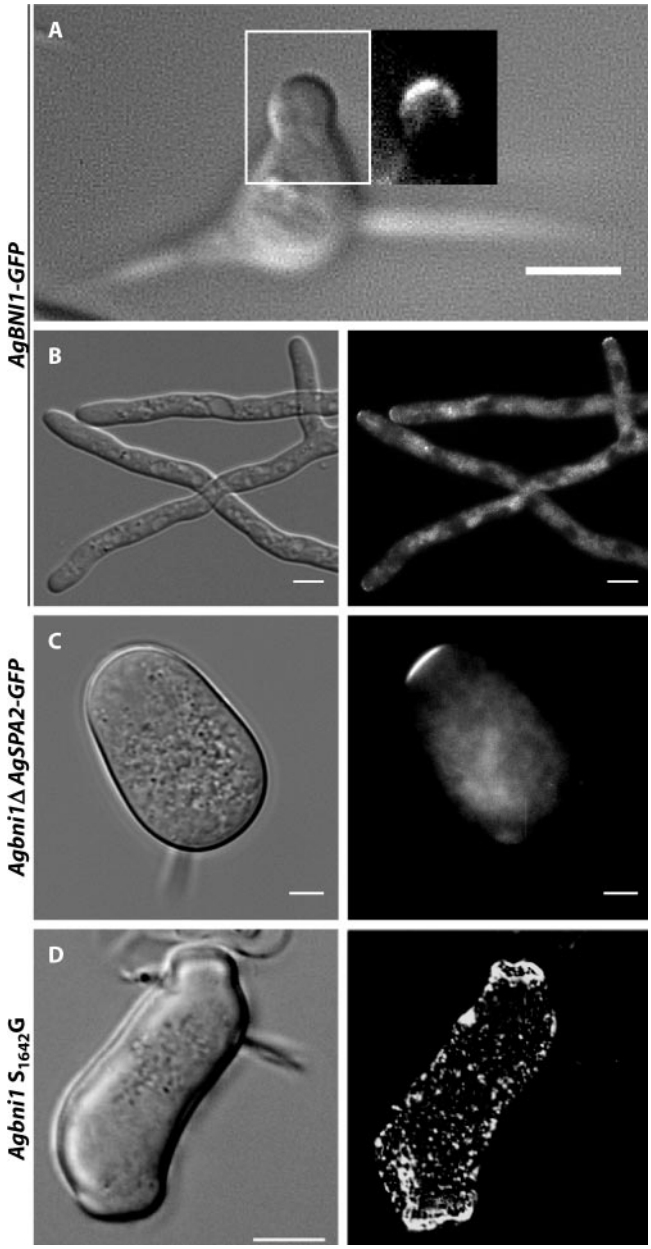

Figure 5. Localization of *Ag*Bni1p-GFP at hyphal tips. (A) Brightfield and fluorescence image of an *A. gossypii* germling carrying one copy of *AgBNI1-GFP* expressed from the endogenous *BNI1* promoter. Because of high autofluorescence of spores, the fluorescence image is only shown for the area corresponding to the white rectangle. Scale bar, 5 μm. (B) Brightfield and fluorescence image of a mature hypha expressing *Ag*Bni1p-GFP from a genomic fusion gene. Scale bar, 5 μm. (C) Localization of *Ag*Spa2p-GFP in *Agbni1*Δ. DIC image and fluorescence images of *Agbni1*Δ cells carrying a *SPA2-GFP* fusion at the *AgSPA2* locus. Spores from heterokaryotic transformants were grown in AFM-Geneticin medium over night at 30°C. Scale bar, 5 μm. (D) Phenotype of the single $S_{1642}G$ substitution in the FH2 domain of *Ag*Bni1p. Spores from heterokaryotic transformants were grown over night in liquid AFM-Geneticin medium at 30°C and stained for actin with Alexa phalloidin. The fluorescence image (top) and the DIC image (bottom) were taken from the same cell. Scale bar, 10 μm.

teins. One important property of *Ag*Bni1p and *Sc*Bni1p is the nucleation of actin cables, which resides within the FH2 domain. We asked whether the characteristic phenotype of the *AgBNI1* deletion is only due to a tip-located loss of actin polymerization capability and subsequent loss of actin cables rather than loss of other functions. To test this, we constructed point mutations in the FH2 domain of *Ag*Bni1p, leading to the amino acid substitutions $S_{1642}G$ in one and $D_{1530}G$, $K_{1620}R$ in a second mutant. Especially the residues mutated in the second mutant are highly conserved throughout all formin proteins (Higgs and Peterson, 2005). In *S. cerevisiae*, both homologous substitutions $S_{1623}G$ and $D_{1511}G$, $K_{1601}R$ lead to temperature-sensitive strains in a background deleted for *ScBNR1*, the second formin gene (Evangelista *et al.*, 2002). We expected to find temperature-sensitive phenotypes for both *A. gossypii* mutants. Surprisingly, the analogous substitutions in *Ag*Bni1p were lethal, even at 16°C. Like the complete deletion, these point mutants were able to form giant cells with many actin patches but without actin cables (Figure 5D). These experiments indicate that the tip-located assembly of actin cables represents the essential function of the *Ag*Bni1p formin, which emphasizes the importance of actin cables for hyphal growth.

Actin Cable-based Vesicle Transport Is Defect in Agbni1D

The loss of actin cables should severely impede delivery of secretory vesicles to hyphal tips. To confirm that *Ag*Bni1p is needed for secretory vesicle transport, we isolated the *AgSEC4* gene by homology to the *S. cerevisiae SEC4* gene and constructed a GFP-fusion. In budding yeast, a GFP-Sec4p fusion protein localizes to secretory vesicles and moves in a directed manner along actin cables toward the bud tip (Schott *et al.*, 2002). We transformed *A. gossypii* with a plasmid expressing an amino-terminal GFP-*Ag*Sec4p fusion under control of the native *AgSEC4* promoter. As shown in Figure 6A, the fusion product localizes mainly to the tip. Addition of latrunculin A, which disrupts actin structures, abolishes vesicular movement and apical localization, giving rise to a uniform fluorescence within hyphae (Figure 6B). To observe the localization of vesicles in the absence of *Ag*Bni1p, we transformed a heterokaryotic *Agbni1*Δ mycelium with the plasmid expressing the GFP-*Ag*Sec4p fusion protein. Spores of these transformants were grown under conditions selective for both, the *Agbni1* deletion and the plasmid. In all growing giant cells the GFP fluorescence was evenly distributed (Figure 6C). This verifies that continuous tip-directed transport of secretory vesicles via actin cables is essential for hyphal growth.

Hyphal Morphogenesis in the Presence of Constitutively Active AgBni1p (AgBNI1ΔD)

We wanted to know whether an overactivation of the *Ag*Bni1 protein would increase hyphal elongation rates. We speculated that such a mutant should assemble more actin cables emanating from the tips, thus enhancing the transport rate of secretory vesicles toward the tip. To test this hypothesis, we deleted in *AgBNI1* the coding sequence of the carboxy-terminal DAD (see Figure 2), thereby eliminating in the expressed protein the inactivating interaction of the DAD domain with the amino terminus.

Several independent mutants were isolated. All show a complete change in branching pattern. Although morphogenesis of young wild-type mycelium exclusively displays lateral branching (Figure 7, A–C), the overactivation of the *Ag*Bni1p formin suppresses this branching mode and induces successive and symmetric hyphal splitting at tips (Figure 7, D–F). Lateral branching events occur only late and very rarely in this mutant, as concluded from videomicroscopy of 10 developing young mycelia. Examples are docu-

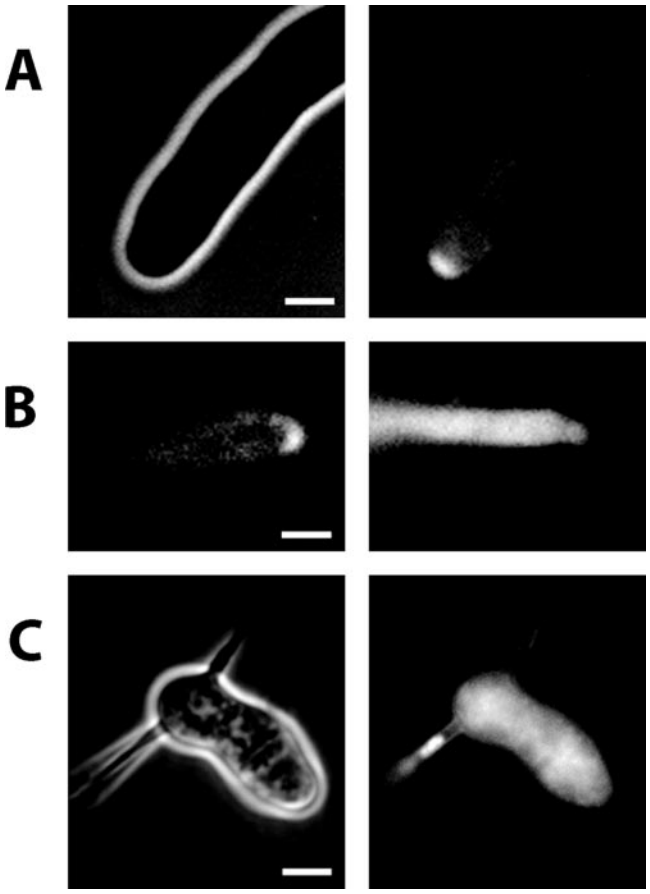

Figure 6. Distribution of GFP-Sec4p in wild type and *Agbni1*Δ. (A) Brightfield (left) and GFP-fluorescence (right) micrographs of a single wild-type hypha carrying a GFP-SEC4 fusion. The main fluorescence localizes to the tip. (B) Localization of GFP-Sec4p prior (left) and after (right) treatment with 200 μM latrunculin A for 1.5 min. (C) Brightfield (left) and GFP-fluorescence (right) images of *Agbni1*Δ carrying a *GFP-SEC4* fusion gene. All strains were grown in liquid selective medium at 30°C over night. Scale bars, 5 μm.

mented in Supplementary Movies S2-S4 for wild type and Supplementary Movies S5-S7 for *AgBNI1ΔD* (see Supplementary Material).

Quantitative evaluation of the movies reveals similar initial tip extension speeds for wild type and *AgBNI1ΔD* (Figure 8A). However, the average diameter of young hyphae of the mutant has almost doubled compared with wild type based on 300 measurements of three hyphae each (4.63 ± 0.46 μm for wild type and 7.52 ± 1.1 μm for mutant hyphae). These parameters allowed us to calculate for each time point the surface expansion rate, which, during the first 4 h, is up to three times higher in the mutant compared with wild type (Figure 8B). This increase in surface growth strongly indicates that an overactivation of *Ag*Bni1p can enhance the traffic of tip-directed secretory vesicles. This idea is supported by three experimental results. First, constitutively activated *Ag*Bni1ΔD proteins still locate to the tips (20/20) of hyphae (Figure 8C). Second, a two to three times higher number of actin cables can be observed in the apical region of mutant hyphae (Figure 8D) compared with wild-type hyphae (Figure 8E). And third, more vesicles are transported to the tip region as evident from the larger area of accumulated secretory vesicles in mutant hyphae (Figure 8, F and G) compared with wild-type hyphae (Figure 6A).

The nonregulatable, overactive *Ag*Bni1ΔD formin leads to a growth advantage during the early mycelial development but has a negative effect on the further development to a fast spreading colony (Figure 8H). Already after 6 to 7 h the elongation rate of mutant hyphae and with that the surface expansion rate reaches a plateau, whereas the elongation of wild-type hyphae continues to accelerate (Figure 8, A and B). This difference in growth rates may be due to the high frequency of premature tip splitting events in the mutant, which impedes hyphal speed acceleration and thus leads to a slower growing mycelium compared with wild type.

AgBni1p Is an Effector of AgCdc42p

The domain composition of *Ag*Bni1p predicts that it is activated when a GTP-bound Rho-type GTPase interacts with the amino-terminal RBD (Figure 2). We searched for candidates of such activator among *A. gossypii* homologues of Rho-type GTPases using two criteria: Its GTP-bound form should interact with the amino-terminus of *Ag*Bni1p, and a GTP-locked form of this protein should induce tip splitting in young hyphae due to a permanent activation of *Ag*Bni1p, similarly as observed for young hyphae of the *AgBNI1ΔD* mutant. By systematic two-hybrid analysis of the *Ag*Bni1p amino-terminus against all *A. gossypii* Rho-type GTPases and by videomicroscopy of GTP-locked mutants of the three Rho-type GTPases, which scored positive in the first test, we identified *Ag*Cdc42p as the only candidate. The two-hybrid result is summarized in Figure 9A and two microscopic images showing tip splitting in young hyphae expressing GTP-locked *Ag*Cdc42p are presented in Figure 9B. These hyphae carry only the mutated *AgCDC42* allele and show growth defects preventing the young mycelia from further development. This is most likely due the multitude of effector proteins that are regulated by *Ag*Cdc42p.

DISCUSSION

The filamentous fungus *A. gossypii* and the budding yeast *S. cerevisiae* have different life styles (see Supplementary Movie S1) despite very similar gene contents and conserved domain compositions of gene products (Dietrich *et al.,* 2004). Both organisms can establish polar growth but in *S. cerevisiae* periods of growth alternate with cell divisions, whereas *A. gossypii* cells (hyphae) grow for unlimited periods without undergoing divisions. In addition, *A. gossypii* hyphae can establish multiple new axes of polarity, e.g., during lateral branching or tip splitting. In contrast, wild-type yeast cells never form more than one new bud at the same time (Caviston *et al.,* 2002). We describe here a role for the *Ag*Bni1p formin in two of these processes: the establishment of polarity (formation of hyphae) and the controlled division of one axis of polarity into two new polarity axes (tip splitting), a novel function for this protein class.

Redundance of Formins in A. gossypii

The lethality of the *Agbni1* deletion was surprising because *A. gossypii* contains two additional formin genes, *AgBNR1* and *AgBNR2*, and because all three formin genes encode proteins with similar domains, notably the actin nucleation domain FH2. The deletion of either one of the *Ag*BNR genes is fully viable indicating overlapping functions in the *Ag*Bnr formins. These results made us at first conclude that the lethality of *Agbni1*Δ is due to distinct functions of members of the *Ag*Bni1p and the *Ag*Bnr proteins. This idea was supported by comparison to the more distantly related fission yeast *S. pombe*, which expresses three members of the formin family with clear separation of functions. For3 is involved in

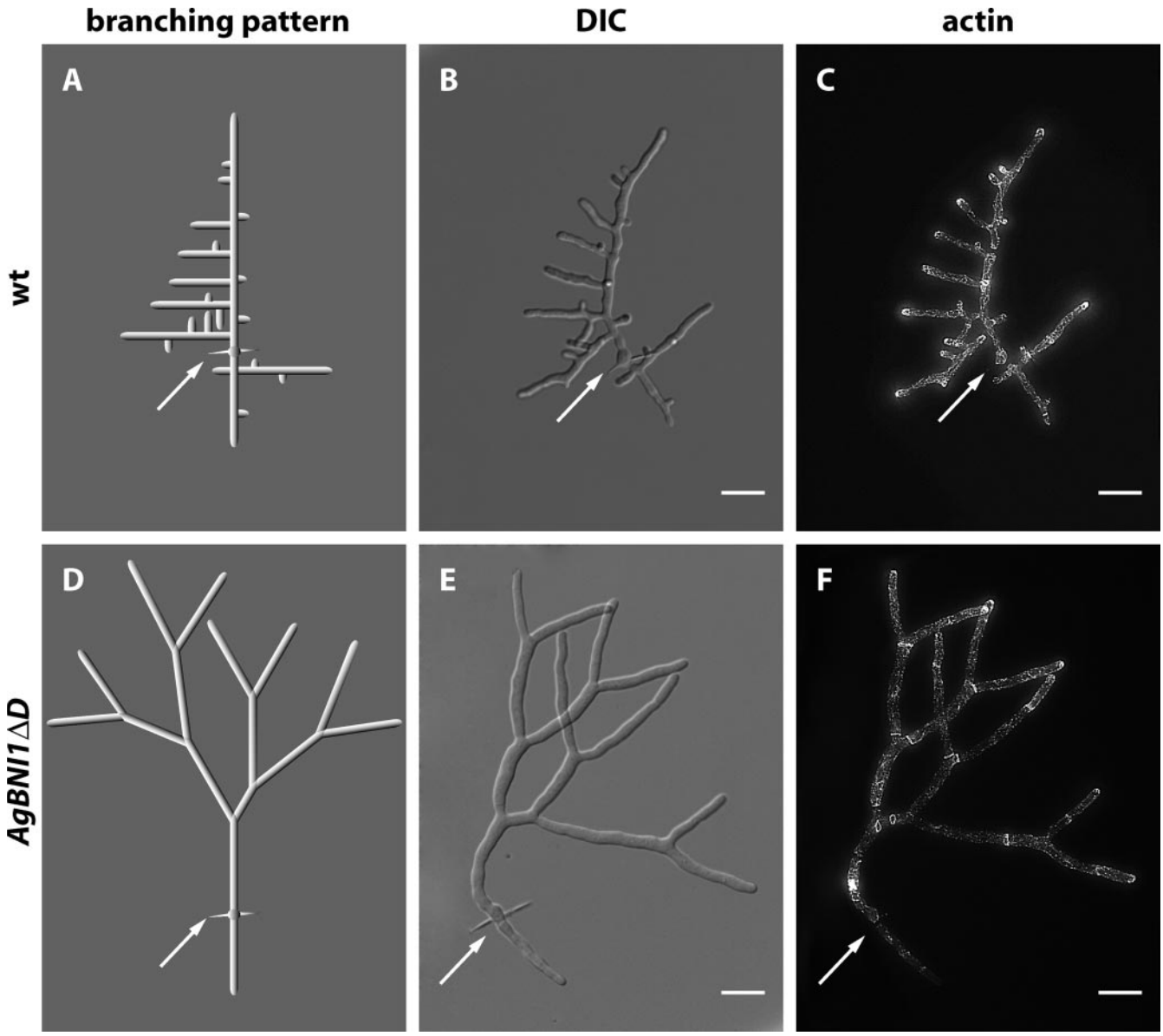

Figure 7. Altered morphogenesis of *AgBNI1ΔD* mycelium. Wild-type and *AgBNI1ΔD* spores were incubated in liquid AFM medium at 30°C. After 18 h aliquots were stained with Alexa-phalloidin and mounted for microscopy. (A) Idealized branching scheme of the young wild-type mycelium shown as DIC image in B and as fluorescence image in C. The white arrows mark the needle of the spore from which two main hyphae developed in opposite directions. New branches always emerged distant from the tip and in an about right angle from the polarity-axis of the main hyphae, leading to a typical "Christmas tree" appearance. (D) Idealized tip splitting pattern of the young *AgBNI1ΔD* mycelium shown as DIC image in E and as fluorescence image in F. The white arrows mark the original position of the spore. Scale bar, 10 μm.

cell polarity (Feierbach and Chang, 2001), Cdc12 is involved in cytokinesis (Chang *et al.*, 1997) and Fus1 is necessary for cell fusion during mating (Petersen *et al.*, 1998a). Although *S. pombe for3*Δ had no visible actin cables (Feierbach and Chang, 2001) or the cables were shorter in size and reduced in number (Nakano *et al.*, 2002), cells were still able to grow in a polarized manner unlike a deletion of *Agbni1*.

Different functions were also described for the baker's yeast formins *Sc*Bni1p and *Sc*Bnr1p (Pruyne *et al.*, 2004). *Sc*Bni1p localizes mainly to the bud tip where it forms actin cables. It is also found at the septum in a very late phase of bud formation, when the direction of growth polarity has already switched. *Sc*Bnr1p in contrast localizes exclusively and already during early phases of bud formation to the forming septum. However, budding yeast cells can still survive in the absence of *Sc*Bni1p because the septum-associated *Sc*Bnr1p is also able to nucleate actin cables, thereby providing the close-by growing bud with secretory vesicles. This short distance between the septum and the growing bud tip, e.g., during axial budding, is probably of key importance for the viability of cells lacking the *Sc*Bni1p formin. At increasing distances between the septum and the growing tip, formin deletion experiments may give different results. For example, assuming similar actin nucleating functions for the formins in *A. gossypii* but distinct protein localization requirements, the lethality of the *Agbni1* dele-

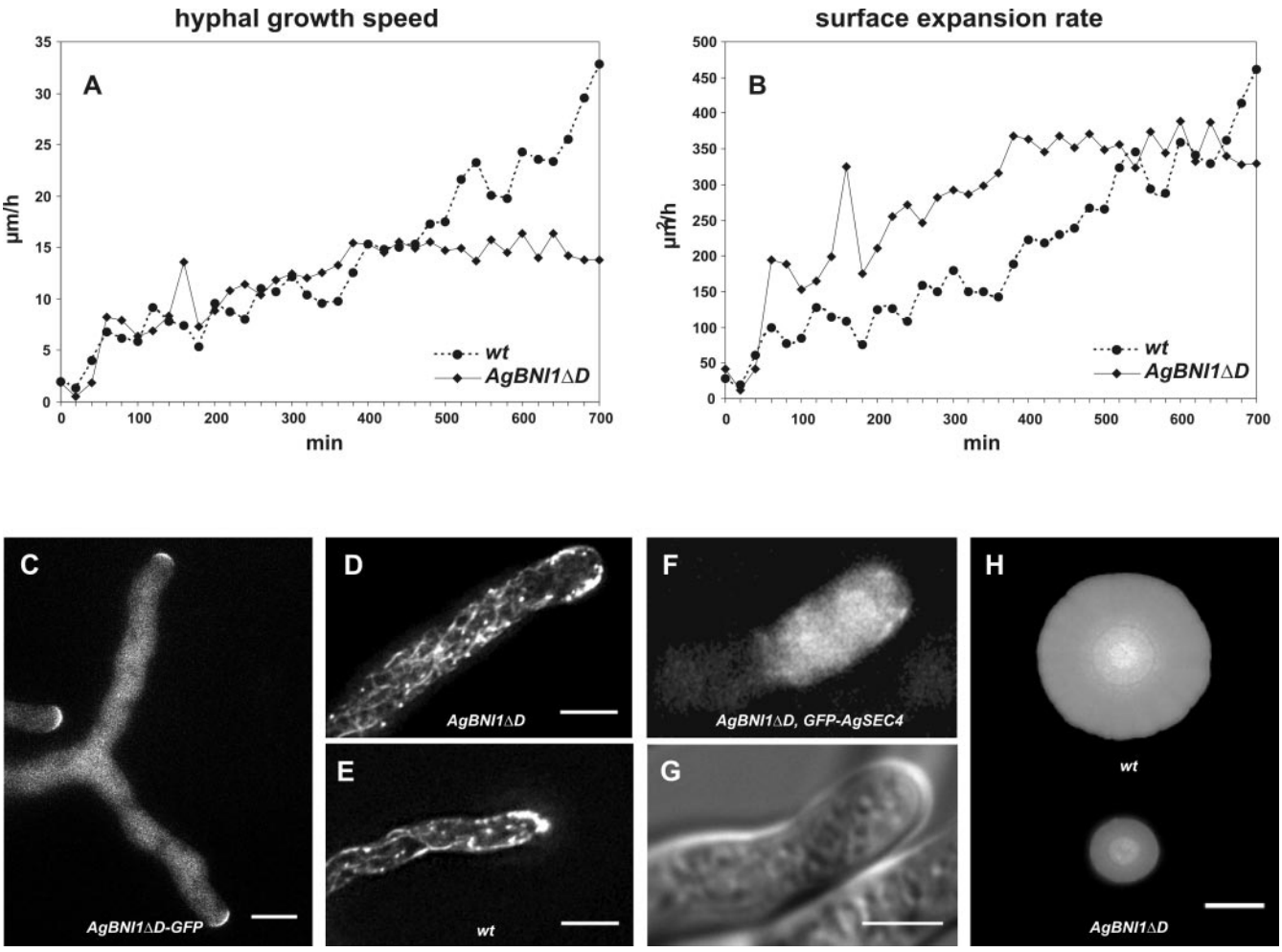

Figure 8. Increase in surface expansion and number of actin cables in *AgBNI1*Δ*D*. (A) Elongation speeds in μm/h of wild-type hyphae (●) and *AgBNI1*Δ*D* hyphae (♦) during the first 700 min of hyphal development. The data points represent the average from two hyphae followed in three young mycelia each, starting shortly after the first hypha has emerged from a germinated spore. (B) Surface expansion rates at hyphal tips of wild type (●) and *AgBNI1*Δ*D* (♦) were calculated from the elongation speeds determined in A, and the hyphal diameters were measured every 10 μm. (C) Localization of *Ag*Bni1ΔD-GFP fusion proteins at hyphal tips. (D) Visualization by epifluorescence microscopy of rhodamine-phalloidin-stained F-actin in *AgBNI1*Δ*D*. For several hyphae a stack of 16 planes taken at 0.4-μm distances was analyzed. Because of the high density of actin cables along the cortex only a maximum projection of the top third of the hypha (three planes) is shown. Four to five actin cables can be seen per cross section, which represents about one-third of the density of cortical actin cables in the hypha. (E) Rhodamine-phalloidin stained F-actin in wild-type *A. gossypii*. The stack of 16 planes was processed as described for D, and only the top third of the hypha is shown. Only one to two cortical actin cables can be seen per cross section. (F and G) Visualization of GFP-*Ag*SEC4-labeled vesicles in the tip region of an *AgBNI1*Δ*D* hypha and the corresponding DIC image. (H) Mycelial colonies of wild type and *AgBNI1*Δ*D* after growth on AFM agar at 30°C for 5 d. Bars, (C–F) 5 μm, (H) 2 cm.

tion could be explained by the large distance between the growing tip and the nearest septum, preventing septum-associated formin functions to complement the loss of such functions at hyphal tips. This alternative interpretation is supported by the fact that we were able to visualize *Ag*Bni1p-GFP at hyphal tips, but not at septa, and *Ag*Bnr2p-GFP at septa but not at hyphal tips.

The fact that *Ag*Bni1p functions in hyphal emergence and elongation, but probably not in septum formation, indicates that it is also functionally different from SepA, the only other formin described in a filamentous fungus so far. SepA from *Aspergillus nidulans* localizes to the tip of hyphae and to septa, and it is essential for morphogenesis. Interestingly, some SepA mutants, defective in septum formation, are still able to form hyphae (Sharpless and Harris, 2002). Therefore, mutant formins can probably still induce actin cables at hyphal tips, or another, so far unidentified formin gene, is present in the genome of *A. nidulans*.

AgBni1p and the Actin Cytoskeleton

The phenotype observed for the *AgBNI1* deletion, lack of actin cables and hyphal growth, indicated that an important function of *Ag*Bni1p might be the regulation of vesicle transport via actin cables. *A. gossypii* hyphae are capable to grow with very high growth speeds of up to 170 μm/h (Knechtle *et al.*, 2003). This speed obviously requires a constant and very efficient transport of growth material toward the elongating tips. Our results show that single amino acid changes in the FH2 domain of *Ag*Bni1p, which is responsible for actin cable assembly, can only expand to potato-shaped cells,

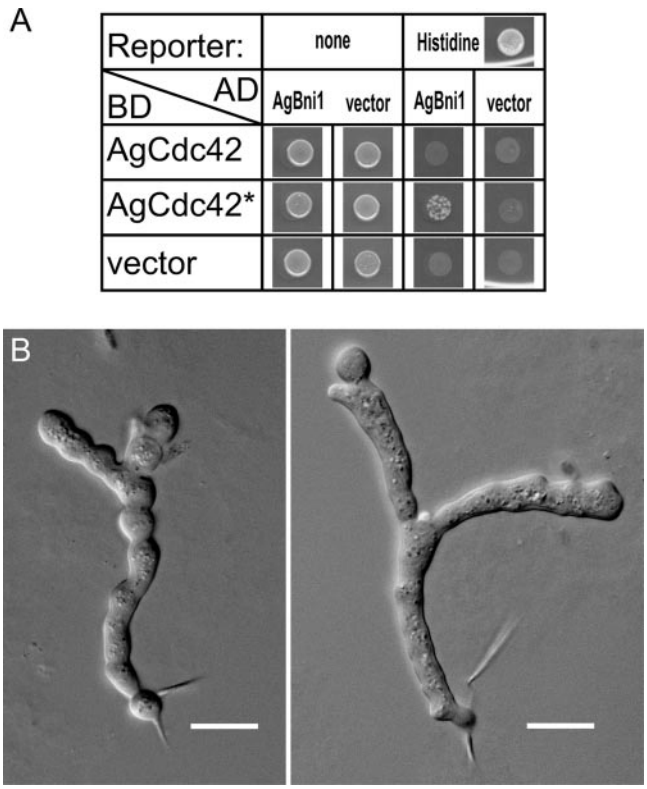

Figure 9. *Ag*Cdc42p regulates tip splitting. (A) Two-hybrid assay of *Ag*Cdc42p-GTP and the amino-terminal half of *Ag*Bni1p. Each spot corresponds to 5 μl of a yeast culture of strain *PJ69–4a* with an OD_{600} of 1, transformed with plasmids encoding fusions of the indicated proteins to either the Gal4-activation domain (AD) or to the Gal4-DNA-binding domain (BD) or, as control, transformed with the vector plasmid. The cells were spotted on a medium allowing to select for the plasmids and were grown overnight at 30°C to screen for protein-protein interactions by growth in the absence of histidine. (B) Altered morphogenesis of *A. gossypii* expressing GTP-locked *Ag*Cdc42p. A heterokaryotic strain of *A. gossypii* was constructed carrying the point mutation *AgCdc42*-Q_{61}H that encodes a protein mimicking the GTP-bound and therefore activated state of the GTPase. Spores were dissected by micromanipulation and allowed to germinate under conditions selecting only for spores carrying the GTP-locked *AgCDC42* allele. The two microscopic images show examples of tip splitting soon after the first hypha emerged from the germling. These hyphae carry only the mutated *AgCDC42* allele and show growth defects preventing the young mycelia from further development. This is most likely due the multitude of effector proteins that are regulated by *Ag*Cdc42p. Scale bar, 10 μm.

which lack polarized actin cables like the deletion mutant. Therefore, it might be the defect of actin cable-based transport, which leads to the phenotype observed when *AgBNI1* is deleted. It is known from several studies, that actin cables can serve as tracks for different cargos such as secretory vesicles (Johnston *et al.*, 1991) and several organelles (Simon *et al.*, 1995; Hill *et al.*, 1996; Hoepfner *et al.*, 2001; Rossanese *et al.*, 2001) as well as mRNA (Bobola *et al.*, 1996; Sil and Herskowitz, 1996; Takizawa *et al.*, 2000). Using the *Ag*Sec4p fused to GFP, we were able to show that secretory vesicles use actin cables for accumulation at the hyphal tips. They no longer do so in *AgBNI1*-deleted hyphae even though the polarisome component *Ag*Spa2p localizes correctly to the cortex at the slowly expanding growth zone, which explains the potatolike shape of the giant mutant cells.

Regulation of Tip Splitting by AgBni1p

Tip splitting, the symmetric division of the polar growth zone of a single growing cell, is to our knowledge limited to filamentous fungi and to dendrites of neuronal cells. Hyphae of *A. gossypii* usually start tip splitting under optimal conditions 12–14 h after the first hyphae emerged from germinated spores (Ayad-Durieux *et al.*, 2000). Premature tip splitting, already after 6–8 h of elongation and before any lateral branching, as found for the constitutively active *Ag*Bni1p protein, was not described before. In an *Agcla4* deletion strain, premature tip splitting was previously observed but after normal development of a young mycelium, including lateral branching (Ayad-Durieux *et al.*, 2000). *Ag*Cla4p is a homologue of the PAK21 kinase Cla4p from *S. cerevisiae*, which is involved in polarization of the cytoskeleton during the cell cycle (Holly and Blumer, 1999). Evidence for an involvement of actin in tip splitting was reported in studies of other filamentous fungi in which tip splitting was not observed in wild type but was seen in different mutants as a neomorphic phenotype. For example, the ramosa-1 mutant of *Aspergillus niger* can divide at hyphal tips when shifted to the restrictive temperature (Reynaga-Pena and Bartnicki-Garcia, 1997), and the authors suggested that tip splitting might be triggered by a transient alteration in the cytoskeletal organization. Similarly, viable mutations in the formin SepA in *A. nidulans* show tip splitting (Sharpless and Harris, 2002). In *Neurospora crassa*, several mutants are known that lead to hyphal tip splitting (Sone and Griffiths, 1999; Bok *et al.*, 2001; Seiler and Plamann, 2003; Virag and Griffiths, 2004). It was suggested that a calcium gradient controls the transport of vesicles. This control mechanism also involves actin and determines whether a tip divides or not. The increased surface expansion rate in *A. gossypii* hyphae with an activated allele of *AgBNI1,* reported here, is most likely caused by the increase in actin cables and thus vesicle transport. This overstimulation in vesicle transport also leads to premature tip splitting. The fact that GTP-bound *Ag*Cdc42p interacts with *Ag*Bni1p in a two-hybrid assay and that mutants expressing the activated allele of *AgCDC42* also show premature tip splitting suggest that this event is regulated by an *Ag*Bni1p branch of the *Ag*Cdc42p signaling network. The observed growth problems of the activated *Agcdc42* mutant compared with the activated *Agbni1* mutant can be explained by the fact that changes in the activity state of *Ag*Cdc42p will influence the interaction with multiple effector proteins (Nelson *et al.*, 2003).

The involvement of the Cdc42 GTPase in tip splitting is also supported by mutants described for the CDC24 homolog of *N. crassa* (Seiler and Plamann, 2003) because Cdc24p is a GDP-GTP exchange factor for the small GTPase Cdc42p.

On the basis of the data discussed here, we suggest a molecular model for tip splitting regulation. *Ag*Cdc42p activates *Ag*Bni1p which in turn increases the number of actin cables emanating from the tip. This leads than to a stimulation of actin cable-based vesicle transport, which first enlarges and finally divides the polar growth site into two new sites. These data, when combined, suggest that altering the activities of formin molecules by Cdc42p can lead to dramatically different cell shapes. Incorporation of future experiments into this model should help to increase our understanding of this unique process like e.g., its growth speed dependence or it might help us to understand in more detail how tip splitting is triggered.

Note added in proof. After submission of this manuscript, two other fungal formins, CaBni1p and CaBnr1p, were shown to play an important but nonessential role in yeast and hyphal growth of *Candida albicans* (Li *et al*., 2005).

ACKNOWLEDGMENTS

We thank Sophie Brachat and Anne-Laure Vitte for their preliminary work on *Agbni1*Δ; Dominic Hoepfner and Anne L'Hernault for providing pUC19NatPS before publication; and Amy Gladfelter, Anja Lorberg, and Tom Bickle for critical reading of the manuscript. This work was supported by the University of Basel and the Swiss National Science Foundation Grant 3100A0-100734.

REFERENCES

Alberts, A. S. (2001). Identification of a carboxyl-terminal diaphanous-related formin homology protein autoregulatory domain. J. Biol. Chem. *276*, 2824–2830.

Altmann-Johl, R., and Philippsen, P. (1996). AgTHR4, a new selection marker for transformation of the filamentous fungus *Ashbya gossypii*, maps in a four-gene cluster that is conserved between *A. gossypii* and *Saccharomyces cerevisiae*. Mol. Gen. Genet. *250*, 69–80.

Ashby, S. F., and Nowell, W. (1926). The fungi of stigmatomycosis. Ann. Botany *40*, 69–86.

Ayad-Durieux, Y., Knechtle, P., Goff, S., Dietrich, F., and Philippsen, P. (2000). A PAK-like protein kinase is required for maturation of young hyphae and septation in the filamentous ascomycete *Ashbya gossypii*. J. Cell Sci. *113* (Pt 24), 4563–4575.

Bartel, P. L., Chien, C.-T., Sternglanz, R., and Fields, S. (1993). Using the two-hybrid system to detect protein-protein interactions. In: Cellular Interactions in Development: A Practical Approach, ed. D. A. Hartley, Oxford: Oxford University Press, 153–179.

Bauer, Y., Knechtle, P., Wendland, J., Helfer, H., and Philippsen, P. (2004). A Ras-like GTPase is involved in hyphal growth guidance in the filamentous fungus *Ashbya gossypii*. Mol. Biol. Cell *15*, 4622–4632.

Bobola, N., Jansen, R. P., Shin, T. H., and Nasmyth, K. (1996). Asymmetric accumulation of Ash1p in postanaphase nuclei depends on a myosin and restricts yeast mating-type switching to mother cells. Cell *84*, 699–709.

Bok, J. W., Sone, T., Silverman-Gavrila, L. B., Lew, R. R., Bowring, F. J., Catcheside, D. E., and Griffiths, A. J. (2001). Structure and function analysis of the calcium-related gene spray in *Neurospora crassa*. Fungal Genet. Biol. *32*, 145–158.

Boles, E., and Miosga, T. (1995). A rapid and highly efficient method for PCR-based site-directed mutagenesis using only one new primer. Curr. Genet. *28*, 197–198.

Caviston, J. P., Tcheperegine, S. E., and Bi, E. (2002). Singularity in budding: a role for the evolutionarily conserved small GTPase Cdc42p. Proc. Natl. Acad. Sci. USA *99*, 12185–12190.

Chang, F., Drubin, D., and Nurse, P. (1997). cdc12p, a protein required for cytokinesis in fission yeast, is a component of the cell division ring and interacts with profilin. J. Cell Biol. *137*, 169–182.

Dietrich, F. S. *et al*. (2004). The *Ashbya gossypii* genome as a tool for mapping the ancient *Saccharomyces cerevisiae* genome. Science *304*, 304–307.

Evangelista, M., Blundell, K., Longtine, M. S., Chow, C. J., Adames, N., Pringle, J. R., Peter, M., and Boone, C. (1997). Bni1p, a yeast formin linking cdc42p and the actin cytoskeleton during polarized morphogenesis. Science *276*, 118–122.

Evangelista, M., Pruyne, D., Amberg, D. C., Boone, C., and Bretscher, A. (2002). Formins direct Arp2/3-independent actin filament assembly to polarize cell growth in yeast. Nat. Cell Biol. *4*, 260–269.

Evangelista, M., Zigmond, S., and Boone, C. (2003). Formins: signaling effectors for assembly and polarization of actin filaments. J. Cell Sci. *116*, 2603–2611.

Feierbach, B., and Chang, F. (2001). Roles of the fission yeast formin for3p in cell polarity, actin cable formation and symmetric cell division. Curr. Biol. *11*, 1656–1665.

Gietz, R. D., and Sugino, A. (1988). New yeast-*Escherichia coli* shuttle vectors constructed with in vitro mutagenized yeast genes lacking six-base pair restriction sites. Gene *74*, 527–534.

Gow, N.A.R. (1995). Tip Growth and Polarity. In: The Growing Fungus, ed. N.A.R. Gow, G. M. Gadd, London: Chapman and Hall, 277–299.

Habas, R., Kato, Y., and He, X. (2001). Wnt/Frizzled activation of Rho regulates vertebrate gastrulation and requires a novel Formin homology protein Daam1. Cell *107*, 843–854.

Hanahan, D. (1983). Studies on transformation of *Escherichia coli* with plasmids. J. Mol. Biol. *166*, 557–580.

Harris, E. S., Li, F., and Higgs, H. N. (2004). The mouse formin, FRLalpha, slows actin filament barbed end elongation, competes with capping protein, accelerates polymerization from monomers, and severs filaments. J. Biol. Chem. *279*, 20076–20087.

Harris, S. D., Read, N. D., Roberson, R. W., Shaw, B., Seiler, S., Plamann, M., and Momany, M. (2005). Polarisome meets spitzenkorper: microscopy, genetics, and genomics converge. Eukaryot. Cell *4*, 225–229.

Harris, S. D., Hamer, L., Sharpless, K. E., and Hamer, J. E. (1997). The *Aspergillus nidulans* sepA gene encodes an FH1/2 protein involved in cytokinesis and the maintenance of cellular polarity. EMBO J. *16*, 3474–3483.

Higgs, H. N., and Peterson, K. J. (2005). Phylogenetic analysis of the formin homology 2 domain. Mol. Biol. Cell *16*, 1–13.

Hill, K. L., Catlett, N. L., and Weisman, L. S. (1996). Actin and myosin function in directed vacuole movement during cell division in *Saccharomyces cerevisiae*. J. Cell Biol. *135*, 1535–1549.

Hoepfner, D., van den Berg, M., Philippsen, P., Tabak, H. F., and Hettema, E. H. (2001). A role for Vps1p, actin, and the Myo2p motor in peroxisome abundance and inheritance in *Saccharomyces cerevisiae*. J. Cell Biol. *155*, 979–990.

Holly, S. P., and Blumer, K. J. (1999). PAK-family kinases regulate cell and actin polarization throughout the cell cycle of *Saccharomyces cerevisiae*. J. Cell Biol. *147*, 845–856.

Imamura, H., Tanaka, K., Hihara, T., Umikawa, M., Kamei, T., Takahashi, K., Sasaki, T., and Takai, Y. (1997). Bni1p and Bnr1p: downstream targets of the Rho family small G-proteins which interact with profilin and regulate actin cytoskeleton in *Saccharomyces cerevisiae*. EMBO J. *16*, 2745–2755.

James, P., Halladay, J., and Craig, E. A. (1996). Genomic libraries and a host strain designed for highly efficient two-hybrid selection in yeast. Genetics *144*, 1425–1436.

Johnston, G. C., Prendergast, J. A., and Singer, R. A. (1991). The *Saccharomyces cerevisiae MYO2* gene encodes an essential myosin for vectorial transport of vesicles. J. Cell Biol. *113*, 539–551.

Kamei, T., Tanaka, K., Hihara, T., Umikawa, M., Imamura, H., Kikyo, M., Ozaki, K., and Takai, Y. (1998). Interaction of Bnr1p with a novel Src homology 3 domain-containing Hof1p. Implication in cytokinesis in *Saccharomyces cerevisiae*. J. Biol. Chem. *273*, 28341–28345.

Knechtle, P., Dietrich, F., and Philippsen, P. (2003). Maximal polar growth potential depends on the polarisome component AgSpa2 in the filamentous fungus *Ashbya gossypii*. Mol. Biol. Cell *14*, 4140–4154.

Kobielak, A., Pasolli, H. A., and Fuchs, E. (2003). Mammalian formin-1 participates in adherens junctions and polymerization of linear actin cables. Nat. Cell Biol. *6*, 21–30.

Kohno, H. *et al*. (1996). Bni1p implicated in cytoskeletal control is a putative target of Rho1p small GTP binding protein in *Saccharomyces cerevisiae*. EMBO J. *15*, 6060–6068.

Kovar, D. R., Kuhn, J. R., Tichy, A. L., and Pollard, T. D. (2003). The fission yeast cytokinesis formin Cdc12p is a barbed end actin filament capping protein gated by profilin. J. Cell Biol. *161*, 875–887.

Li, C. R., Wang, Y. M., DeZheng, X., Liang, H. Y., Tang, J. C., and Wang, Y. (2005). The formin family protein CaBni1p has a role in cell polarity control during both yeast and hyphal growth in *Candida albicans*. J. Cell. Sci. *118*, 2637–2648.

Li, F., and Higgs, H. N. (2003). The mouse Formin mDia1 is a potent actin nucleation factor regulated by autoinhibition. Curr. Biol. *13*, 1335–1340.

Momany, M. (2002). Polarity in filamentous fungi: establishment, maintenance and new axes. Curr. Opin. Microbiol. *5*, 580–585.

Moseley, J. B., Sagot, I., Manning, A. L., Xu, Y., Eck, M. J., Pellman, D., and Goode, B. L. (2004). A conserved mechanism for Bni1- and mDia1-induced actin assembly and dual regulation of Bni1 by Bud6 and profilin. Mol. Biol. Cell *15*, 896–907.

Nakano, K., Imai, J., Arai, R., Toh, E. A., Matsui, Y., and Mabuchi, I. (2002). The small GTPase Rho3 and the diaphanous/formin For3 function in polarized cell growth in fission yeast. J. Cell Sci. *115*, 4629–4639.

Needleman, S. B., and Wunsch, C. D. (1970). A general method applicable to the search for similarities in the amino acid sequence of two proteins. J. Mol. Biol. *48*, 443–453.

Nelson, B. *et al.* (2003).. RAM: a conserved signaling network that regulates Ace2p transcriptional activity and polarized morphogenesis. Mol. Biol. Cell *14*, 3782–3803.

Ozaki-Kuroda, K., Yamamoto, Y., Nohara, H., Kinoshita, M., Fujiwara, T., Irie, K., and Takai, Y. (2001). Dynamic localization and function of Bni1p at the sites of directed growth in *Saccharomyces cerevisiae.* Mol. Cell. Biol. *21*, 827–839.

Pearson, W. R. (1990). Rapid and sensitive sequence comparison with FASTP and FASTA. Methods Enzymol. *183*, 63–98.

Petersen, J., Nielsen, O., Egel, R., and Hagan, I. M. (1998a). F-actin distribution and function during sexual differentiation in *Schizosaccharomyces pombe.* J. Cell Sci. *111 (Pt 7),* 867–876.

Petersen, J., Nielsen, O., Egel, R., and Hagan, I. M. (1998b). FH3, a domain found in formins, targets the fission yeast formin Fus1 to the projection tip during conjugation. J. Cell Biol. *141*, 1217–1228.

Pruyne, D., Evangelista, M., Yang, C., Bi, E., Zigmond, S., Bretscher, A., and Boone, C. (2002). Role of formins in actin assembly: nucleation and barbed-end association. Science *297*, 612–615.

Pruyne, D., Gao, L., Bi, E., and Bretscher, A. (2004). Stable and dynamic axes of polarity use distinct formin isoforms in budding yeast. Mol. Biol. Cell *15*, 4971–4989.

Reynaga-Pena, C. G., and Bartnicki-Garcia, S. (1997). Apical branching in a temperature sensitive mutant of *Aspergillus niger.* Fungal Genet. Biol. *22*, 153–167.

Rossanese, O. W., Reinke, C. A., Bevis, B. J., Hammond, A. T., Sears, I. B., O'Connor, J., and Glick, B. S. (2001). A role for actin, Cdc1p, and Myo2p in the inheritance of late Golgi elements in *Saccharomyces cerevisiae.* J. Cell Biol. *153*, 47–62.

Sagot, I., Klee, S. K., and Pellman, D. (2002a). Yeast formins regulate cell polarity by controlling the assembly of actin cables. Nat. Cell Biol. *4*, 42–50.

Sagot, I., Rodal, A. A., Moseley, J., Goode, B. L., and Pellman, D. (2002b). An actin nucleation mechanism mediated by Bni1 and profilin. Nat. Cell Biol. *4*, 626–631.

Sambrook, J., Russel, D. W., and Sambrook, J. (2001). Molecular Cloning: A Laboratory Manual, Cold Spring Harbor, NY: Cold Spring Harbor Laboratory.

Schott, D. H., Collins, R. N., and Bretscher, A. (2002). Secretory vesicle transport velocity in living cells depends on the myosin-V lever arm length. J. Cell Biol. *156*, 35–39.

Seiler, S., and Plamann, M. (2003). The genetic basis of cellular morphogenesis in the filamentous fungus *Neurospora crassa.* Mol. Biol. Cell *14*, 4352–4364.

Sharpless, K. E., and Harris, S. D. (2002). Functional characterization and localization of the *Aspergillus nidulans* formin SEPA. Mol. Biol. Cell *13*, 469–479.

Sheu, Y. J., Santos, B., Fortin, N., Costigan, C., and Snyder, M. (1998). Spa2p interacts with cell polarity proteins and signaling components involved in yeast cell morphogenesis. Mol. Cell. Biol. *18*, 4053–4069.

Shimada, A., Nyitrai, M., Vetter, I. R., Kuhlmann, D., Bugyi, B., Narumiya, S., Geeves, M. A., and Wittinghofer, A. (2004). The core FH2 domain of diaphanous-related formins is an elongated actin binding protein that inhibits polymerization. Mol. Cell *13*, 511–522.

Sikorski, R. S., and Hieter, P. (1989). A system of shuttle vectors and yeast host strains designed for efficient manipulation of DNA in *Saccharomyces cerevisiae.* Genetics *122*, 19–27.

Sil, A., and Herskowitz, I. (1996). Identification of asymmetrically localized determinant, Ash1p, required for lineage-specific transcription of the yeast *HO* gene. Cell *84*, 711–722.

Simon, V. R., Swayne, T. C., and Pon, L. A. (1995). Actin-dependent mitochondrial motility in mitotic yeast and cell-free systems: identification of a motor activity on the mitochondrial surface. J. Cell Biol. *130*, 345–354.

Sone, T., and Griffiths, A. J. (1999). The frost gene of *Neurospora crassa* is a homolog of yeast *cdc1* and affects hyphal branching via manganese homeostasis. Fungal Genet. Biol. *28*, 227–237.

Steiner, S., and Philippsen, P. (1994). Sequence and promoter analysis of the highly expressed *TEF* gene of the filamentous fungus *Ashbya gossypii.* Mol. Gen. Genet. *242*, 263–271.

Steiner, S., Wendland, J., Wright, M. C., and Philippsen, P. (1995). Homologous recombination as the main mechanism for DNA integration and cause of rearrangements in the filamentous ascomycete *Ashbya gossypii.* Genetics *140*, 973–987.

Storici, F., Lewis, L. K., and Resnick, M. A. (2001). In vivo site-directed mutagenesis using oligonucleotides. Nat. Biotechnol. *19*, 773–776.

Takizawa, P. A., DeRisi, J. L., Wilhelm, J. E., and Vale, R. D. (2000). Plasma membrane compartmentalization in yeast by messenger RNA transport and a septin diffusion barrier. Science *290*, 341–344.

Vieira, J., and Messing, J. (1991). New pUC-derived cloning vectors with different selectable markers and DNA replication origins. Gene *100*, 189–194.

Virag, A., and Griffiths, A. J. (2004). A mutation in the *Neurospora crassa* actin gene results in multiple defects in tip growth and branching. Fungal Genet. Biol. *41*, 213–225.

Wallar, B. J., and Alberts, A. S. (2003). The formins: active scaffolds that remodel the cytoskeleton. Trends Cell Biol. *13*, 435–446.

Watanabe, N., Kato, T., Fujita, A., Ishizaki, T., and Narumiya, S. (1999). Cooperation between mDia1 and ROCK in Rho-induced actin reorganization. Nat. Cell Biol. *1*, 136–143.

Watanabe, N., Madaule, P., Reid, T., Ishizaki, T., Watanabe, G., Kakizuka, A., Saito, Y., Nakao, K., Jockusch, B. M., and Narumiya, S. (1997). p140mDia, a mammalian homolog of *Drosophila* diaphanous, is a target protein for Rho small GTPase and is a ligand for profilin. EMBO J. *16*, 3044–3056.

Wendland, J., Ayad-Durieux, Y., Knechtle, P., Rebischung, C., and Philippsen, P. (2000). PCR-based gene targeting in the filamentous fungus *Ashbya gossypii.* Gene *242*, 381–391.

Wendland, J., and Philippsen, P. (2000). Determination of cell polarity in germinated spores and hyphal tips of the filamentous ascomycete *Ashbya gossypii* requires a rhoGAP homolog. J. Cell Sci. *113*(Pt 9), 1611–1621.

Wendland, J., and Philippsen, P. (2001). Cell polarity and hyphal morphogenesis are controlled by multiple rho-protein modules in the filamentous ascomycete *Ashbya gossypii.* Genetics *157*, 601–610.

Wright, M. C., and Philippsen, P. (1991). Replicative transformation of the filamentous fungus *Ashbya gossypii* with plasmids containing *Saccharomyces cerevisiae* ARS elements. Gene *109*, 99–105.

Xu, Y., Moseley, J. B., Sagot, I., Poy, F., Pellman, D., Goode, B. L., and Eck, M. J. (2004). Crystal structures of a Formin Homology-2 domain reveal a tethered dimer architecture. Cell *116*, 711–723.

Zahner, J. E., Harkins, H. A., and Pringle, J. R. (1996). Genetic analysis of the bipolar pattern of bud site selection in the yeast *Saccharomyces cerevisiae.* Mol. Cell. Biol. *16*, 1857–1870.

Part II

Cytokinesis and septation in the filamentous fungus *Ashbya gossypii*

Cytokinesis and septation in *Saccharomyces cerevisiae* and *Schizosaccharomyces pombe* occurs by the action of over sixty components including those of the actomyosin system. Although homologs of all these genes are present in the genome of *Ashbya gossypii*, cell separation does not occur in its multinucleated hyphae. Here we present the events that take place during septation in *A. gossypii*. By 3D live cell imaging we analyzed the role of cytokinetic key players, i.e. actin, PCH protein, septins, myosin II, formins, landmark proteins, and IQGAP. Septins constantly localize as thin filaments to the cortex of apical compartments. They mark future septa at the very hyphal tip when localizing as a collar of cortical bars (CCB). The PCH protein *Ag*Hof1 colocalizes with septins as CCBs at future septa. These bars condense to a single ring colocalizing with the actin ring. The ring contracts as the septum is formed. CCBs and rings can persist up to 5 hours but the ring closure rate is comparable to *S. cerevisiae* and *S. pombe*. Concomitant with ring contraction cytokinesis occurs and the chitin-rich septum is formed but the hyphal compartments do not separate. This allows us to divide septation in *A. gossypii* into five stages: Site selection, septal proteins localize as CCBs to future septa. Bar-to-ring transition, CCBs of landmark proteins condense to double rings that delimit the single rings of adaptor proteins. Contractile ring assembly and persistence, actin localizes to the single rings. Ring contraction and cytokinesis, the single rings contract, the plasma membrane is constricted and the septum is deposited. Septum maturation, the proteins involved in septation delocalize from the septum while the septum is strengthened. It is to emphasize that all these events take place simultaneously in a continuous cytoplasm at different septa of one hypha. A possible reason for cell separation not to occur is that two major enzymes required for cell separation in *S. cerevisiae* are not present in *A. gossypii.*

Introduction

Cytokinesis (division of the cytoplasm) is a process that is conserved between higher eukaryotes and fungi and precedes cell separation (Nanninga, 2001). Basically all these cells, except plants, use an actin-based contractile ring to constrict the plasma membrane and to separate the cytoplasm of the two daughter cells during cytokinesis. In animal cells a contractile actin ring forming at the cleavage furrow was described more than thirty years ago (Forer and Behnke, 1972; Perry *et al.*, 1971; Schroeder, 1973). In 1986 such a cytokinetic ring was described in the fission yeast *Schizosaccharomyces pombe* (Marks *et al.*, 1986) and only in 1998 in the budding yeast *Saccharomyces cerevisiae* (Bi *et al.*, 1998). More than sixty components contribute to the process of cytokines and most of them are conserved from yeast to humans (revied by Balasubramanian *et al.*, 2004).

One main difference between fungal and animal cells is that fungi possess rigid cell walls, composed mainly of mannoproteins, glucan, and chitin (Carlile *et al.*, 2000), allowing them to grow in a variety of osmotic conditions. This osmotic barrier must be maintained during cytokinesis. Therefore, contraction of an actomyosin ring is followed by the formation of a chitin-rich septum. In yeasts, secondary septa and new cell walls will form on either side of the primary septum that is finally degraded leading to complete cell separation and to the formation of two daughter cells. In contrast to unicellular fungi, actin ring contraction and septation do not lead to cell separation in filamentous ascomycetes. The cells stay attached and form hyphae. Hyphal filaments are multinucleated, with either multiple nuclei between two septa or one nucleus per compartment, depending on how the nuclear cycle is coordinated with septation. Although the outcome of actin ring contraction and septation is fundamentally different in yeast-like and filamentous ascomycetes, the components involved seem to be conserved as well (reviewed by Gladfelter, 2006; Walther and Wendland, 2003).

The septin protein family (Cdc3, Cdc10, Cdc11, and Cdc12) was initially discovered in the Hartwell screen for yeast cell division cycle (Cdc) mutants as factors essential for cytokinesis (Hartwell, 1971). In budding yeast they help control the morphogenesis checkpoint, the spindle-alignment checkpoint, chitin deposition, and bud-site selection (Byers and Goetsch, 1976; Dobbelaere and Barral, 2004; Gladfelter *et al.*, 2005). Additionally, they work as diffusion barriers to maintain the polarity of the mother-bud plasma membrane (Barral *et al.*, 2000; Takizawa *et al.*, 2000) and act as 'corral' to trap proteins at the site of cytokinesis (Dobbelaere and Barral, 2004). In fission yeast septin homologs are not essential, but

the absence of any or all of them causes a delay in the completion of cell division (An *et al.*, 2004; Berlin *et al.*, 2003; Tasto *et al.*, 2003; Wood *et al.*, 2002). Septin homologs with conserved function in cytokinesis have been found throughout eukaryotes, with the exception of plants.

To date, septins have been characterized to some extent in the filamentous fungi *Ashbya gossypii*, *Candida albicans*, and *Aspergillus nidulans*. Strikingly, septins of filamentous fungi form higher-order structures with different appearances and potentially different functions within one hypha. *A. gossypii* septins localize to cortical bars at hyphal tips, rings at septation sites, and asymmetric bar structures at branch bases (Helfer, 2006; Helfer and Gladfelter, 2006). Septins of *C. albicans* form a diffuse cap at hyphal tips, double and single rings at septation sites, a diffuse band at the base of hyphae, and filaments in chlamydospores (Sudbery, 2001; Warenda and Konopka, 2002). In *A. nidulans* septins localize to single and double rings at septation sites and prior to branch emergence at the cortex of hyphae (Momany *et al.*, 2001; Westfall and Momany, 2002). Apart from septins several other proteins that play conserved roles in cytokinesis have been characterized in *A. gossypii*. The IQGAP-related proteins *Sc*Iqg1, *Sp*Rng2, and *Ag*Cyk1 are all essential for actin ring formation (Eng *et al.*, 1998; Epp and Chant, 1997; Lippincott and Li, 1998b; Wendland and Philippsen, 2002). The N-terminal calponin homology domain of *Sc*Iqg1 is responsible for actin ring assembly, whereas the C-terminal GTPase activating domain is required for ring constriction (Shannon and Li, 1999). Analysis of *AgBUD3*, a homolog of the *S. cerevisiae* bud gene *ScBUD3*, showed that *Ag*Bud3 is involved in septation due to its role in correctly localizing *Ag*Cyk1 (Wendland, 2003a). Additionally, deletion of the PAK-like protein kinase *Ag*Cla4, a putative downstream effector of the well conserved Rho-type GTPase *Ag*Cdc42, severely impairs actin ring formation and septation (Ayad-Durieux *et al.*, 2000). This indicates that *Ag*Cdc42 signalling is not only essential for polarized growth (Wendland and Philippsen, 2001) but for septation as well.

Only recently, Pombe Cdc15 homology (PCH) proteins have emerged in many species as important coordinators of actomyosin assembly and membrane dynamics. *S. pombe* Cdc15 is the founding member of the PCH protein family (Fankhauser et al., 1995). Genes encoding PCH proteins have been identified in most eukaryotes, except in plants, and are implicated in many human diseases reaching from autoinflammatory diseases to cancer (revieved by Aspenstrom et al., 2006). These proteins are characterized by the presence of several conserved sequence and structural motifs. Most PCH family proteins contain an N-terminal FER-CIP4 Homology (FCH) domain (Aspenstrom, 1997), a region with coiled-coil forming potential near their amino termini, a Src homology domain 3 (SH3) at the carboxyl termini, and proline - glutamic acid - serine - threonine rich (PEST) sequences between the coiled-coil region and the SH3 domain (reviewed by Aspenstrom et al., 2006); Lippincott and Li, 2000). Many of the PCH proteins are involved in actin based processes, especially in cytokinesis. *S. pombe* Cdc15 interacts directly with the Arp2/3 complex in actin patches and the formin *Sp*Cdc12 during cytokinesis (Carnahan and Gould, 2003; Chang et al., 1997). It is a key element downstream of the septation initiation network (SIN) and plays an essential role in actomyosin ring assembly and maintenance after anaphase, but it is dispensable for ring assembly early in mitosis (Wachtler et al., 2006). Consistent with the results from *S. pombe*, *S. cerevisiae* Hof1/Cyk2 interacts via its SH3 domain with the formin *Sc*Bnr1 (Kamei et al., 1998) and disruption of *ScHOF1* does not affect the assembly of the actomyosin ring but results in rapid disassembly of the ring during the contraction phase, leading to incomplete cytokinesis (Lippincott and Li, 1998a). *Sc*Hof1 is bound by *Sc*Grr1 at its PEST domain to promote its cell-cycle dependent degradation by $Sc\text{SCF}^{\text{Grr1}}$ after mitotic exit network (MEN) activation at the end of mitosis, which is necessary to allow efficient contraction of the actomyosin ring and cell separation during cytokinesis (Blondel et al., 2005). Recently it was shown for the human formin-binding protein 17 (FBP17) that the FCH domain together with the predicted coiled-coil region shows weak homology to the Bin-amphiphysin-Rvs (BAR) domain, that it binds phospholipids, and that it can deform membranes *in vitro*. Thus, the FCH and coiled-coil domains are likely to be one unit involved in the interaction with membrane phospholipids and have been referred to as both an EFC (extended FCH) domain (Tsujita et al., 2006) and an F-BAR (FCH and BAR) domain (Itoh et al., 2005). This indicates that PCH protein family members can couple membrane deformation to the actin cytoskeleton as it is required during cytokinesis when the actin ring contracts.

So far, PCH proteins have not been characterized in filamentous fungi. Here, we identify a PCH protein in the filamentous fungus *A. gossypii* and characterize its role in septation. Deletion of *AgHOF1* results in the inability to undergo septation, as concluded by the absence of actin ring formation and the lack of chitin accumulation at sites where septa would be expected. The absence of *Ag*Hof1 does not interfere with polarized hyphal tip growth, lateral branching, and tip splitting. *Ag*Hof1 firstly localizes as a collar of cortical bars at incipient sites of septation, similar to septins, then forms a cortical ring that finally contracts concomitantly with septum formation. *Ag*Hof1 interacts via its SH3 domain with formins and we propose a role for this domain in actin ring integrity. Furthermore, for the first time in

filamentous fungi, we analyze the dynamics of proteins essential for septation, using 4D microscopy. Thereby we cannot only draw a time scale for septation but we also gain new insights into the behavior of the septin *Ag*Sep7, the IQGAP *Ag*Cyk1, the cortical landmark protein *Ag*Bud3, and the type II myosin *Ag*Myo1.

Materials and Methods

Ashbya gossypii strains, media and transformation

Strains *ATCC10895* (Ashby and Nowell, 1926) and *ΔlΔt* (Altmann-Johl and Philippsen, 1996) will be referred to as wild type. All strains were cultured as described in (Steiner *et al.*, 1995; Wright and Philippsen, 1991). Apart form full medium (AFM; Wright and Philippsen (1991) two slightly different synthetic defined drop-out media were used: ASD (*Ashbya* drop-out medium) is composed of 20 g/l D-glucose, 1.7 g/l YNB without amino acids and ammonium sulfate (Becton, Dickinson and Co., Sparks, MD, USA), 0.69 g/l CSM-LEU (Bio101 Systems, Qbiogene, Morgan Irvine, CA, USA), 1 g/l L-asparagine, 1 g/l myo-inositol, pH 6.2. ASC (*Ashbya* synthetic complete) contains instead of CSM-LEU 1.8 g/l SC-LEU (Bio101 Systems, Qbiogene, Morgan Irvine, CA, USA) and instead of L-asparagine 7 g/l L-glutamic acid monopotassium salt monohydrate and 7 g/l L-aspartic acid potassium salt hemihydrate. Both media were supplemented with 100 mg/l L-leucine when necessary. We found that general growth of *A. gossypii* but especially sporulation was better on ASC compared to ASD or previously published synthetic defined media for *A. gossypii* (data not shown). Strains were constructed either by PCR-based gene targeting as described by (Wendland *et al.*, 2000) or by transformation with linear DNA fragments with long flanking homology regions (~ 200 – 1000 bp) made from plasmids that carry the gene with the mutation to be introduced. All strains with description are listed in Table 1. PCR templates and primer names or plasmids and restriction enzymes used for strain construction are given in Table 1. All oligonucleotides used and purpose of use are listed in Table 2. Description of plasmids used for strain constructions are listed in Table 3. Strains were verified by analytical PCR according to (Wendland *et al.*, 2000) using a PTC 100 thermocycler (MJ Research, Waltham, MA, USA).

DNA manipulations and sequencing

All DNA manipulations were carried out according to Sambrook and Russell (2001) with *E. coli* strain DH5αF' as host (Hanahan, 1983). For recombination of plasmids and PCR products they were cotransformed according to Gietz *et al.* (1995) into yeast host strain FY1679 (Winston *et al.*, 1995) derivative DY3 (*MATα his3Δ200 trp1Δ63 leu2Δ1 ura3-52Δ*). Plasmids were isolated from yeast using the 'High Pure Plasmid Purification Kit' (Roche Diagnostics, Rotkreuz, Switzerland) with a modified protocol as described in Schmitz *et al.* (2006). Sequencing was done by Microsynth AG (Balgach, Switzerland).

Plasmids and constructs

All plasmids and details of construction are listed in Table 3. PCR products were either cloned into the backbones, using restriction sites added by the primers, or cotransformed together with the vectors into yeast to allow recombination of the vectors and the PCR products, which contained flanking homologies to the vector added by the primers. If selection for the PCR product was not possible the vectors were linearized prior to cotransformation to allow selection for the backbone. All primers, templates, and restriction enzymes used are listed in Table 3.

Actin, chitin, membrane, and immunofluorescence stainings

Actin staining with either Alexa Fluor® 488, Alexa Fluor® 568, or rhodamine phalloidin (Molecular Probes, Eugene, OR, USA) and chitin staining with calcofluor white (fluorescent brightener 28; Sigma-Aldrich Chemie GmbH, Steinheim, Germany) was done as previously described (Ayad-Durieux *et al.*, 2000; Knechtle *et al.*, 2003; Pringle *et al.*, 1989). The protocol for membrane staining with the lipophilic styryl compound FM® 4-64 (Molecular Probes, Eugene, OR, USA) was adapted from Fischer-Parton *et al.* (2000). To visualize the septins *Ag*Cdc11A/B and *A. gossypii* cells were processed for immunofluorescence as described for yeast cells (Pringle *et al.*, 1991) with slight modifications for *A. gossypii* (Gladfelter *et al.*, 2006a). Primary antibody rabbit anti-*Sc*Cdc11 (Santa Cruz Biotechnology, Santa Cruz, CA, USA) was used 1:20. Secondary antibody Alexa Fluor® 568 goat anti-rabbit IgG (H+L) (Molecular Probes, Eugene, OR, USA) was used 1:200.

Microscopy techniques, image acquisition and processing

The microscopy setup used was the same as described in (Knechtle *et al.*, 2003) except that a CoolSNAP HQ camera (Photometrics, Tucson, AZ, USA) was used. The illumination light source for fluorescence microscopy was either a 75 W XBO® short arc lamp (OSRAM GmbH, Augsburg, Germany) or a Polychrome V monochromator (TILL Photonics GmbH, Gräfelfing, Germany). The Z distance between two planes in stack acquisitions was set between 0.3 – 1 µm. DIC and single plane fluorescence images were processed using the 'Scale image' feature in MetaMorph 6.2r6 (Molecular

Table 1: *A. gossypii* strains used in this study

Strain	Genotype	Construction	Reference
ATCC10895	*wild type*	-	Ashby and Nowell, 1926
ΔlΔt	*leu2Δ thr4Δ*	-	Altmann-Johl and Philippsen (1996)
AgHPH08	*SEP7-GFP-NATPS leu2Δ thr4Δ*	-	Helfer and Gladfelter, 2006
AgHPH04	*ade2::ADE2-HHF1-GFP leu2Δ thr4Δ*	-	Helfer, 2006
PK62	*cyk1Δ::nat1 BOI1/2-GFP-GEN3 leu2 thr4*	-	Knechtle *et al.*, 2006
AMK007	hof1Δ::GEN3	pGEN3; PCR 02.126/02127	this study
AMK009	*hof1Δ::NATPS leu2Δ thr4Δ*	pAMK171, AatII, SacII	this study
AMK010	*hof1Δ::GEN3 SEP7-GFP-NAT1 leu2Δ thr4Δ*	pGEN3; PCR 02.126/02127	this study
AMK032	*hof1Δ::NATPS BUD3-GFP-GEN3 leu2Δ thr4Δ*	pAMK171, AatII, SacII	this study
AMK034	*hof1Δ::NATPS MYO1-GFP-GEN3leu2Δ thr4Δ*	pAMK171, AatII, SacII	this study
AMK012	*HOF1-GFP-NATPS leu2Δ thr4Δ*	pAMK157; StuI, SacII	this study
AMK036	*HOF1-CFP-NATPS leu2Δ thr4Δ*	pAMK105; BsmI, StuI, XmnI	this study
AMK036	*bud3Δ::GEN3 HOF1-GFP-NATPS leu2Δ thr4Δ*	pAMK134; BssSI, BsrBI	this study
AMK015	*BUD3-GFP-GEN3 leu2Δ thr4Δ*	pAMK121; BssSI, XhoI	this study
AMK016	*BUD3-YFP-GEN3 HOF1-CFP-NATPS leu2Δ thr4Δ*	pAMK122; BssSI, XhoI	this study
AMK030	*cyk1Δ::GEN3 HOF1-GFP-NATPS leu2Δ thr4Δ*	pAMK133; MunI, BsrBI	this study
AMK020	*CYK1-YFP-GEN3 HOF1-CFP-NATPS leu2Δ thr4Δ*	pAMK127; BsrBI, AvaI, ApaLI, BspHI	this study
AMK021	*MYO1-GFP-GEN3 leu2Δ thr4Δ*	pAMK138; BssSI, BsrBI	this study
AMK022	*MYO1-RedStar2-GEN3 HOF1-GFP-NATPS leu2Δ thr4Δ*	pAMK141; BssSI, BsrBI	this study
AMK029	*myo1Δ::GEN3 HOF1-CFP-NATPS leu2Δ thr4Δ*	pAGT140; PCR M1-S1, M1-S2	this study
AMK025	*hof1Δ7-210-GFP-NATPS leu2Δ thr4Δ*	pAMK153; AatII, SacII	this study
AMK023	*hof1Δ1333-1404-GFP-NATPS leu2Δ thr4Δ*	pAMK155; AatII, SacII	this study
AMK024	*hof1Δ1861-2052-YFP-NATPS leu2Δ thr4Δ*	pAMK156; StuI, SacII	this study

Devices Corp., Downingtown, PA, USA). If necessary, stacks were deblurred with either MetaMorph's 'Nearest Neighbors' or 'No Neighbors' tool or using '3D blind deconvolution' of AutoDeblur 7 (MediaCybernetics, Silver Spring, MD, USA), flattened by maximum projection with MetaMorph's 'Stack Arithmetics' and scaled as mentioned above. Tilted views of stacks were made with MetaMorph's '3D reconstruction'. Fluorescence and DIC images were colored and overlaid using MetaMorph's 'Overlay Images' tool. For time-lapse acquisitions spores or small pieces of mature mycelium were cultured on 'time-lapse slides', glass slides with a cavity (ROTH AG, Reinach, Switzerland) that were filled with 1 % agarose in ¾ ASC or ASD and ¼ AFM to reduce autofluorescence of the medium but to provide enough nutrients for optimal growth. Ideally 'time-lapse slides' should have an air bubble in the center of the agarose-filled cavity, which is believed to provide oxygen during time-lapse acquisitions. The slides were incubated in a humid chamber without cover slip until the mycelia reached the desired developmental stage. Then a cover slip was applied and the slides were placed under the microscope. Alternatively, 1 ml of the same medium was spread onto normal microscopy slides. After solidification of the thin agarose layer small pieces of mycelium were placed on the slide, 100 µl of liquid medium were added and a cover slip was applied. The slides were incubated as described above. The acquisition frequencies varied between 1 – 0.2 min^{-1}. The time-lapse picture series were exported from MetaMorph

Table 2: Primers used in this study

	Name	Sequence (5'→3')	use
02.126	AgHOF1-S1	**AGGCGGGCGCGAGGAAAAGACAGCTGGGTGGTAAAGGAGC**GCTAGGGATAACAGGGTAAT	gene targeting
02.127	AgHOF1-S2	**CAGGCGCCACGCTTTGTTACAGTTTTGATTGGTCTTCGCT**AGGCATGCAAGCTTAGATCT	gene targeting
02.128	AgHOF1-G1	GAGCGGGCCTCGAGGAGATG	analytical PCR
02.129	AgHOF1-G4	GCAGTCGATGGCCATCCTTG	analytical PCR
02.130	AgHOF1-I1	GTTTCGAGTGGCTCTGGGCC	analytical PCR
03.476	AgHOF1-I2	CAACGCACGGAAATGAGTGG	analytical PCR
03.477	AgHOF1-G5	AATAGTCCTTTGCGGTGGCC	analytical PCR
04.273	AgHOF1Fus1	**TATCGGGGAAGTCCACAATGGGAACGGCAAGCAGGGGCTCATTCCGATGAACTACGTG GAACTGCTCTC**CAAAACGACGGCCAGTGAATTCG	gene targeting
04.274	AgHOF1 S2	**CGTTACAACGTCCTAATATGTAATAGTCCTTTGCGGTGGCCAGGCGCCACGCTTTGT TACAGTTTTGATT**ACCATGATTACGCCAAGCTTGC	gene targeting
04.474	AgHOF1-NS1	**AGGCGGGCGCGAGGAAAAGACAGCTGGGTGGTAAAGGAGC**CCAGTGAATTCGAGCTCGG	gene targeting
04.485	AgHOF1-5'SmaI	GAATAAcccgggCAGACACAAGGGACATATCG	cloning
04.486	AgHOF1-3'ApaI	GAATgggcccCCAGATAGAACAGGCTACAC	cloning
05.257	AgHOF1dSH3-F1	**ACCAAAAGCGTTGCGATGGAGTGGCCCAAGGTCACCAGCAAGGGTCGC** AAAACGACGGCCAGTGAATTCG	gene targeting
05.297	AgHOF1-I3	ACGTAGGGCTGTTCGTGAGC	analytical PCR
05.350	AgHOF1-I4	AAACTGGAGAAGGCGAAGGC	analytical PCR
05.363	AgHOF1-G1.1	CACGCGGGACGTGTATCATC	analytical PCR
05.364	AgHOF1-I5	CGCTTGGCGCTCTTGTACTC	analytical PCR
04.481	AgCYK1-5'SmaI	GAATAAcccgggGAAACGCTTTCACTTTACAC	cloning
04.482	AgCYK1-3'ApaI	GAATgggcccTGCTTCGACAACTTACTATG	cloning
05.009	CYK-G1	TAGAGACCACGGCATTTG	analytical PCR
05.010	CYK-G4	GGCTGCTTTCTCCTATTG	analytical PCR
05.135	AgCYK1-F1	**AGGAGCGCAACTTTTAAAATATCAGCGCTAATAGACCTACTTTGTGAAGTGTTTTTTAGG** AAAACGACGGCCAGTGAATTCG	gene targeting
05.196	AgCYK1-F2	**CCGTATTAATTATTATTGTTGTCCTTATCCATCGTTACGTAAGTATAA** ACCATGATTACGCCAAGCTTGC	gene targeting
06.330	S1_cyk1_gen3	**ACTCGAGTTGGCAGCTGGTAATTCAATGCGCGACGGCTATTTTTT** GCTAGGGATAACAGGGTAATACAGAT	gene targeting
06.331	S2_cyk1_gen3	**CGCCTACCAAATCCATCAGCGAAAAAAAAGCATTAATATTCTGTG** AGGCATGCAAGCTTAGATCTGATGA	gene targeting
06.332	G1_cyk1	GAATTTCTCTGTAGAGTTGG	analytical PCR
06.333	G4_cyk1	GGCTGCTTTCTCCTATTG	analytical PCR
05.196	AgCYK1-F2	CCGTATTAATTATTATTGTTGTCCTTATCCATCGTTACGTAAGTATAA**ACC** ATGATTACGCCAAGCTTGC	gene targeting
04.483	AgBUD3-5'SmaI	GAATAAcccgggAGCACCAGATGCAATGTACG	cloning
04.484	AgBUD3-3'ApaI	GATAgggcccATGGCTTCAGCTCACAGAAC	cloning
05.044	AgBUD3-F1	**GAGCAGCAAGATAAGAAATTGGCAGCTAACACGGACGAGATGGATTCCGCTAGACGTCTT** AAAACGACGGCCAGTGAATTCG	gene targeting
05.045	AgBUD3-F2	**AATATTCATTGTATACAGACTAGCATTGGCAATATGATAACTGGCTTACGGTGTAATATT** ACCATGATTACGCCAAGCTTG	gene targeting
06.334	G1_bud3	CGACTAGAACGTTGGTATGCGTG	analytical PCR
06.335	G4_bud3	CATGGCATCGCGCCTGATGGTATG	analytical PCR
06.336	I1_bud3	CACGGAGTGCAGGTGCATGAC	analytical PCR
06.337	Agbud3_S1_gen3	**GTCACGGCCATATCAGATTTCAACGACGGGTAGTTGACTGAGCT** GCTAGGGATAACAGGGTAATACAGAT	gene targeting
06.338	Agbud3_S2_gen3	**GATAACTGGCTTACGGTGTAATATTAGTTGAGTATAATTATGAT** AGGCATGCAAGCTTAGATCTGATGA	gene targeting
	M1-S1	**AAGGAACGAGAAGTGCTGGAGGTGGAGACCGCGGCGGTGAATCCG** GCTAGGGATAACAGGGTAAT	gene targeting
	M1-S2	**TTGATTCTCAGAGCTTCTTCCTGTATCTGCTCAATAAGCGATTCA** AGGCATGCAAGCTTAGATCT	gene targeting
05.040	AgMYO1-F1	**TACAAAGGACTATCGACACATCGCAGGAGTTTGGCGCAGTCAACGGAGGAGGTGTTAATA** AAAACGACGGCCAGTGAATTCG	gene targeting

05.041	AgMYO1-F2	**CATATATGCCTCATAAACAAGAACAAAATTACATATTACATCATTGCTGAATCGCATATA** ACCATGATTACGCCAAGCTTG	gene targeting
05.042	AgMYO1-I1	CTTGAAATGCGGCTGAACG	analytical PCR
05.043	AgMYO1-G4	GTCACACCCGAAGACTGTATG	analytical PCR
04.011	green2.2	TGTAGTTCCCGTCATCTTTG	analytical PCR
04.199	V2PDC1P	GAACAAACCCAAATCTGATTGCAAGGAGAGTGAAAGAGCCTT	analytical PCR
04.200	V3PDC1T	GACCAGACAAGAAGTTGCCGACAGTCTGTTGAATTGGCCTG	analytical PCR
04.314	G3.2	ctccaactcggcactattttac	analytical PCR
05.291	RedI	GAATGGCAGTGGACCACCCTTAG	analytical PCR
05.293	dFCH-5'	CGCATAGGCGGGCGCGAGGAAAAGACAGCTGGGTGGTAAAGGAGCATGGCAtacgggaac	recombination
05.294	dFCH-3'	TTGCTCTGCTCCGCCCGGCAGAGCTCCGCACACTTCTGCATGTTCCCGTAtgccatgctc	recombination
05.295	dPEST-5'	ACTGAGATACGTAGGGCTGTTCGTGAGCAGCAGCTACAGCATCGCGAGGGCagcatggcc	recombination
05.296	dPEST-3'	TGCGTACGAGGAGATGGACGTTACCATCGAGTCCGCACTCGTGGCCATGCTgccctcgcg	recombination
05.349	G2.3	GGAGGTAGTTTGCTGATTGG	analytical PCR
06.204	V3*nat1	ACATGAGCATGCCCTGCCCC	analytical PCR
05.287	AgHOF1 5'-SH3	**gacgtaccagattacgctcatatggccatggaggccagtgaattc**CGTGTTATCGGCTACGCGC	2-hybrid
05.288	AgHOF1 3'-SH3	**tctgcagctcgagctcgatg**	2-hybrid
05.275	AgBNI1 5'-FH1	**ctgatctcagaggaggacctgcatatggccatggaggccgaattc**ACTGATGCGAAAGATGTACAG	2-hybrid
05.276	AgBNI1 3'-FH1	**ggttatgctagttatgcggccgctgcaggtcgacggatcccccggg**TTAGGAACGACCCAGTTGTGG	2-hybrid
05.277	AgBNI1 5'-FH2	**ctgatctcagaggaggacctgcatatggccatggaggccgaattc**TATCCTCGTCCGAAGAAGAAG	2-hybrid
05.278	AgBNI1 3'-FH2	**ggttatgctagttatgcggccgctgcaggtcgacggatcccccggg**TTACTTGCGTGCGGAGGACGG	2-hybrid
05.279	AgBNR1 5'-FH1	**ctgatctcagaggaggacctgcatatggccatggaggccgaattc**ACCAGACCTTTGATACCACCG	2-hybrid
05.280	AgBNR1 3'-FH1	**ggttatgctagttatgcggccgctgcaggtcgacggatcccccggg**TTATGTCGAAGGTGGTGATGGC	2-hybrid
05.281	AgBNR1 5'-FH2	**ctgatctcagaggaggacctgcatatggccatggaggccgaattc**CGGATCAAGCTCAAACAGATC	2-hybrid
05.282	AgBNR1 3'-FH2	**ggttatgctagttatgcggccgctgcaggtcgacggatcccccggg**TTACAGAAGCCGGCGGCGCTTC	2-hybrid
05.283	AgBNR2 5'-FH1	**ctgatctcagaggaggacctgcatatggccatggaggccgaattc**CATAGAAAGTTGCACGAAACC	2-hybrid
05.284	AgBNR2 3'-FH1	**ggttatgctagttatgcggccgctgcaggtcgacggatcccccggg**TTATGGACCCTGCAATGAACAAC	2-hybrid
05.285	AgBNR2 5'-FH2	**ctgatctcagaggaggacctgcatatggccatggaggccgaattc**TCTCCTACTTCACAGCGTGTG	2-hybrid
05.286	AgBNR2 3'-FH2	**ggttatgctagttatgcggccgctgcaggtcgacggatcccccggg**TTACTTGAACAAAGCAACAAAGTC	2-hybrid

Flanking homologous sequences are indicated in bold

Restriction sites are indicated in lower case characters

Table 3: Plasmids used in this study

Plasmid	Description	Source or Reference
pUC19	-	Yanisch-Perron *et al.*, 1985
pRS415	-	Sikorski and Hieter, 1989
pRS314	-	Sikorski and Hieter, 1989
pBSII SK(+) Sca-	pBlueskript II lacking ScaI site	Knechtle, P., unpublished
pGADT7	two-hybrid Gal4-activation domain vector	Chien *et al.*, 1991
pGBKT7	two-hybrid Gal4-binding domain vector	Louvet *et al.*, 1997
pVA3	two-hybrid binding domain positive control vector	Clonetech, Mountain View, CA, USA
pTD1	two-hybrid binding domain positive control vector	Clonetech, Mountain View, CA, USA
pAG8331	pRS416-'AgMYO1; *A. gossypii* chromosome 3 from 484569-489257	Mohr, 1997
pHPS218	pGBT9-HOF1	Schmitz, H.P., unpublished
pAGT100	pUC19NATPS; NATPS cassette	Part III of this thesis
pAGT140	GEN3 cassette	Part III of this thesis
pAGT101	GFP-NATPS cassette	Part III of this thesis
pAGT102	CFP-NATPS cassette	Part III of this thesis
pAGT103	YFP-NATPS cassette	Part III of this thesis
pAGT141	GFP-GEN3 cassette	Part III of this thesis
pAGT143	YFP-GEN3 cassette	Part III of this thesis
pGAT144	RedStar2-GEN3 cassette	Part III of this thesis
pAMK100	pRS415-AgHOF1; PCR product amplified from *A. gossypii* genomic DNA with primers 04.485 /04.486., cloned with SmaI/ApaI	this study

pAMK101	pRS415-AgCYK1; PCR product amplified from *A. gossypii* genomic DNA with primers 04.481 /04.482, cloned with SmaI/ApaI	this study
pAMK102	pRS415-AgBUD3, PCR product amplified from *A. gossypii* genomic DNA with primers 04.483/04.484, cloned with SmaI/ApaI	this study
pAMK129	pAghof1Δ::NATPS; pAMK100 recombined with PCR product from pUC19NATPS with primers 04.474/04.274	this study
pAMK104	pAgHOF1-GFP-NATPS; pAMK100 recombined with PCR product from pAGT101 with primers 04.273/04.274	this study
pAMK105	pAgHOF1-CFP-NATPS; pAMK100 recombined with PCR product from pAGT102 with primers 04.273/04.274	this study
pAMK121	pAgBUD3-GFP-GEN3; pAMK102 recombined with PCR product from pAGT141 with primers 05.044/05.045	this study
pAMK122	pAgBUD3-YFP-GEN3; pAMK102 recombined with PCR product from pAGT143 with primers 05.044/05.045	this study
pAMK127	pAgCYK1-YFP-GEN3; pAMK101 recombined with PCR product from pAGT143 with primers 05.135/05.196	this study
pAMK133	pAgcyk1Δ::GEN3; pAMK103 recombined with PCR product from pAGT140 with primers S1_cyk1_gen3/S2_cyk1_gen3	this study
pAMK134	pAgbud3Δ::GEN3; pAMK102 recombined with PCR product from pAGT140 with primers Agbud3_S1_gen3/Agbud3_S2_gen3	this study
pAMK135	pAghof1ΔSH3-YFP-NATPS; pAMK100 recombined with PCR product from pAGT103 with primers 05.257/04.274	this study
pAMK138	p'AgMYO1-GFP-GEN3; pAG8331 recombined with PCR product from pAGT141 with primers 05.040/05.041	this study
pAMK141	p'AgMYO1-RFP-GEN3; pAG8331 recombined with PCR product from pAGT144 with primers 05.040/05.041	this study
pAMK145	pAghof1ΔFCH-GFP-NATPS; AsiSI linearized pAMK104 recombined with annealed and extended primers 05.293/05.294	this study
pAMK128	pRS314 carrying ApaI/XmaI fragment from pAMK100	this study
pAMK149	pRS314-Aghof1ΔPEST; BstBI linearized pAMK128 recombined with annealed and extended primers 05.295/05.296	this study
pAMK150	pAghof1ΔPEST-GFP-NATPS; pAMK104 carrying AsiSI/StuI fragment from pAMK149	this study
pAMK153	pBSII-Aghof1ΔFCH-GFP-NATPS; pBSII SK(+) Sca- carrying SacII fragment from pAMK145	this study
pAMK155	pBSII-Aghof1ΔPEST-GFP-NATPS; pBSII SK(+) Sca- carrying SacII fragment from pAMK150	this study
pAMK156	pBSII-Aghof1ΔSH3-YFP-NATPS; pBSII SK(+) Sca- carrying SacII fragment from pAMK135	this study
pAMK171	pBSII-Aghof1Δ::NATPS; pBSII SK(+) Sca- carrying SacII fragment from pAMK129	this study
pAMK172	pGADT7-HOF1; pGADT7 carrying EcoRI/XmaI fragment from pHPS218	this study
pHPS178	pGBT9-BNI1; pGBT9 carrying complete AgBNI1 ORF in EcoRI/BamHI sites	Schmitz, H.P., unpublished
pHPS177	pGBT9-BNR1; pGBT9 carrying complete AgBNR1 ORF in EcoRI/BamHI sites	Schmitz, H.P., unpublished
pHPS179	pGBT9-BNR2; pGBT9 carrying complete AgBNR2 ORF in EcoRI/BamHI sites	Schmitz, H.P., unpublished
pHPS218	pGBT9-HOF1; pGBT9 carrying complete AgHOF1 ORF in EcoRI/BamHI sites	Schmitz, H.P., unpublished
pAMK179	pGADT7-HOF1SH3; SmaI linearized pGADT7 recombined with PCR product from pAMK100 with primers 05.287/05.288	this study
pBDBNI1FH1	pGBKT7-BNI1FH1; SmaI linearized pGBKT7 recombined with PCR product from pHPS178with primers 05.275/05.276	this study
pAMK180	pGBKT7-BNI1FH2; SmaI linearized pGBKT7 recombined with PCR product from pHPS178 with primers 05.277/05.278	this study
pAMK181	pGBKT7-BNI1FH12; SmaI linearized pGBKT7 recombined with PCR product from pHPS178 with primers 05.275/05.278	this study
pAMK182	pGBKT7-BNR1FH1; SmaI linearized pGBKT7 recombined with PCR product from pHPS177 with primers 05.279/05.280	this study

pAMK183	pGBKT7-BNR1FH2; SmaI linearized pGBKT7 recombined with PCR product from pHPS177 with primers 05.281/05.282	this study
pAMK184	pGBKT7-BNR1FH12; SmaI linearized pGBKT7 recombined with PCR product from pHPS177 with primers 05.279/05.282	this study
pBDBNR2FH1	pGBKT7-BNR2FH1; SmaI linearized pGBKT7 recombined with PCR product from pHPS179 with primers 05.283/05.284	this study
pAMK185	pGBKT7-BNR2FH2; SmaI linearized pGBKT7 recombined with PCR product from pHPS179 with primers 05.285/05.286	this study
pAMK186	pGBKT7-BNR2FH12; SmaI linearized pGBKT7 recombined with PCR product from pHPS179 with primers 05.283/05.286	this study

as 8-bit TIFF files and converted to AVI movies with ImageJ (Wayne Rasband, NIH, Bethesda, MD, USA). Conversion to QuickTime or MPEG4 format was done with QuickTime Pro 7 (Apple Computer, Inc.).

Two-hybrid assay

For two-hybrid experiments pGADT7 and pGBKT7, linearized with SmaI, were cotransformed with PCR products into *S. cerevisiae* strains PJ69-4a (James *et al.*, 1996) and PJ69-4α (Uetz *et al.*, 2000) to construct bait and prey plasmids, respectively, or with previously made bait and prey plasmids. For details of plasmids, primers and templates used see Table 3. Transformants with correct bait and prey plasmids, as judged by colony PCR, were allowed to mate and diploids were selected on plates lacking both, tryptophan and leucine but containing a four-fold concentration of adenine sulfate (80 mg/ml). To monitor the activity of the reporter genes cell suspensions were spotted on plates lacking in addition to leucine and tryptophan either histidine or adenine. The empty vectors pGADT7 and pGBKT7 were used as negative and pTD1 and pVA3 as positive controls.

Movie legends

Movie S01: *AgHOF1-GFP*
DIC (top left), *Ag*Hof1-GFP maximum projection (bottom right), overlay (top left), 3D reconstruction 50° tilted (bottom left). Acquisition frequency 0.2 min^{-1}. Scale bar represents 5 µm.

Movie S02: *AgHOF1-GFP*, FM4-64, calcofluor
DIC, *Ag*Hof1-GFP maximum projection (green), FM4-64 (red), calcofluor (blue), and overlays of the 3 fluorescent channels. Acquisition frequency 0.2 min^{-1}. Scale bar represents 5 µm.

Movie S03: *AgMYO1-RedStar2 AgHOF1-GFP* colocalization.
DIC (top left), *Ag*Hof1-GFP maximum projection (bottom left), *Ag*Myo1-RedStar2 (bottom right), and overlay (top right). Acquisition frequency 0.2 min^{-1}. Scale bar represents 5 µm.

Movie S04: *AgMYO1-RedStar2* tip localization.
DIC (top), *Ag*Myo1-RedStar2 (bottom). Acquisition frequency 0.2 min^{-1}. Scale bar represents 20 µm.

Movie S05: *AgSEP7-GFP* localization at young hyphal tip.
DIC (top), *Ag*Sep7-GFP maximum projection (bottom). Acquisition frequency 0.2 min^{-1}. Scale bar represents 5 µm.

Movie S06: *AgSEP7-GFP* localization at mature hyphal tip.
DIC (top), *Ag*Sep7-GFP maximum projection (bottom). Acquisition frequency 0.2 min^{-1}. Scale bar represents 5 µm.

Movie S07: *AgBUD3-GFP* localization at mature hyphal tip.
DIC (top), *Ag*Bud3-GFP maximum projection (bottom). Acquisition frequency 0.2 min^{-1}. Scale bar represents 5 µm.

Movie S08: *AgHOF1-GFP* localization at mature hyphal tip.
DIC (top), *Ag*Hof1-GFP maximum projection (bottom). Acquisition frequency 0.2 min^{-1}. Scale bar represents 5 µm.

Movie S09: *AgHOF1-GFP* ring contraction.
DIC (top row), *Ag*Hof1-GFP maximum projection (bottom row). Acquisition frequency 0.2 min^{-1}. Scale bar represents 5 µm.

Movie S10: *AgHOF1-GFP* ring contraction.
DIC (left), *Ag*Hof1-GFP maximum projection (right). Acquisition frequency 0.2 min^{-1}. Scale bar represents 5 µm.

Movie S11: *Aghof1ΔSH3-GFP* filaments.
Overlay (left), *Ag*hof1ΔSH3-GFP maximum projection (right). Acquisition frequency 0.2 min^{-1}. Scale bar represents 5 µm.

Movie S12: Open septum.
Calcofluor (left frame, blue), FM4-64 (middle frame, red), and overlay (right frame). Deconvolved Z stack. Z distance 0.3 µm. Scale bar represents 5 µm.

Movie S13: Closed septum.
Calcofluor (left frame, blue), FM4-64 (middle frame, red), and overlay (right frame). Deconvolved Z stack. Z distance 0.3 µm. Scale bar represents 5 µm.

Movie S14: Nuclear migration and cytoplasmic streaming through closing septum.
DIC (left), *AgHHF1-GFP* maximum projection (green), calcofluor (blue).Acquisition frequency 1 min^{-1}. Scale bar represents 5 µm.

Results

*Ag*Hof1: a PCH protein

In the *A. gossypii* sequencing project ABR082W was annotated as a syntenic homolog of *S. cerevisiae* YMR032W (*HOF1/CYK2*) and as a putative homolog of *S. pombe* SPAC20G8.05C (*cdc15*) with an ORF length of 2,052 bps (Dietrich *et al.*, 2004). On protein level it shares 32 % sequence identity with *S. cerevisiae* Hof1 and was named *Ag*Hof1 (Figure 1). Sequence analysis with PROSITE (Hulo *et al.*, 2006) revealed a N-terminal FCH (FER-CIP4 homology) domain located at residues 3 – 70 and a C-terminal SH3 (Src homology 3) domain located at residues 621 – 683. The software COILS (Lupas *et al.*, 1991) predicted two coiled-coil regions between residues 121 – 157 and 173 – 200 with a high probability of 1 and 0.982, respectively. An N-terminal FCH domain followed by potential coiled-coil regions is a conserved domain feature of all PCH proteins and was referred to as EFC (Tsujita *et al.*, 2006) or F-BAR domain (Itoh *et al.*, 2005). In addition, PESTfind Analysis (www.at.embnet.org) revealed a potential PEST sequence between residues 445 – 468 with a PESTfind score of 5.27 (Rogers *et al.*, 1986). The presence of all of these features (Figure 1) confirms *Ag*Hof1 as member of the PCH (*pombe cdc15* homology) protein family.

Actin ring formation and septation requires *Ag*Hof1

If *Ag*Hof1 was a member of the PCH protein family, as predicted by its amino acid sequence, it could potentially be involved in actin-based processes. *A. gossypii* wild type has three distinct F-actin structures that are visible in phalloidin stainings: tip-polarized cortical actin patches, cortical actin cables, and actin rings (Figure 2, lower left panel, white arrowheads and Knechtle *et al.*, 2003). Septa are visible in DIC images (Figure 2, upper left panel, black arrowhead) and can be stained with calcofluor white. To test the hypothesis if *Ag*Hof1, like other PCH proteins, is involved in actin-based processes the complete ORF of *AgHOF1* was deleted. In homokaryotic *Aghof1Δ* hyphae polarized actin patches and actin cables were wild type-like, but actin rings were lacking (Figure 2, lower right panel). This was surprising, as *S. cerevisiae hof1Δ* and *S. pombe cdc15-140* cells, although having cytokinesis defects, still form actin rings (Balasubramanian *et al.*, 1998; Lippincott and Li, 1998a). There were also no indications of septa in DIC images (Figure 2, upper right panel) as well as in images of calcofluor white-stained mycelia (not shown). Apart from the septation defect no other polarity defects were discernable: radial mycelial growth speed, tip growth speed, tip-splitting, and branching index (total mycelial length per number of tips) were not affected by the lack of *Ag*Hof1 (data not shown). The mycelial developmental pattern was indistinguishable form wild type as previously described (Ayad-Durieux *et al.*, 2000; Knechtle, 2002; Knechtle *et al.*, 2003; Schmitz *et al.*, 2006).

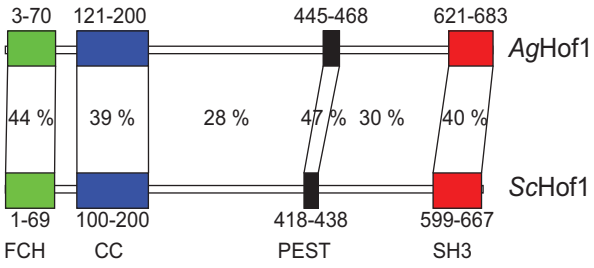

Figure 1: Domain comparison of *A. gossypii* and *S. cerevisiae* PCH proteins.

The two proteins were aligned using the 'Align plus' tool of SECentral (Scientific & Educational Software, Cary, NC, USA). The domains were predicted as described in the main text. Each domain was realigned and the identity values were taken from the output. All distances are drawn to a relative scale. FCH, FER-CIP4 homology; CC, coiled-coil region; PEST, PEST sequence; SH3, Src homology 3.

Septum maturation revealed by *Ag*Hof1 localization

Previous studies showed that the IQGAP *Ag*Cyk1 (Wendland and Philippsen, 2002) and *Ag*Bud3 (Wendland, 2003a), proteins whose homologs in *S. cerevisiae* are involved in cytokinesis, localize as cortical rings at sites where septa will form. Hence these sites will be referred to as future septa. Recently it was observed that septins of *A. gossypii* localize as collars of cortical bars (CCBs) and as cortical rings (Helfer, 2006; Helfer and Gladfelter, 2006). As *Aghof1Δ* mutants, like *Agcyk1Δ* (Wendland and Philippsen, 2002), lack actin rings, we wanted to know whether *Ag*Hof1 localizes to future septa as well. We constructed an *AgHOF1-GFP* fusion at its chromosomal locus expressed under control of its native promoter. *Ag*Hof1 localized as CCBs and as cortical rings (Figure 3), similar to the septin localization pattern. Closer analyses of the localization pattern revealed that CCBs were only found at future septa close to the hyphal tip, whereas rings were found much further subapical, in the older part of the hypha. Actin rings, always found at future septa (Knechtle *et al.*, 2003), were only colocalizing with *Ag*Hof1 rings and not with CCBs (Figure 3), indicating that actin is only recruited to future septa when *Ag*Hof1 localizes as rings.

In Figure 4 six independent future septa can be seen. The images were arranged according to the part of the hyphae where they were acquired, i.e. close to hyphal tips or in older parts of the hyphae (from left to right), and upon progression of septum formation, visible in the DIC images as a dark band that constricts the hyphae

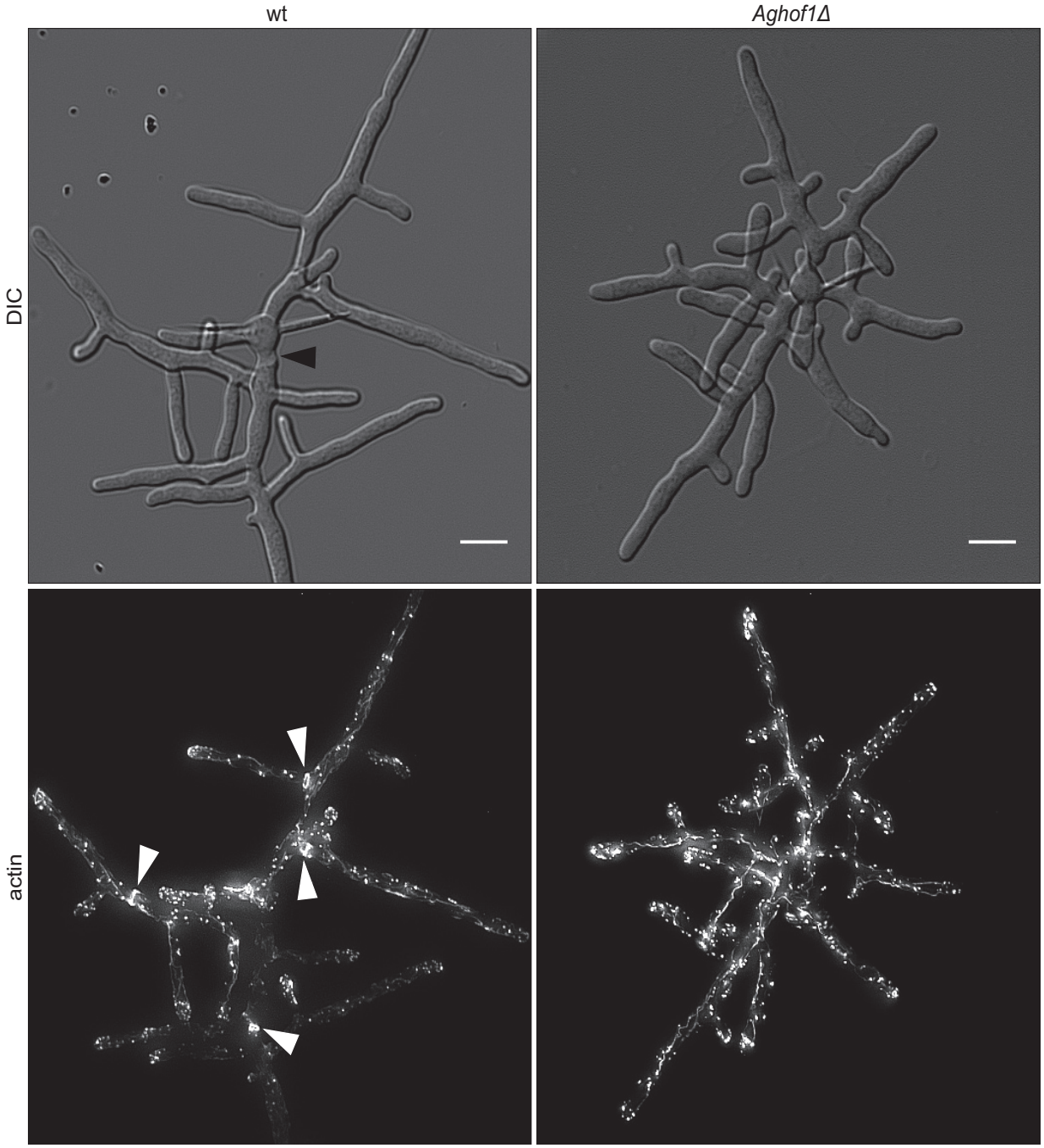

Figure 2: Actin ring formation and septation require *Ag*Hof1.

DIC images (top) and florescence images of the rhodamine phalloidin-stained actin cytoskeleton (bottom) of young wild-type (left column) and *Aghof1Δ* (right column) mycelia. Black and white arrowheads point to septa and actin rings, respectively, in wild type. Both structures are not found in *Aghof1Δ* mutants. Scale bars represent 10 µm.

(top row, column 4 – 6, arrowheads). *Ag*Hof1 localizes as ~12 distinct bars parallel to the hyphal growth axis with an average length of 2.62 ± 0.11µm (mean ± *SE*; n = 29) forming a collar inside the hyphal cortex (first column). The second column shows an apparently intermediate stage between the CCB and cortical ring localization. In the third column *Ag*Hof1 localizes as a single continuous cortical ring that corresponds with the hyphal diameter. As the septum grows inward, seen in the DIC images, the ring diameter becomes smaller (columns 4 and 5). Shortly before and after septum completion *Ag*Hof1 localizes in a spotted manner around the septum (columns 5 and 6, respectively).

The localization patterns of *Ag*Hof1 suggest that the position of future septa is already marked at or close to

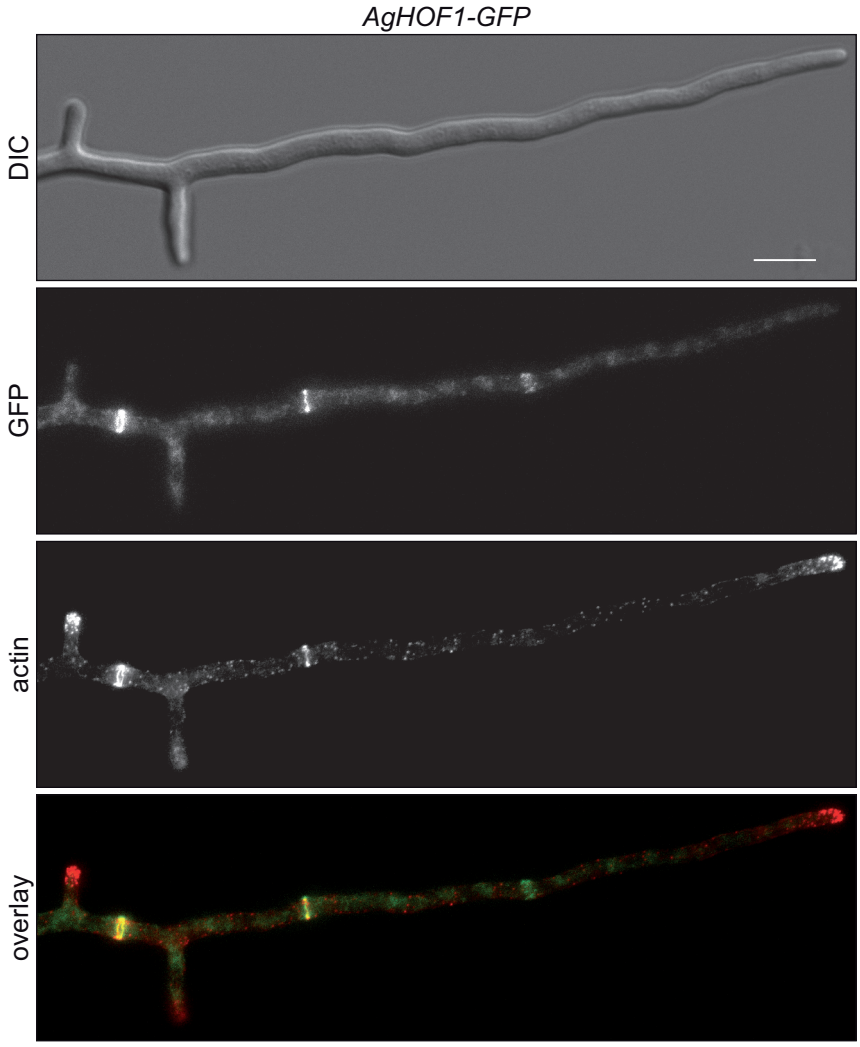

Figure 3: Colocalization of *Ag*Hof1 and actin.
DIC, GFP, rhodamine phalloidin-stained actin, and overlay of GFP and actin images (from top to bottom). *Ag*Hof1 localizes as CCB in the apical part and as cortical rings in the subapical parts of the hypha shown. Actin rings only colocalize with *Ag*Hof1 rings but not with the *Ag*Hof1 CCB. Scale bar represents 10 µm.

the growing tip but septation only takes place in older parts of the hyphae. To test if this is a gradual maturation process of the future septum we made 3D time-lapse movies of growing hyphae expressing *AgHOF1-GFP* (Movies S1 and S2). Figure 4, B shows selected frames from Movie S1. At time point 0 min *Ag*Hof1 localizes as a CCB, clearly visible in the 50°-tilted views of the 3D reconstructions of the stacks. As time progresses these bars become shorter and after ~30 min a single continuous ring is formed. After this bar-to-ring transition the ring contracts and the septum is formed, as seen in the bright field images by the dark line constricting the hypha. In Movie S2 we incubated mycelia expressing *AgHOF1-GFP* in presence of the lipophilic membrane dye FM 4-64 and calcofluor white to visualize the contractile ring, the plasma membrane, and the cell wall, respectively. After bar-to-ring transition, when the *Ag*Hof1 ring contracts, the plasma membrane starts to invaginate and chitin accumulates as a ring around the plasma membrane (185 min). Concomitant with the invagination of the plasma membrane the chitin-rich septum grows inward. Upon complete contraction of the *Ag*Hof1 ring (215 min) the plasma membrane of the two adjacent hyphal compartments separate leaving a gap of about 0.3 µm that is filled with the continuous disc of the septum. Following septum completion the plasma membranes become slightly curved, bending away from the septum as it is strengthened.

This clearly demonstrates the maturation steps that sites of septation within one hypha undergo. The youngest site, i.e. the one closest to the growing tip, is at the stage when *Ag*Hof1 forms a CCB. As the tip elongates and new future septa are marked, the older sites mature characterized by a bar-to-ring transition of *Ag*Hof1. After this transition, further back in the hypha, actin is recruited to form a contractile ring that finally leads to septation. The time frame for complete septation is very variable and is described below in more detail.

Proteins involved in septation localize to bars and rings

As the localization pattern of *Ag*Hof1 demonstrates its role in septation, we were interested to know, if it colocalizes with other proteins known to be involved in septation, i.e. *Ag*Bud3 (Wendland, 2003a), *Ag*Cyk1 (Wendland and Philippsen, 2002), and type II myosin *Ag*Myo1 (Helfer, 2001). We constructed strains expressing pairs of fluorescent fusion proteins and observed their localization pattern. *Ag*Hof1 was found to colocalize with *Ag*Cyk1, *Ag*Bud3, and *Ag*Myo1 (Figure 5). Interestingly, we found, in addition to the previously reported localization to cortical rings, that *Ag*Cyk1 and *Ag*Bud3 localize to CCBs as well (Figure 5, A and C). It is to mention, that not all investigated proteins form single rings. It was reported, that *Ag*Bud3 (Wendland, 2003a) and septins (Helfer, 2006; Helfer and Gladfelter,

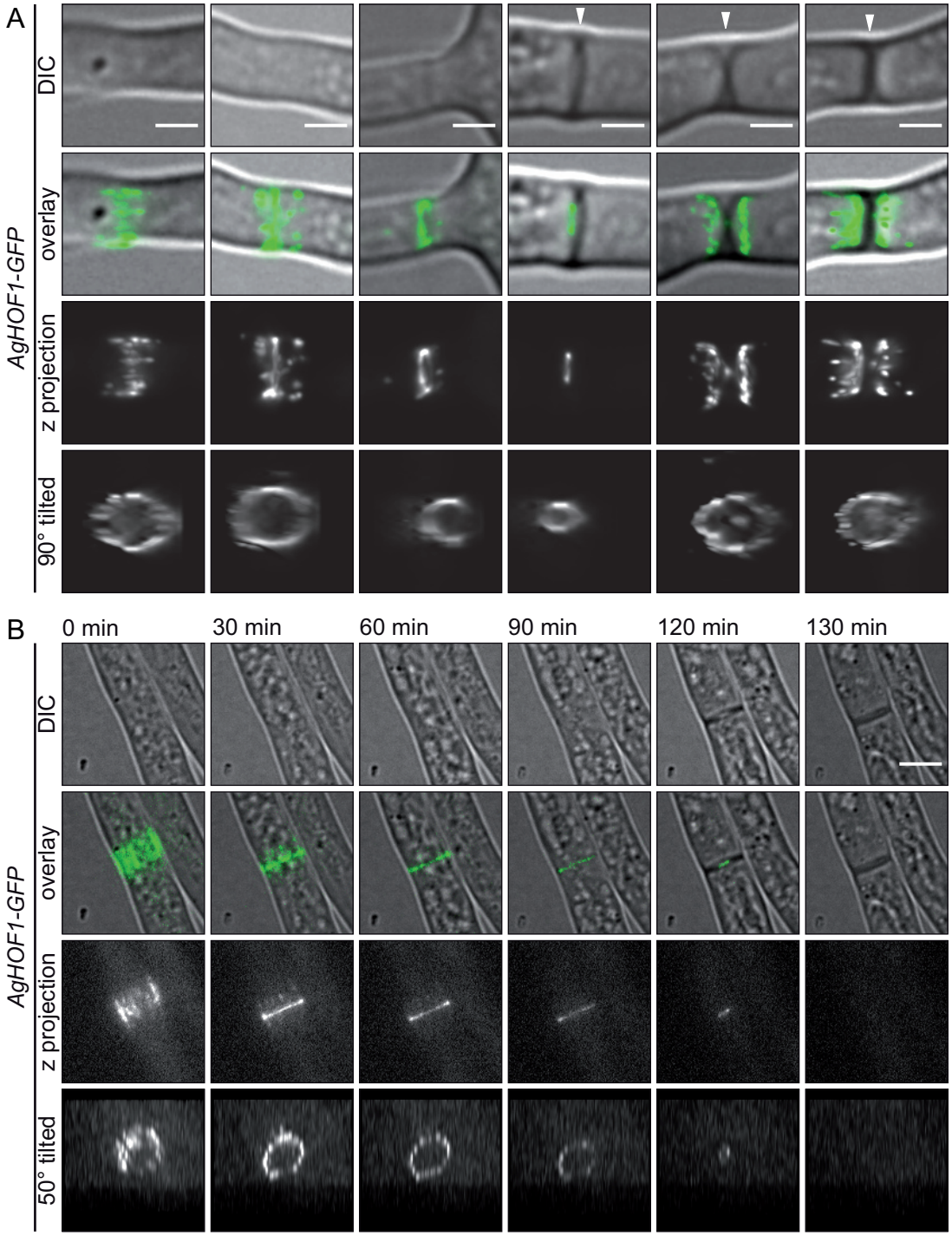

Figure 4: Septum maturation revealed by *Ag*Hof1 localization.

(A) DIC images, maximum projections, and 90°-tilted views of 3D-reconstructed blind-deconvolved stacks with a Z resolution of 0.3 µm of six independent septa, arranged based upon the part of the hyphae where they were acquired, i.e. close to hyphal tips or in older parts of the hyphae (from left to right), and upon progression of septum formation, dark band in DIC images (top row, column 4 – 6, arrowheads). Scale bars represent 2.5 µm. (B) Selected frames from Movie S01 show the dynamics of *Ag*Hof1. Every 5 min a stack of 5 planes spaced 1 µm apart was acquired. *Ag*Hof1 localizes first as a CCB (0 min). After bar-to-ring transition (30 min) *Ag*Hof1 localizes as a single cortical ring (60 min) that contracts concomitantly with septum formation (90 – 130 min). Scale bar represent 5 µm.

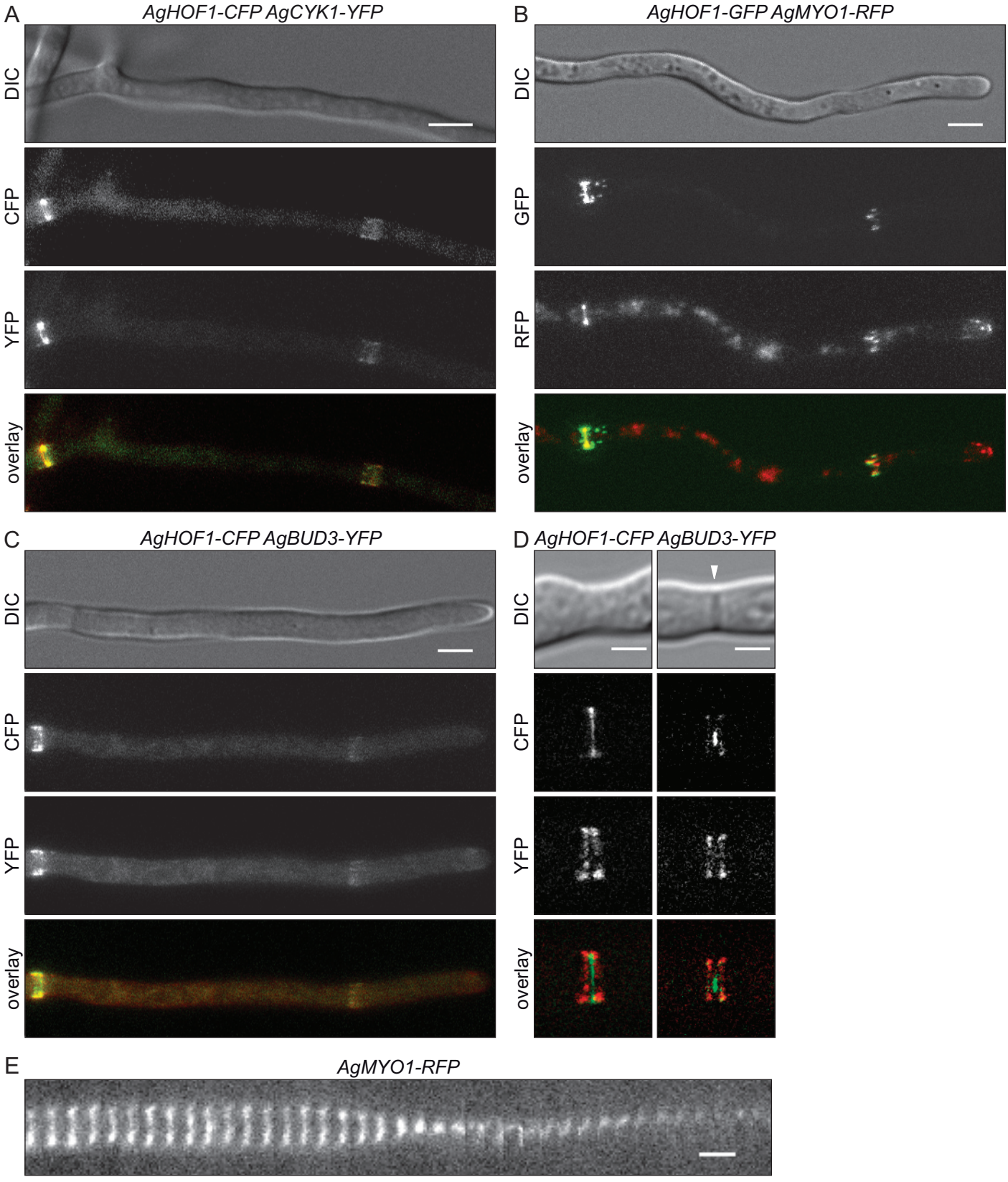

Figure 5: Proteins involved in septation localize to bars and rings.
*Ag*Hof1 colocalizes with *Ag*Cyk1 (A), *Ag*Myo1 (B), and *Ag*Bud3 (C) as CCBs and cortical rings. Scale bars represent 5 µm. (D) Before *Ag*Hof1 ring contraction *Ag*Bud3 double rings delimit the *Ag*Hof1 single ring (top row). The *Ag*Hof1 ring contracts whereas the *Ag*Bud3 double rings do not. The arrowhead indicates the progressing septum formation. Scale bars represent 2.5 µm. (E) Kymograph made from Movie S03 illustrating *Ag*Myo1 ring contraction. Time points are 5 min apart. Scale bar represents 2.5 µm.

2006) localize as double rings, i.e. two rings right next to each other, at future septa. We found that the *Ag*Bud3 double rings delimit the single rings formed by *Ag*Hof1, *Ag*Myo1, *Ag*Cyk1, and actin. When septation takes place, visible in DIC images as a dark band that constricts the hypha (Figure 5, D, arrowhead), the single rings of *Ag*Hof1, *Ag*Myo1, *Ag*Cyk1, and actin contract, whereas the double rings of *Ag*Bud3 do not (shown for *Ag*Bud3 and *Ag*Hof1 in Figure 5, D).

The localization pattern of the single type II myosin of *A. gossypii* *Ag*Myo1 was so far uncharacterized. It localizes to CCBs and cortical contractile rings and, as mentioned above, it colocalizes with *Ag*Hof1 (Figure 5, B and E; Movie S3). Occasionally we observed localization to the hyphal tip (Figure 5, B; Movie S4). However, we only observed this localization for *Ag*Myo1-RedStar2 and never for *Ag*Myo1-GFP. Whether this tip localization is an artifact because RedStar2 dimerizes or whether it is of biologially important and cannot be seen for *Ag*Myo1-GFP for some reasons, should be tested with antibodies risen against *Ag*Myo1 (so far unavailable).

Very recently it was observed that septins supposedly form contractile rings, i.e. rings smaller than the hyphal diameter (Amy Gladfelter, personal communication). This is very surprising as septin rings contract neither in *S. pombe* nor in *S. cerevisiae* (Wu *et al.*, 2003; reviewed by Gladfelter *et al.*, 2005; Gladfelter *et al.*, 2001). We therefore analyzed the localization pattern of the septin *Ag*Sep7. Firstly, we could confirm its published localization to CCBs (Figure 6, A, top row; (Helfer, 2006; Helfer and Gladfelter, 2006)). Secondly, we could confirm Amy Gladfelter's observations that *Ag*Sep7 localizes to presumably contractile rings at contracting septa (Figure 6, A, middle and bottom row). It is to mention that these rings were of a rather splotchy appearance and did not seem to be as continuous as for example an actin ring. Additionally and most interestingly we found *Ag*Sep7 not only to localize as CCBs and cortical rings but also as very thin cortical filaments that run in parallel to the growth axis of the hyphae (Figure 6, B). These filaments were of very low signal intensity and thus difficult to visualize but were observed in more than 30 hyphae. They were mainly found between the hyphal tip and the first CCB but also in more subapical parts of the hyphae (counted from the hyphal tip). The *Ag*Sep7 CCBs are of higher signal intensity compared to the filaments (Figure 6, B, arrowhead).

Septation site selection

In young *A. gossypii* mycelia the site of septation is apparently marked as tip growth slows down concomitant with lateral branch emergence further back in the hypha (Knechtle *et al.*, 2003), but nothing was known about the order of appearance of the cytokinetic proteins. We therefore acquired time-lapse movies from strains expressing GFP-tagged cytokinetic proteins (Movies S05-08; Figure 7). The septin *Ag*Sep7 localizes as cortical filaments to the apical part of the hypha in young and mature mycelia (Movies S05 and S06; Figure 7, A and B, respectively). Due to the much shorter exposure time used for acquisition of time-lapse movies the cortical septin filaments, as seen in Figure 6, B, appear only as diffuse clouds of fluorescence close to the growing tip. In young and mature mycelia *Ag*Sep7-GFP localization to a CCB could be observed already five minutes after the growing tip passed the site of the future septa, i.e. 1.3 and

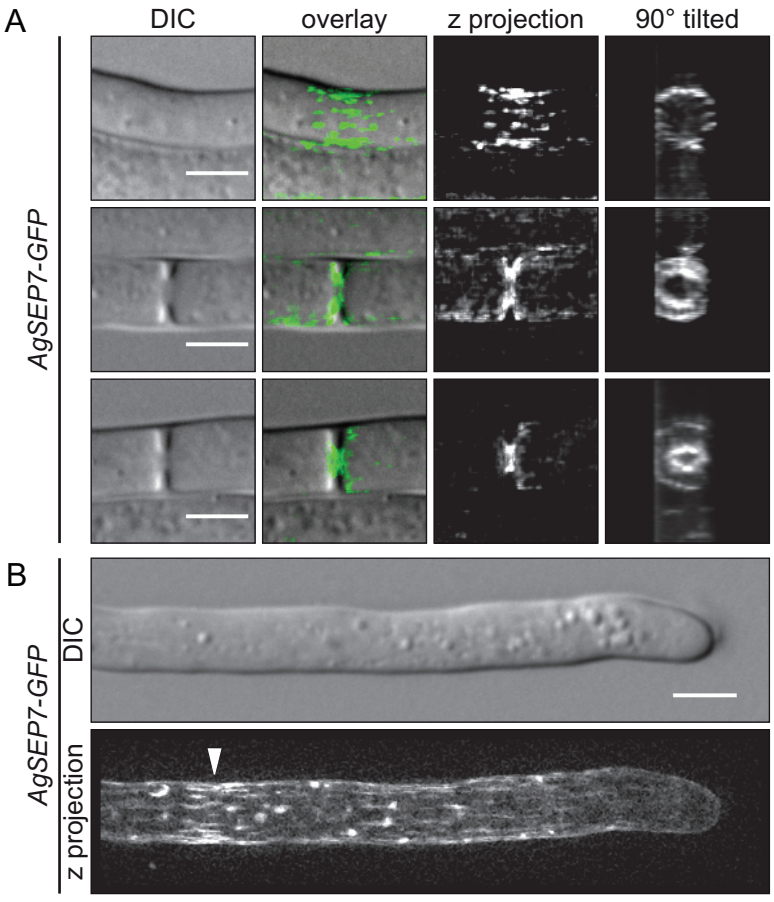

Figure 6: Septins localize to CCBs, contractile rings, and cortical filaments.
(A) *Ag*Sep7 localizes as a CCB to future site of septation (top row). During septum formation it localizes as an apparently contractile ring (middle and bottom row). (B) In apical parts of hyphae *Ag*Sep7 localizes to thin cortical filaments and CCBs (arrowhead). Scale bars represent 5 µm.

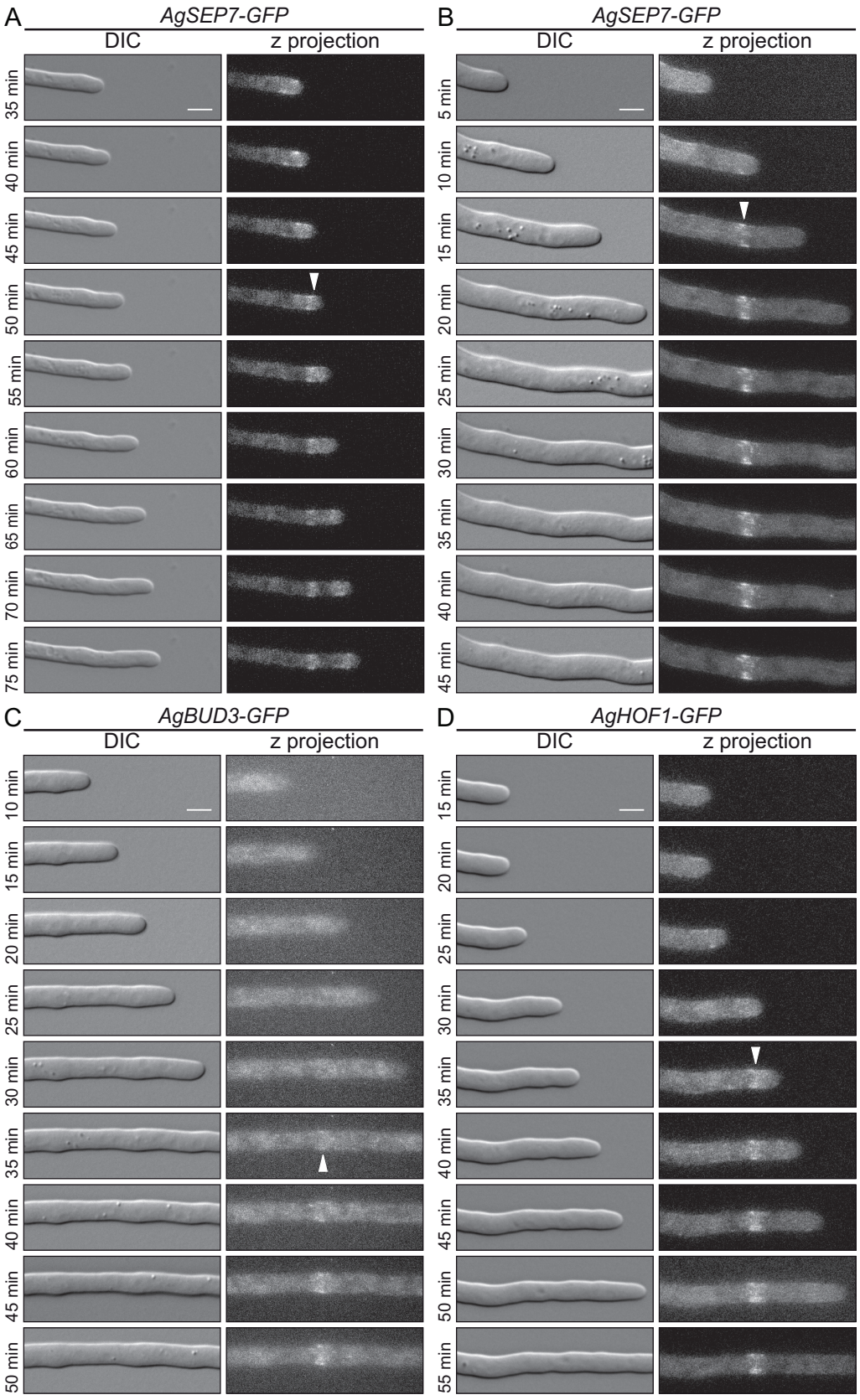

Figure 7: Septation site selection.

Selected frames of Movies S05-08. *Ag*Sep7 can be observed localizing as CCBs in young (A) and mature (B) hyphae directly after the growing tip has passed the site of the future septa. The same can be observed for *Ag*Hof1 (D). *Ag*Bud3 becomes only visible 20 min after the growing tip has passed the site of the future septa (C). Arrowheads indicate where GFP signals become first visible. Scale bars represent 5 µm.

9.4 µm behind the tip, respectively (arrowheads at time-points 50 and 15 min in Figure 7, A and B, respectively). Localization of the landmark protein *Ag*Bud3 to a CCB became barely visible 20 minutes after the growing tip passed the site of the future septa, i.e. 23.3 µm behind the tip (arrowhead at time point 35 min in Figure 7, C; Movie S07). Interestingly *Ag*Hof1-GFP, like *Ag*Sep7-GFP, could be observed already 5 minutes after the growing tip passed the site of the future septa, 3.6 µm behind the tip (arrowhead at time point 35 min in Figure 7, D; Movie S08).

Based only on the early appearance of *Ag*Hof1 at the future septum we could not conclude if it is involved in septation site selection. To test if *Ag*Hof1 is required to localize other septal proteins to the future septa we deleted *AgHOF1* in strains expressing *AgSEP7-GFP*, *AgBUD3-GFP*, or *AgMYO1-GFP*. The septin *Ag*Sep7 and the landmark protein *Ag*Bud3 still localized to bars and rings as they do in wild type (Figure 8), demonstrating that *Ag*Hof1 is not required for septation site selection and bar-to-ring transition. Type II myosin *Ag*Myo1 localized as well to bars and rings (Figure 8), but these rings did not contract anymore. As actin rings are missing in *Aghof1Δ* mutants it is conceivable that the *Ag*Myo1 rings did not contract. Only the motor protein *Ag*Myo1 together with the actin ring can exert the force necessary for contraction. These results suggest that *Ag*Hof1, although appearing early at future septa, is not involved in septation site selection but in recruiting the machinery, needed for actin ring formation.

Next we wanted to test if *Ag*Hof1 depends on *Ag*Cyk1, *Ag*Myo1, and *Ag*Bud3 for localization to future septa. To do so we deleted *AgCYK1*, *AgMYO1,* and *AgBUD3* in strains expressing either *AgHOF1-GFP* or *AgHOF1-CFP*. As seen in Figure 9 *Ag*Hof1 is able to localize in all three mutants. Although actin, *Ag*Cyk1 (Wendland, 2003a) and *Ag*Hof1 (data not shown) form bundles instead of rings, septation sites are normally selected and contractile rings can eventually form in *Agbud3Δ* hyphae. These results, together with the rather late appearance of *Ag*Bud3 at future septa (Figure 7, C; Movie S7), compared to *Ag*Sep7 and *Ag*Hof1, indicate that *Ag*Bud3 cannot be regarded as a bona fide landmark protein for septation site selection in *A. gossypii*. It rather functions in delimiting septal proteins to form a proper contractile ring, as suggested by its localization as double rings on both sides of contractile rings (Figure 5, D)

Time frame of septation: ring persistence and contraction

With the results presented above we could divide the process of septation into different stages: CCB formation, bar-to-ring transition, ring persistence, and ring contraction concomitant with septum formation. Interestingly, ring contraction does not always follow bar-to-ring transition immediately. In one instance a hypha, taken from liquid media-grown cells, could be observed in which, over a distance of 590 µm, 7 future septa persisted at the same time without ring contraction and septum formation (Figure 10, arrowheads). Assuming a tip growth speed of 180 µm/h would mean that the oldest future septa (i.e. the most subapical of the 7 septa in the hypha) remained open for over 3 hours. To determine more precisely on what time scale these events occur we acquired time-lapse movies where we tried to follow the dynamic localization of *Ag*Hof1-GFP from CCB formation until the end of ring contraction. *Ag*Hof1-GFP localization at 6 future septa was followed

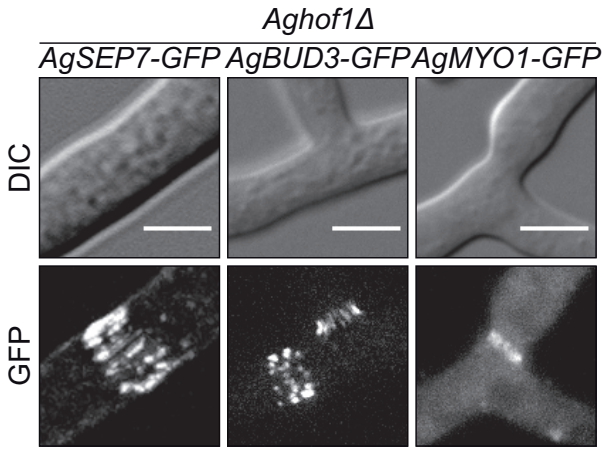

Figure 8: Localization of septal proteins in *Aghof1Δ*.
*Ag*Sep7 (left), *Ag*Bud3 (middle), and *Ag*Myo1 (right) are still localizing to CCBs and cortical rings in *Aghof1Δ* mutants. Scale bars represent 5 µm.

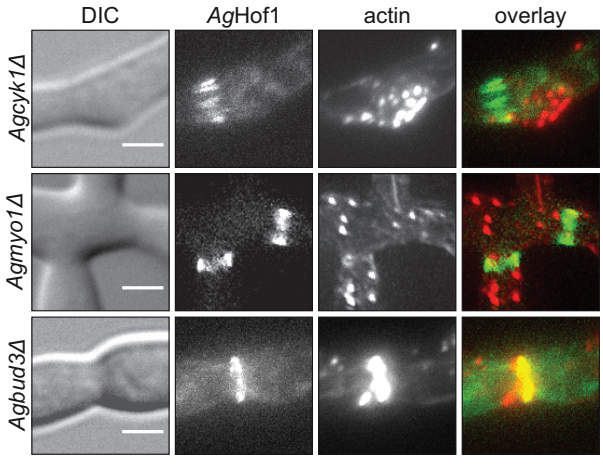

Figure 9: *Ag*Hof1 localization in *Agcyk1Δ*, *Agmyo1Δ*, and *Agbud3Δ*.
Deletion of *AgCYK1* (top), *AgMYO1* (middle), or *AgBUD3* (bottom) does not abolish *Ag*Hof1 localization to CCBs and cortical rings. Scale bars represent 2.5 µm.

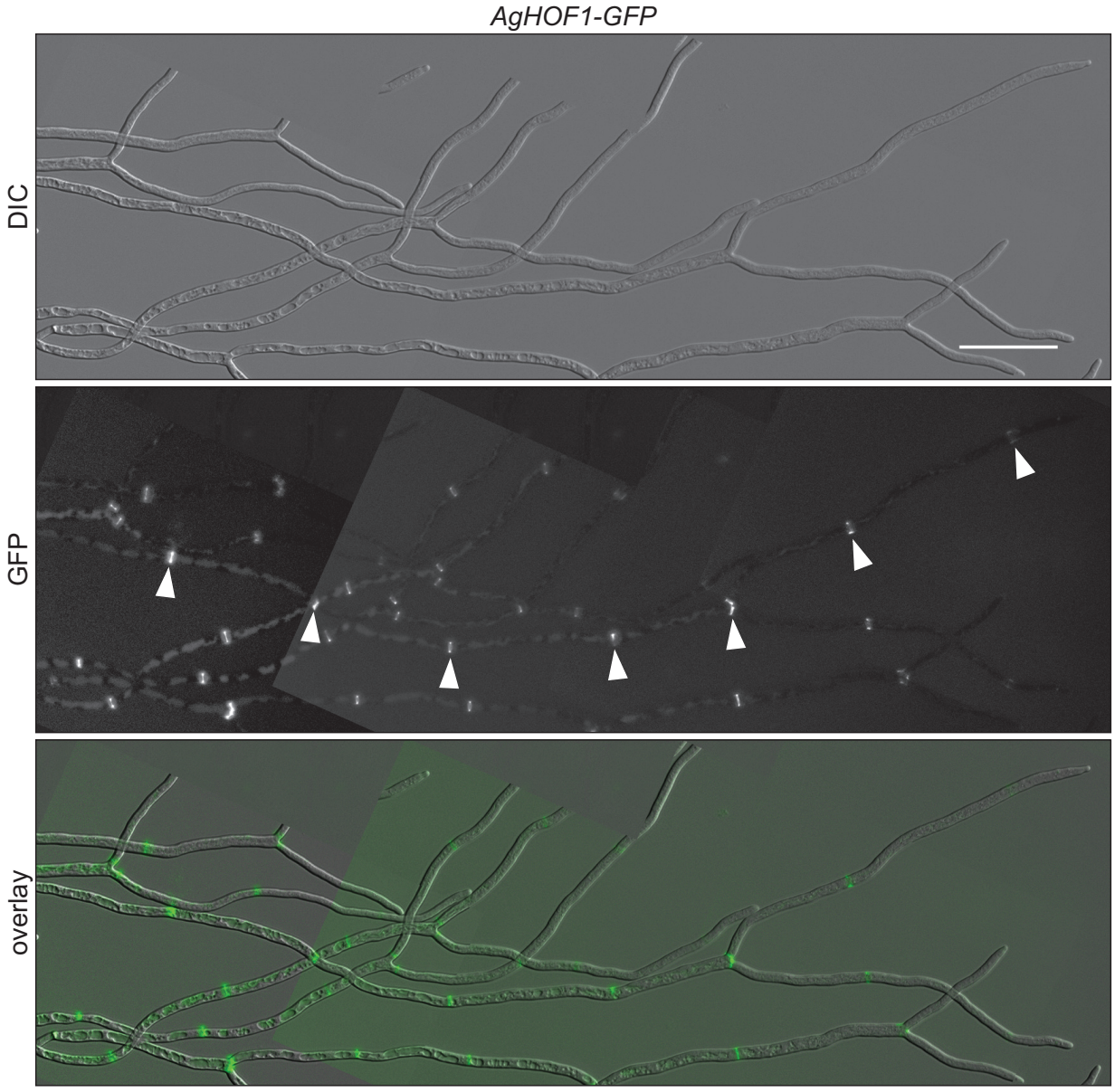

Figure 10: Ring persistence.

Montage of 4 images showing the simultaneous persistence of 7 future septa (CCBs and open rings; arrowheads) in one hypha from liquid media-grown mycelia over a distance of 590 µm. Scale bar represents 50 µm.

in 4 independent movies (Figure 11, A; Movies S1, S2, S9, and S10). As reference time point we chose closure of the *Ag*Hof1 ring. Arrows indicate the time points when bar-to-ring transition has completed and a continuous ring has formed. The longest time where we were able to monitor a single future septum was 325 min (Figure 11, A, black line; Movie S9, middle frame), but still we were unable to follow the future septum from initial *Ag*Hof1 localization to the closure of the ring. In this movie CCB localization and bar-to-ring transition took over 135 min. The time for ring persistence varied considerably as well: in 5 of the 6 movies we measured ring persistence between 60 – 160 min, which is consistent with the data from Figure 10. During ring persistence the ring diameter stays constant. Only in one case we observed a slow decrease in ring diameter of about 1.5 µm over 160 min (Figure 11, A, black line; Movie S9, middle frame). After ring persistence the actual ring contraction occurs within 30 min. Figure 11, C, left and middle graph, shows the average decrease in ring diameter and standard errors of the six septa during the last 50 min. A linear regression through the last 5 time points (20 min) results in a ring closure rate of 0.18 µm/min. This is comparable to fission and budding yeast. For the myosin light chain Cdc4 of *S. pombe* a ring closure rate of 0.14 µm/min was measured (Pelham

and Chang, 2002). The much smaller *S. cerevisiae* Myo1 rings contract within 5.1 min (Dobbelaere and Barral, 2004). With a bud neck width of 1 µm this results in a ring closure rate of 0.20 µm/min, .

In *S. cerevisiae Sc*Hof1 interacts via its PEST domain with the SCF component *Sc*Grr1. This interaction leads to the degradation of *Sc*Hof1 by SCF^{Grr1} late in mitosis and is required for normal actomyosin ring contraction. *Sc*Myo1 ring contraction takes almost twice as long in cells expressing *ScHOF1* lacking its PEST sequence (Blondel *et al.*, 2005). We tested whether the predicted PEST domain in *Ag*Hof1 has a similar role in ring persistence or contraction in *A. gossypii*. Therefore we constructed a strain expressing *AghofΔPEST-GFP* from the endogenous *AgHOF1* promoter and analyzed the dynamics of *Ag*Hof1ΔPEST by 4D microscopy. *Ag*Hof1ΔPEST localized to CCBs that underwent bar-to-ring transition like *Ag*Hof1 (not shown). In Figure 11, B *Ag*Hof1ΔPEST localization at 11 future septa from 2 independent movies was analyzed from the time-point when a continuous ring had formed until ring

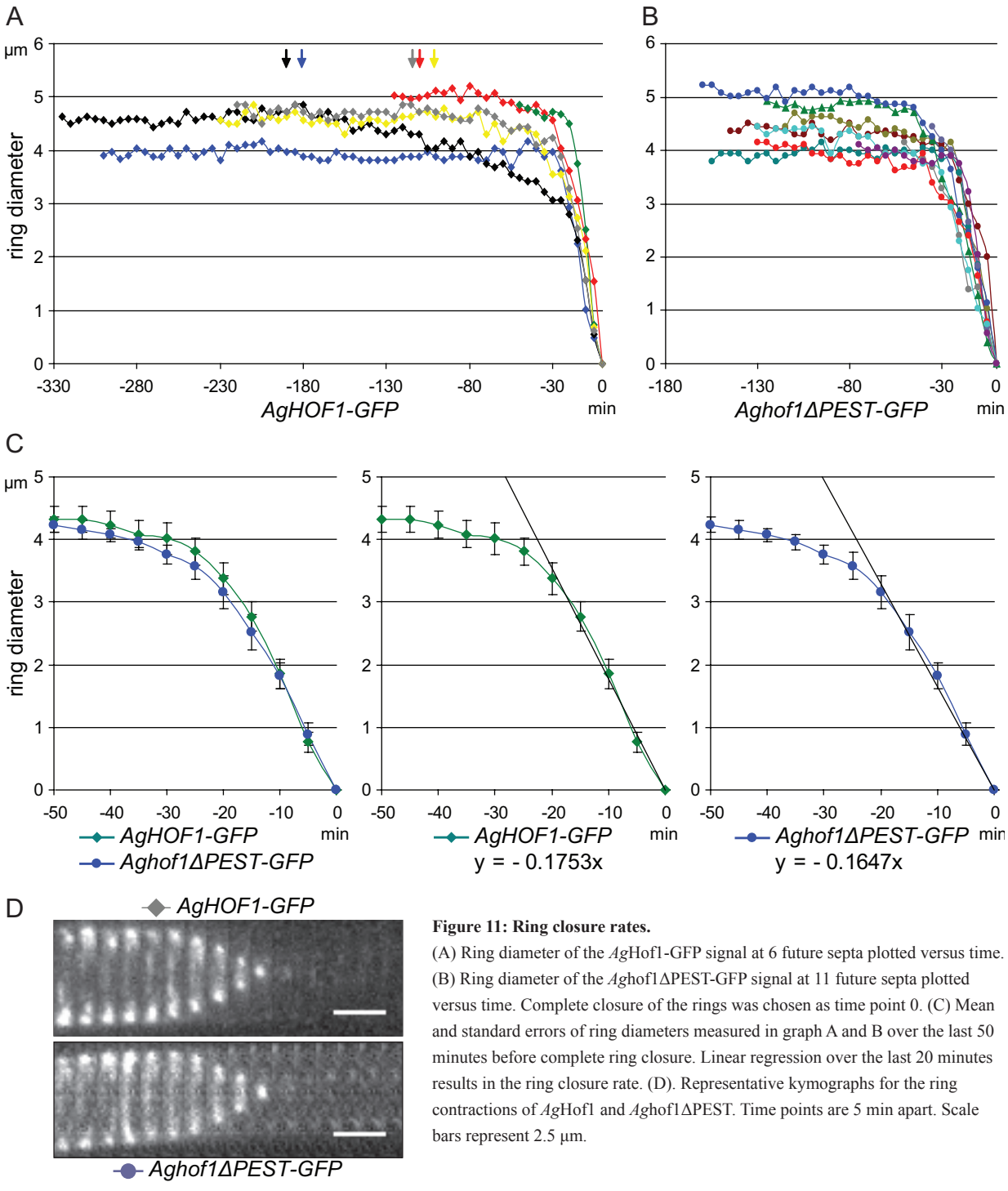

Figure 11: Ring closure rates.
(A) Ring diameter of the *Ag*Hof1-GFP signal at 6 future septa plotted versus time. (B) Ring diameter of the *Ag*hof1ΔPEST-GFP signal at 11 future septa plotted versus time. Complete closure of the rings was chosen as time point 0. (C) Mean and standard errors of ring diameters measured in graph A and B over the last 50 minutes before complete ring closure. Linear regression over the last 20 minutes results in the ring closure rate. (D). Representative kymographs for the ring contractions of *Ag*Hof1 and *Ag*hof1ΔPEST. Time points are 5 min apart. Scale bars represent 2.5 µm.

contraction. We measured ring persistence up to 130 min which is in the range we observed for *Ag*Hof1. The average ring closure rate of 0.16 µm/min does not differ significantly form 0.18 µm/min measured for *Ag*Hof1 (Figure 11, C and D). This indicates that either *Ag*Hof1 degradation is not necessary for normal ring contraction or the predicted PEST sequence has no function and Hof1 degradation is regulated differently in *A. gossypii* than in *S. cerevisiae*.

What finally triggers ring contraction is still unclear. Apparently it is not just a simple time-based maturation process as ring persistence can vary in the range of hours. Nutrient depletion or stress might be involved. Septation occurs further back in the mycelium, where nutrients are probably limited. On the other hand, it can be assumed that hyphae grown under time-lapse conditions are subjected to several forms of stress, e.g. oxygen limitation and irradiation, which could trigger ring contraction sooner or later, depending on the actual place and the total incubation time of the hyphae on the time-lapse slide.

*Ag*Hof1 interacts with formins

One reason why actin rings are missing in cells lacking *Ag*Hof1 could be that *Ag*Hof1 would normally recruit proteins to the septation site that are nucleators of the actin filaments required to form the actin ring. One of the three formins present in *A. gossypii* (Schmitz *et al.*, 2006) could be such a nucleator. It was shown that formins nucleate actin filaments (Harris *et al.*, 2004; Kovar *et al.*, 2003; Moseley *et al.*, 2004; Pruyne *et al.*, 2002; Sagot *et al.*, 2002) and that their proline-rich FH1 (formin homology 1) domain can interact with the SH3 domain of PCH proteins (Kamei *et al.*, 1998). Therefore we tested in a two-hybrid assay the interactions between *Ag*Hof1 and the three formins *Ag*Bni1, *Ag*Bnr1, and *Ag*Bnr2 (Figure 12). We found strong interactions between full length *Ag*Hof1 and the FH1 domains of both *Ag*Bni1 and *Ag*Bnr1 (residues 1241 – 1349 and 697 – 1162, respectively). The same, but slightly weaker interactions were found for the SH3 domain (residues 621 – 683) of *Ag*Hof1 alone. Additionally, we found a weak interaction between the FH1 domain (residues 640 – 762) of *Ag*Bnr2 and full length *Ag*Hof1. Here, no interaction between the FH1 domain and the SH3 domain alone could be detected. Interactions between full length formins and *Ag*Hof1

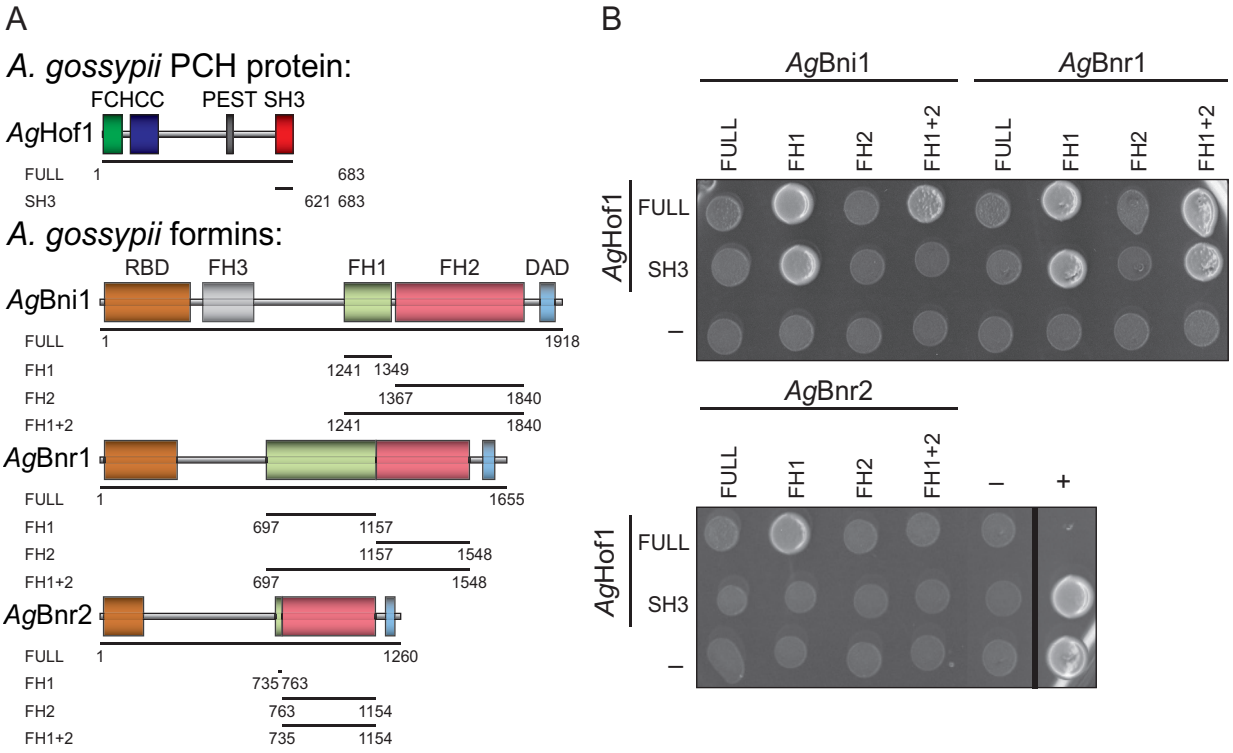

Figure 12: *Ag*Hof1 interacts with formins.

(A) Domain composition and fragments of *Ag*Hof1, *Ag*Bni1, *Ag*Bnr1, and *Ag*Bnr2 that were used to assay protein-protein interactions. (B) Two-hybrid assay. Each spot corresponds to 5 µl of a yeast culture of strain PJ69-4a/α harboring respective bait and prey plasmids with an OD_{600} of 1. Cells were spotted on medium lacking tryptophan, leucine, and histidine to select for the bait and prey plasmid and to monitor protein-protein interactions, respectively. + indicates pTD1 and pVA3 bait and prey plasmids, respectively, used as positive control. – indicates empty pGADT7 and pGBKT7 vectors used as negative controls.

were barely detectable. This is probably due to the autoinhibitory intramolecular interaction between the N-terminal RBD (Rho binding domain) and the C-terminal DAD (diaphanous autoregulatory domain) common to many formins (Alberts, 2001). These results show that, indeed, one of the three formins could be recruited to the septation site by *Ag*Hof1 to nucleate actin filaments needed for the actin ring.

The SH3 domain of *Ag*Hof1 is required for ring integrity

If the SH3 domain of *Ag*Hof1 alone was responsible for recruiting actin ring nucleators to the future septa, then cells expressing *Ag*Hof1 without its SH3 domain should display a similar phenotype as *Aghof1Δ* cells, i.e. lacking actin rings. Therefore we deleted the C-terminal SH3 domain (residues 621 – 683) by fusing YFP in frame to the last amino acid upstream of the SH3 domain. Interestingly, cells expressing *Aghof1ΔSH3-YFP* were still able to form actin rings and septa. In addition, this truncated version of *Ag*Hof1 still localized seemingly correctly as CCBs and rings to future septation sites (Figure 13, A, top and middle row). Only time-lapse movies revealed that there is a phenotype. In some cases *Ag*hof1ΔSH3 rings broke open and septation did not occur (Figure 14, A; Movie S11). In other cases *Ag*hof1ΔSH3 did not form closed rings but spiral-like filaments (Figure 14, B; Movie S11). These filaments were cortical as normal *Ag*Hof1 rings are. Interestingly, the spiral-like filaments straightened, moved inside the hyphae and became shorter over time. The length of these filaments roughly corresponds to the circumference of normal *Ag*Hof1 rings, indicating that these filaments are of similar origin as normal rings except that they could not be closed due to the lacking SH3 domain. The shortening of theses filaments occurs much slower than the ring closure rates measured for *Ag*Hof1 rings. The filaments in Movie S11 constantly become shorter during more than 9 hours but do not disappear completely. This indicates that the shortening of these filaments cannot be compared with normal ring contraction and is rather due to disassembly of the filaments at their ends. We tested whether these filaments influenced the structural organization at the future septa. Actin staining revealed that *Ag*hof1ΔSH3 filaments partially colocalize with abnormally thick actin filaments (Figure 13, A, bottom row). Immunofluorescence stainings of septins with antibodies against Cdc11 showed that septins colocalize with normal looking *Ag*hof1ΔSH3 rings (Figure 13, B, top row) but not with open rings or filaments (Figure 13, B, middle and bottom row). This demonstrates that the SH3 domain deletion influences proteins that are downstream of *Ag*Hof1 in septation. Although the results from the two-hybrid assay suggest that the SH3 domain of *Ag*Hof1 recruits the formins to nucleate actin filaments at the sites of septation, the data presented here, indicates that

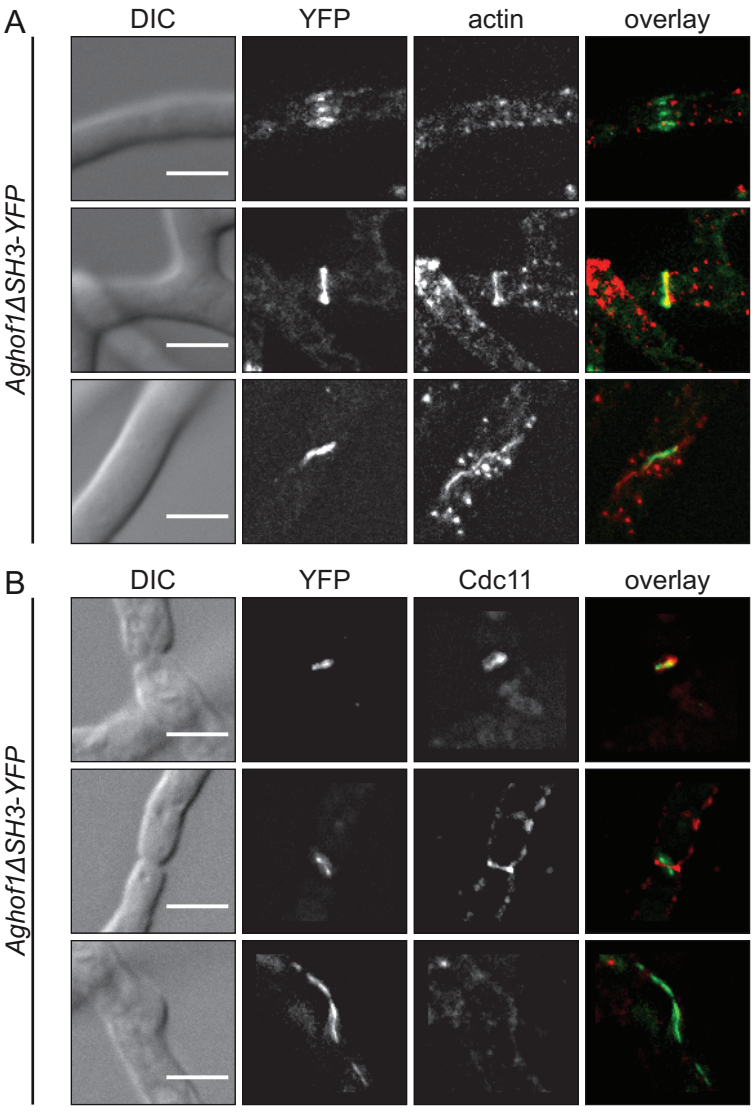

Figure 13: *Ag*Hof1 SH3 domain deletion.
(A) *Ag*hof1ΔSH3 localizes as normal CCB at future septa (top row) and colocalizes with actin rings after bar-to-ring transition (middle row). *Ag*hof1ΔSH3 forms abnormal cortical filaments that colocalize with thick actin filaments (bottom row). (B) Immunofluorescence staining of septins in mycelia expressing *Aghof1ΔSH3-YFP* using anti-*Sc*Cdc11 antibodies. *Ag*hof1ΔSH3 colocalizes with septins if *Ag*hof1ΔSH3 forms a closed ring (top row) but not if the rings are open (middle row) or if *Ag*hof1ΔSH3 forms cortical filaments (bottom row). Scale bars represent 5 µm.

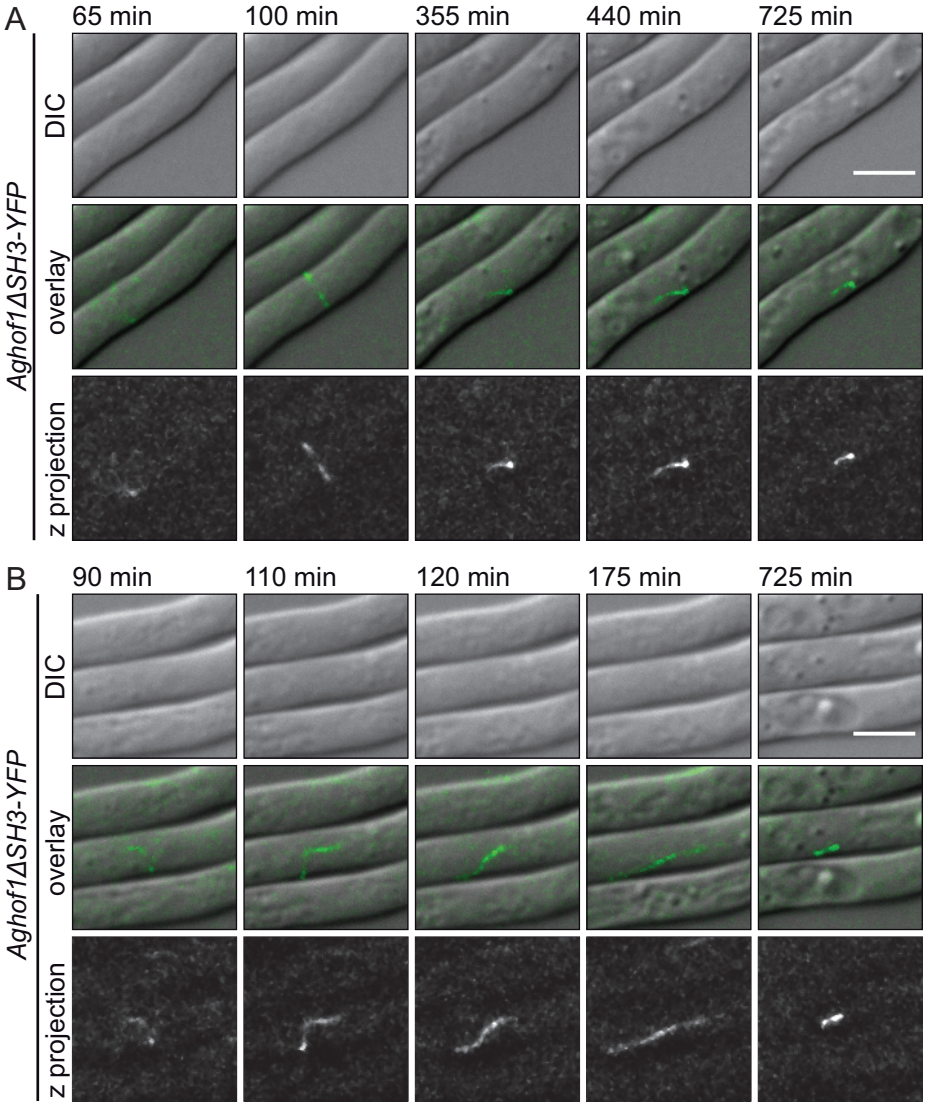

Figure 14: *Ag*Hof1ΔSH3 dynamics.
(A) Region of selected frames from Movie S11 showing a closed *Ag*hof1ΔSH3 ring that is not stable and brakes open. (B) Region of selected frames from Movie S11 showing the formation, stretching, movements, and shortening of a cortical *Ag*hof1ΔSH3 filament within the hypha. Scale bars represent 5 µm.

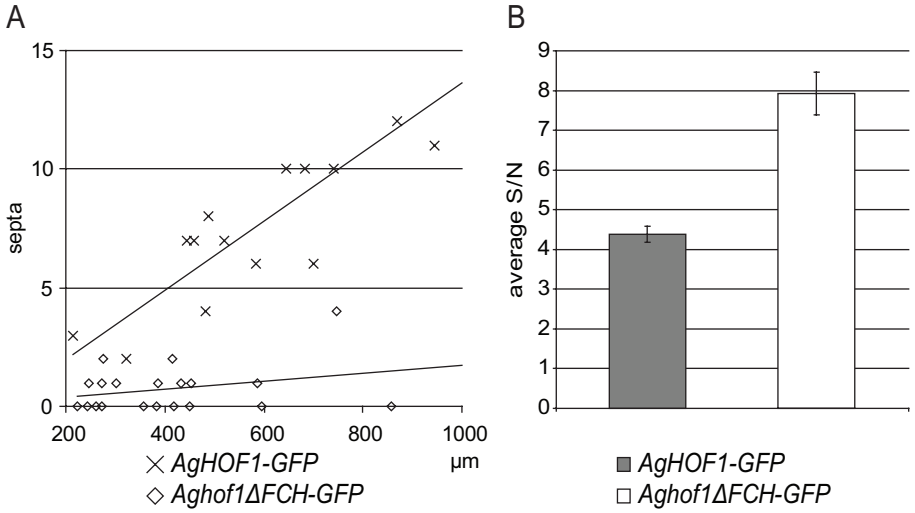

Figure 15: Deletion the *Ag*Hof1 FCH domain impairs septum formation.
(A) Number of calcofluor white-stained future and mature septa of young lateral-branching *Aghof1ΔFCH-GFP* and *AgHOF1-GFP* mycelia plotted versus total mycelium length. (B) Average signal to noise ratio (average intensity value divided by the standard deviation around the mean of the average intensity value) in a 9 µm² region around each septum. Higher signal intensities result in a lower average S/N. *Ag*Hof1-GFP: average S/N = 4.4 ± 0.2 (SEM; n = 24). *Ag*hof1ΔFCH-GFP: average S/N = 7.9 ± 0.5 (SEM; n = 21).

the function of *Ag*Hof1's SH3 domain rather lies in stabilizing the contractile ring.

Deletion the *Ag*Hof1 FCH domain impairs septum formation

It has been suggested that PCH protein family members couple via its FCH domain membrane deformation to the actin cytoskeleton during cytokinesis when the actin ring contracts (Aspenstrom *et al.*, 2006). We tested if the predicted N-terminal FCH domain of *Ag*Hof1 was required for its localization and thus the recruitment of the actin ring to the future septum. We deleted the predicted FCH domain (bps 7-210) on a plasmid carrying *AgHOF1-GFP* and integrated the construct at the chromosomal locus of *AgHOF1*. *Ag*hof1ΔFCH was able to localize to future septa as CCBs and rings (not shown). Actin rings and septa formed but less frequently. For quantification of this effect we stained septa in young mycelia of strains expressing either *AgHOF1-GFP* or *Aghof1ΔFCH-GFP* and determined the number of septa per total length of mycelium (Figure 15, A). In *AgHOF1-GFP* the number of septa increases linearly with about 1.5 septa per 100 µm of mycelium. In *Aghof1ΔFCH-GFP* the number of septa increases linearly as well but only with about 0.16 septa per 100 µm of mycelium. For most *AgHOF1-GFP* mycelia with a total length of over 600 µm 10 or more septa have formed whereas *Aghof1ΔFCH-GFP* mycelia of similar length were found to contain a maximum of 4 septa. It also appeared as if the GPF signal at future septa was less intense in *Aghof1ΔFCH-GFP* mycelia compared to *AgHOF1-GFP* mycelia. Thus, we measured the average signal to noise ratio in a 9 μm^2 region around each septum. The average S/N is calculated by dividing the average intensity value by the standard deviation around the mean of the average intensity value for the entire region. Higher signal intensities result in a higher standard deviation and, thus, in a lower average S/N. For *Ag*Hof1-GFP we measure an average S/N of 4.4 ± 0.2 (SEM; n = 24) which was significantly lower than 7.9 ± 0.5 (SEM; n = 21) of *Ag*hof1ΔFCH-GFP (ttest P < 10^{-5}) (Figure 15, B). Similarly, stained actin rings in *Aghof1ΔFCH-GFP* displayed weaker signal intensities (not shown). Together this suggests that the missing FCH domain impairs the localization of *Ag*Hof1 to future septa and thus actin rings and septa can less frequently form.

Septation is not essential for sporulation

Spores of *A. gossypii* are formed within the hyphae in compartments, called sporangia, which are closed at both ends by septa (Figure 16, A). *A. gossypii* mutants that do not form actin rings and septa do not sporulate, as reported, for example, for the IQGAP mutant *Agcyk1Δ* (Wendland and Philippsen, 2002). Thus, it was assumed that septation is essential for sporulation. Initially, we found that *Aghof1Δ* mycelia do not seem to sporulate like *Agcyk1Δ*. To our surprise, we found spores in *Aghof1Δ* mycelia when grown on synthetic defined media (ASD). Close examination of *Aghof1Δ*, *Agcyk1Δ* and *Agmyo1Δ* (lacking actin rings and septa as well; Helfer, 2001) mutants revealed that all sporulate. Sporulation efficiency (spores per mg mycelia compared to a reference strain) was 30 % for *Aghof1Δ*, 34 % for *Agcyk1Δ*, and 25 % for *Agmyo1Δ* grown on ASD (Figure 16, B). Interestingly, sporulation was affected by the culture medium. When grown on full medium (AFM), sporulation efficiency of *Aghof1Δ* was as low as 1.7 % compared to 30 % when grown on ASD (Figure 16, C). The reason for this difference between the two media is unclear.

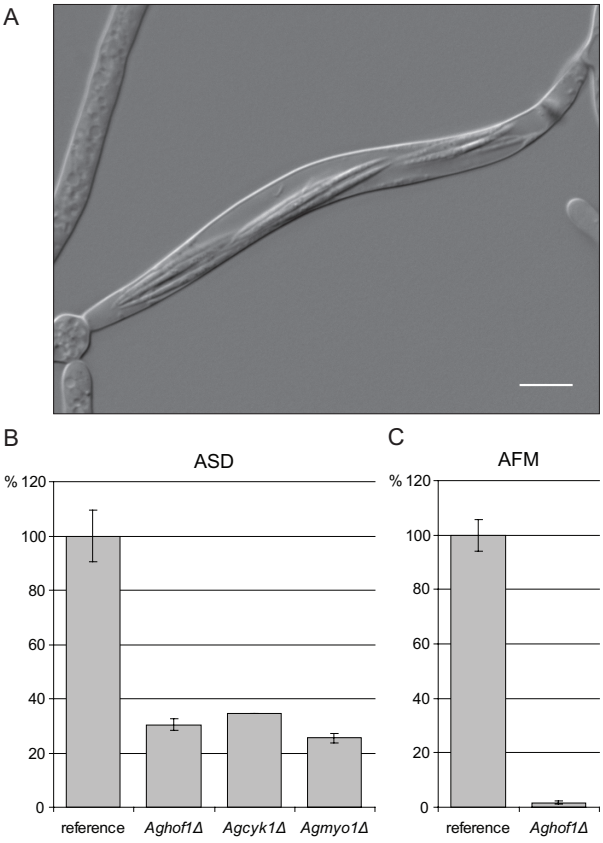

Figure 16: Septation is not essential for sporulation.
(A) Representative DIC image of an *A. gossypii* sporangium containing spores closed off by septa on either end. Scale bar represents 10 µm. (B) Mean sporulation efficiency and standard errors of septation mutants grown on ASD. (C) Mean sporulation efficiency and standard errors of *Aghof1Δ* mycelia grown on AFM. To determine sporulation efficiency mycelia were grown on plates for 7 days at 30 °C. The mycelia were scraped from the plates and weighed. Spores were isolated by digesting the mycelium with Zymolyase-20T (Seikagaku Corp., Tokyo, Japan).The spore titer was determined using a Thoma chamber. Sporulation efficiency was calculated as spores per mg mycelia normalized to a reference strain.

Cytokinesis and septation without cell separation

Filamentous ascomycetes of the subgroup *Pezizomycotinas* (*Euascomycetes*) possess septal pores that connect hyphal compartments and allow the transport of cytoplasm and organelles. These pores are usually associated with an organelle known as the Woronin body (Buller, 1933; Markham and Collinge, 1987; Woronin, 1864). The Woronin body rapidly occludes the septal pore after cell lysis limiting mycelial death, by preventing extensive cytoplasmic loss from ruptured hyphae (Trinci and Collinge, 1974). It was first purified from *Neurospora crassa*, and this allowed the identification of a key Woronin body-associated protein, HEX-1 (Jedd and Chua, 2000; Tenney *et al.*, 2000), which has homologs in many *Pezizomycotinas* such as *Aspergillus spp.* or *Magnaporthe grisea*. For *Saccharomycotinas*, the second subgroup of ascomycetes, Woronin bodies have only been observed in *Geotrichum candidum* (Cole and Samson, 1979) that posses pores (plasmodesmata) with a diameter of 20 – 70 nm (Hashimoto *et al.*, 1964). In *Candida albicans* 25 nm wide micropores connect adjacent hyphal compartments (Carlile *et al.*, 2000) but Woronin bodies

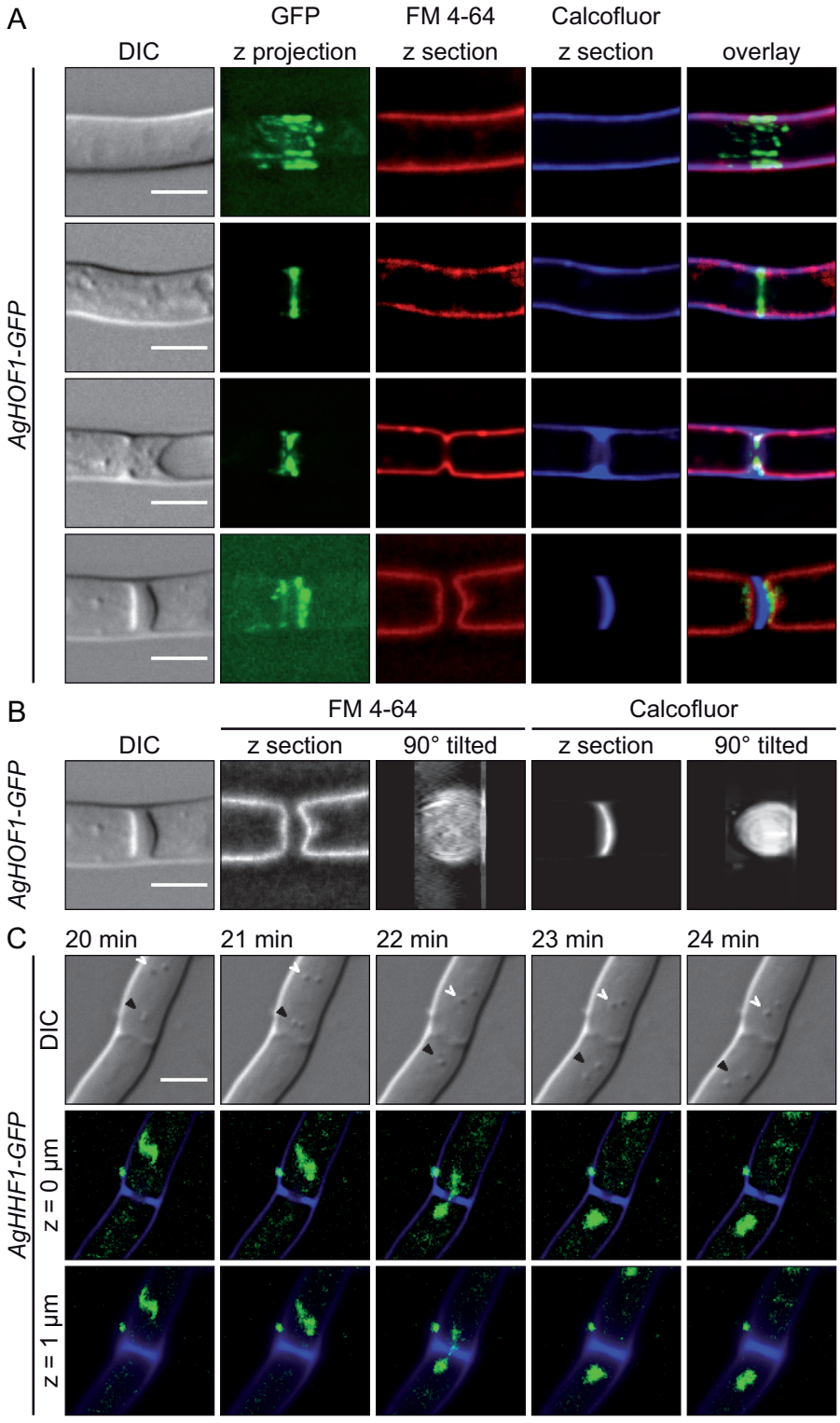

Figure 17: Cytokinesis and septation without cell separation. (A) Representative images of sites of septation at 4 different maturation stages form mycelia expressing *AgHOF1-GFP* (contractile ring, green) grown in presence of FM 4-64 (membrane, red) and calcofluor white (chitin/cell wall, blue). (B) DIC image, 3D blind-deconvolved z sections, and 90°-tilted views of 3D-reconstructed blind-deconvolved FM 4-64 and calcofluor white stacks with a z resolution of 0.3 µm of the mature septum shown at the bottom row in A. (C) Selected frames from Movie S14 showing nuclei (green) passing through a closing septum (chitin, blue). Granules in the DIC images (black and white arrowheads, top row) move with the cytoplasmic streaming. Middle row: overlay of in-focus 2D deconvolved ('No neighbors' algorithm) z section of GFP and calcofluor white stacks with a z resolution of 1 µm. Bottom row: 1 µm out-of-focus not-deconvolved z section of GFP and calcofluor white stacks. Scale bars represent 5 µm.

have not been observed. For the *Saccharomycotina A. gossypii* it has been reported that nuclei can migrate through septa (Alberti-Segui, 2001; Alberti-Segui *et al.*, 2001) and Wendland and Walter (2005) mentioned that 'cell compartments are interconnected by septal pores'. This would suggest that septa in *A. gossypii* are comparable rather with those of *Pezizomycotinas* than of other *Saccharomycotinas* and that cytokinesis, i.e. the division of the cytoplasm, in *A. gossypii* is incomplete.

Here we wanted to address the question if septa in *A. gossypii* are indeed related to those of *Pezizomycotinas* and if cytokinesis in *A. gossypii* is incomplete. If septa of *A. gossypii* would contain pores that allow the passage of nuclei then an organelle like a Woronin body may be present, as after cell lysis leakage of cytoplasm stops at septa (Movie S9, middle frame, after time point 350 min). Woronin bodies of *N. crassa* can be observed by light microscopy as a short hexagonal rod up to 1 µm in diameter (Jedd and Chua, 2000), but such a structure has not been observed in *A. gossypii*. Additionally, a blastp search (Altschul *et al.*, 1997) with *N. crassa* Hex1 as query against the *A. gossypii* proteome did not yield a potential homolog. This suggests that no Woronin body-like organelle exists in *A. gossypii*. Evidence for the lack of septal pores and complete cytokinesis came from mycelia expressing *AgHOF1-GFP* in presence of FM 4-64 and calcofluor white to visualize the contractile ring, the plasma membrane, and the cell wall, respectively (Figure 17; Movie S2). It revealed that concomitant with *Ag*Hof1 ring contraction the plasma membrane invaginates and the chitin-rich septum grows inward. Upon closing of the *Ag*Hof1 ring the membrane splits and a continuous chitin-rich septum is formed between the two hyphal compartments. Deconvolved high resolution sections (Z distance 0.3 µm) of septa at different stages and 3D reconstructed 90°-tilted views thereof (Figure 17, A and B; Movies S12 and S13) show that the plasma membranes of two adjacent hyphal compartments do not touch and that the chitin-rich septum forms a continuous disc. No pores could be detected. Even if the diameter of such pores (~50 nm) would lie below the theoretical resolution of the light microscope (i.e. ~300 nm for FM 4-64) they could be visible in fluorescence micrographs, as they are lined with plasma membrane that is, with a thickness of only 5 nm, visible as well, just not at its true size. Furthermore, we incubated mycelia expressing GFP-labeled histone H4 in presence of calcofluor white to visualize nuclear dynamics and the cell wall during septation, respectively. In 3D time-lapse movies (Movie S14, middle frame, and Figure 17, C) we could observe nuclei passing through closing septa, when there was still a hole of at least 1 µm in diameter in the septum. Passing of nuclei through completely closed septa, judged by calcofluor staining, was never observed. In the data presented by Alberti-Segui (2001) only a single focal plane was used to image the calcofluor-stained septa. We realized, even if slightly out of focus (i.e. 1 µm), calcofluor-stained closing septa appear as continuous line thus looking like completely closed septa (Movie S14, right frame, and Figure 17, C). We think that this could have led to the impression of nuclei migrating through septal pores and to the assumption that in *A. gossypii* cytokinesis is incomplete. Additionally, granules visible in the DIC images of Movie S14 (left frame) moved with the cytoplasmic flow. Two granules (closed black arrowhead) just pass through the closing septum in front of a nucleus. Two others (open white arrowhead) that follow the first two are stopped as the septum closes. At the same time cytoplasmic flow through the septum stops. From these results we conclude that cytokinesis in *A. gossypii* is complete and there are no pores that would allow the exchange of nuclei or other organelles between two compartments. Electron micrographs of septa should be made to finally test for the absence or presence of mircropores and plasmodesmata comparable to those found in *C. albicans* and *G. candidum*, respectively. Another way to test the discontinuity of the cytoplasm would be photobleaching of cytoplasmic GFP on one side of a septum to see if fluorescence is recovered by exchange of cytoplasm between the two compartments.

Discussion

First, we report on the identification and characterization of *Ag*Hof1, a novel member of the PCH protein family. Although the overall homology to *Sc*Hof1 is rather weak the individual domains are conserved. Up to date, no other PCH proteins have been described in filamentous fungi. Second, starting from the assumed role of *Ag*Hof1, we analyzed the events that lead to cytokinesis and septation in *A. gossypii*. Our analysis of the sequence of events in cytokinesis and septation in *A. gossypii* helps to clarify information on these processes from previous studies in this organism and leads to new insights in the role and function of PCH proteins and septins in filamentous fungi. We see that cytokines and septation take place in five discernable stages (Figure 18). We focused our efforts on 6 proteins, i.e. actin, *Ag*Hof1, *Ag*Sep7, *Ag*Myo1, *Ag*Bud3, *Ag*Cyk1, where we anticipated that they would be involved in these stages, but recognize that many other proteins contribute to cytokinesis and septation. The data set the frame for future more refined analyses of molecular interactions during cytokinesis and septation in filamentous fungi as well as new studies at the cellular level.

The first stage of septation is site selection. The hyphal tips of *A. gossypii* elongate constantly and proteins with a conserved role in cell polarization permanently localize to the hyphal tip, e.g., the Rho-type GTPase *Ag*Cdc42 (Michael Köhli, personal communication) and its effector *Ag*Cla4 (Ayad-Durieux *et al.*, 2000). In *S. cerevisiae*

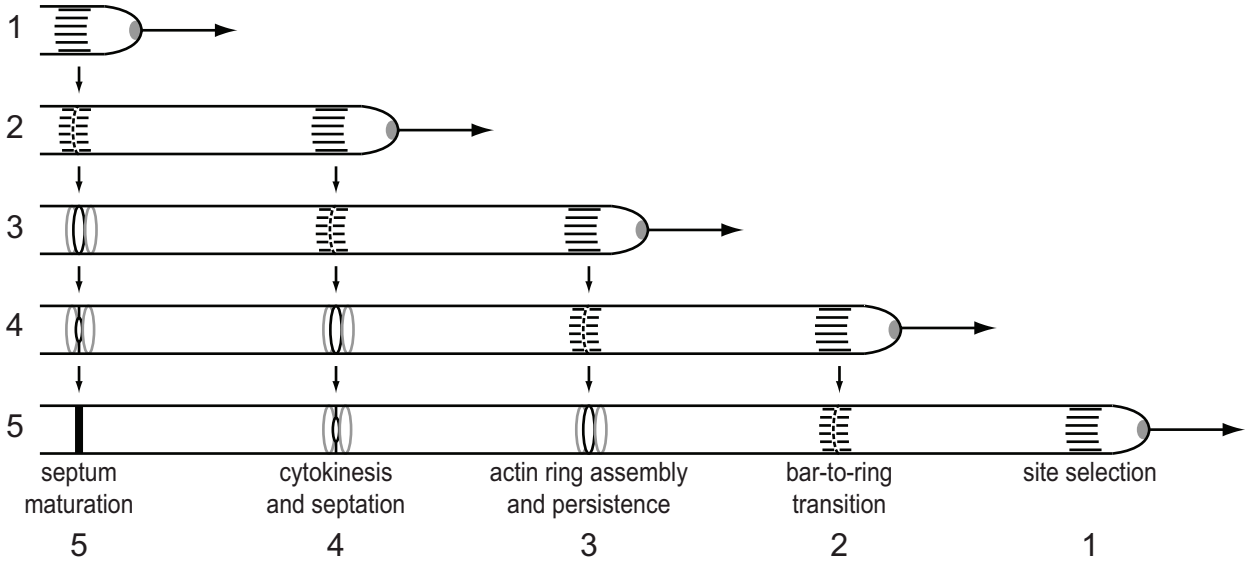

Figure 18: Current model on septation in *A. gossypii*.

1. Site selection: Polarity factors (grey spheroid), e.g., the Rho GTPase *Ag*Cdc42 and its effector *Ag*Cla4, permanently localize to the growing tip (long horizontal arrow) and signal to septins to mark the site of septation. Septins, the PCH protein *Ag*Hof1, the landmark *Ag*Bud3, the IQGAP *Ag*Cyk1, and type II myosin *Ag*Myo1 localize as a collar of 12 cortical bars (black horizontal lines). **2. Bar-to-ring transition:** The bars become gradually shorter and *Ag*Hof1, *Ag*Cyk1, and *Ag*Myo1 assemble as single cortical rings (black circles) that are delimited by two *Ag*Bud3 rings (grey circles). **3. Actin ring assembly and persistence:** Actin is recruited to form the contractile actomyosin ring. The rings can persist for variable time periods. **4. Cytokinesis and septation:** The actomyosin, *Ag*Hof1, and *Ag*Cyk1 rings contract leading to the constriction of the plasma membrane. The septum grows concomitantly inward. **5. Septum maturation:** The plasma membranes of the adjacent compartments delimit the septum (thick black vertical line). No cell separation occurs. All five stages of septation take place at the same time within a hypha only spatially separated.

*Sc*Cla4 is activated by *Sc*Cdc42 and is involved in septin ring assembly by directly phosphorylating the septins *Sc*Cdc3 and *Sc*Cdc10 (Caviston *et al.*, 2003; Versele and Thorner, 2004). We found that the septin *Ag*Sep7 constantly localizes as thin filaments to the cortex of the apical hyphal compartment before localization as CCBs at future septa. Together with the septation defect of *Agcla4Δ* mutants it is likely that *Ag*Cdc42 signals via *Ag*Cla4 to the septins. The septins then assemble at the growing tip a CCB and thereby mark the future septa. This CCB of septins becomes reinforced (as GFP signals are usually brighter in subapical regions of the hyphae) and serves as positional cue for the recruitment of all the other proteins we analyzed. Although the PCH protein *Ag*Hof1 localizes as CCB to future septa as early as the septins it is not involved in site selection as it is not essential for localization of the septins, *Ag*Bud3, and *Ag*Myo1.

In the next stage, the bar-to-ring transition, the bars become gradually shorter and the proteins eventually assemble as a cortical ring. In this stage the landmark protein *Ag*Bud3 becomes important for delimiting the future septa and proper ring formation. In *Agbud3Δ* mutants actin, *Ag*Cyk1 and *Ag*Hof1 often form cortical filaments instead of closed rings.

After bar-to-ring transition the contractile actin ring assembles. *Ag*Hof1, *Ag*Myo1, and *Ag*Cyk1 are essential for the assembly of the contractile actin ring. In deletion mutants of all three genes actin rings cannot form. The bar-to-ring transition as well as the persistence of the contractile ring can be very variable in time. In one instance bar-to-ring transition took over 135 min and we measured ring persistence between 60 – 160 min. This stage highlights particularly the differences between unicellular and filamentous fungi. Cytokinesis and septation in the yeasts *S. cerevisiae* and *S. pombe* are tightly coupled to the nuclear cycle and happen only once per cell cycle after completion of mitosis. The generation time of *S. cerevisiae* and *S. pombe* is roughly 1.5 – 2 and 2 – 4 hours, respectively, which sets the time frame for septation. The hyphae of *A. gossypii* contain multiple nuclei that share a common cytoplasm and the nuclear cycle length varies form 46 to 250 min (Gladfelter *et al.*, 2006a). Thus, septation in *A. gossypii* is obviously uncoupled from single nuclear division events.

Next the actomyosin ring as well as the *Ag*Hof1 and *Ag*Cyk1 ring contract and initiate cytokinesis. At this stage *Ag*Bud3 forms double rings that delimit the contractile single rings further confirming its role as a landmark protein. In contrast to the bar-to-ring transition and ring persistence the ring closure rates are very

constant and similar to those observed in *S. cerevisiae* and *S. pombe*. The contraction of the actomyosin ring leads to the invagination and constriction of the plasma membrane. Concomitant with constriction of the plasma membrane a chitin-rich ring forms around the future septum that grows inward. Upon completion of ring contraction cytokinesis occurs: the plasma membranes of the two adjacent hyphal compartments separate. In between the two compartments a chitin-rich continuous disc forms the septum.

In the last stage the completed septum matures. The plasma membranes of the adjacent hyphal compartments become slightly curved, bending away from the septum as it is strengthened. The compartments stay attached because cell separation does not occur. This is a crucial step for filamentous fungi as only the lack of cell separation enables them to form a continuous mycelium. And it highlights again the differences between unicellular and filamentous fungi. In *S. cerevisiae*, after cytokinesis and formation of the primary septum, secondary septa form and new cell wall material is deposited on either side of the primary septum, which is finally degraded and this allows cell separation to occur.

On a genetic level *A. gossypii* and *S. cerevisiae* are very closely related and their lineages have separated only about 100 million years ago. Furthermore, the complete synteny map of both genomes reveals that 95 % of *A. gossypii* genes are orthologs of *S. cerevisiae* genes and 90 % map within blocks of synteny (syntenic homologs) (Dietrich *et al.*, 2004). We wondered why two organisms with so many similar genes adapted so different life styles, especially why one undergoes cell separation whereas the other does not. Therefore we screened the SGD database (Hong *et al.*, 2007) for all *S. cerevisiae* genes that were annotated with the gene ontology term cytokinesis. The query yielded 89 genes. Next we were looking for the homologs of these genes in *A. gossypii* (Dietrich *et al.*, 2004; Gattiker *et al.*, 2007). Two genes were found to have duplicated in *A. gossypii*: the septin *CDC11* and the formin *BNR1*. These genes are known to play a role in septation in *A. gossypii* (Helfer, 2006; Helfer and Gladfelter, 2006); Hans-Peter Schmitz, personal communication) but are unlikely to have an active role in cell separation. Four of those 89 genes have no homolog in *A. gossypii*. One of them is *ScSLA2* which encodes a transmembrane actin-binding protein linking clathrin and endocytosis and is associated with actin patches (Baggett *et al.*, 2003; Pruyne and Bretscher, 2000; Yang *et al.*, 1999), but it is as well rather unlikely to be directly involved in cell separation. Most interesting are the three other genes that have no homolog in *A. gossypii*. These are *ScCTS1* encoding an endochitinase, required for cell separation (Kuranda and Robbins, 1991; O'Conallain *et al.*, 1999), *ScEGT2* encoding a cell wall endoglucanase, required for proper cell separation (Kovacech *et al.*, 1996; Pan and Heitman, 2000; Terashima *et al.*, 2003), and *ScSCW11* encoding a cell wall protein with similarity to glucanases (Cappellaro *et al.*, 1998; Zeitlinger *et al.*, 2003). In other words 3 of the 4 genes missing in *A. gossypii* are directly involved in cell separation. The synteny map of the related ascomycetes ***S. cerevisiae,*** *S. castellii, C. glabrata, A. gossypii, K. lactis, K. waltii* and *S. kluyveri* (Byrne and Wolfe, 2005) shows that *EGT2* is only missing in *A. gossypii* and most likely got lost as a consequence of a translocation between chromosome 7 and chromosome 4. At the syntenic position of *CTS1* is a simple gap in the *A. gossypii* genome but no break of synteny. It is also missing in *S. kluyveri* but there is a break of synteny. A similar situation presents for *SCW11*, no break of synteny in *A. gossypii* but in *S. kluyveri*. These findings allow speculations on the evolution of filamentous growth. Is filamentous growth just a consequence of gene loss? Can one reverse evolution by simple reintroduction of lost genes?

Part III

Construction of a versatile toolbox for PCR-based gene targeting in the filamentous fungus *Ashbya gossypii*

Tagging of genes by chromosomal integration of heterologous PCR-amplified cassettes is an efficient and widely used method to label proteins *in vivo*. This strategy directs the amplified tags and markers to the desired chromosomal loci due to flanking homologous sequences provided by PCR primers. Generation of N- and C-terminally tagged proteins or the exchange of the promoter of a gene has thus become a straightforward method to analyze protein function. For the yeast *Saccharomyces cerevisiae* many plasmid collections covering a wide selection of tags and markers are available. Unfortunately, most of these cassettes cannot be used in the filamentous ascomycete *Ashbya gossypii* as they include the KanMX marker that contains sequences homologous to the *A. gossypii* genome. Furthermore, the *S. cerevisiae ADH1* terminator, which is used for many tags, displays ARS activity in *A. gossypii.* So far, only a limited number of C-terminal tags and no N-terminal tags were available for *A. gossypii*. Therefore we constructed a series of novel cassettes, containing a broad variety of C-terminal epitope tags as well as promoter substitutions in combination with N-terminal tags. We found that the expression of *AgTHI13* is transcriptionally regulated and that the promoter of its homolog from *S. cerevisiae* can be used to regulate gene expression in *A. gossypii*. Using the provided cassettes for N- and C-terminal tagging, promoter exchange and deletion of any given gene, a set of only six primers is required, which makes this method very cost-effective and reproducible. This new toolbox should help to speed up the analysis of gene function in *A. gossypii* and potentially in other ascomycetes in which *S. cerevisiae* promoter sequences are functional.

Introduction

Deletion and tagging of genes by chromosomal integration of heterologous PCR-amplified DNA is a widely used and a fast method to analyze protein function. This simple strategy directs the amplified module to the desired chromosomal loci due to flanking homologous sequences provided by the PCR primers, thus enabling the selective introduction of any sequence at any place of a gene. This method has been shown to be a powerful tool in systematic gene deletion (Winzeler *et al.*, 1999), protein localization (Huh *et al.*, 2003) and protein complex purification (Gavin *et al.*, 2002; Ho *et al.*, 2002), as well as for single gene function analysis. It was first established in the yeast *Saccharomyces cerevisiae* (Wach *et al.*, 1997; Wach *et al.*, 1994) and later in *Schizosaccharomyces pombe* (Bahler *et al.*, 1998). Since then it became a standard method not only in yeasts and bacteria (Gust *et al.*, 2003; Zhang *et al.*, 1998), but also in the ascomycete *A. gossypii* that was the first filamentous fungus in which a PCR-based gene disruption technique had been established (Wendland *et al.*, 2000).

For *S. cerevisiae* many plasmid collections covering a wide selection of modules for protein tagging are available (Bahler *et al.*, 1998; Goldstein and McCusker, 1999; Janke *et al.*, 2004; Knop *et al.*, 1999; Longtine *et al.*, 1998; Sheff and Thorn, 2004; Wach *et al.*, 1997; Wach *et al.*, 1994). This makes the technique most powerful and cost-efficient, as many of these collections contain identical primer-binding sites, which allow the amplification of the cassettes with a minimal set of primers. Unfortunately, these cassettes cannot be used in *A. gossypii* for several reasons: first, the KanMX cassette (Wach *et al.*, 1994), which is widely used in *S. cerevisiae* and other fungi, consists of the *kan*^{R}-ORF flanked by the *A. gossypii TEF1* promoter and terminator and is therefore not heterologous to the *A. gossypii* genome. Second, the HIS3MX6 module (Wach *et al.*, 1997), which would consist of heterologous sequences, cannot be used, because presently no non-reverting *Aghis3* strain is available. Third, the *S. cerevisiae ADH1* terminator, which is used to terminate the transcription of the ORF fusions, shows ARS activity in *A. gossypii* (Knechtle *et al.*, 2003). To circumvent these incompatibilities gene-targeting modules analogous to those used in *S. cerevisiae* have been constructed for the use in *A. gossypii*. The GEN3 cassette consists of the *kan*^{R}-ORF flanked by the *S. cerevisiae TEF2* promoter and terminator and can be used for gene deletions (Wendland *et al.*, 2000). The GUG cassette combines GFP(S65T), the *S. cerevisiae URA3* terminator, and the GEN3 cassette for C-terminal tagging (Knechtle *et al.*, 2003). And the *S. cerevisiae LEU2* gene is used as selection marker for gene deletions in non-reverting *Agleu2Δ* strains (Bauer *et al.*, 2004).

So far, only a limited number of C-terminal and no N-terminal tags were available for *A. gossypii*. Here we

present a total of 103 new modules, including a wide range of C-terminal tags and describe new cassettes that allow the replacement of the promoter of any gene, with the addition of an N-terminal epitope tag to the gene. Use of these modules allows the initial characterization of a candidate gene including its deletion, promoter swap, and tagging experiments with a minimal set of gene specific primers and a small set of standard diagnostic primers. Due to the modular design of the plasmid collection, the construction of PCR-cassettes is straightforward and can be done via standard cloning strategies. Therefore, it will be easy to create new cassettes, e.g., to introduce new combinations of tags, markers, and promoters (in the case of N-terminal tagging). Additionally we show that the expression of *AgTHI13* is transcriptionally regulated. It is repressed in the presence and derepressed in the absence of thiamine. The promoter of *S. cerevisiae THI13* is functional in *A. gossypii* and can be used to regulate gene expression in *A. gossypii.* This is a tool that as not been available for functional genomics in *A. gossypii*.

Materials and Methods

DNA manipulations and sequencing

All DNA manipulations were carried out according to Sambrook and Russell (2001) with *E. coli* strain DH5αF' as host (Hanahan, 1983). Sequencing was done using an ABI prism 377 DNA sequencer (PE Applied Biosystems, Foster City, CA, USA) according to the instructions of the manufacturer or by Microsynth AG (Balgach, Switzerland).

Plasmids and constructs

All plasmids that were used for the construction of the new cassettes are summarized in Table 1; all primers used are listed in Table 2. A comprehensive overview of all new cassettes, with regard to selection markers and tags, is given in Table 3, 4, and 6, and Figure 2.

Deletion cassettes:

pUC19NATPS was constructed by Anne L'Hernault during an internship in the group of Peter Philippsen under the supervision of Dominic Hoepfner (unpublished). NATPS consists of the *nat1*-ORF from *Streptomyces noursei* flanked by the *S. cerevisiae PDC1* promoter and terminator and confers clonNAT/ Nourseothricin (WERNER BioAgents, Jena-Cospeda, Germany) resistance. The *nat1*-ORF was PCR-amplified from pAG25 (Goldstein and McCusker, 1999) using primers PDC1PAG25 S1 and S2 (Table 2) thereby adding 45 bp flanking homologies to the *S. cerevisiae PDC1*-ORF. The PCR product was transformed into *S. cerevisiae* strain DHY6 to knock out the *PDC1*-ORF. Genomic DNA from a *PDC1Δ::nat1* knock-out strain was used as a template to PCR-amplify the *nat1*-ORF including the *PDC1* promoter and terminator sequences using primers (PDC1PST1-AMP1 and -AMP2, Table 2) that add PstI sites to the PCR product. The NATPS cassette was cloned into the PstI site of pUC19 (Vieira and Messing, 1991) to construct pUC19NATPS. We renamed, in agreement with D. Hoepfner, pUC19NATPS to pAGT100. The LEU2 and GEN3 cassettes were cut out with PstI from pScLEU2 (Bauer *et al.*, 2004) and pGEN3 (Wendland *et al.*, 2000) and cloned into the PstI site of pUC19 to construct pAGT120 and pAGT140, respectively. The correct integration of the markers of pAGT100, pAGT120, and pAGT140 has been verified by sequencing.

pAGT100 series: classical C-terminal tags:

The three plasmids encoding the deletion cassettes, pAGT100, pAGT120, and pAGT140, served as backbones for all C-terminal tags. All tags and terminators were PCR-amplified and cloned into the SacI site of each plasmid, upstream of and in the same orientation as the deletion cassettes. Restriction sites not present in the tags and terminators were added by PCR. All tags and terminators have been completely sequenced and verified. For and overview see Table 3.

GFP(S65T) and the *S. cerevisiae URA3* terminator were PCR-amplified from pGUG (Knechtle *et al.*, 2003) with 04.146 and 04.147. The PCR product was cut with SacI and cloned into the three backbones resulting in pAGT101, pAGT121, and pAGT141.

YFP and the *S. cerevisiae URA3* terminator were PCR-amplified from pHPS146 (Hailey *et al.*, 2002); Schmitz, H.P. unpublished) with 04.146 and 04.147. The PCR product was cut with SacI and cloned into the three backbones resulting in pAGT103, pAGT123, and pAGT143.

CFP was PCR-amplified from pHPS144 (Hailey *et al.*, 2002); Schmitz, H.P. unpublished) with 04.146 and 04.147. The PCR product was cut with AscI and ligated to the *S. cerevisiae LYS2* terminator that was amplified with 06.010 and 06.011 from pDP6 (Fleig *et al.*, 1986) and also cut with AscI. The ligation reaction was used as template to PCR-amplify CFP and the *S. cerevisiae LYS2* terminator with 04.146 and 06.011. The PCR product was cut with SacI and cloned into the three backbones resulting in pAGT102, pAGT122, and pAGT142.

RedStar2 was PCR-amplified from pAgRedStar (Gladfelter *et al.*, 2006a; Janke *et al.*, 2004) with 04.368 and 06.034. The PCR product was cut with AscI and ligated to the *S. cerevisiae LYS2* terminator that was

Table 1: Plasmids used in this study

Plasmid	Description	Source or Reference
pUC19	-	Yanisch-Perron *et al.*, 1985
pBSII SK(+) Sca-	pBlueskript II lacking ScaI site	Knechtle, P., unpublished
pUC19NATPS	NATPS cassette	Hoepfner, D., unpublished
pScLEU2	LEU2 cassette	Bauer *et al.*, 2004
pGEN3	GEN3 cassette	Wendland *et al.*, 2000
pGUG	GFP(S65T)-T_{ScURA3}-GEN3	Knechtle *et al.*, 2003
pHPS144	CFP-T_{ScURA3}-GEN3	Schmitz, H.P., unpublished
pHPS146	YFP-T_{ScURA3}-GEN3	Schmitz, H.P., unpublished
pAgRedStar	RedStar2	Gladfelter *et al.*, 2006a
pYM3	6HA	Knop *et al.*, 1999
pFA6a-13Myc-KanMX	13Myc	Longtine *et al.*, 1998
pBS7	Venus	Nagai *et al.*, 2002; YeastResourceCenter, 2006
pBS10	Cerulean	Rizzo *et al.*, 2004; YeastResourceCenter, 2006
pFA6a-GST-KanMX	GST	Longtine *et al.*, 1998
pDP6	ScLYS2	Fleig *et al.*, 1986
pKT127	yEGFP	Sheff and Thorn, 2004
pKT101	yECFP	Sheff and Thorn, 2004
pKT210	yEmCFP	Sheff and Thorn, 2004
pKT220	yECFP-3HA	Sheff and Thorn, 2004
pKT232	yECFP-13Myc	Sheff and Thorn, 2004
pKT090	yEVenus	Sheff and Thorn, 2004
pKT139	yECitrine	Sheff and Thorn, 2004
pKT211	yEmCitrine	Sheff and Thorn, 2004
pKT221	yECitrine-3HA	Sheff and Thorn, 2004
pKT233	yECitrine-13Myc	Sheff and Thorn, 2004
pRSET B-mCherry	mCherry	Shaner *et al.*, 2004
pRSET B-mStrawberry	mStrawberry	Shaner *et al.*, 2004
pRSET B-tdTomato	tdTomato	Shaner *et al.*, 2004
pAG13375	AgTHI13 (AER451W)	Mohr, 1997
pAG1163	AgICL1 (ADL066C)	Mohr, 1997
pAG19274	AgBNI5 (AFR027C)	Mohr, 1997
pAG17217	AgVRP1 (ABR083C)	Mohr, 1997
pAG1807	AgMLC2 (AEL280W)	Mohr, 1997
pG3i PacI^{-}	inverse GEN3 cassette	Köhli, M., unpublished
pN1i	inverse NATPS cassette	this study
pL2i	inverse LEU2 cassette	this study
pK50.3	P_{ScHIS3}	Köhli, M., unpublished
pAN5	P_{ScMEP2}-*lacZ*; YCplac111	Lorberg, A., unpublished
pAMK161	$P_{AgTHI13}$L-lacZ-KanMX; YCplac111	this study
pAMK162	$P_{AgTHI13}$S-lacZ-KanMX; YCplac111	this study
pAMK163	$P_{ScTHI13}$L-lacZ-KanMX; YCplac111	this study
pAMK164	$P_{ScTHI13}$S-lacZ-KanMX; YCplac111	this study
pAMK173	$P_{AgTHI13}$L; pUC19	this study
pAMK174	$P_{AgTHI13}$S; pUC19	this study
pAMK175	$P_{ScTHI13}$L; pUC19	this study
pAMK176	$P_{ScTHI13}$S; pUC19	this study
pAMK1	*AgBNI1* from nucleotide -682 to +523	Schmitz *et al.*, 2006
pAMK177	NATPS-P_{ScHIS3}L-BNI1; pAMK1	this study
pAMK178	NATPS-P_{ScHIS3}S-BNI1; pAMK1	this study
pAMK169	NATPS-P_{ScHIS3}L-BNI1; pBSII	this study
pAMK170	NATPS-P_{ScHIS3}S-BNI1; pBSII	this study
pAMK100	pRS415-AgHOF1	Part II of this thesis
pAMK101	pRS415-AgCYK1	Part II of this thesis

pAMK102	pRS415-AgBUD3	Part II of this thesis
pAMK104	pAgHOF1-GFP-NATPS	Part II of this thesis
pAMK105	pAgHOF1-CFP-NATPS	Part II of this thesis
pAMK106	pAgHOF1-YFP-NATPS; pAMK100 recombined with PCR product from pAGT103 with primers 04.273/04.274	this study
-	pAgHOF1-RedStar2-NATPS; pAMK100 recombined with PCR product from pAGT104 with primers 04.273/04.274	this study
pAMK121	pAgBUD3-GFP-GEN3	Part II of this thesis
pAMK122	pAgBUD3-YFP-GEN3	Part II of this thesis
pAMK127	pAgCYK1-YFP-GEN3; pAMK101 recombined with PCR product from pAGT143 with primers 05.135/05.196	this study
pAMK116	pAgBNI5-GFP-GEN3; pAG19274 recombined with PCR product from pAGT141 with primers 04.477/04.476	this study
pAMK117	pAgBNI5-YFP-GEN3; pAG19274 recombined with PCR product from pAGT143 with primers 04.477/04.476	this study
pAMK118	pAgVRP1-GFP-GEN3; pAG17217 recombined with PCR product from pAGT141 with primers 04.480/04.479	this study
pMV	pAgMLC2-Venus; pAG1807 recombined with PCR product from pAGT147 with primers 06.009/05.322	this study

Table 2: Primers used in this study

	Name	Sequence (5'→3')	use
	PDC1PAG25 S1	**TCTCAATTATTATTTTCTACTCATAACCTCACGCAAAATAACACAGTCAAATCAATCA** AAATGGGTACCACTCTTGACGAC	gene targeting
	PDC1PAG25 S2	**CGTTACATAAAAATGCTTATAAAACTTTAACTAATAATTAGAGATTAAATCGC** TTAGGGGCAGGGCATGCTCATG	gene targeting
	PDC1PST1-AMP1	AAActgcagAACCGTTACGGTATTTTACTATGGAATAATCAATCAATTGAGG	cloning
	PDC1PST1-AMP2	AAActgcagCCAAACAGTGTTCCTTAATCAAGGATACCTC	cloning
04.146	GFPS65T	CCAAgagctcAGTAAAGGAGAAGAACTTTTCAC	cloning
04.147	URA3T	CCAAgagctcTATGCGTCCATCTTTACAGTC	cloning
06.010	LYS2-AscI	AGggcgcgccGGTTGAGCATTACGTATGATATG	cloning
06.011	LYS2-SacI	ATTCgagctcTCATTTTAGACCCATGGTGG	cloning
04.368	DsRed5'	CCAAgagctcATGAGTGCTTCTTCTGAAGATG	cloning
06.034	Red-AscI	AGggcgcgccTTACAAGAACAAGTGGTGTCTAC	cloning
04.150	6HA	CCAAgagctcTACCCATACGATGTTCCTGAC	cloning
06.035	6HA-AscI	AGggcgcgccTTAGCTAGAAGCGTAATCTGG	cloning
06.036	13Myc-SacI	ATTCgagctcAACGGTGAACAAAAGCTAATC	cloning
06.037	13Myc-AscI	AGggcgcgccCTAGTGATTGATTAATTTTTGTTC	cloning
	URA3t_AscI	ggcgcgccATTATAAGTAAATGCATGTATAC	cloning
04.366	TADH	CCAAgagctcATATTACCCTGTTATCCCTAGC	cloning
06.038	GST-SacI	ATTCgagctcATGTCCCCTATACTAGGTTATTG	cloning
06.269	SacI-PacI-RFP	GTACCgagctcttaattaaCATGGTGAGCAAGGGCGAG	cloning
06.271	RFP-AscI	CAACCggcgcgccTTACTTGTACAGCTCGTCCATGC	cloning
06.267	SacI-PacI-XFP	GTACCgagctcttaattaaCATGTCTAAAGGTGAAG	cloning
06.268	XFP-link-SacI	AATTCgagctcAATGCACCGTCACCTGCGCCCGCGCCTTTGTACAATTCATCCATACC	cloning
06.270	RFP-link-SacI	AATTCgagctcAATGCACCGTCACCTGCGCCCGCGCCCTTGTACAGCTCGTCCATGC	cloning
04.488	F1-37	TGTGCTGCAAGGCGATTAAG	sequencing
05.028	SEQ-GCYFP	CAAGAGTGCCATGCCCGAAG	sequencing
05.029	SEQ-RFP	GGTGGCGTTGTTACTGTTAC	sequencing
05.030	SEQ-REV	CTGCAGGTCGACTCTAGAGG	sequencing
04.489	F2+49	TTATGCTTCCGGCTCGTATG	sequencing
04.050	AgACT1-N1	CACGGTATCGTCACAAACTG	Northern blot
04.051	AgACT1-N2	AGAGGCCAAGATAGAACCAC	Northern blot
04.052	AgICL1-N1	GCCGAAGCCGAGGATATTAG	Northern blot

04.053	AgICL1-N2	TGACGGCTTCATGGAATAAC	Northern blot
04.056	AgTHI13-N1	TTTCCCGGTCACTTCTGTTG	Northern blot
04.057	AgTHI13-N2	TGATGGACCGCCATTAAACG	Northern blot
04.168	ScTHI13-P1.1	CTATcccgggCGAGCGTATTTAATATGTCC	cloning
04.169	ScTHI13-P1.2	CTATcccgggTAAGATTGGCGCGTTAATGC	cloning
04.170	ScTHI13-P2	GCTAggatccAGCTTGGAAGTATGTGTATTG	cloning
04.171	AgTHI13-P1	CATAcccgggCTATATTAGCTGTGAAGCTCG	cloning
04.172	AgTHI13-P1.1	CATAcccgggGACGGGGGTTGAATATGTAG	cloning
04.173	AgTHI13-P2	CATAggatccGGCTCATCAGCCGCTTTATATACC	cloning
04.379	AgBNI1-PFUS1	**CAGTGGGACAAGGCAGCAGGTGTGGAACACGGCGGGACGCAGGATTTACCG GTATAGTGG**ACGGCCAGTGAATTCGAG	gene targeting
04.380	AgBNI1-PFUS2	**GGCAACCTGCCCCGCGTGCTGTGTTTTGGAGTGTTTGTTCGAGTGCGTGGAC TTCTTCAT**CAGCTTGGAAGTATGTGTATTG	gene targeting
01.059	AgBNI1-G1	CCCGACCACCGTCTTGGACC	analytical PCR
02.101	AgBNI1-G1.1	AAGCCTACCACCCTGTGGGGGA	analytical PCR
01.060	AgBNI1-I1	CAGATCGGGCCTGTGTTACC	analytical PCR
02.102	V2PDC1P	GAACAAACCCAAATCTGATTGCAAGGAGAGTGAAAGAGCCTT	analytical PCR
04.381	VPT13	CTCTTGTGACGACAGCAAAC	analytical PCR
06.039	proHIS-pacI-5	GCttaattaaTATTACTCTTGGCCTCCTC	cloning
06.040	proHis-pacI-3	GCttaattaaTTTGCCTTCGTTTATCTTGC	cloning
06.009	AgMLC2-F1	**GGCCAGCAGCTGTTCAAGGGCAAACGGTTCCTCGACGCGGTGAGCGAG** AAAACGACGGCCAGTGAATTCG	gene targeting
05.322	AgMLC2-F2	**CTTATAGGCGCTCCGCGCGTATACACCCTACGTACTTGTATAATATAATACAT** GATTACGCCAAGCTTGC	gene targeting
05.321	AgMLC2-G1	CCCTTCCAAGCCACCAATTC	analytical PCR
05.323	AgMLC2-I1	GGCAGTCGCTCGGAAAGAAG	analytical PCR
05.324	AgMLC2-G4	CAGCAGCAGGAGCAGCATAG	analytical PCR
04.289	AgBNI5-G1	GAGAACACGGAGCAGAAGG	analytical PCR
04.290	AgBNI5-G4	ATTCGTCGGGATTTGGAAG	analytical PCR
04.291	AgBNI5-I1	CTGACGAACCTGATGAAGAC	analytical PCR
04.292	AgVRP1-G1	TTGTTCTGGTCGTCGCTTTG	analytical PCR
04.293	AgVRP1-G4	TGACGGGTTGGGAATAGTTG	analytical PCR
04.294	AgVRP1-I1	TATGAAACCGCTGACACTCC	analytical PCR
04.476	AgBNI5-NS2	**AAATTTTCGTCAGCCCGCGGCCACGTGACCGGCGGCGGCC** TACGCCAAGCTTGCATGCCT	gene targeting
04.477	AgBNI5-FUS1	**GCAAGCATATCAACAACGGGTCCAACGGGCAGTTCTGGCTCAGCGGCAAG** AAAACGACGGCCAGTGAATTCG	gene targeting
04.479	AgVRP1-NS2	AATGACTTCTAACACATGATATATACACCCGCACGTGTGCTACGCCA AGCTTGCATGCCT	gene targeting
04.480	AgVRP1-FUS1	**ACCCCAGCGGTAGAGGCAGCAGCGTTCCGTTAGATTTAAGTTTATATTCC** AAAACGACGGCCAGTGAATTCG	gene targeting
05.009	CYK-G1	TAGAGACCACGGCATTTG	analytical PCR
05.010	CYK-G4	GGCTGCTTTCTCCTATTG	analytical PCR
05.135	AgCYK1-F1	**AGGAGCGCAACTTTTAAAATATCAGCGCTAATAGACCTACTTTGTGAAGTGT TTTTTAGG**AAAACGACGGCCAGTGAATTCG	gene targeting
05.146	AgCYK1-F2	**TTATACTTACGTAACGATGGATAAGGACAACAATAATAATTAATACGGACGAATT** CATCAACCATGATTACGCCAAGCTTGC	gene targeting
02.129	AgHOF1-G4	GCAGTCGATGGCCATCCTTG	analytical PCR
03.476	AgHOF1-I2	CAACGCACGGAAATGAGTGG	analytical PCR
03.477	AgHOF1-G5	AATAGTCCTTTGCGGTGGCC	analytical PCR
04.273	AgHOF1Fus1	**TATCGGGGAAGTCCACAATGGGAACGGCAAGCAGGGGCTCATTCCGATGAA CTACGTGGAACTGCTCTCC**AAAACGACGGCCAGTGAATTCG	gene targeting
04.274	AgHOF1 S2	**CGTTACAACGTCCTAATATGTAATAGTCCTTTGCGGTGGCCAGGCGCCACGCT TTGTTACAGTTTTGATTAC**CATGATTACGCCAAGCTTGC	gene targeting
05.350	AgHOF1-I4	AAACTGGAGAAGGCGAAGGC	analytical PCR
05.364	AgHOF1-I5	CGCTTGGCGCTCTTGTACTC	analytical PCR

Flanking homologous sequences are indicated in bold

Restriction sites are indicated in lower case characters

Table 7: Standard annealing sequences for the amplification of pAGT cassettes

Primer	Sequence (5'→3')
NS1	Homology region + CCAGTGAATTCGAGCTCGG
F1	Homology region + AAAACGACGGCCAGTGAATTCG
F5	Homology region + GGTGACGGTGCTGGTTTA
NF5	Homology region + ACACAGGAAACAGCTATGAC
R3	Homology region + ACACAGGAAACAGCTATGAC
NR3	Homology region + CAATGCACCGTCACCTGC
PF1	Homology region + ACGGCCAGTGAATTCGAG
PF2	Homology region + CAGCTTGGAAGTATGTGTATTG

Table 8: Standard primer sequences for analytical PCR

Use	Primer	Sequence (5'→3')
NATPS 5'	V2*NAT1	GTGTCGTCAAGAGTGGTACC
NATPS 3'	V3*NAT1	ACATGAGCATGCCCTGCCCC
LEU2 5'	L2	TTTAGGACCAGCCACAGCACC
LEU2 3'	L3	AACTGGTGATTTAGGTGGTTCC
GEN3 5'	G2.3	GGAGGTAGTTTGCTGATTGG
GEN3 3'	G3.3	ATGTTGGACGAGTCGGAATC
green, cyan and yellow C-terminal tags	green2.2	TGTAGTTCCCGTCATCTTTG
yeast-optimized green, cyan and yellow C-terminal tags	ygreen	CTTCAGCTCTGGTCTTGTAG
green, cyan and yellow N-terminal tags	Nygreen	TTGGTGATGGTCCAGTCTTG
RedStar2 C-terminal tag	RedI	GAATGGCAGTGGACCACCCTTAG
mCherry, mStrawberry, tdTomato C-terminal tags	Red2	TCATCACGCGCTCCCACTTG
mCherry, mStrawberry, tdTomato N-terminal tags	RedN	CCCGTAATGCAGAAGAAG
13Myc	MycI	CGAGTCCGTTCAAGTCTTCTTCTGAG
$P_{ScTHI13}$	VPT13	CTCTTGTGACGACAGCAAAC

Table 9: *A. gossypii* strains used in this study

Strain	Genotype	Reference
ΔlΔt	*leu2Δ thr4Δ*	Altmann-Johl and Philippsen, 1996
K51.52	*GEN3*-P_{ScHIS3}*-GFP(S65T)-BUD6 leu2Δ thr4Δ*	Köhli, M., unpublished
K67.52	*GEN3*-P_{ScHIS3}*-yEGFP-BUD6 leu2Δ thr4Δ*	Köhli, M., unpublished
AMK009	*hof1Δ::NATPS leu2Δ thr4Δ*	Part II of this thesis
AMK012	*HOF1-GFP-NATPS leu2Δ thr4Δ*	Part II of this thesis
AMK027	*NATPS*-P_{ScHIS3}*L-BNI1 leu2Δ thr4Δ*	this study
AMK028	*NATPS*-P_{ScHIS3}*S-BNI1 leu2Δ thr4Δ*	this study
AMK047	P_{ScMEP2}*-lacZ-KanMX*(pAN5) *leu2Δ thr4Δ*	this study
AMK048	$P_{AgTHI13}$*L-lacZ-KanMX*(pAMK161) *leu2Δ thr4Δ*	this study
AMK049	$P_{AgTHI13}$*S-lacZ-KanMX*(pAMK162) *leu2Δ thr4Δ*	this study
AMK050	$P_{ScTHI13}$*L-lacZ-KanMX*(pAMK163) *leu2Δ thr4Δ*	this study
AMK051	$P_{ScTHI13}$*S-lacZ-KanMX*(pAMK164) *leu2Δ thr4Δ*	this study

amplified with 06.010 and 06.011 from pDP6 and also cut with AscI. The ligation reaction was used as template to PCR-amplify RedStar2 and the *S. cerevisiae LYS2* terminator with 04.368 and 06.011. The PCR product was cut with SacI and cloned into the three backbones resulting in pAGT104, pAGT124, and pAGT144.

6HA was PCR-amplified from pYM3 (Knop *et al.*, 1999) with 04.150 and 06.035. The PCR product was cut with AscI and ligated to the *S. cerevisiae LYS2* terminator that was amplified from pDP6 with 06.010 and 06.011 and also cut with AscI. The ligation reaction was used as template to PCR-amplify 6HA and the *S. cerevisiae LYS2* terminator with 04.150 and 06.011. The PCR product was cut with SacI and cloned into the three backbones resulting in pAGT105, pAGT125, and pAGT145.

13Myc was PCR-amplified from pFA6a-13Myc-KanMX (Longtine *et al.*, 1998) with 06.036 and 06.037. The PCR product was cut with AscI and ligated to the *S. cerevisiae URA3* terminator that was amplified from

pGUG with URA3t_AscI and 04.147 and also cut with AscI. The ligation reaction was used as template to PCR-amplify 13Myc and the *S. cerevisiae URA3* terminator with 06.036 and 04.147. The PCR product was cut with SacI and cloned into the three backbones resulting in pAGT106, pAGT126, and pAGT146.

Cerulean was PCR-amplified from pBS10 (Rizzo *et al.*, 2004; YeastResourceCenter, 2006) with 04.146 and 04.366. The PCR product was cut with AscI and ligated to the *S. cerevisiae LYS2* terminator that was amplified with 06.010 and 06.011 from pDP6 and also cut with AscI. The ligation reaction was used as template to PCR-amplify Cerulean and the *S. cerevisiae LYS2* terminator with 04.146 and 06.011. The PCR product was cut with SacI and cloned into the three backbones resulting in pAGT108, pAGT128, and pAGT148.

Venus was PCR-amplified from pBS7 (Nagai *et al.*, 2002; YeastResourceCenter, 2006) with 04.146 and 04.366. The PCR product was cut with AscI and ligated to the *S. cerevisiae URA3* terminator that was amplified from pGUG with URA3t_AscI and 04.147 and also cut with AscI. The ligation reaction was used as template to PCR-amplify Venus and the *S. cerevisiae URA3* terminator with 04.146 and 04.147. The PCR product was cut with SacI and cloned into the three backbones resulting in pAGT107, pAGT127, and pAGT147.

GST was PCR-amplified from pFA6a-GST-KanMX (Longtine *et al.*, 1998) with 06.038 and 04.366. The PCR product was cut with AscI and ligated to the *S. cerevisiae URA3* terminator that was amplified from pGUG with URA3t_AscI and 04.147 and also cut with AscI. The ligation reaction was used as template to PCR-amplify GST and the *S. cerevisiae URA3* terminator with 06.038 and 04.147. The PCR product was cut with SacI and cloned into the three backbones resulting in pAGT109, pAGT129, and pAGT149.

pAGT200 series: enhanced C-terminal tags:

For and overview see Table 3. The AatII and AscI fragments of plasmids pKT127(yEGFP), pKT090(yEVenus), pKT139 (yECitrine), pKT211(yEmCitrine), and pKT233(yECitrine-13Myc) (Sheff and Thorn, 2004), containing the linkers and tags, were ligated into the AatII and AscI backbone fragments of pAGT103, pAGT123, and pAGT143, containing the terminators and markers, resulting in pAGT201, pAGT221, pAGT241, pAGT206, pAGT226, pAGT246, pAGT207, pAGT227, pAGT247, pAGT208, pAGT228, pAGT248, pAGT210, pAGT230, and pAGT240, respectively.

The AatII and AscI fragments of plasmids pKT101(yECFP), pKT210(yEmCFP), and pKT232(yECFP-13Myc) (Sheff and Thorn, 2004), containing the linkers and tags, were ligated into the AatII and AscI backbone fragments of pAGT102, pAGT122, and pAGT142, containing the terminators and markers, resulting in pAGT202, pAGT222, pAGT242, pAGT203, pAGT223, pAGT243, pAGT205, pAGT225, and pAGT245, respectively.

The NotI and AscI fragment of plasmid pKT221(yECFP-3HA) (Sheff and Thorn, 2004), containing the linker and tag, was ligated into the NotI and AscI backbone fragments of pAGT205, pAGT222, and pAGT242, containing the terminators and markers, resulting in pAGT204, pAGT224, and pAGT244, respectively.

The NotI and AscI fragment of plasmid pKT220(yECitrne-3HA) (Sheff and Thorn, 2004), containing the linker and tag, was ligated into the NotI and AscI backbone fragments of pAGT210, pAGT230, and pAGT250, containing the terminators and markers, resulting in pAGT209, pAGT229, and pAGT249, respectively.

mCherry, mStrawberry, and tdTomato were amplified with the primers 06.269 and 06.271 from the plasmids pRSET B-mCherry, pRSET B-mStrawberry, and pRSET B-tdTomato (Shaner *et al.*, 2004), respectively. The PCR products and the plasmid pAGT205 were cut with PacI and AscI and the PCR products, providing the tags, were cloned into the plasmid, providing the linker, terminator and marker, resulting in pAGT211, pAGT212, pAGT213. After cloning, all linker and tags have been verified by sequencing. Then the AatII and AscI fragments of plasmids pAGT211, pAGT212, and pAGT213, containing the linker and tags, were ligated into the AatII and AscI backbone fragments of pAGT122 and pAGT142, containing the terminators and markers, resulting in pAGT231, pAGT251, pAGT232, pAGT252, pAGT233, and pAGT253, respectively. These resulting plasmids have not yet been verified by sequencing at the time this manuscript was written. All other linkers and tags of the pAGT200 series have been completely sequenced and verified.

pAGT300 series: enhanced N-terminal tags and promoter substitution:

For and overview see Table 4. To construct the plasmid collection for N-terminal tagging we had to switch the orientation of the 3 selection markers of pAGT100, pAGT120, and pATG140 in order to give the selection markers the same orientation as the tags and to be able to use the SacI site to insert the tag. pAGT100 and pAGT120 were cut with PstI and religated. Plasmids with desired orientation of the markers were isolated and named pN1i and pL2i, respectively. pG3i PacI-, a derivative of

pAGT140, where the marker has reversed orientation and the PacI site in the *ScTEF2* terminator has been removed was obtained from M. Kohli (unpublished). The primers 06.267 and 06.268 were used to PCR-amplify the tags from pAGT201, pAGT202, pAGT203, pAGT206, pAGT207, and pAGT208 and the primers 06.269 and 06.270 were used to PCR-amplify the tags from pRSET B-mCherry, pRSET B-mStrawberry, and pRSET B-tdTomato. After SacI restriction digest of the PCR products and pG3i PacI-, the PCR products were ligated into the vector backbone, resulting in pAGT341, pAGT342, pAGT343, pAGT346, pAGT347, pAGT348, pAGT351, pAGT352, pAGT353. After verification of all linkers and tags by sequencing the SacI fragments of these plasmids were cloned into the SacI site of pN1i and pL2i, resulting in pAGT301, pAGT302, pAGT303, pAGT306, pAGT307, pAGT308, pAGT301, pAGT302, and pAGT303 and pAGT321, pAGT322, pAGT323, pAGT326, pAGT327, pAGT328, pAGT321, pAGT322, and pAGT323, respectively. These resulting plasmids have not yet been verified by sequencing at the time this manuscript was written.

The *ScHIS3* promoter was PCR-amplified using primers 06.040 and 06.039 and pK50.3 (Michael Köhli, unpublished) as template. The PCR product was cut with PacI and cloned into the PacI site of pAGT341 to construct pAGT341-PHIS3.

S. cerevisiae THI13 promoter-substitution cassettes:

For and overview see Table 6. A long (692 bps) and a short (348 bps) fragment of the *AgTHI13* promoter was amplified using primers 04.171/04.173 and 04.172/04.173, respectively, and pAG13375 (Mohr, 1997) as template. The long and short PCR products were cut with SmaI and BamHI and cloned into pUC19, resulting in pAMK173 and pAMK174, respectively. The long and short promoter fragments were cut out with AvaI and BamHI and cloned into SalI/BamHI-cut pAN5 (Lorberg, A. unpublished), resulting in pAMK161 and pAMK162, respectively.

A long (744 bps) and a short (358 bps) fragment of the *ScTHI13* promoter was amplified using primers 04.168/04.170 and 04.169/04.170, respectively, and genomic DNA from CEN.PK2 (van Dijken *et al.*, 2000) as template. The long and short PCR products were cut with SmaI and BamHI and cloned into pUC19, resulting in pAMK175 and pAMK176, respectively. The long and short promoter fragments were cut out with NspI and BamHI and cloned into SphI/BamHI-cut pAN5 (Lorberg, A. unpublished.), resulting in pAMK163 and pAMK164, respectively.

The HindIII/XbaI fragment of pAGT100 was blunt-ended with Pwo polymerase and cloned into the SmaI site of pAMK175 and pAMK176 to construct pN1PT13L and pN1PT13S, respectively. The HindIII/XbaI fragment of pScLEU2 was blunt-ended with Pwo polymerase and cloned into the SmaI site of pAMK175 and pAMK176 to construct pL2PT13L and pL2PT13S, respectively. The selection markers were integrated upstream of and in the same orientation as the promoter. The SmaI/AflIII fragment of pAMK175 and pAMK176 was cloned into the EcoRV/AflIII sites of pGEN3 to construct pG3PT13L and pG3PT13S, respectively. The promoters were integrated upstream of and in the inverse orientation as the selection marker. pN1PT13L, pN1PT13S, pL2PT13L, pL2PT13SL, pG3PT13L, and pG3PT13S have not yet been verified by sequencing at the time this manuscript was written.

Amplification of PCR cassettes

A set of six gene-specific primers allows amplifying all N- and C-terminal tags and to generate gene deletions. NS1/R3 to amplify all deletion cassettes. F1/R3 to amplify all C-terminal fusion cassettes of the pAGT100 series. F5/R3 to amplify all C-terminal fusion cassettes of the pAGT200 series. NF5/NR3 to amplify all N-terminal fusion cassettes of the pAGT300 series. The standard annealing sequences of these primers are given in Table 7.

Isolation of genomic DNA and analytical PCR

Isolation of genomic DNA from *A. gossypii* as described in Wright and Philippsen (1991) is a time-consuming procedure and therefore not suited to screen a large number of potential transformants. On the other hand colony PCR, i.e. adding a small piece of mycelia directly into the PCR tube, as described in Wendland *et al.* (2000), is, based on our observations, unreliable and only rarely gives a PCR product (not shown). We describe here a new protocol to quickly isolate genomic DNA and a PCR protocol for consistent and reliable results in diagnostic PCR. To isolate genomic DNA for diagnostic PCR, small piece of mycelium (about the size of two pinheads) was mixed in a 1.5 ml tube with 0.2 g of 0.5 mm glass beads, 200 µl 'DNA extraction buffer' (50 mM NaCl, 1 mM EDTA pH 8.0, 10 mM Tris-HCl pH 8.0, 0.5 % v/v Triton X-100) and 100 µl of water-saturated 70 % phenol/chloroform solution. The tube was vortexed for 10 min at 4 °C and centrifuged at 17'000 x g for 15 min at room temperature for phase separation. Of the upper aqueous phase 10 µl were carefully taken away, diluted with 90 µl of ddH_2O. Although traces of phenol/chloroform would inhibit the PCR reaction we never experienced any difficulties of that kind and further purification of the DNA by ethanol precipitation was not necessary. This DNA solution was directly used as template in the following PCR mix: 3 µl template DNA, 1 µl each of 10 µM primer 1 and 2, 3 µl dNTPs (2mM for each nucleotide), 6 µl 5 M Betaine, 2 µl 10x

PCR reaction buffer with $MgCl_2$ (Roche Diagnostics GmbH, Penberg, Germany), 4 µl ddH_2O. After10 min at 96 °C the following mix was added (hot start PCR): 1 µl 10x PCR reaction buffer with $MgCl_2$, 0.1 µl Taq DNA Polymerase (5 U/ µl; Roche Diagnostics GmbH, Penberg, Germany), 8.9 µl ddH_2O. The PCR was done using the following conditions: 30 s denaturation at 94 °C, 30 s annealing at 50 °C, 1 min elongation at 72 °C, 35 cycles. Because of the high GC content (52 %) of the *A. gossypii* genome (Dietrich *et al.*, 2004) and as the addition of betaine has been reported to reduce the base pair composition dependence on DNA strand melting (Rees *et al.*, 1993) we found it helpful to add betaine at a relatively high concentration to the PCR mixture. Following these protocols we could quickly and reliably screen large numbers of potential transformants (data not shown).

Analytical PCR (Wendland *et al.*, 2000; reviewed by Wendland, 2003b) is used to verify the correct integration of the pAGT cassettes into the target locus. 3 gene-specific together with 2 standard primers that bind within the cassettes are used. One gene-specific primer binds upstream (G1) of, one downstream (G4) of and one within (I1) the target ORF. One standard primer binds in the 5' region (G2) and one in the 3' region (G3) of the cassettes. The following primer combinations are used to verify the correct integration of the cassettes: G1/G2, G4/G3, and I1/G2. Names and sequences of standard primers are given in Table 8.

Ashbya gossypii strains, media and transformation

A. gossypii media and transformation protocols are described in part II of this manuscript. All strains used in this study are listed in Table 9.

Saccharomyces cerevisiae strains and methods

PCR products were transformed according to (Gietz *et al.*, 1995) into yeast strain DHY6 (*MATα/a HHF2:: GFP-KanMX6/HHF2 ura3-52Δ1/ura3-52Δ1 trp1Δ63/ TRP1 leu2Δ1/LEU2 his3Δ 200/HIS3*; (Hoepfner *et al.*, 2000)). Genomic DNA from CEN.PK2 (*MAT*a/α *ura3-52Δ/ura3-52Δ trp1-289/trp1-289 leu2-3,112/leu2-3,112 his3Δ1/his3Δ1 MAL2-8C/MAL2-8C SUC2/SUC2*; (Entian and Kötter, 1998; van Dijken *et al.*, 2000) was used to amplify promoter fragments.

RNA isolation

A. gossypii mycelia of liquid cultures were collected by filtration and used to generate protoplasts (adapted from (Beggs, 1978; Hinnen *et al.*, 1978; Wright and Philippsen, 1991)). About 500 mg mycelia (wet weight) were resuspended in 1.5 ml SPEZ buffer (1 M sorbitol, 10 mM sodium phosphate buffer pH 5.8, 10 mM EDTA, 2 mg/ml Zymolyase®-20T (Seikagaku Corp., Tokyo, Japan), 1 µl/ml 2-mercaptoethanol) and incubated with gentle agitation at 30 °C for about 35 min until, judged by microscopic inspection, protoplasts had formed. Protoplasts were collected by centrifugation at 500 x g for 5 min. From this point total RNA was isolated using the RNeasy Kit (Qiagen AG, Hombrechtikon, Switzerland) according to the protocol for filamentous fungi.

Probe generation, Northern blotting, hybridization and detection

Probes for Northern blotting were generated by PCR. 04.050 and 04.051 were used to generate the probe for *AgACT1* using genomic DNA as template. 04.052 and 04.053 were used to generate the probe for *AgICL1* using pAG1163 (Mohr, 1997) as template. 04.056 and 04.057 were used to generate the probe for *AgTHI13* using pAG13375 (Mohr, 1997) as template. PCR products were biotinylated using the BrightStar Psoralen-Biotin Nonisotopic Labeling Kit (Ambion, Austin, Texas, USA). 15 – 25 µg total RNA and a RNA Ladder (New England BioLabs, Ipswich, Massachusetts, USA) were separated on a 7 mm 1.2 % denaturing agarose gel at 62 V 400 mA for 4 h and blotted for 3 h on Biodyne® B Nylon Membranes (PIERCE, Rockford, Illinois, USA) using the NorthernMax® Kit and Protocol (Ambion, Austin, Texas, USA). After blotting the RNA was cross-linked to the membrane by UV irradiation at 254 nm for 1 min 45 sec at 1.5 J/cm^2. 15 – 25 ng/ml biotinylated probes were used to hybridize to and detect the immobilized RNA using the North2South Chemiluminescent Hybridization and Detection Kit (PIERCE, Rockford, Illinois, USA). Pre-hybridization for 1 h 15 min and overnight hybridization at 55 °C was carried out in a Hybaid Hybridisation Oven (Hybaid Ltd., Teddington, Middlesex, England).

X-Gal overlay assay

A. gossypii mycelia were grown on agar plates for 3 days. 10 ml of each 1M sodium phosphate buffer pH 7.0 and 1 % w/v agarose in H_2O were boiled separately and let cool down while stirring. Just before solidification the two solutions were pooled and 20 µl 10 % w/v SDS and 400 µl 5 mg/ml X-Gal in DMF were added. This solution was used to overlay the agar plates. Blue coloration was visible within hours after incubation at 37 °C.

Protein extraction and β-galactosidase activity assay

A. gossypii mycelia grown overnight in 40 ml ASC were centrifuged for 5 min at 2,500 x g at 4 °C. 500 µl

'pellet' was mixed with 500 µl LacZ buffer (0.1 M sodium phosphate pH 7, 10 mM KCl, 1 mM $MgSO_4$,) and 500 µl 0.5 mm Zirconia/Silica beads (BioSpec Products Inc., Bartlesville, Oklahoma, USA) and vortexed at 4 °C for 4 times 10 min. Before and in between each interval the tubes were put on ice for 1 min. The samples were centrifuged at 17,900 x g for 10 min at 4 °C and the crude protein extract (supernatant) was collected. β-galactosidase activity in the crude protein extracts was determined using the protocol described in (Burke *et al.*, 2000).

Microscopy techniques, image acquisition and processing

Microscopy techniques, image acquisition and processing are described in detail in Part II of this thesis.

Results

Deletion cassettes

Currently, three heterologous selection markers are used in *A. gossypii* for PCR-based gene targeting: The auxotrophic marker LEU2 and the dominant drug resistance markers GEN3 and NATPS. LEU2, encoded on pScLEU2 (Bauer *et al.*, 2004), consists of the *S. cerevisiae LEU2* gene. GEN3, encoded on pGEN3, was constructed analogous to the KanMX cassette used in *S. cerevisiae* (Wach *et al.*, 1994). It consists of the *kan*^{R}–ORF flanked by the *S. cerevisiae TEF*2 promoter and terminator and confers G418/ Geneticin resistance (Wendland *et al.*, 2000). NATPS encoded on pUC19NATPS consists of the *nat1*-ORF from *Streptomyces noursei* flanked by the *S. cerevisiae PDC1* promoter and terminator and confers clonNAT resistance (Goldstein and McCusker, 1999; Dominic Hoepfner, unpublished; Figure 1). Because pGEN3 (Wendland *et al.*, 2000) and pScLEU2 (Bauer *et al.*, 2004) are not pUC19-based as pUC19NATPS, different pairs of primers were necessary to delete one gene with the three different markers. To be able to use only one set of gene-specific primers for the deletion of one gene with the three different markers, the GEN3 and the LEU2 cassettes were cloned from pGEN3 and pScLEU2 into pUC19. The three pUC19-based plasmids were named pAGT100 (NATPS), pAGT120 (LEU2), and pAGT140 (GEN3) (Table 3 and Figure 2, A).

pAGT100 series: classical C-terminal tags

So far, only a limited number of C-terminal tags were available for *A. gossypii*. Namely GFP(S65T)-GEN3 from the GUG cassette (Knechtle *et al.*, 2003) and YFP, CFP and GST in combination with the GEN3 or the NATPS cassette (Hans-Peter Schmitz and Hans-Peter Helfer, unpublished). Additionally, the red fluorescent protein variant RedStar2 (Janke *et al.*, 2004) was successfully used to tag *A. gossypii* genes on plasmids (Gladfelter *et al.*, 2006a) but this cassette, for the above mentioned reasons, is not suitable to tag *A. gossypii* genes at their chromosomal loci as it contains the *S. cerevisiae ADH1* terminator. No tags were available in combination with the *S. cerevisiae LEU2* gene as marker. Furthermore, different pairs of primers were necessary to amplify these tags for labeling the same gene with different fluorophores. Thus, we decided to build up a plasmid collection that contains a wide array of different tags, all three markers, and can be amplified with only one pair of gene-specific primers.

We included 3 variants of fluorescent proteins that are well established and widely used (GFP(S65T), CFP, and YFP) as well as 3 newer variants (Cerulean, Venus, and RedStar2). Additionally we included 3 epitope tags that can be used for protein purification or immunostaining (6HA, 13Myc, and GST). The cassettes for C-terminal tagging were all constructed in the same modular way. The 3 plasmids containing the deletion cassettes served as backbones. All tags, linked to either the *ScURA3* or *ScLYS2* terminator via an AscI site, were cloned upstream of and in the same orientation as the markers

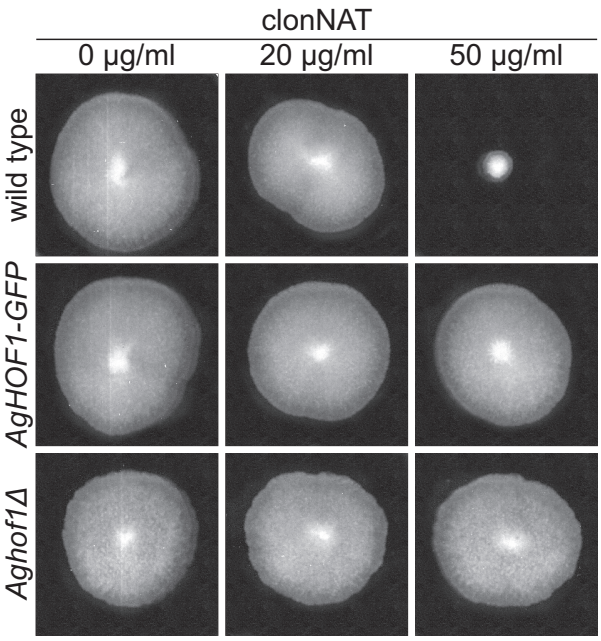

Figure 1: Effects of clonNAT on growth of different *A. gossypii* strains.

3 strains were grown on AFM plates in presence of 0, 20, or 50 µg/ml clonNAT. The reference strain *AlΔt* is able to grow at a clonNAT concentration of 20 but not at a concentration of 50 µg/ml. The strains transformed with either the GFP cassette GFP-NATPS from pAGT101 (*AgHOF1-GFP*) or the deletion cassette NATPS from pAGT100 (*Aghof1Δ*) show no growth defect at a clonNAT concentration of 50 µg/ml.

into the SacI site. An overview of all tag/terminator/marker combinations and the names of the resulting plasmids are given in Table 3 and Figure 2, A. The tag/terminator combinations were chosen in ways that in the case of colabeling no homologous sequences are present (except for the homologies between the *Aquorea victoria* derived fluorescent proteins). For example, all cyan tags come with the *ScLYS2* and all yellow tags with the *ScURA3* terminator.

For successful and unsuccessful applications of the GFP, CFP, YFP, and RedStar2 tags in combination with either the NATPS or the GEN3 marker see Figure 3, Part II of this thesis manuscript (Figures 2-11, 13-15, and 17), Gladfelter *et al.* (2006b), and Schmitz *et al.* (2006).

pAGT200 series: enhanced C-terminal tags

The pAGT100 series makes it possible to delete one gene with three different markers and to use seven different C-terminal tags in combination with the three different markers using only three gene specific primers. But this plasmid collection has drawbacks: Firstly, the green yellow and cyan fluorescent protein variants used (except for Venus and Cerulean), although well established, are not 'enhanced'. They are basically the first variants that became available for gene tagging *in vivo*. For example, the GFP variant used differs only in one point mutation (S65T) from wild-type GFP of *A. victoria*. In recent years, many new variants became available that have been improved with respect to brightness, photostability, folding efficiency and dimerization (reviewed by Shaner *et al.*, 2005). Secondly, the red fluorescent protein used, RedStar2, is an obligate dimer. Although protein fusions can be successful (Figure 5 in Part II of this thesis and Gladfelter *et al.*, 2006a), it is known from its progenitor, DsRed, that chimeras can form intracellular aggregates (Baird *et al.*, 2000; Campbell *et al.*, 2002; Lauf *et al.*, 2001; Mizuno *et al.*, 2001). These protein fusions can even be detectable but often mislocalize and the tagged proteins are not functional. Thirdly, the amino acid sequence that links the tag to the protein is a random sequence resulting from the primer binding site on the pUC19 vector backbone (linker1; Table 5). An ideal linker should fulfill (at least) three criteria: firstly, it is the primer binding site for PCR amplification of the tagging cassette, and so should be GC-rich to give a high T_m. Secondly, it forms a linker between the protein and the tag and should be flexible (i.e. a Gly-rich sequence) and probably not hydrophobic. Thirdly, it should be codon-optimized to improve translation. It was shown by Sheff and Thorn (2004) that optimizing the linker sequence according to these three criteria can increase the detectability of a tagged protein.

Sheff and Thorn (2004) constructed a collection of plasmids with yeast codon usage-optimized tags and linkers for C-terminal tagging in *S. cerevisiae*. As these plasmids contain the KanMX cassette and the *S. cerevisiae ADH1* terminator they cannot be used

Table 3: Systematic table of all available pAGT plasmids for C-terminal tagging and deletion

Tag	Ex/Em[1]	Terminator	NATPS	LEU2	GEN3
Deletion module	na	na	pAGT100	pAGT120	pAGT140
linker1-GFP(S65T)	489/509	T_{ScURA3}	pAGT101	pAGT121	pAGT141
linker1-CFP	434/474	T_{ScLYS2}	pAGT102	pAGT122	pAGT142
linker1-YFP	514/526	T_{ScURA3}	pAGT103	pAGT123	pAGT143
linker1-RedStar2	558/583	T_{ScLYS2}	pAGT104	pAGT124	pAGT144
linker1-6HA	na	T_{ScLYS2}	pAGT105	pAGT125	pAGT145
linker1-13Myc	na	T_{ScURA3}	pAGT106	pAGT126	pAGT146
linker1-Venus	515/528	T_{ScURA3}	pAGT107	pAGT127	pAGT147
linker1-Cerulean	433/475	T_{ScLYS2}	pAGT108	pAGT128	pAGT148
linker1-GST	na	T_{ScURA3}	pAGT109	pAGT129	pAGT149
linker2-yEGFP	488/509	T_{ScURA3}	pAGT201	pAGT221	pAGT241
linker2-yECFP	437/476	T_{ScLYS2}	pAGT202	pAGT222	pAGT242
linker2-yEmCFP	437/476	T_{ScLYS2}	pAGT203	pAGT223	pAGT243
linker2-yECFP-3HA	437/476	T_{ScLYS2}	pAGT204	pAGT224	pAGT244
linker2-yECFP-13Myc	437/476	T_{ScLYS2}	pAGT205	pAGT225	pAGT245
linker2-yEVenus	515/528	T_{ScURA3}	pAGT206	pAGT226	pAGT246
linker2-yECitrine	516/526	T_{ScURA3}	pAGT207	pAGT227	pAGT247
linker2-yEmCitrine	516/526	T_{ScURA3}	pAGT208	pAGT228	pAGT248
linker2-yECitrine-3HA	516/526	T_{ScURA3}	pAGT209	pAGT229	pAGT249
linker2-yECitrine-13Myc	516/526	T_{ScURA3}	pAGT210	pAGT230	pAGT250
linker2-mCherry	574/596	T_{ScLYS2}	pAGT211	pAGT231	pAGT251
linker2-mStrawberry	587/610	T_{ScLYS2}	pAGT212	pAGT232	pAGT252
linker2-tdTomato	554/581	T_{ScLYS2}	pAGT213	pAGT233	pAGT253

[1] Excitation and emission maxima of the fluorescent spectra in nm.

na not applicable

Figure 2: Schematic illustration of the pAGT collection.

(A) Illustration of the pUC19 vector backbone, its multiple-cloning site (MSC) and the restrictions sites used to insert the tags and terminators (SacI) and the markers (PstI) used in the pAGT100 series. (B) Illustration of the cloning principle of the pAGT200 series. (C) Scheme how to introduce a promoter of choice into the pAGT300 series for N-terminal tagging and promoter substitutions.

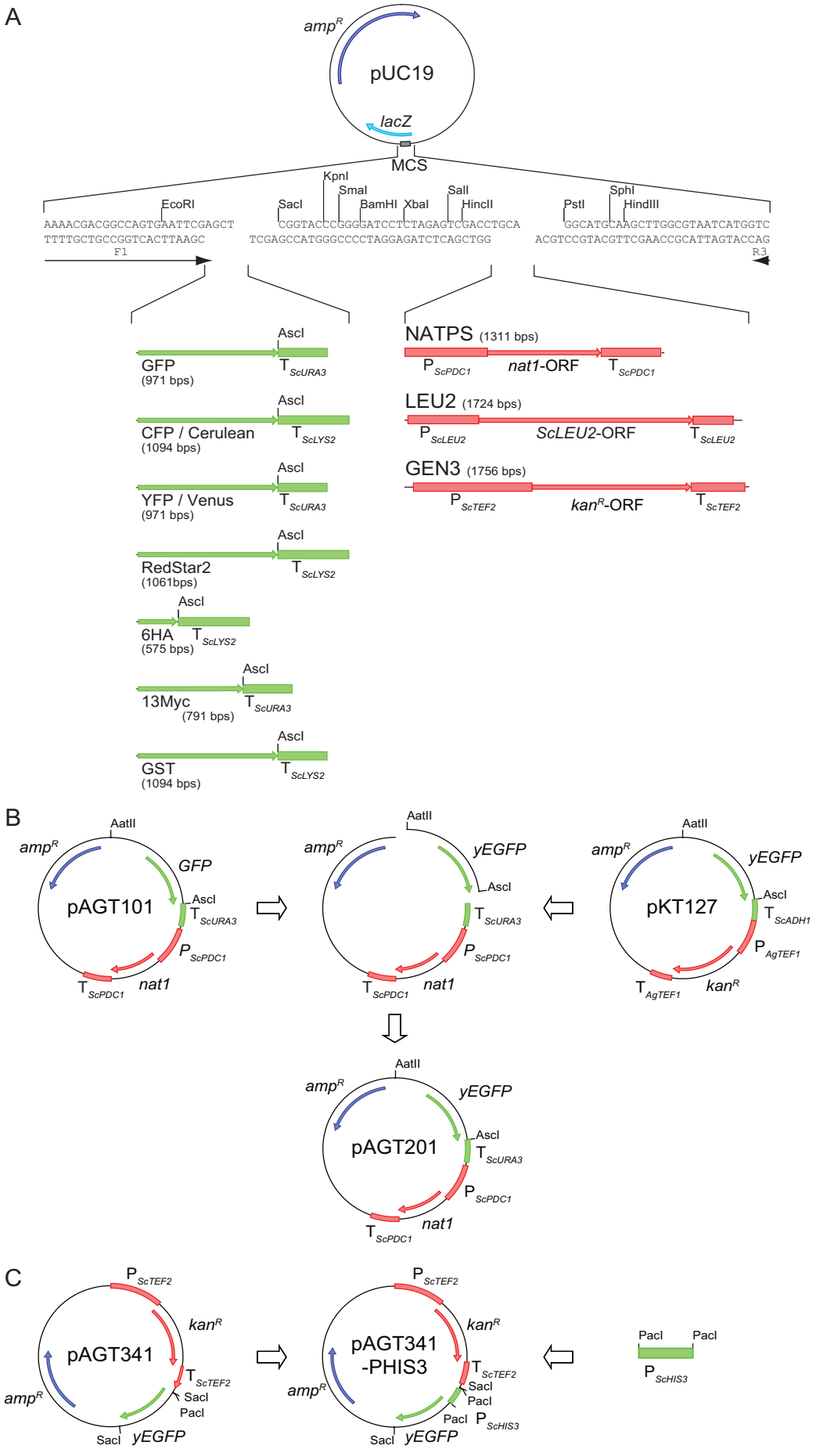
A
ampR
pUC19
lacZ
MCS
KpnI
SmaI
SalI
SphI
EcoRI
SacI
BamHI
XbaI
HincII
PstI
HindIII
AAAACGACGGCCAGTGAATTCGAGCT
CGGTACCCGGGGATCCTCTAGAGTCGACCTGCA
GGCATGCAAGCTTGGCGTAATCATGGTC
TTTTGCTGCCGGTCACTTAAGC
TCGAGCCATGGGCCCCTAGGAGATCTCAGCTGG
ACGTCCGTACGTTCGAACCGCATTAGTACCAG
F1
R3
AscI
GFP
(971 bps)
TScURA3
CFP / Cerulean
(1094 bps)
TScLYS2
YFP / Venus
(971 bps)
RedStar2
(1061bps)
6HA
(575 bps)
13Myc
(791 bps)
GST
(1094 bps)
NATPS (1311 bps)
PScPDC1
nat1-ORF
TScPDC1
LEU2 (1724 bps)
PScLEU2
ScLEU2-ORF
TScLEU2
GEN3 (1756 bps)
PScTEF2
kanR-ORF
TScTEF2
B
AatII
pAGT101
GFP
PScPDC1
nat1
yEGFP
pAGT201
pKT127
TScADH1
PAgTEF1
TAgTEF1
kanR
C
pAGT341
pAGT341
-PHIS3
SacI
PacI
PScHIS3

in *A. gossypii* for the reasons mentioned above. To be able to use these enhanced tags and linkers in *A. gossypii* we had to integrate these tags into our pAGT100 series of plasmids. Because of the similar modular design of these two plasmid collections, we could simply clone their tags and linkers upstream of the terminators and selection markers of our collection (for details see Table 3 and Figure 2, B).

As already mentioned for RedStar2, using red fluorescent proteins derived from *Discosoma* sp. DsRed is problematic, as they are obligate tetramers and often toxic (Baird *et al.*, 2000; Matz *et al.*, 1999) and the half time for maturation of DsRed is with >10 hours very slow (Shaner *et al.*, 2004). Shaner *et al.* (2004) developed by random and directed mutagenesis of DsRed several red fluorescent protein variants that are true monomers and have maturation half times in the range of minutes to one hour. We obtained from Shaner *et al.* (2004) the three variants mCherry, mStrawberry, and tdTomato and included them into our pAGT200 series (for details see Table 3).

pAGT300 series: enhanced N-terminal tags and promoter substitution

For many proteins C-terminal tagging is not possible as the attachment of a tag to the C-terminus renders the protein nonfunctional. For example, small Rho-type GTPases, as many other proteins, have a lipid modification near their C-termini that is essential for their proper localization and function. Addition of any tag to their C-termini inhibits this modification and results in nonfunctional fusion proteins. Therefore it is necessary to be able to tag proteins at their N-terminus instead of their C-terminus. N-terminal tagging of proteins is often more complicated because the promoter region of the gene has to be located between the marker and the tag. On the other hand regulatable promoters, from existing modules, that allow controlled up- or downregulation or simple overexpression of the gene can be used.

We wanted to apply the same simple modular architecture, which was used to construct the plasmid collections for C-terminal tagging, to a plasmid collection that allows N-terminal tagging of genes as well as promoter swap experiments. First, we switched the orientation of the 3 cassettes in pAGT100, pAGT120, and pAGT140, in order to use the SacI site for insertion of the tags and that in the final cassettes the selection markers would have the same orientation as the tagged gene. Second, we PCR-amplified the tags from the pAGT200 series with primers that add on the 5'-end of the PCR product a SacI and a PacI site just upstream of the tag ATG and on the 3'-end omit the STOP codon and add an in-frame linker sequence followed by a SacI site. The PCR products were then cloned into the SacI site downstream of the selection markers. The linker sequence was designed according to the criteria mentioned above (Table 5). PacI serves as restriction site to introduce the promoter of choice under which the gene to be tagged should be expressed. Such a promoter can either be of heterologous origin used to regulate the expression of the gene or the endogenous promoter that has been PCR-amplified from *A. gossypii* genomic DNA adding PacI sites. We chose to use a PacI site, as PacI has an 8 bp recognition site that only rarely occurs in the *A. gossypii* genome.

Helfer and Gladfelter (2006) showed recently that the promoter of *ScHIS3* is functional in *A. gossypii* and can be used for constant overexpression of genes. To make this promoter available for the

Table 4: Systematic table of all available plasmids for N-terminal tagging

Tag	Promoter	NATPS	LEU2	GEN3
yEGFP-linker3	none	pAGT301	pAGT321	pAGT341
yECFP-linker3	none	pAGT302	pAGT322	pAGT342
yEmCFP-linker3	none	pAGT303	pAGT323	pAGT343
yEVenus-linker3	none	pAGT306	pAGT326	pAGT346
yECitrine-linker3	none	pAGT307	pAGT327	pAGT347
yEmCitrine-linker3	none	pAGT308	pAGT328	pAGT348
mCherry-linker3	none	pAGT311	pAGT331	pAGT351
mStrawberry-linker3	none	pAGT312	pAGT332	pAGT352
tdTomato-linker3	none	pAGT313	pAGT333	pAGT353
yEGFP-linker3	P_{ScHIS3}	na	na	pAGT341-PHIS3[1]
yECFP-linker3	P_{ScHIS3}	na	na	na
yEmCFP-linker3	P_{ScHIS3}	na	na	na
yEVenus-linker3	P_{ScHIS3}	na	na	na
yECitrine-linker3	P_{ScHIS3}	na	na	na
yEmCitrine-linker3	P_{ScHIS3}	na	na	na
mCherry-linker3	P_{ScHIS3}	na	na	na
mStrawberry-linker3	P_{ScHIS3}	na	na	na
tdTomato-linker3	P_{ScHIS3}	na	na	na

[1] Not sequenced at the time this manuscript was written.

na Not available at the time this manuscript was written.

Table 5: Linker sequences

Linker	Nucleotide sequence (5'→3')	AA sequence (N→C)
linker1	AAAACGACGGCCAGTGAATTCGAGCTC	KTTASEFEL
linker2	GGTGACGGTGCTGGTTTAATTAAC	GDGAGLIN
linker3	GGCGCGGGCGCAGGTGACGGTGCATTG	GAGAGDGGAL

Primer annealing sites are in bold

pAGT300 series we PCR-amplified it and cloned it into the PacI site of the plasmids for N-terminal gene tagging. For an application of the *GEN3*-P_{ScHIS3}-*yEGP* module (pAGT341-PHIS3) see next section and Figure 3.

For an overview of all available modules of the pAGT300 series for N-terminal gene tagging and promoter substitutions see Table 4 and for an illustration of the principle how to clone promoters into the plasmids of the pAGT300 series see Figure 2, C.

Heterologous gene expression in yeast

Mohr (1997) constructed a genomic library of *A. gossypii* of size-selected 3.5 – 5.5 kb partial Sau3AI fragments in the CEN/ARS vector pRS416. This library, which covers over 85 % of the genome, a BAC collection and another plasmid library were used to sequence the *A. gossypii* genome (Dietrich *et al.*, 2004). In our lab we routinely use the pRS416-based so-called pAG clones to directly tag genes of interest on a plasmid. This is done by cotransformation of the pAG clones and PCR products amplified from the pAGT plasmids into yeast to allow homologous recombination. This strategy has, at least, three advantages over direct gene targeting in *A. gossypii*. Firstly, transformation of yeast cells requires much less DNA compared to *A. gossypii* (Gietz and Woods, 2002; Wendland *et al.*, 2000). Secondly, if the whole gene is present on the pAG clone heterologous expression and complementation, i.e. the functionality of *A. gossypii* genes in yeast, can be directly assayed. And thirdly, if the promoter is functional in yeast, yeast transformants can easily be screened for functional GFP fusions. Interestingly, not only promoters of *A. gossypii* are often functional in yeast but *A. gossypii* proteins often localize to the same structures as their yeast homolog. We observed this for *Ag*Hof1, *Ag*Bud3, *Ag*Cyk1, *Ag*Vrp1, *Ag*Mlc2, and *Ag*Bni5 (Figure 3). *Ag*Hof1-RedStar2 is an example for a non-functional fusion of RedStar2, probably for the reasons mentioned above, and this was already observable in yeast. Interestingly, *Ag*Bni5-GFP and *Ag*Bni5-YFP localized in yeast where expected but displayed a dominant negative phenotype when transformed into *A. gossypii* (not shown).

GFP(S65T) vs. yEGFP

We wanted to test if yEGFP was superior to GFP(S65T) in terms of brightness and detectability when expressed in *A. gossypii*. The strains K51.52 and K67.52 (Michael Köhli, unpublished) carry P_{ScHIS3}-*GFP(S65T)-BUD6* and P_{ScHIS3}-*yEGFP-BUD6*, respectively, at the native chromosomal locus. *AgBUD6* is a component of the polarisome and constantly localizes to tips of *A. gossypii* hypha (Michael Köhli, personal communication). P_{ScHIS3}-*yEGFP-BUD6* was constructed using pAGT341-PHIS3. We inoculated one agar slide with the two strains, acquired GFP image stacks of ~35 hyphae for each

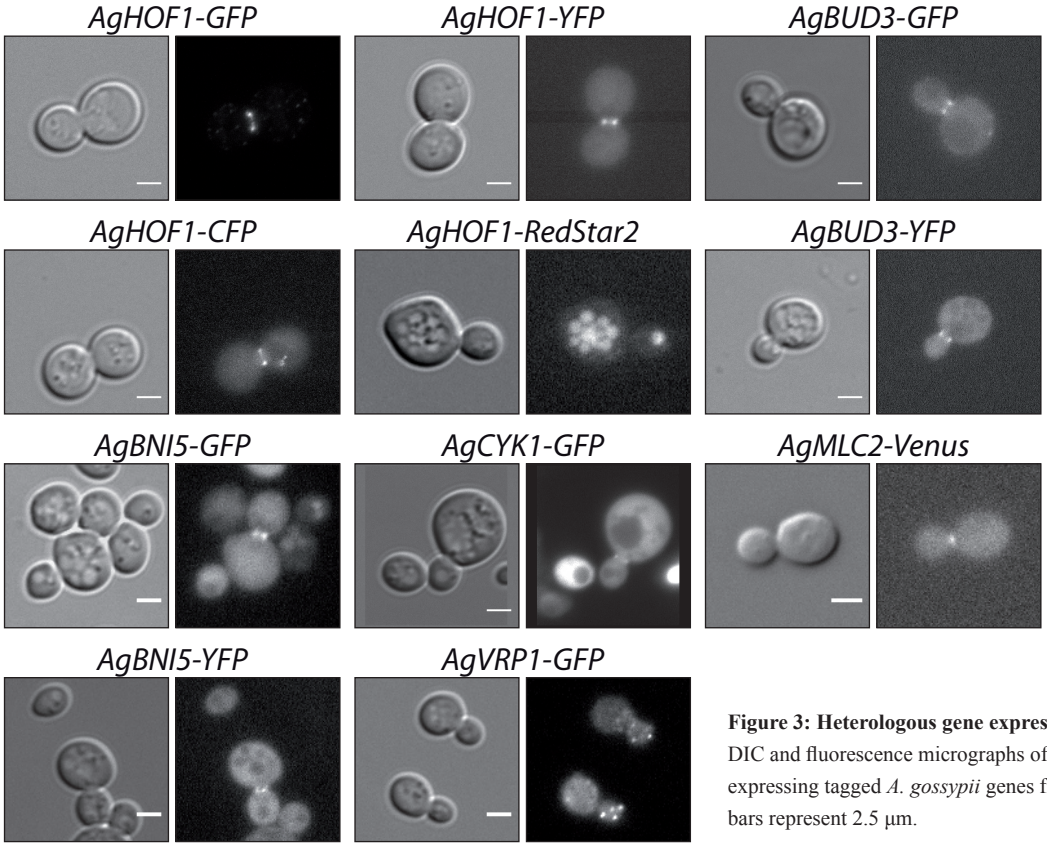

Figure 3: Heterologous gene expression in yeast. DIC and fluorescence micrographs of yeast cells expressing tagged *A. gossypii* genes from plasmids. Scale bars represent 2.5 µm.

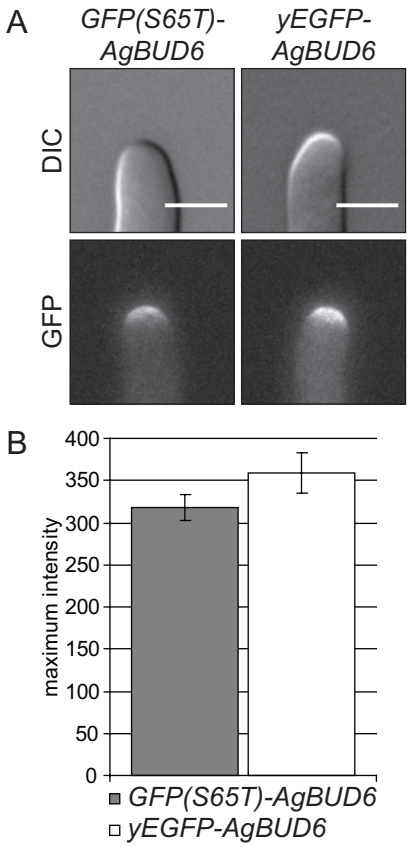

Figure 4: GFP(S65T) vs. yEGFP.
(A) Representative DIC images and maximum projections of 9-plane GFP image stacks (z distance = 0.5 µm) of two hyphal tips expressing either *GFP(S65T)-AgBUD6* (left panel) or *yEGFP-AgBUD6* (right panel), corresponding to the average maximum intensities measured for the respective signals. GFP images were scaled identically. Scale bars represent 5 µm. (B) Average and standard errors of the maximum intensities of GFP(S65T) and yEGFP signals measured in 36 *GFP(S65T)-AgBUD6* and 35 *yEGFP-AgBUD6* hyphal tips, respectively.

strain, and measured the maximum intensity of the GFP signal in each hyphal tip. What was already obvious during image acquisition and by visual inspection of the image stacks (Figure 4, A) was confirmed by statistical analysis. Although the average maximum intensity of the GFP signal in *GFP(S65T)-BUD6* 318 ± 15 (SEM; n = 36) was slightly lower than of *yEGFP-BUD6* 358 ± 23(SEM; n = 35) (Figure 4, B), this difference was not significant (ttest P = 0.15). At the time this manuscript was written we had not yet compared other 'classical' and 'enhanced' fluorescent proteins.

$P_{ScTHI13}$: a regulatable promoter for use in *A. gossypii*

An important tool in the analysis of gene and protein function is the potential to regulate the expression of a gene, i.e. to switch transcription on or off at any given time point or to even alter the strength of expression. This is usually achieved by putting a gene under control of an inducible or repressible promoter. The most commonly used regulatable promoters in *S. cerevisiae* are those of the *GAL* genes (St John and Davis, 1981). All galactose structural genes (*GAL1, GAL10, GAL7, GAL2*) are coordinately regulated at the level of transcription in response to galactose by Gal4, Gal80, and Gal3 (De Robichon-Szulmajster, 1958; Platt and Reece, 1998; and reviewed by Lohr *et al.*, 1995). Unfortunately, no homologs of the galactose structural genes are present in the genome of *A. gossypii* and it cannot utilize galactose as a carbon source. Thus, it is not possible to use the *GAL* promoters for controlled gene induction and repression in *A. gossypii*. The promoter of *nmt1* (no message on thiamine) has been well established to control gene expression in *S. pombe* (Bahler *et al.*, 1998; Maundrell, 1993). It is repressed in presence and derepressed in absence of thiamine. When we were looking for potential regulatable promoters for the use in *A. gossypii* we found a homolog of *nmt1* present in its genome: AER451W. We named it *AgTHI13* after its (non-syntenic) homolog in *S. cerevisiae*. A second potential candidate for a regulatable promoter was the promoter of the isocitrate lyase-encoding gene *AgICL1* (ADL066C). *AgICL1* is subject to glucose repression, derepressed by glycerol, partially induced by the C_2 compounds ethanol and acetate, and full induced on soybean oil (Maeting *et al.*, 1999).

To test the suitability of these two promoters we analyzed by northern blotting the expression of *AgTHI13* in cells grown in either presence or absence of thiamine and of *AgICL1* in cells grown on glucose, glycerol, ethanol, or oleate. For *AgTHI13* we found a strong induction in cells grown in medium lacking thiamine and no detectable signal in cells grown in presence of thiamine (Figure 5, A). For *AgICL1* we could confirm a strong expression in cells grown on oleate and no expression in cells grown on glucose, but we could not detect any expression in cells grown on glycerol or ethanol (data not shown). This could probably be due to the lacking sensitivity of our northern blots as we were using a non-isotopic detection kit. Radial colony growth speed is severely reduced when *A. gossypii* is grown on

Table 6: Systematic table of all available plasmids for *ScTHI13* promoter substitutions

Promoter	Induction	NATPS	LEU2	GEN3
$P_{ScTHI13}$L 744 bps	strong	pN1PT13L[1]	pL2PT13L[1]	pG3PT13L[1]
$P_{ScTHI13}$S 358 bps	weak	pN1PT13S[1]	pL2PT13L[1]	pG3PT13L[1]

[1] Not sequenced at the time this manuscript was written.

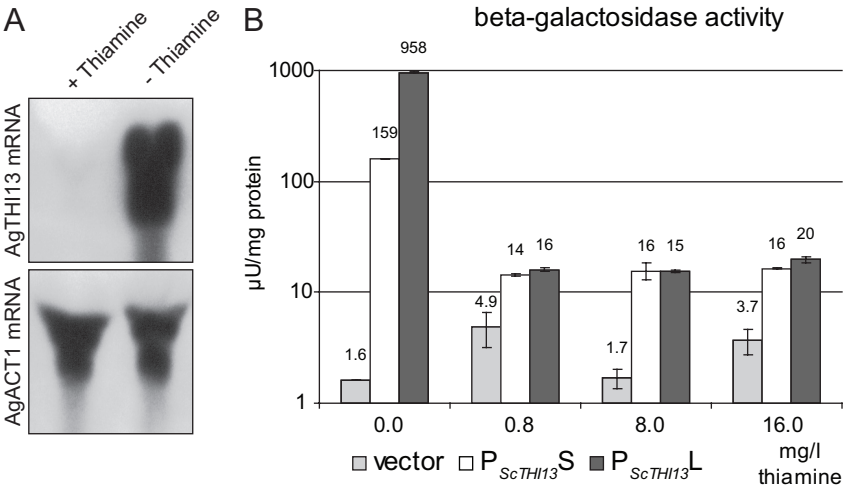

Figure 5: Regulation of *A. gossypii* and *S. cerevisiae THI13* promoter.
(A) Northern blot of total mRNA extracted from strain *AlΔt* grown in liquid media with thiamine (left lane) and without thiamine (right lane) probed for mRNA of *AgTHI13* (upper panel) and *AgACT1* (lower panel; loading control). (B) β-galactosidase activity (average of 3 measurements and standard error) measured in crude protein extracts of strain *AlΔt* carrying the plasmids pAN5 (vector), pAMK163 ($P_{ScTHI13}$L-*lacZ*), or pAMK164 ($P_{ScTHI13}$S-*lacZ*) grown in media containing 0, 0.8, 8, or 16 mg/l thiamine.

other carbon sources than glucose (Figure 6). Because such effects on normal growth are not desirable for a regulatable promoter we discarded the *AgICL1* promoter as a potential candidate.

For PCR-based gene targeting to be efficient and precise the cassettes have to be heterologous to the genome of the organism (Wach *et al.*, 1994). Therefore we tested if the *S. cerevisiae THI13* promoter is functional in *A. gossypii.* We cloned fragments of different sizes from the promoter regions of *AgTHI13* and *ScTHI13* in front of the *lacZ* reporter gene and transformed the plasmids in *A. gossypii* to measure β-galactosidase activity. Transformed mycelia were grown on plates either with or without thiamine. After 3 days the mycelia were overlaid with X-gal-containing agarose. 4 hours after the overlay a blue coloration could be observed for the strains grown without thiamine expressing *lacZ* under control of the long and short promoter fragment of *ScTHI13*. After 24 hours the blue coloration was very intense for the long *ScTHI13* promoter fragment and slightly less intense for the short fragment. At this time point a slight blue coloration was also detectable for those two strains grown in presence of thiamine indicating a low basal expression of *lacZ* under the control of the *ScTHI13* promoter. To quantify the strength of those two *ScTHI13* promoter fragments and the basal expression level in presence of different concentrations of thiamine we made a colorimetric assay to determine the β-galactosidase activity in crude protein extracts (Figure 5, C). When induced, the long *ScTHI13* promoter fragment gave rise to a 6 times higher β-galactosidase activity compared to the short promoter fragment. Not induced, independent of the thiamine concentration tested, β-galactosidase activity was identical for both fragments: 10 fold and 60 fold lower compared to the induced state of the short and long promoter fragment, respectively, but about 5 fold higher than the average background activity measured for the negative control.

The short and long *ScTHI13* promoter fragments were used to construct promoter replacement modules in combination with the markers NATPS, LEU2, and GEN3 (pN1PT13S, pN1PT13L, pL2PT13S, pL2PT13L,

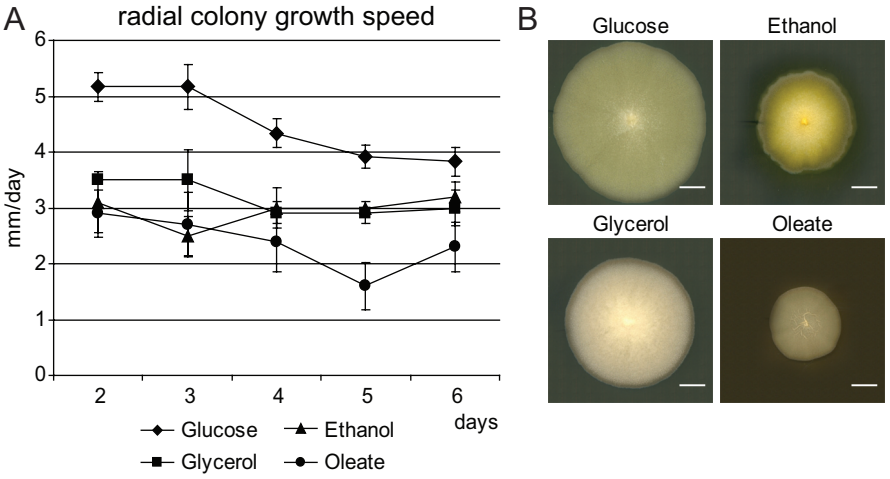

Figure 6: Radial colony growth speed of *A. gossypii* grown on different C sources.
(A) Average radial colony growth speed and standard deviations of 6 mycelia each of strain *AlΔt* grown on AFM plates containing D-glucose, glycerol, ethanol, or oleate as C source. (B) Representative images of the colonies from A after 6 days. Scale bars represent 1 cm.

pG3PT13S, and pG3PT13L, respectively; Table 6). These 6 cassettes can be amplified with one pair of gene-specific primers (PF1 and PF2; Table 7) and can be used to directly replace the promoter of any given gene in *A. gossypii*.

To test if the expression levels of the two promoter fragments in the uninduced state are low enough to approximate the situation of a gene knock out we replaced the promoter of an essential gene. We chose the essential formin *AgBNI1* because its deletion phenotype was well characterized (Schmitz *et al.*, 2006). The N1PT13S and N1PT13L cassettes were amplified and used to transform *A. gossypii* strain *ΔlΔt* (Altmann-Johl and Philippsen, 1996). Preliminary results show that homokaryotic $P_{ScTHI13}$-*AgBNI1* spores are viable and do not show the deletion phenotype even in the presence of thiamine (data not shown). This suggests that the two *ScTHI13* promoter fragments are too leaky to completely repress the expression of an essential gene. Whether they can be used to up- or downregulate the expression of other genes remains to be tested.

Discussion

In this report we present three sets of new gene targeting modules to allow rapid strain construction in *A. gossypii* and related fungi using previously established PCR-based gene targeting protocols. In our collection we have integrated all heterologous auxotrophic and dominant drug resistance markers currently available for *A. gossypii* and 14 different fluorescent protein variants and 3 different epitope tags for C-terminal protein fusions. Furthermore, we constructed modules for N-terminal fusions that allow the use of any promoter to drive gene expression. In our lab we have started using these modules routinely for rapid and efficient gene targeting experiments at various loci (Gladfelter *et al.*, 2006b; Schmitz *et al.*, 2006); Part II of this manuscript; Michael Köhli, Claudia Birrer, Katrin Hungerbühler, and Sandrine Grava, personal communication).

In recent years random and site-directed mutagenesis lead to many new fluorescent protein (FP) variants that are supposed to be superior over classical, well-established variants in terms of brightness, photostability, folding efficiency, dimerization, and translation efficiency (Janke *et al.*, 2004; Nagai *et al.*, 2002; Rizzo *et al.*, 2004; Shaner *et al.*, 2004; Sheff and Thorn, 2004). To make use of these new FP variants in *A. gossypii* we integrated 11 of them in our plasmid collection. For the case of GFP(S65T) and yEGFP, we demonstrated that the use of an 'enhanced' FP variant does not significantly improve the detectability of a tagged protein in *A. gossypii*. Whether the same is true for other proteins and FP variants remains to be tested.

Colabeling of two proteins with different FP variants is usually done with a cyan and a yellow variant, as the spectra of these two proteins differ enough so that they can be separated using different sets of excitation and emission filters. The main drawback using these two FP variants is that they are significantly less bright, especially CFP, and bleach faster compared to conventional GFP, still the most reliable FP variant available. In *A. gossypii* many strains exist where one gene is tagged with GFP. Thus a FP variant that can be used to colable proteins in combination with GFP would be of great advantage. Such a FP variant is DsRed and all its derivatives. The problems using these *Discosoma* sp. derived FP variants were their slow maturation half time and tendency to tetramerize (Baird *et al.*, 2000). With the development of RedStar2 (Janke *et al.*, 2004), mCherry, mStrawberry, and tdTomato (Shaner *et al.*, 2004) some of these problems could be solved. Which of these red FP variants is best suitable for colabeling of proteins in combination with GFP in *A. gossypii* remains to be established. RedStar2 is a dimer and can cause potential localization artifacts (see Part II of this thesis) or lead to non-functional protein fusions (Figure 3 and data not shown). When used in *A. gossypii* mCherry is significantly less bright compared to GFP (Sandrine Grava, personal communication). tdTomato consists of a tandem repeat of a DsRed variant and folds back on itself to prevent dimerization of the fusion protein but has twice the molecular weight. The fluorescent spectra of mCherry and mStrawberry are shifted far enough into the red part of the light spectrum, so that they could potentially be used together with yellow FP variants, thus enabling colabeling of three proteins with a cyan, yellow, and red FP variant.

An important tool for the functional analysis of genes and proteins is overexpression and controlled up- and downregulation. To be able to do so one has to use a regulatable promoter. The most commonly used promoters in *S. cerevisiae* are those of the *GAL* structural genes that are repressed when glucose is present and induced when galactose is present. Unfortunately homologs of these *GAL* genes are not present in the *A. gossypii* genome. Thus the *GAL* promoters may be active but are most likely differently regulated in *A. gossypii*. We found that the expression of *AgTHI13* is repressed in the presence and derepressed in the absence of thiamine. Additionally we show that the promoter of *S. cerevisiae THI13* is functional in *A. gossypii*, is regulated in the same manner, and can be used to regulate gene expression in *A. gossypii.* This regulatable promoter is a novel tool for the functional analysis of genes and proteins in *A. gossypii*.

In summary, the pAGT toolbox for *A. gossypii* provides a versatile array of modules that allows the rapid

analysis of gene function by eliminating time consuming cloning steps while providing ample choices of element combinations that will be made freely available to the scientific community.

Acknowledgements

Acknowledgements

I am very grateful to Peter Philippsen for giving me the opportunity to work in his laboratory. He was always very generous in terms of supporting all my experimental projects, giving me the opportunity to visit many important conferences, and supplying the whole group with treats. Whenever I was seeking his advice he would listen to me and was never short of theoretical advice and scientific anecdotes. Peter gave me many suggestions while I was writing my thesis and I especially appreciate his efficient reading of this manuscript.

Hans-Peter Schmitz is an excellent mentor and did a great job introducing me to the practical side of science. I am indebted to him for being very helpful, patient, and encouraging whenever I faced a problem and for critical reading of this thesis.

Working in the Philippsen group was always characterized by a very pleasant, friendly atmosphere and I would like to thank all the former and current group members as well as the technical staff who contributed to this. I could always bother you and got help: Michael Köhli, Claudia Birrer, Ivan Schlatter, Katrin Hungerbühler, Hans-Peter Helfer, Riccarda Rischatsch, Hans-Peter Schmitz, Amy Gladfelter, Pierre Philippe Laissue, Philipp Knechtle, Sylvia Vögeli, Brigitte Berglas, Dominic Hoepfner, Kamila Boudier, Juliet Odathekal, Jeannine Winkler, Mark Finlayson, Sandrine Grava, Virginie Galati, and Bettina Hersberger.

To my friends who were there.

I would like to appreciate all the support I received from Claudia Birrer. She made me looking ahead when I was looking back.

Special thanks go to Guenda Berthold who accompanied me for many years.

My very special thanks go to my parents and sisters. Without their constant love and support I would not be where I am now.

References

References

Adamo, J. E., Rossi, G. and Brennwald, P. (1999). The Rho GTPase Rho3 has a direct role in exocytosis that is distinct from its role in actin polarity. *Mol Biol Cell* **10**, 4121-33.

Agrios, G. (1980). Insect involvement in the transmission of fungal pathogens. In *Vectors of plant pathogens*, (eds K. Maramorosch and K. Harris), pp. 467. New York, NY: Academic Press.

Agrios, G. (1997). Plant pathology. San Diego, CA: Academic Press.

Alberti-Segui, C. (2001). Control of nuclear dynamics by microtubule-based motors in the filamentous fungus *Ashbya gossypii*. In *Biozentrum*, vol. PhD, pp. 82. Basel: Universität Basel.

Alberti-Segui, C., Dietrich, F., Altmann-Johl, R., Hoepfner, D. and Philippsen, P. (2001). Cytoplasmic dynein is required to oppose the force that moves nuclei towards the hyphal tip in the filamentous ascomycete *Ashbya gossypii*. *J Cell Sci* **114**, 975-86.

Alberts, A. S. (2001). Identification of a carboxyl-terminal diaphanous-related formin homology protein autoregulatory domain. *J Biol Chem* **276**, 2824-30.

Altmann-Johl, R. and Philippsen, P. (1996). *AgTHR4*, a new selection marker for transformation of the filamentous fungus *Ashbya gossypii*, maps in a four-gene cluster that is conserved between *A. gossypii* and *Saccharomyces cerevisiae*. *Mol Gen Genet* **250**, 69-80.

Altschul, S. F., Madden, T. L., Schaffer, A. A., Zhang, J., Zhang, Z., Miller, W. and Lipman, D. J. (1997). Gapped BLAST and PSI-BLAST: a new generation of protein database search programs. *Nucleic Acids Res* **25**, 3389-402.

An, H., Morrell, J. L., Jennings, J. L., Link, A. J. and Gould, K. L. (2004). Requirements of fission yeast septins for complex formation, localization, and function. *Mol Biol Cell* **15**, 5551-64.

Ashby, S. F. and Nowell, W. (1926). The fungi of stigmatomycosis. *Ann Botany* **40**, 69 - 84.

Aspenstrom, P. (1997). A Cdc42 target protein with homology to the non-kinase domain of FER has a potential role in regulating the actin cytoskeleton. *Curr Biol* **7**, 479-87.

Aspenstrom, P., Fransson, A. and Richnau, N. (2006). Pombe Cdc15 homology proteins: regulators of membrane dynamics and the actin cytoskeleton. *Trends Biochem Sci* **31**, 670-9.

Ayad-Durieux, Y., Knechtle, P., Goff, S., Dietrich, F. and Philippsen, P. (2000). A PAK-like protein kinase is required for maturation of young hyphae and septation in the filamentous ascomycete *Ashbya gossypii*. *J Cell Sci* **113 Pt 24**, 4563-75.

Baggett, J. J., D'Aquino, K. E. and Wendland, B. (2003). The Sla2p Talin Domain Plays a Role in Endocytosis in *Saccharomyces cerevisiae*. *Genetics* **165**, 1661-1674.

Bahler, J., Wu, J. Q., Longtine, M. S., Shah, N. G., McKenzie, A., 3rd, Steever, A. B., Wach, A., Philippsen, P. and Pringle, J. R. (1998). Heterologous modules for efficient and versatile PCR-based gene targeting in *Schizosaccharomyces pombe*. *Yeast* **14**, 943-51.

Baird, G. S., Zacharias, D. A. and Tsien, R. Y. (2000). Biochemistry, mutagenesis, and oligomerization of DsRed, a red fluorescent protein from coral. *Proc Natl Acad Sci U S A* **97**, 11984-9.

Balasubramanian, M. K., Bi, E. and Glotzer, M. (2004). Comparative analysis of cytokinesis in budding yeast, fission yeast and animal cells. *Curr Biol* **14**, R806-18.

Balasubramanian, M. K., McCollum, D., Chang, L., Wong, K. C., Naqvi, N. I., He, X., Sazer, S. and Gould, K. L. (1998). Isolation and characterization of new fission yeast cytokinesis mutants. *Genetics* **149**, 1265-75.

Barral, Y., Mermall, V., Mooseker, M. S. and Snyder, M. (2000). Compartmentalization of the cell cortex by septins is required for maintenance of cell polarity in yeast. *Mol Cell* **5**, 841-51.

Batra, L. R. (1973). *Nematosporaceae* (*Hemiascomycetidae*): taxonomy, pathogenicity, distribution and vector relations. *USDA Technol Bull*, 1–71.

Bauer, Y., Knechtle, P., Wendland, J., Helfer, H. and Philippsen, P. (2004). A Ras-like GTPase is involved in hyphal growth guidance in the filamentous fungus *Ashbya gossypii*. *Mol Biol Cell* **15**, 4622-32.

Beggs, J. D. (1978). Transformation of yeast by a replicating hybrid plasmid. *Nature* **275**, 104-9.

Bender, A. and Pringle, J. R. (1989). Multicopy suppression of the *cdc24* budding defect in yeast by *CDC42* and three newly identified genes including the ras-related gene *RSR1*. *Proc Natl Acad Sci U S A* **86**, 9976-80.

Berlin, A., Paoletti, A. and Chang, F. (2003). Mid2p stabilizes septin rings during cytokinesis in fission yeast. *J Cell Biol* **160**, 1083-92.

Bi, E., Maddox, P., Lew, D. J., Salmon, E. D., McMillan, J. N., Yeh, E. and Pringle, J. R. (1998). Involvement of an actomyosin contractile ring in *Saccharomyces cerevisiae* cytokinesis. *J Cell Biol* **142**, 1301-12.

Blondel, M., Bach, S., Bamps, S., Dobbelaere, J., Wiget, P., Longaretti, C., Barral, Y., Meijer, L. and Peter, M. (2005). Degradation of Hof1 by SCF(Grr1) is important for actomyosin contraction during cytokinesis in yeast. *Embo J*.

Buller, A. H. R. (1933). The translocation of protoplasm through septate mycelium of certain *Pyrenomycetes*, *Discomycetes* and *Hymenomycetes*. In *Researches on Fungi*, vol. 5, pp. 75–167. London: Longmans, Green and Co.

Burke, D., Dawson, T. and Stearns, T. (2000). Methods in Yeast Genetics: A Cold Spring Harbor Laboratory Course Manual. Cold Spring Harbor: Cold Spring Harbor Laboratory Press.

Buss, L. J. Dorsal view of adult cotton stainer, *Dysdercus suturellus* (Herrich-Schaeffer): University of Florida.

Byers, B. and Goetsch, L. (1976). A highly ordered ring of membrane-associated filaments in budding yeast. *J Cell Biol* **69**, 717-21.

Byrne, K. P. and Wolfe, K. H. (2005). The Yeast Gene Order Browser: combining curated homology and syntenic context reveals gene fate in polyploid species. *Genome Res* **15**, 1456-61.

Campbell, R. E., Tour, O., Palmer, A. E., Steinbach, P. A., Baird, G. S., Zacharias, D. A. and Tsien, R. Y. (2002). A monomeric red fluorescent protein. *Proc Natl Acad Sci U S A* **99**, 7877-82.

Cappellaro, C., Mrsa, V. and Tanner, W. (1998). New potential cell wall glucanases of *Saccharomyces cerevisiae* and their involvement in mating. *J Bacteriol* **180**, 5030-7.

Carlile, M. J., Watkinson, S. C. and Gooday, G. W. (2000). The Fungi: Academic Press.

Carnahan, R. H. and Gould, K. L. (2003). The PCH family protein, Cdc15p, recruits two F-actin nucleation pathways to coordinate cytokinetic actin ring formation in *Schizosaccharomyces pombe*. *J Cell Biol* **162**, 851-62.

Caviston, J. P., Longtine, M., Pringle, J. R. and Bi, E. (2003). The role of Cdc42p GTPase-activating proteins in assembly of the septin ring in yeast. *Mol Biol Cell* **14**, 4051-66.

Chalfie, M., Tu, Y., Euskirchen, G., Ward, W. W. and Prasher, D. C. (1994). Green fluorescent protein as a marker for gene expression. *Science* **263**, 802-5.

Chang, F., Drubin, D. and Nurse, P. (1997). cdc12p, a protein required for cytokinesis in fission yeast, is a component of the cell division ring and interacts with profilin. *J Cell Biol* **137**, 169-82.

Chien, C. T., Bartel, P. L., Sternglanz, R. and Fields, S. (1991). The two-hybrid system: a method to identify and clone genes for proteins that interact with a protein of interest. *Proc Natl Acad Sci U S A* **88**, 9578-82.

Cid, V. J., Cenamor, R., Sanchez, M. and Nombela, C. (1998). A mutation in the Rho1-GAP-encoding gene *BEM2* of *Saccharomyces* cerevisiae affects morphogenesis and cell wall functionality. *Microbiology* **144 (Pt 1)**, 25-36.

Cole, G. T. and Samson, R. A. (1979). Patterns of Development in Conidial Fungi. London: Pitman.

Cormack, B. P., Bertram, G., Egerton, M., Gow, N. A., Falkow, S. and Brown, A. J. (1997). Yeast-enhanced green fluorescent protein (yEGFP)a reporter of gene expression in *Candida albicans*. *Microbiology* **143 (Pt 2)**, 303-11.

Dammer, K. H. and Ravelo, H. G. (1990). Verseuchung von *Leptoglossus gonagra* (Fabr.) mit *Nematospora coryli* Peglion und *Ashbya gossypii* (Ashby et Nowell) Guilliermond in einer Zitrusanlage der Republik Kuba. *Arch Phytopathol Pflanzenschutz Berlin* **26**, 71-8.

De Robichon-Szulmajster, H. (1958). Induction of enzymes of the galactose pathway in mutants of *Saccharomyces cerevisiae*. *Science* **127**, 28-9.

Demain, A. L. (1972). Riboflavin oversynthesis. *Annu Rev Microbiol* **26**, 369-88.

Dietrich, F. S., Voegeli, S., Brachat, S., Lerch, A., Gates, K., Steiner, S., Mohr, C., Pohlmann, R., Luedi, P., Choi, S. et al. (2004). The *Ashbya gossypii* Genome as a Tool for Mapping the Ancient *Saccharomyces cerevisiae* Genome. *Science*.

Dobbelaere, J. and Barral, Y. (2004). Spatial coordination of cytokinetic events by compartmentalization of the cell cortex. *Science* **305**, 393-6.

Ellenberg, J., Lippincott-Schwartz, J. and Presley, J. F. (1998). Two-color green fluorescent protein time-lapse imaging. *Biotechniques* **25**, 838-42, 844-6.

Eng, K., Naqvi, N. I., Wong, K. C. and Balasubramanian, M. K. (1998). Rng2p, a protein required for cytokinesis in fission yeast, is a component of the actomyosin ring and the spindle pole body. *Curr Biol* **8**, 611-21.

Entian, K. D. and Kötter, P. (1998). Yeast Mutant and Plasmid Collections. In *Yeast Gene Analysis*, vol. 26, pp. 431-449. Academic Press.

Epp, J. A. and Chant, J. (1997). An IQGAP-related protein controls actin-ring formation and cytokinesis in yeast. *Curr Biol* **7**, 921-9.

Etienne-Manneville, S. (2004). Cdc42--the centre of polarity. *J Cell Sci* **117**, 1291-300.

Fankhauser, C., Reymond, A., Cerutti, L., Utzig, S., Hofmann, K. and Simanis, V. (1995). The *S. pombe cdc15* gene is a key element in the reorganization of F-actin at mitosis. *Cell* **82**, 435-44.

FAO. Organic cotton: farmingsolutions.

Fischer-Parton, S., Parton, R. M., Hickey, P. C., Dijksterhuis, J., Atkinson, H. A. and Read, N. D. (2000). Confocal microscopy of

FM4-64 as a tool for analysing endocytosis and vesicle trafficking in living fungal hyphae. *J Microsc* **198**, 246-59.

Fleig, U. N., Pridmore, R. D. and Philippsen, P. (1986). Construction of *LYS2* cartridges for use in genetic manipulations of *Saccharomyces cerevisiae*. *Gene* **46**, 237-45.

Forer, A. and Behnke, O. (1972). An actin-like component in sperm tails of a crane fly (*Nephrotoma suturalis* Loew). *J Cell Sci* **11**, 491-519.

Frazer, H. L. (1944). Obserrvations on the method of transmission of internal boll diseases of cotton by the cotton stainer bug. *Ann Appl Biol* **31**, 271-90.

Gattiker, A., Rischatsch, R., Demougin, P., Voegeli, S., Dietrich, F. S., Philippsen, P. and Primig, M. (2007). Ashbya Genome Database 3.0: a cross-species genome and transcriptome browser for yeast biologists. *BMC Genomics* **8**, 9.

Gavin, A. C., Bosche, M., Krause, R., Grandi, P., Marzioch, M., Bauer, A., Schultz, J., Rick, J. M., Michon, A. M., Cruciat, C. M. et al. (2002). Functional organization of the yeast proteome by systematic analysis of protein complexes. *Nature* **415**, 141-7.

Gietz, R. D., Schiestl, R. H., Willems, A. R. and Woods, R. A. (1995). Studies on the transformation of intact yeast cells by the LiAc/SS-DNA/PEG procedure. *Yeast* **11**, 355-60.

Gietz, R. D. and Woods, R. A. (2002). Transformation of yeast by lithium acetate/single-stranded carrier DNA/polyethylene glycol method. *Methods Enzymol* **350**, 87-96.

Gladfelter, A. S. (2006). Control of filamentous fungal cell shape by septins and formins. *Nat Rev Microbiol* **4**, 223-9.

Gladfelter, A. S., Hungerbuehler, A. K. and Philippsen, P. (2006a). Asynchronous nuclear division cycles in multinucleated cells. *J Cell Biol* **172**, 347-62.

Gladfelter, A. S., Kozubowski, L., Zyla, T. R. and Lew, D. J. (2005). Interplay between septin organization, cell cycle and cell shape in yeast. *J Cell Sci* **118**, 1617-28.

Gladfelter, A. S., Pringle, J. R. and Lew, D. J. (2001). The septin cortex at the yeast mother-bud neck. *Curr Opin Microbiol* **4**, 681-9.

Gladfelter, A. S., Sustreanu, N., Hungerbuehler, A. K., Voegeli, S., Galati, V. and Philippsen, P. (2006b). The anaphase promoting complex/cyclosome (APC/C) is required for anaphase progression in multinucleated *A. gossypii* cells. *Eukaryot Cell*.

Goldstein, A. L. and McCusker, J. H. (1999). Three new dominant drug resistance cassettes for gene disruption in *Saccharomyces cerevisiae*. *Yeast* **15**, 1541-53.

Griesbeck, O., Baird, G. S., Campbell, R. E., Zacharias, D. A. and Tsien, R. Y. (2001). Reducing the environmental sensitivity of yellow fluorescent protein. Mechanism and applications. *J Biol Chem* **276**, 29188-94.

Gust, B., Challis, G. L., Fowler, K., Kieser, T. and Chater, K. F. (2003). PCR-targeted *Streptomyces* gene replacement identifies a protein domain needed for biosynthesis of the sesquiterpene soil odor geosmin. *Proc Natl Acad Sci U S A* **100**, 1541-6.

Hailey, D. W., Davis, T. N. and Muller, E. G. (2002). Fluorescence resonance energy transfer using color variants of green fluorescent protein. *Methods Enzymol* **351**, 34-49.

Hanahan, D. (1983). Studies on transformation of *Escherichia coli* with plasmids. *J Mol Biol* **166**, 557-80.

Harris, E. S., Li, F. and Higgs, H. N. (2004). The mouse formin, FRLalpha, slows actin filament barbed end elongation, competes with capping protein, accelerates polymerization from monomers, and severs filaments. *J Biol Chem* **279**, 20076-87.

Hartwell, L. H. (1971). Genetic control of the cell division cycle in yeast. IV. Genes controlling bud emergence and cytokinesis. *Exp Cell Res* **69**, 265-76.

Hashimoto, T., Kishi, T. and Yoshida, N. (1964). Demonstration of Microspores in Fungal Cross-Wall. *Nature* **202**, 1353.

Heim, R., Cubitt, A. B. and Tsien, R. Y. (1995). Improved green fluorescence. *Nature* **373**, 663-4.

Heim, R., Prasher, D. C. and Tsien, R. Y. (1994). Wavelength mutations and posttranslational autoxidation of green fluorescent protein. *Proc Natl Acad Sci U S A* **91**, 12501-4.

Helfer, H. (2001). Effects of myosin gene deletions on growth and development of the filamentous fungus *Ashbya gossypii*. In *Biozentrum*, vol. MSc, pp. 59. Basel: University of Basel.

Helfer, H. (2006). New aspects of septin assembly and cell cycle control in multinucleated *A. gossypii*. In *Biozentrum*, vol. PhD, pp. 111. Basel: University of Basel.

Helfer, H. and Gladfelter, A. S. (2006). AgSwe1p regulates mitosis in response to morphogenesis and nutrients in multinucleated *Ashbya gossypii* cells. *Mol Biol Cell* **17**, 4494-512.

Hinnen, A., Hicks, J. B. and Fink, G. R. (1978). Transformation of yeast. *Proc Natl Acad Sci U S A* **75**, 1929-33.

Ho, Y., Gruhler, A., Heilbut, A., Bader, G. D., Moore, L., Adams, S. L., Millar, A., Taylor, P., Bennett, K., Boutilier, K. et al. (2002). Systematic identification of protein complexes in *Saccharomyces cerevisiae* by mass spectrometry. *Nature* **415**, 180-3.

Hoepfner, D., Brachat, A. and Philippsen, P. (2000). Time-lapse video microscopy analysis reveals astral microtubule detachment in

the yeast spindle pole mutant *cnm67*. *Mol Biol Cell* **11**, 1197-211.

Hong, E. L., Balakrishnan, R., Christie, K. R., Costanzo, M. C., Dwight, S. S., Engel, S. R., Fisk, D. G., Hirschman, J. E., Livstone, M. S., Nash, R. et al. (2007). *Saccharomyces* Genome Database.

Huh, W. K., Falvo, J. V., Gerke, L. C., Carroll, A. S., Howson, R. W., Weissman, J. S. and O'Shea, E. K. (2003). Global analysis of protein localization in budding yeast. *Nature* **425**, 686-91.

Hulo, N., Bairoch, A., Bulliard, V., Cerutti, L., De Castro, E., Langendijk-Genevaux, P. S., Pagni, M. and Sigrist, C. J. (2006). The PROSITE database. *Nucleic Acids Res* **34**, D227-30.

Imamura, H., Tanaka, K., Hihara, T., Umikawa, M., Kamei, T., Takahashi, K., Sasaki, T. and Takai, Y. (1997). Bni1p and Bnr1p: downstream targets of the Rho family small G-proteins which interact with profilin and regulate actin cytoskeleton in *Saccharomyces cerevisiae*. *Embo J* **16**, 2745-55.

Inouye, S. and Tsuji, F. I. (1994). *Aequorea* green fluorescent protein. Expression of the gene and fluorescence characteristics of the recombinant protein. *FEBS Lett* **341**, 277-80.

Itoh, T., Erdmann, K. S., Roux, A., Habermann, B., Werner, H. and De Camilli, P. (2005). Dynamin and the actin cytoskeleton cooperatively regulate plasma membrane invagination by BAR and F-BAR proteins. *Dev Cell* **9**, 791-804.

James, P., Halladay, J. and Craig, E. A. (1996). Genomic libraries and a host strain designed for highly efficient two-hybrid selection in yeast. *Genetics* **144**, 1425-36.

Janke, C., Magiera, M. M., Rathfelder, N., Taxis, C., Reber, S., Maekawa, H., Moreno-Borchart, A., Doenges, G., Schwob, E., Schiebel, E. et al. (2004). A versatile toolbox for PCR-based tagging of yeast genes: new fluorescent proteins, more markers and promoter substitution cassettes. *Yeast* **21**, 947-62.

Jedd, G. and Chua, N. H. (2000). A new self-assembled peroxisomal vesicle required for efficient resealing of the plasma membrane. *Nat Cell Biol* **2**, 226-31.

Kamei, T., Tanaka, K., Hihara, T., Umikawa, M., Imamura, H., Kikyo, M., Ozaki, K. and Takai, Y. (1998). Interaction of Bnr1p with a novel Src homology 3 domain-containing Hof1p. Implication in cytokinesis in *Saccharomyces cerevisiae*. *J Biol Chem* **273**, 28341-5.

Knechtle, P. (2002). *AgSPA2* and *AgBOI* control landmarks of filamentous growth in the filamentous ascomycete *Ashbya gossypii*. In *Biozentrum*, vol. PhD, pp. 65. Basel: University of Basel.

Knechtle, P., Dietrich, F. and Philippsen, P. (2003). Maximal polar growth potential depends on the polarisome component *Ag*Spa2 in the filamentous fungus *Ashbya gossypii*. *Mol Biol Cell* **14**, 4140-54.

Knechtle, P., Wendland, J. and Philippsen, P. (2006). The SH3/PH domain protein *Ag*Boi1/2 collaborates with the Rho-type GTPase *Ag*Rho3 to prevent nonpolar growth at hyphal tips of *Ashbya gossypii*. *Eukaryot Cell* **5**, 1635-47.

Knop, M., Barr, F., Riedel, C. G., Heckel, T. and Reichel, C. (2002). Improved version of the red fluorescent protein (drFP583/DsRed/RFP). *Biotechniques* **33**, 592, 594, 596-8 passim.

Knop, M., Siegers, K., Pereira, G., Zachariae, W., Winsor, B., Nasmyth, K. and Schiebel, E. (1999). Epitope tagging of yeast genes using a PCR-based strategy: more tags and improved practical routines. *Yeast* **15**, 963-72.

Kovacech, B., Nasmyth, K. and Schuster, T. (1996). *EGT2* gene transcription is induced predominantly by Swi5 in early G1. *Mol. Cell. Biol.* **16**, 3264-3274.

Kovar, D. R. (2006). Molecular details of formin-mediated actin assembly. *Curr Opin Cell Biol* **18**, 11-7.

Kovar, D. R., Kuhn, J. R., Tichy, A. L. and Pollard, T. D. (2003). The fission yeast cytokinesis formin Cdc12p is a barbed end actin filament capping protein gated by profilin. *J Cell Biol* **161**, 875-87.

Kuranda, M. J. and Robbins, P. W. (1991). Chitinase is required for cell separation during growth of *Saccharomyces cerevisiae*. *J Biol Chem* **266**, 19758-67.

Lauf, U., Lopez, P. and Falk, M. M. (2001). Expression of fluorescently tagged connexins: a novel approach to rescue function of oligomeric DsRed-tagged proteins. *FEBS Lett* **498**, 11-5.

Lippincott, J. and Li, R. (1998a). Dual function of Cyk2, a cdc15/PSTPIP family protein, in regulating actomyosin ring dynamics and septin distribution. *J Cell Biol* **143**, 1947-60.

Lippincott, J. and Li, R. (1998b). Sequential assembly of myosin II, an IQGAP-like protein, and filamentous actin to a ring structure involved in budding yeast cytokinesis. *J Cell Biol* **140**, 355-66.

Lippincott, J. and Li, R. (2000). Involvement of PCH family proteins in cytokinesis and actin distribution. *Microsc Res Tech* **49**, 168-72.

Lohr, D., Venkov, P. and Zlatanova, J. (1995). Transcriptional regulation in the yeast GAL gene family: a complex genetic network. *Faseb J* **9**, 777-87.

Longtine, M. S., McKenzie, A., 3rd, Demarini, D. J., Shah, N. G., Wach, A., Brachat, A., Philippsen, P. and Pringle, J. R. (1998). Additional modules for versatile and economical PCR-based gene deletion and modification in *Saccharomyces cerevisiae*. *Yeast* **14**, 953-61.

Louvet, O., Doignon, F. and Crouzet, M. (1997). Stable DNA-binding yeast vector allowing high-bait expression for use in the two-hybrid system. *Biotechniques* **23**, 816-8, 820.

Lupas, A., Van Dyke, M. and Stock, J. (1991). Predicting coiled coils from protein sequences. *Science* **252**, 1162-4.

Maeting, I., Schmidt, G., Sahm, H., Revuelta, J. L., Stierhof, Y. D. and Stahmann, K. P. (1999). Isocitrate lyase of *Ashbya gossypii*--transcriptional regulation and peroxisomal localization. *FEBS Lett* **444**, 15-21.

Markham, P. and Collinge, A. J. (1987). Woronin bodies of filamentous fungi. *FEMS Microbiology Letters* **46**, 1-11.

Marks, J., Hagan, I. M. and Hyams, J. S. (1986). Growth polarity and cytokinesis in fission yeast: the role of the cytoskeleton. *J Cell Sci Suppl* **5**, 229-41.

Matz, M. V., Fradkov, A. F., Labas, Y. A., Savitsky, A. P., Zaraisky, A. G., Markelov, M. L. and Lukyanov, S. A. (1999). Fluorescent proteins from nonbioluminescent *Anthozoa* species. *Nat Biotechnol* **17**, 969-73.

Maundrell, K. (1993). Thiamine-repressible expression vectors pREP and pRIP for fission yeast. *Gene* **123**, 127-30.

Michailides, T. J. and Moragan, D. P. (1990). Etiology and transmission of stigmatomycosis disease of pistachio in California. In *Calif Pistachio Industry (ed.), Annu Rpt Crop Year 1989-90*, pp. 88-95. Fresno, CA.

Mitchell, P. L. (2004). *Heteroptera* as vectors of plant pathogens. *Neotropical Entomology* **33**, 519-545.

Mizuno, H., Sawano, A., Eli, P., Hama, H. and Miyawaki, A. (2001). Red fluorescent protein from *Discosoma* as a fusion tag and a partner for fluorescence resonance energy transfer. *Biochemistry* **40**, 2502-10.

Mohr, C. (1997). Genetic engineering of the filamentous fungus *Ashbya gossypii*: construction of a genomic library, isolation of genes for beta-isopropylmalate-dehydrogenase (*LEU2*) and a protein kinase (*APK1*) by heterologous complementation, and characterization of non-reverting mutants. In *Biozentrum*, vol. PhD. Basel: University of Basel.

Momany, M., Zhao, J., Lindsey, R. and Westfall, P. J. (2001). Characterization of the *Aspergillus nidulans* septin (*asp*) gene family. *Genetics* **157**, 969-77.

Moseley, J. B., Sagot, I., Manning, A. L., Xu, Y., Eck, M. J., Pellman, D. and Goode, B. L. (2004). A conserved mechanism for Bni1- and mDia1-induced actin assembly and dual regulation of Bni1 by Bud6 and profilin. *Mol Biol Cell* **15**, 896-907.

Mulholland, J., Wesp, A., Riezman, H. and Botstein, D. (1997). Yeast actin cytoskeleton mutants accumulate a new class of Golgi-derived secretory vesicles. *Mol Biol Cell* **8**, 1481-99.

Nagai, T., Ibata, K., Park, E. S., Kubota, M., Mikoshiba, K. and Miyawaki, A. (2002). A variant of yellow fluorescent protein with fast and efficient maturation for cell-biological applications. *Nat Biotechnol* **20**, 87-90.

Nanninga, N. (2001). Cytokinesis in prokaryotes and eukaryotes: common principles and different solutions. *Microbiol Mol Biol Rev* **65**, 319-33 ; third page, table of contents.

Nguyen, A. W. and Daugherty, P. S. (2005). Evolutionary optimization of fluorescent proteins for intracellular FRET. *Nat Biotechnol* **23**, 355-60.

O'Conallain, C., Doolin, M. T., Taggart, C., Thornton, F. and Butler, G. (1999). Regulated nuclear localisation of the yeast transcription factor Ace2p controls expression of chitinase (*CTS1*) in *Saccharomyces cerevisiae*. *Mol Gen Genet* **262**, 275-82.

Ormo, M., Cubitt, A. B., Kallio, K., Gross, L. A., Tsien, R. Y. and Remington, S. J. (1996). Crystal structure of the *Aequorea victoria* green fluorescent protein. *Science* **273**, 1392-1395.

Pan, X. and Heitman, J. (2000). Sok2 Regulates Yeast Pseudohyphal Differentiation via a Transcription Factor Cascade That Regulates Cell-Cell Adhesion. *Mol. Cell. Biol.* **20**, 8364-8372.

Pelham, R. J. and Chang, F. (2002). Actin dynamics in the contractile ring during cytokinesis in fission yeast. *Nature* **419**, 82-6.

Perry, M. M., John, H. A. and Thomas, N. S. (1971). Actin-like filaments in the cleavage furrow of newt egg. *Exp Cell Res* **65**, 249-53.

Philippsen, P., Kaufmann, A. and Schmitz, H. P. (2005). Homologues of yeast polarity genes control the development of multinucleated hyphae in *Ashbya gossypii*. *Curr Opin Microbiol* **8**, 370-7.

Platt, A. and Reece, R. J. (1998). The yeast galactose genetic switch is mediated by the formation of a Gal4p-Gal80p-Gal3p complex. *Embo J* **17**, 4086-91.

Prasher, D. C., Eckenrode, V. K., Ward, W. W., Prendergast, F. G. and Cormier, M. J. (1992). Primary structure of the *Aequorea victoria* green-fluorescent protein. *Gene* **111**, 229-33.

Pringle, J. R., Adams, A. E., Drubin, D. G. and Haarer, B. K. (1991). Immunofluorescence methods for yeast. *Methods Enzymol* **194**, 565-602.

Pringle, J. R., Preston, R. A., Adams, A. E., Stearns, T., Drubin, D. G., Haarer, B. K. and Jones, E. W. (1989). Fluorescence microscopy methods for yeast. *Methods Cell Biol* **31**, 357-435.

Pruyne, D. and Bretscher, A. (2000). Polarization of cell growth in yeast. *J Cell Sci* **113**, 571-585.

Pruyne, D., Evangelista, M., Yang, C., Bi, E., Zigmond, S., Bretscher, A. and Boone, C. (2002). Role of formins in actin

assembly: nucleation and barbed-end association. *Science* **297**, 612-5.

Rees, W. A., Yager, T. D., Korte, J. and von Hippel, P. H. (1993). Betaine can eliminate the base pair composition dependence of DNA melting. *Biochemistry* **32**, 137-44.

Rizzo, M. A., Springer, G. H., Granada, B. and Piston, D. W. (2004). An improved cyan fluorescent protein variant useful for FRET. *Nat Biotechnol* **22**, 445-9.

Rogers, S., Wells, R. and Rechsteiner, M. (1986). Amino acid sequences common to rapidly degraded proteins: the PEST hypothesis. *Science* **234**, 364-8.

Sagot, I., Rodal, A. A., Moseley, J., Goode, B. L. and Pellman, D. (2002). An actin nucleation mechanism mediated by Bni1 and profilin. *Nat Cell Biol* **4**, 626-31.

Sambrook, J. and Russell, D. W. (2001). Molecular Cloning - A Laboratory Manual. Cold Spring Harbor, New York: Cold Spring Harbor Laboratory Press.

Schmitz, H. P., Kaufmann, A., Kohli, M., Laissue, P. P. and Philippsen, P. (2006). From function to shape: a novel role of a formin in morphogenesis of the fungus *Ashbya gossypii*. *Mol Biol Cell* **17**, 130-45.

Schroeder, T. E. (1973). Actin in dividing cells: contractile ring filaments bind heavy meromyosin. *Proc Natl Acad Sci U S A* **70**, 1688-92.

Shaner, N. C., Campbell, R. E., Steinbach, P. A., Giepmans, B. N., Palmer, A. E. and Tsien, R. Y. (2004). Improved monomeric red, orange and yellow fluorescent proteins derived from Discosoma sp. red fluorescent protein. *Nat Biotechnol* **22**, 1567-72.

Shaner, N. C., Steinbach, P. A. and Tsien, R. Y. (2005). A guide to choosing fluorescent proteins. *Nat Methods* **2**, 905-9.

Shannon, K. B. and Li, R. (1999). The multiple roles of Cyk1p in the assembly and function of the actomyosin ring in budding yeast. *Mol Biol Cell* **10**, 283-96.

Sheff, M. A. and Thorn, K. S. (2004). Optimized cassettes for fluorescent protein tagging in *Saccharomyces cerevisiae*. *Yeast* **21**, 661-70.

Shimomura, O., Johnson, F. H. and Saiga, Y. (1962). Extraction, purification and properties of aequorin, a bioluminescent protein from the luminous hydromedusan, *Aequorea*. *J Cell Comp Physiol* **59**, 223-39.

Siegel, M. S. and Isacoff, E. Y. (1997). A genetically encoded optical probe of membrane voltage. *Neuron* **19**, 735-741.

Sikorski, R. S. and Hieter, P. (1989). A system of shuttle vectors and yeast host strains designed for efficient manipulation of DNA in *Saccharomyces cerevisiae*. *Genetics* **122**, 19-27.

SquashBug. Cotton Stainer *Dysdercus voelkeri*: SquashBug.

St John, T. P. and Davis, R. W. (1981). The organization and transcription of the galactose gene cluster of *Saccharomyces*. *J Mol Biol* **152**, 285-315.

Stahmann, K. P., Arst, H. N., Jr., Althofer, H., Revuelta, J. L., Monschau, N., Schlupen, C., Gatgens, C., Wiesenburg, A. and Schlosser, T. (2001). Riboflavin, overproduced during sporulation of *Ashbya gossypii*, protects its hyaline spores against ultraviolet light. *Environ Microbiol* **3**, 545-50.

Steiner, S., Wendland, J., Wright, M. C. and Philippsen, P. (1995). Homologous recombination as the main mechanism for DNA integration and cause of rearrangements in the filamentous ascomycete *Ashbya gossypii*. *Genetics* **140**, 973-87.

Stewart, C. N., Jr. (2006). Go with the glow: fluorescent proteins to light transgenic organisms. *Trends Biotechnol* **24**, 155-62.

Straight, A. F., Marshall, W. F., Sedat, J. W. and Murray, A. W. (1997). Mitosis in living budding yeast: Anaphase a but no metaphase plate. *Science* **277**, 574-578.

Sudbery, P. E. (2001). The germ tubes of *Candida albicans* hyphae and pseudohyphae show different patterns of septin ring localization. *Mol Microbiol* **41**, 19-31.

Takizawa, P. A., DeRisi, J. L., Wilhelm, J. E. and Vale, R. D. (2000). Plasma membrane compartmentalization in yeast by messenger RNA transport and a septin diffusion barrier. *Science* **290**, 341-4.

Tasto, J. J., Morrell, J. L. and Gould, K. L. (2003). An anillin homologue, Mid2p, acts during fission yeast cytokinesis to organize the septin ring and promote cell separation. *J Cell Biol* **160**, 1093-103.

Tenney, K., Hunt, I., Sweigard, J., Pounder, J. I., McClain, C., Bowman, E. J. and Bowman, B. J. (2000). *Hex-1*, a gene unique to filamentous fungi, encodes the major protein of the Woronin body and functions as a plug for septal pores. *Fungal Genet Biol* **31**, 205-17.

Terashima, H., Hamada, K. and Kitada, K. (2003). The localization change of Ybr078w/Ecm33, a yeast GPI-associated protein, from the plasma membrane to the cell wall, affecting the cellular function. *FEMS Microbiology Letters* **218**, 175-180.

TransGEN. (2007). Vitamin B2: Herstellung mit gv-Mikroorganismen: TransGEN - Transparenz für Gentechnik bei Lebensmittel.

Trinci, A. P. and Collinge, A. J. (1974). Occlusion of the septal pores of damaged hyphae of *Neurospora crassa* by hexagonal crystals. *Protoplasma* **80**, 57-67.

Tsien, R. Y. (1998). The green fluorescent protein. *Annu Rev Biochem* **67**, 509-44.

Tsujita, K., Suetsugu, S., Sasaki, N., Furutani, M., Oikawa, T. and Takenawa, T. (2006). Coordination between the actin cytoskeleton and membrane deformation by a novel membrane tubulation domain of PCH proteins is involved in endocytosis. *J Cell Biol* **172**, 269-79.

Uetz, P., Giot, L., Cagney, G., Mansfield, T. A., Judson, R. S., Knight, J. R., Lockshon, D., Narayan, V., Srinivasan, M., Pochart, P. et al. (2000). A comprehensive analysis of protein-protein interactions in *Saccharomyces cerevisiae*. *Nature* **403**, 623-7.

van Dijken, J. P., Bauer, J., Brambilla, L., Duboc, P., Francois, J. M., Gancedo, C., Giuseppin, M. L., Heijnen, J. J., Hoare, M., Lange, H. C. et al. (2000). An interlaboratory comparison of physiological and genetic properties of four *Saccharomyces cerevisiae* strains. *Enzyme Microb Technol* **26**, 706-714.

Versele, M. and Thorner, J. (2004). Septin collar formation in budding yeast requires GTP binding and direct phosphorylation by the PAK, Cla4. *J Cell Biol* **164**, 701-15.

Vieira, J. and Messing, J. (1991). New pUC-derived cloning vectors with different selectable markers and DNA replication origins. *Gene* **100**, 189-94.

Wach, A., Brachat, A., Alberti-Segui, C., Rebischung, C. and Philippsen, P. (1997). Heterologous *HIS3* marker and GFP reporter modules for PCR-targeting in *Saccharomyces cerevisiae*. *Yeast* **13**, 1065-75.

Wach, A., Brachat, A., Pohlmann, R. and Philippsen, P. (1994). New heterologous modules for classical or PCR-based gene disruptions in *Saccharomyces cerevisiae*. *Yeast* **10**, 1793-808.

Wachtler, V., Huang, Y., Karagiannis, J. and Balasubramanian, M. K. (2006). Cell Cycle-dependent Roles for the FCH-Domain Protein Cdc15p in Formation of the Actomyosin Ring in *Schizosaccharomyces pombe*. *Mol Biol Cell* **17**, 3254-66.

Walther, A. and Wendland, J. (2003). Septation and cytokinesis in fungi. *Fungal Genet Biol* **40**, 187-96.

Wang, S. and Hazelrigg, T. (1994). Implications for bcd mRNA localization from spatial distribution of exu protein in *Drosophila* oogenesis. *Nature* **369**, 400-03.

Wang, T. and Bretscher, A. (1995). The rho-GAP encoded by *BEM2* regulates cytoskeletal structure in budding yeast. *Mol Biol Cell* **6**, 1011-24.

Ward, W. W., Cody, C. W., Hart, R. C. and Cormier, M. J. (1980). Spectrophotometric Identity of the Energy-Transfer Chromophores in Renilla and *Aequorea* Green-Fluorescent Proteins. *Photochemistry and Photobiology* **31**, 611-615.

Warenda, A. J. and Konopka, J. B. (2002). Septin function in *Candida albicans* morphogenesis. *Mol Biol Cell* **13**, 2732-46.

Wendland, J. (2003a). Analysis of the landmark protein Bud3 of *Ashbya gossypii* reveals a novel role in septum construction. *EMBO Rep* **4**, 200-4.

Wendland, J. (2003b). PCR-based methods facilitate targeted gene manipulations and cloning procedures. *Curr Genet* **44**, 115-23.

Wendland, J., Ayad-Durieux, Y., Knechtle, P., Rebischung, C. and Philippsen, P. (2000). PCR-based gene targeting in the filamentous fungus *Ashbya gossypii*. *Gene* **242**, 381-91.

Wendland, J. and Philippsen, P. (2000). Determination of cell polarity in germinated spores and hyphal tips of the filamentous ascomycete *Ashbya gossypii* requires a rhoGAP homolog. *J Cell Sci* **113 (Pt 9)**, 1611-21.

Wendland, J. and Philippsen, P. (2001). Cell polarity and hyphal morphogenesis are controlled by multiple rho-protein modules in the filamentous ascomycete *Ashbya gossypii*. *Genetics* **157**, 601-10.

Wendland, J. and Philippsen, P. (2002). An IQGAP-related protein, encoded by *AgCYK1*, is required for septation in the filamentous fungus *Ashbya gossypii*. *Fungal Genet Biol* **37**, 81-8.

Wendland, J. and Walther, A. (2005). *Ashbya gossypii*: a model for fungal developmental biology. *Nat Rev Microbiol* **3**, 421-9.

Westfall, P. J. and Momany, M. (2002). *Aspergillus nidulans* septin AspB plays pre- and postmitotic roles in septum, branch, and conidiophore development. *Mol Biol Cell* **13**, 110-8.

Wickerham, L. J., Flickinger, M. H. and Johnston, R. M. (1946). The production of riboflavin by *Ashbya gossypii*. *Arch Biochem* **9**, 95-8.

Winston, F., Dollard, C. and Ricupero-Hovasse, S. L. (1995). Construction of a set of convenient *Saccharomyces cerevisiae* strains that are isogenic to S288C. *Yeast* **11**, 53-5.

Winzeler, E. A., Shoemaker, D. D., Astromoff, A., Liang, H., Anderson, K., Andre, B., Bangham, R., Benito, R., Boeke, J. D., Bussey, H. et al. (1999). Functional characterization of the *S. cerevisiae* genome by gene deletion and parallel analysis. *Science* **285**, 901-6.

Wood, V. Gwilliam, R. Rajandream, M. A. Lyne, M. Lyne, R. Stewart, A. Sgouros, J. Peat, N. Hayles, J. Baker, S. et al. (2002). The genome sequence of Schizosaccharomyces pombe. *Nature* **415**, 871-80.

Woronin, M. (1864). Zur Entwicklungsgeschichte des *Ascobolus pulcherrimus* Cr. und einiger Pezizen. *Abh. Senkenb. Naturforsch.* **5**, 333-344.

Wright, M. C. and Philippsen, P. (1991). Replicative transformation of the filamentous fungus *Ashbya gossypii* with plasmids containing *Saccharomyces cerevisiae* ARS elements. *Gene* **109**, 99-105.

Wu, J. Q., Kuhn, J. R., Kovar, D. R. and Pollard, T. D. (2003). Spatial and temporal pathway for assembly and constriction of the contractile ring in fission yeast cytokinesis. *Dev Cell* **5**, 723-34.

Yang, F., Moss, L. G. and Phillips, G. N. (1996). The molecular structure of green fluorescent protein. *Nature Biotechnology* **14**, 1246-1251.

Yang, S., Cope, M. J. T. V. and Drubin, D. G. (1999). Sla2p Is Associated with the Yeast Cortical Actin Cytoskeleton via Redundant Localization Signals. *Mol. Biol. Cell* **10**, 2265-2283.

Yanisch-Perron, C., Vieira, J. and Messing, J. (1985). Improved M13 phage cloning vectors and host strains: nucleotide sequences of the M13mp18 and pUC19 vectors. *Gene* **33**, 103-19.

YeastResourceCenter. (2006). This work is supported by the National Center for Research Resources of the National Institutes of Health by a grant to T.N.D. entitled 'Comprehensive Biology: Exploiting the Yeast Genome', P41 RR11823. Seattle.

Zacharias, D. A., Violin, J. D., Newton, A. C. and Tsien, R. Y. (2002). Partitioning of lipid-modified monomeric GFPs into membrane microdomains of live cells. *Science* **296**, 913-6.

Zeitlinger, J., Simon, I., Harbison, C. T., Hannett, N. M., Volkert, T. L., Fink, G. R. and Young, R. A. (2003). Program-specific distribution of a transcription factor dependent on partner transcription factor and MAPK signaling. *Cell* **113**, 395-404.

Zhang, Y., Buchholz, F., Muyrers, J. P. and Stewart, A. F. (1998). A new logic for DNA engineering using recombination in Escherichia coli. *Nat Genet* **20**, 123-8.

Curriculum vitae

CURRICULUM VITAE

PERSONAL INFORMATION

Name	Andreas Michael Kaufmann
Address	Jägerstrasse 14, Basel, Switzerland
Mobile	+4178 629 5939
Email	andreas.kaufmann@unibas.ch

EDUCATION

2003 – 2007 **Doctor of Philosophy in Microbiology**; Biozentrum, University of Basel, Switzerland
Grade: Summa cum laude (5.8 / 6)
Thesis title "Polarized growth and septation in the filamentous ascomycete *Ashbya gossypii* analyzed by live cell imaging".
Supervisor: Prof. Peter Philippsen, University of Basel, Switzerland.
Committee: Prof. Anne Spang, University of Basel, Switzerland; Dr. Robert Arkowitz, University of Nice, France.

1998 – 2003 **Diploma degree in Molecular Biology**; Biozentrum, University of Basel, Switzerland
equivalent to a degree of a Master of Science
Grade: 5.6 / 6
Thesis title "*AgBNI1* and *AgHOF1*: Two genes involved in hyphal development in the filamentous fungus *A. gossypii*".
Supervisor: Prof. Peter Philippsen, University of Basel, Switzerland.
Courses in Biophysics and Structural Biology, Biochemistry, Microbiology, Microscopy, Genetics, Cell and Developmental Biology, Neurobiology, and Immunology.

1993 – 1997 **Matura, Type E (Economics)**; Gymnasium Bern-Neufeld, Bern, Switzerland
Grade: 5.2 / 6
Award for highest grades in science classes.

PUBLICATIONS

Kaufmann, A. (manuscript in preparation). A versatile toolbox for PCR-based gene targeting in *Ashbya gossypii*.

Kaufmann, A. and Philippsen, P. (manuscript in revision). Of collars and rings: Hof1-dependent cytokinesis in multiseptated hyphae of *Ashbya gossypii*.

Knechtle, P., Kaufmann, A., Cavicchioli, D., and Philippsen, P. (2008). The Paxillin-like protein AgPxl1 is required for apical branching and maximal hyphal growth in *A. gossypii*. *Fungal Genet Biol.* ***45****, 829-38*.

Schmitz, H. P., Kaufmann, A., Kohli, M., Laiussue, P. P. and Philippsen, P. (2006). From function to shape: a novel role of a formin in morphogenesis of the fungus *Ashbya gossypii*. *Mol Biol Cell* ***17****, 130-45*.

Philippsen, P., Kaufmann, A. and Schmitz, H. P. (2005). Homologues of yeast polarity genes control the development of multinucleated hyphae in *Ashbya gossypii*. *Curr Opin Microbiol* ***8****, 370-7*.

CURRICULUM VITAE

PRESENTATIONS

First German/French/European Meeting on Yeast and Filamentous Fungi; Strasbourg, 2008
Platform: Cytokinesis and septation in the filamentous ascomycete *Ashbya gossypii*.

ECFG 9th European Conference on Fungal Genetics; Edinburgh, 2008
Poster: Cytokinesis and septation in the filamentous ascomycete *Ashbya gossypii*.

XXIIIrd International Conference on Yeast Genetics and Molecular Biology; Melbourne, 2007
Workshop and poster: Cytokinesis and septation in the filamentous ascomycete *Ashbya gossypii*.

Swiss Yeast Meeting 2006; Basel, 2006
Platform: Septation in the filamentous ascomycete *Ashbya gossypii*.

GSA Yeast Genetics and Molecular Biology Meeting; Princeton, 2006.
Workshop and poster: Incomplete cytokinesis in the filamentous yeast *Ashbya gossypii*.

CSH Yeast Cell Biology Meeting; Cold Spring Harbor, 2005.
Platform: Hof1 is essential for actin ring formation during septation in *A. gossypii*.

GSA Yeast Genetics and Molecular Biology Meeting; Seattle, 2004.
Poster: From function to shape – the role of a Formin in tip-branching and hyphal formation in *Ashbya gossypii*.

ECFG 6th European Conference on Fungal Genetics; Pisa, 2002.
Poster: Functional analysis of the Formins of the filamentous fungus *Ashbya gossypii*.

Erklärung

Erklärung

Ich erkläre, dass ich die Dissertation „Polarized growth and septation in the filamentous ascomycete *Ashbya gossypii* analyzed by live cell imaging“ nur mit der darin angegebenen Hilfe verfasst und bei keiner anderen Universität und keiner anderen Fakultät der Universität Basel eingereicht habe.

Basel, 10. April 2007

Andreas Kaufmann